Design, Characterization and Pharmacokinetic Evaluation of Lopinavir Nanoparticles for Oral Delivery in the Effective Treatment of HIV/AIDS

THESIS

Submitted in partial fulfilment
of the requirements for the degree of
DOCTOR OF PHILOSOPHY

by

Rahul Vats
ID. No. 2010PHXF034H

Under the Supervision of
Dr. PUNNA RAO RAVI

BIRLA INSTITUTE OF TECHNOLOGY AND SCIENCE, PILANI
2014

BIRLA INSTITUTE OF TECHNOLOGY AND SCIENCE, PILANI

CERTIFICATE

This is to certify that the thesis entitled **Design, Characterization and Pharmacokinetic Evaluation of Lopinavir Nanoparticles for Oral Delivery in the Effective Treatment of HIV/AIDS** and submitted by **Rahul Vats** ID No **2010PHXF034H** for award of Ph.D. of the Institute embodies original work done by him under my supervision.

Signature of the Supervisor:

Name in capital letters : **PUNNA RAO RAVI**

Designation : **Assistant Professor**

Date :

ACKNOWLEDGEMENT

Words cannot express my heartfelt gratitude to my mentor and guide, Dr Punna Rao Ravi, Assistant Professor, Department of Pharmacy, BITS Pilani, Hyderabad Campus. He has been a constant source of support and inspiration to me throughout my course of work. His boundless enthusiasm coupled with his sharp intellectual abilities has left an indelible mark on me. His moral support and timely advice at crucial times are unforgettable. I am highly indebted to him and sincerely acknowledge his help at all times.

It is my duty to express my sincere thanks to the Chancellor, BITS Pilani for providing necessary infrastructural support to carry out my research work. I am thankful to Prof. Bijendra Nath Jain, Vice Chancellor, BITS Pilani for facilitating my research work at the institute. I am also thankful to Prof. V.S. Rao, Director, BITS Pilani, Hyderabad Campus for his support during the course of my stay at this campus. I am thankful to Prof S.K. Verma, Dean, Academic Research Division, BITS Pilani, for his co-operation and encouragement at every stage of this research work.

I am thankful to Dr V. Vamsi Krishna, Head, Department of Pharmacy and senior professors, Dr D Sriram and Dr Yogeeswari Sriram for providing me with all the laboratory facilities and moral support during the course of my stay at the campus.

I sincerely acknowledge the help provided by other faculty members, Dr Srikant Charde, Dr Onkar Kulkarni, Dr Sajeli Begum, Dr Swati Biswas, Dr Balram Ghosh and Dr Arti Dhar for sharing their vast experience and technical knowledge with me at needy times.

I am also grateful to the non-teaching staff, Mr Rajesh, Mrs Saritha, Mr Ramu, Mr Srinivas and Mrs Rekha for their support in maintaining the supply of chemicals, glassware and animals during the course of my research work.

I am very grateful to my colleagues and friends, Mr N. Aditya, Mr Praveen Kumar, Mr Shailender, Mr Madhubabu, Mr Ram and many others for their invaluable support, encouragement and help at all times. They have been extremely patient and bearing with me and have helped in gaining a lot through mutual exchange of knowledge. Their constructive criticism and technical inputs have been invaluable for my work.

The undergraduate and postgraduate students of pharmacy department deserve a special mention here. I cannot forget the help rendered by our students, Mr Upendra Reddy, Mr Jagadeesh Balija, Mr Sathya Prabhu Naidu, Mr Vikash Dalal, Mr Nitin Gadekar and Mr Rahul Thakur.

I acknowledge the help of Department of Science and Technology (DST) for providing financial assistance through a major research grant (DST Ref. No.: SR/FT/CS-122/2010 for the project. I also thank SERB, Department of Science and Technology, Govt. of India and BITS-Pilani for providing travel assistance to present my research work at various conferences in India and abroad.

This section would be incomplete without thanking my family for their unwavering support throughout this period. My heartfelt thanks to my parents, Mr Umakant Mishra and Mrs Shakuntala Mishra for being pillars of my life and for providing me with unconditional support at all times. I can hardly find words to express my gratitude to my wife Pooja Mishra for her patience and sacrifice.

Rahul Vats

Abstract

The principle objective of the present work was to design and evaluate suitable nanocarriers to improve therapeutic effectiveness of lopinavir by improving plasma exposure and selective distribution towards viral reservoir sites. Lopinavir is a potent HIV protease inhibitor and integral part of highly active antiretroviral treatment. Lopinavir shows poor plasma exposure after oral administration and high inter-patient variability in humans due to its poor aqueous solubility, extensive pre-systemic metabolism and P-gp efflux. To improve oral bioavailability, currently marketed formulation of lopinavir (Kaletra[@]; co-formulation of lopinavir/ritonavir in combination of 4:1) contains sub-therapeutic dose of ritonavir. Ritonavir, being CYP and P-gp inhibitor, significantly improves plasma exposure of lopinavir.

In order to achieve the broader objective of the present work, suitable analytical and bioanalytical methods were developed using liquid chromatography for determination of lopinavir in bulk formulation and biological matrices. Pre-formulation studies were performed to establish necessary physicochemical data of lopinavir prior to formulation development. Nanoparticulate formulations were developed by identifying and optimizing critical factors in the manufacturing process using optimization techniques (DoE). The prepared nanoparticles were extensively characterized for surface morphology, particle size, encapsulation efficiency and *in vitro* drug release.

Extensive pharmacokinetic studies (single dose-oral, IV and tissue distribution studies) were performed against marketed formulation to investigate the *in vivo* performance of the prepared nanoparticles in the healthy rat model. Mechanistic studies such as microsomal stability, intestinal permeability study and lymph transport inhibition study were carried out to explain the mechanism involved in absorption and disposition of nanoparticles.

Results indicated that developed and validated analytical and bioanalytical methods were sensitive and selective for determination of lopinavir in bulk, formulation and biological samples. Extensive pre-formulation studies indicated the lipophilic nature and pH independent ionization characteristics. Results from drug-excipient studies revealed no significant interaction of drug with various excipients used in formulation.

Biodegradable and biocompatible lipid based (stearic acid) and polymeric nanocarriers (poly-ε-caprolactone and pullulan acetate) were chosen for delivery of

lopinavir. Critical variables such as polymer, surfactant concentrations and time of homogenization demonstrated significant impact on particle size, surface charge and encapsulation efficiency of nanoparticles. Microscopic imaging and particle size measurement confirmed that nanoparticles are near spherical with size in the range of 200 nm. In vitro drug release from the loaded nanoparticles was controlled over 45-75h. This could be explained by reciprocal powered time model release kinetics. The optimized nanoparticles (SLNs and PCL NPs) have shown high drug entrapment efficiency (>90%).

Single dose pharmacokinetic studies demonstrated a significant improvement in plasma exposure of lopinavir following oral administration of lopinavir nanoparticles. SLNs showed highest improvement in oral bioavailability (>5 folds) of lopinavir followed by PCL NPs (>4 folds) and PA NPs (>2 folds). Significant improvement in oral bioavailability was attributed to protection from pre-systemic metabolism and P-gp efflux and improvement in both active and passive uptake of lopinavir from the GIT. Lymph transport inhibition studies demonstrate the role of the lymphatic system in transport of SLNs. Tissue distribution studies revealed increased availability of the drug towards viral reservoir sites such as liver, spleen and lymph nodes. Co-administration of ritonavir showed significant improvement of plasma exposure of lopinavir but failed to maintain higher drug concentration at targeted organs. Collectively, these results indicate that prepared nanocarriers have great potential for delivering lopinavir to HIV viral reservoir sites. Drug delivery using nanoparticles would be advantageous over the currently available marketed formulation of lopinavir.

List of Abbreviations and Symbols	
µg	Microgram
AIDS	Acquired immunodeficiency syndrome
AFM	Atomic Force Microscopy
AP-2	Assembly Polypeptide 2
AUC	Area Under concentration versus time Curve
AUMC	Area Under first Moments Curve of concentration versus time profile
BBB	Blood Brain Barrier
Caco-2	Colorectal adenocarcinoma cells
CD	Cluster of Differentiation
CI	Confidence Intervals
CL	Clearance
CL/F	Clearance scaled by bioavailability
C_{max}	Maximum concentration of the drug
CME	Clathrin Mediated Endocytosis
CNS	Central Nervous System
CPCSEA	Committee for the Purpose of Control and Supervision of Experiments on Animals
CR	Complement Receptor
CYP	Cytochrome P450 enzyme system
DDS	Drug Delivery System
DLS	Dynamic Light Scattering
DSC	Differential Scanning Calorimetry
EE	Entrapment Efficiency
EPR	Enhanced Permeation and Retention
F	Absolute Bioavailability

FAE	Follicle Associated Epithelium
FDA	Food and Drug Administration
F_{rel}	Relative Bioavailability
g	Gram
GALT	Gut-associated Lymphoid Tissue
GIT	Gastrointestinal Tract
GMS	Glyceryl Monostearate
GDS	Glyceryl Distearate
GB	Glyceryl Behenate
GTS	Glyceryl Tristearate
h	Hour
HIV	Human Immunodeficiency Virus
HPLC	High Performance Liquid Chromatography
HQC	Higher Level Quality Control Standard
IAEC	Institutional Animal Ethics Committee
ICH	International Conference on Harmonization
J	Joules
k	Degradation rate constant
K	Release rate constant
K_e	Rate of elimination of the drug
KHB	Krebs-Henseleit Buffer
L	Litre
LC-MS	Liquid Chromatography coupled with Mass Spectroscopy
LLOQ	Lowest Limit Of Quantification
LOD	Limit of Detection

Log D	Log of oil/water partition coefficient at a given pH
Log P	Log of oil/water partition coefficient
LPV	Lopinavir
LQC	Lower Level Quality Control Standard
M	Molar
MAT	Mean Absorption Time
M-Cells	Manifold Cells
MEC	Minimum Effective Concentration
mg	Milligram
min	Minutes
mm	Millimeter
MPS	Mononuclear Phagocyte System
MQC	Medium Level Quality Control Standard
MRT	Mean Retention Time
N	Newton
NPs	Nanoparticles
NDDS	Novel Drug Delivery System
NF	National Formulary
ng	Nano gram
O/W	Oil-in-water
^{o}C	Degree Centigrade
O-MALT	Mucosa Associated Lymphoid Tissue
P188	Poloxamer 188
P407	Poloxamer 407
PA	Pullulan acetate

PCL	Poly(ε-caprolactone)
PCS	Photon correlation spectroscopy
PD	Pharmacodynamics
PDI	Polydispersity Index
PECA	Poly(ethyl cyanoacrylate)
PEG	Polyethylene glycol
PK	Pharmacokinetics
PLA	Poly Lactic acid
PLGA	Poly(lactide-co-glycolic acid) copolymer
PSD	Particle size distribution
PVA	Polyvinyl Alcohol
QC	Quality Control Standard
R^2	Regression coefficient
RES	Reticuloendothelial System
RESOLV	Rapid expansion of supercritical solution into liquid solvent
RESS	Rapid expansion of supercritical solution
R_f	Retention Factor
RI	Recrystallization Index
RTV	Ritonavir
rpm	Revolutions per minute
RSD	Relative Standard Deviation
RT	Room Temperature (25 ± 2 ºC/60 ± 5% RH)
s	Seconds
SA	Stearic Acid
SD	Standard Deviation

SEM	Scanning Electron Microscopy
SLN	Solid Lipid Nanoparticles
$T_{1/2}$	Half-life
TEM	Transmission Electron Microscopy
T_f	Tailing Factor
TG-LPs	Triglycerides rich lipoproteins
T_{max}	Time to reach maximum concentration of the drug
USP	United States Pharmacopoeia
UV	Ultraviolet Light
V_d	Volume of distribution
O/W	Oil-in-Water
WAXS	Wide angle X-ray Scattering
Δ H	Melting Enthalpy
ε	Epsilon
ζ-potential	Zeta Potential
λmax	Wavelength Maxima for UV-Absorbance

Chapter 1

Introduction

1.1 AIDS and human immunodeficiency virus

The human immunodeficiency virus (HIV) was unknown until the early 1980's but since then it has infected millions of people in a worldwide pandemic. HIV is a member of the genus lentivirus from the retroviridae family responsible for acquired immunodeficiency syndrome (AIDS). At present there are two known types of HIV: HIV-1 and HIV-2. Of the two, HIV-1 is more virulent, transmittable and prevalent and is the cause of the majority of the HIV infections globally [1, 2].

The term AIDS represents the entire range of diseases caused by the HIV from early infection to late stage symptoms. This condition progressively reduces the effectiveness of the immune system and leaves individuals susceptible to opportunistic infections and tumors. The disease naturally targets only a few cell types including cluster of differentiation 4 ($CD4^+$) T cells, $CD4^+$ monocytes/macrophages, dendritic cells and microglial cells [3, 4]. Nearly 99% of all viral replication occur in activated and productively infected $CD4^+$ T cells of the blood and lymphoid tissues such as peripheral secondary lymphoid organs, the spleen, lymph nodes and gut associated lymphoid tissues [5].

1.2 Incidence of HIV/AIDS

AIDS is now a pandemic; in 2012, it was estimated that 35.3 million people lived with the disease worldwide. According to the report, the new HIV infections have fallen by 33% since 2001. Nevertheless, in 2012, 2.3 million people became newly infected with HIV worldwide [6]. Till today, over 36 million deaths due to HIV related illness have been reported. Out of which, 1.6 million people have died in 2012 [6]. Asia, home to 60% of the world's population, is only second to sub-Saharan Africa in terms of the number of people living with HIV. India accounts for roughly half of Asia's HIV prevalence. HIV estimations of 2012 corroborate the fact that the HIV epidemic in India continues to decline at the national level including new infections and AIDS related deaths. However, still around 2.09 million people in India are living with HIV. Of these, an estimated 36% are women and 3.5% are children [7].

The spread of HIV in India has been uneven. HIV epidemics are more severe in the southern half of the country and the far northeast. The highest HIV prevalence rates are found in Andhra Pradesh, Maharashtra, Tamil Nadu and Karnataka in the south; and Manipur and Nagaland in the northeast [8].

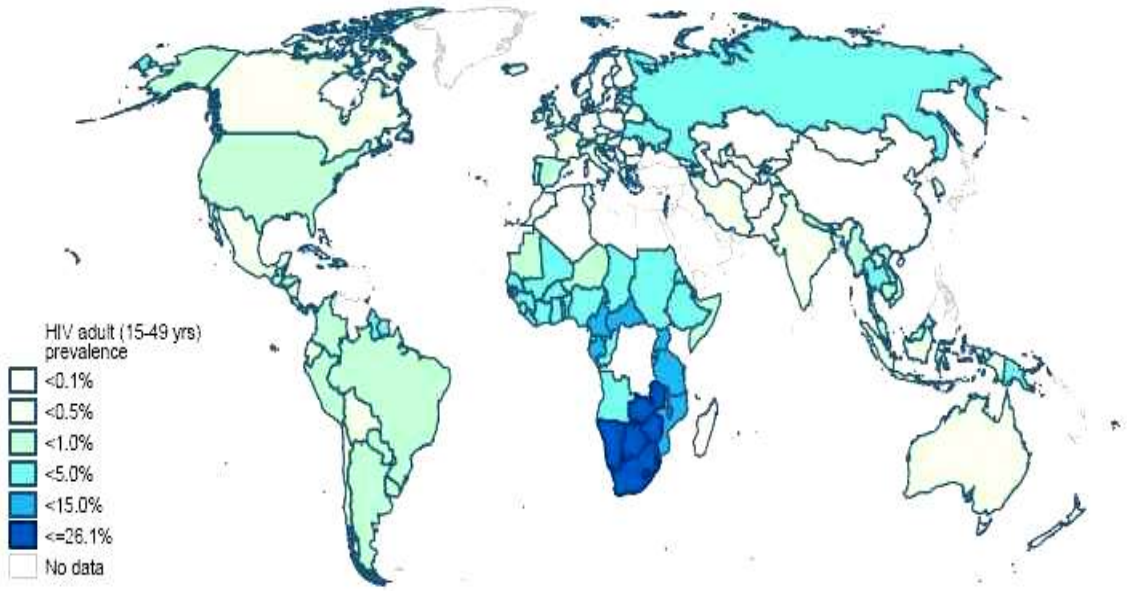

Fig. 1.1: Global Prevalence of HIV infection. Fig. source: Global report. UNAIDS report on the global AIDS epidemic 2013.

1.3 Viral structure and pathogenesis of HIV infection

A mature HIV virus consists of a bar-shaped electron dense core containing the viral genome; two short strands of ribonucleic acid (RNA) along with enzyme reverse transcriptase, protease, ribonuclease, and integrals, all encased in an outer lipid envelope derived from a host cell [9]. This envelope has 72 surface projections or spikes, containing antigens gp 120 and gp 41 that aid in the binding of the virus to the target cells expressed with the $CD4^+$ receptors. The genome of HIV contains three major genes: gag, pol, and env. These genes code for the major structural and functional components of HIV. The structural components encoded by env include the envelope glycoproteins (gp 120 and gp 41). Components encoded by the gag gene include core nucleocapsid proteins p55, p40, p24 (capsid, or “core" antigen), p17 (matrix), and p7 (nucleocapsid) and the important proteins encoded by pol are the enzyme proteins p66, p51 (reverse transcriptase), p11 (protease), and p32 (integrase) [10, 11].

The pathogenesis of HIV infection is a function of the virus life cycle, host cellular environment, and quantity of viruses in the infected individual. HIV requires living host cells to replicate. After entering the body, the viral particle is attracted to a cell with the appropriate $CD4^+$ receptor molecules where it attaches by fusion to a susceptible cell membrane or by endocytosis and then enters into the cell. The likelihood of infection depends on both the initial viral load in the body fluids which contacts the host and the number of cells containing $CD4^+$ receptors at the point of contact [12]. $CD4^+$ is a glycoprotein found on the surface of immune cells, such as T lymphocytes, natural killer

(NK) lymphocytes, monocytes, macrophages, microglial cells in the brain, and dendritic cells (epithelial Langerhans cells and follicular dendritic cells in lymph nodes) [13].

HIV entry into a host cell begins with gp120 binding to the $CD4^+$ receptor, which induces a conformational change in gp 120, exposing co-receptor binding sites which leads to the fusion of gp 41 of HIV and host cell membranes. Once within the cell, the viral particle releases its genetic material; the RNA. The enzyme reverse transcriptase that is bound to the HIV RNA then triggers the synthesis of linear double-stranded cDNA (proviral) from RNA. The HIV proviral DNA is inserted into the host cell genomic DNA by the integrase enzyme of the HIV and that initiates the translation process. Viral components such as gag proteins are assembled in the inner part of the host cell membrane, and virions then begin to bud off. During the budding process, HIV protease cleaves viral proteins into their functional forms. The infected cells can then release virions by surface budding, or infected cells can undergo lysis with a burst release of new HIV virions, that can then infect additional cells [14]. The life cycle of HIV is illustrated in Fig 1.2.

1.4 HIV and viral reservoirs

HIV can gain access in the human body even through the intact oropharyngeal, cervical, vaginal, and gastrointestinal mucosal surfaces. Routes of HIV entry into mucosal lamina propria include dendritic cells, epithelial cells, and microfold (M) cells. Dendritic cells that squeeze between "tight" epithelium may capture HIV and deliver it to underlying T cells, resulting in dissemination to lymphoid organs. The conventional dendritic cells, such as langerhans cells are found in epithelia and can cross endothelium and circulate freely into both lymphoid and mucosal tissues. Thus, dendritic cells play a key role in dissemination of HIV infection [15, 16].

Within the lymph nodes, HIV virions are trapped in the processes of follicular dendritic cells, where they reside in endosomal compartments formed from invaginations of the cell surface membrane. These compartmentalized virions in dendritic cells may further infect $CD4^+$ lymphocytes that are percolating through the nodes. Cells of the mononuclear phagocyte system, including those in lymph nodes, spleen, liver, and bone marrow can then become infected with HIV. Besides lymph nodes, the gut associated lymphoid tissues (GALT) in gastrointestinal sub-mucosa provides a substantial reservoir for HIV. When HIV is carried to local sites in the body, particularly to regional lymph nodes and to GALT, the antigen-presenting cells such as macrophages or dendritic cells act as a "Trojan horse" [17-19].

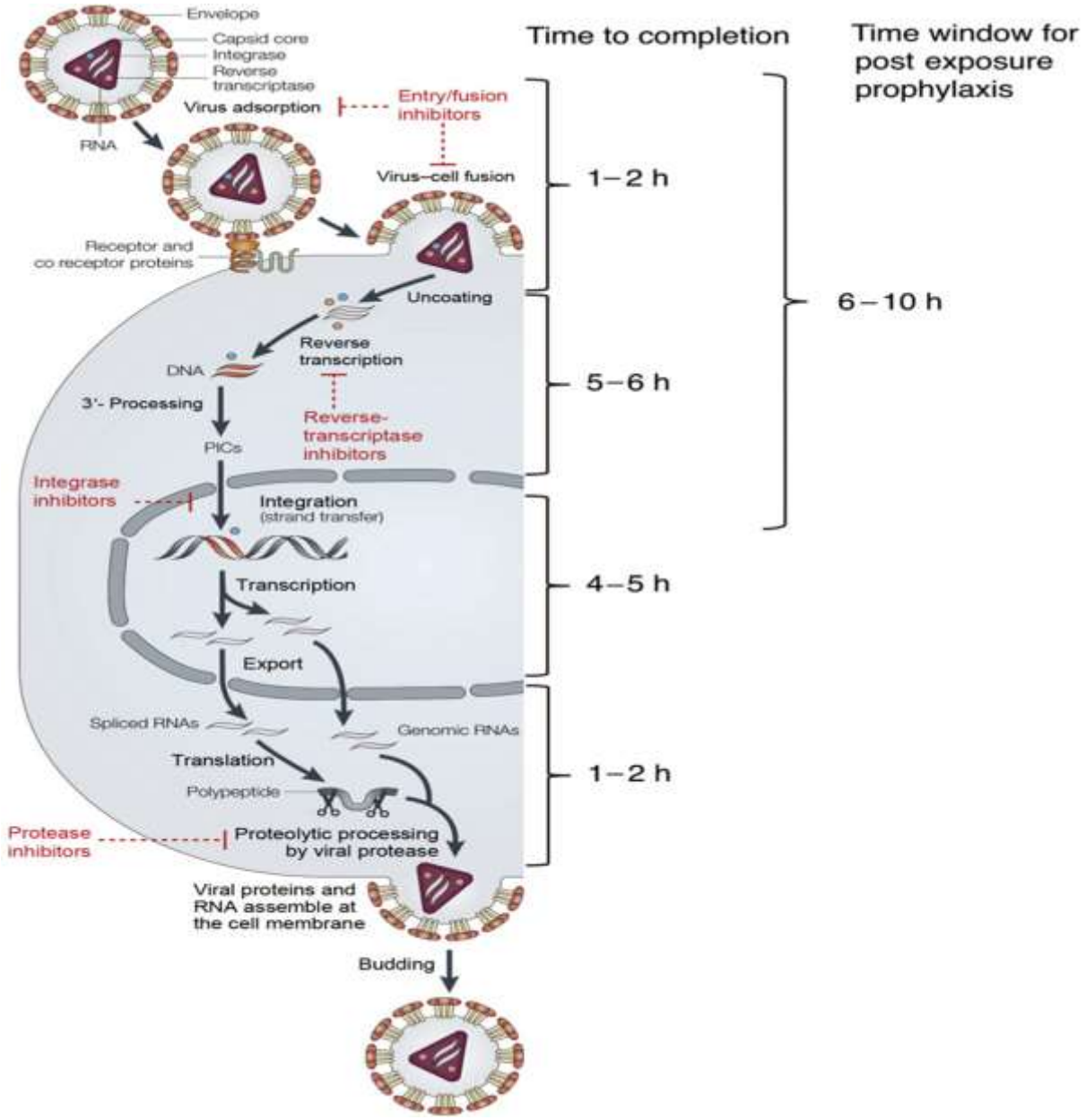

Fig. 1.2: Life cycle of HIV-I. Figure source: Métifiot M, Marchand C, Pommier Y. HIV integrase inhibitors: 20-year landmark and challenges. Adv Pharmacol. 2013; 67: 75-105.

1.5 Antiretroviral therapy

Since 1984, several strategies have been adopted for the effective treatment of HIV/AIDS. In line with this, bone marrow transplantation, lymphocyte transfusions, thymus transplantation, and therapeutic apheresis to remove virus-bearing cells have been tried without much success against HIV infection and are therefore no longer employed. Later, research focus was shifted to the development of effective and safe antiretroviral (ARV) drugs with an aim to block HIV replication and subsequent progression of AIDS. Presently, the greatest success in the clinical management of HIV/AIDS has been observed

with the use of ARV drugs such as reverse transcriptase inhibitors and protease inhibitors [20].

1.5.1 Reverse transcriptase inhibitors

Two sub-classes of reverse transcriptase inhibitors have been developed since 1990s against HIV infections. Nucleoside reverse transcriptase inhibitors (NTRIs) were first class of drugs that include zidovudine (ZDV), didanosine (ddI), zalcitabine (ddC), stavudine (d4T), lamivudine (3TC), and abacavir (ABC). Reverse transcriptase is an enzyme found in retroviruses that is necessary for their replication. The reverse transcriptase inhibitors have shown effectiveness in preventing infection of uninfected $CD4^+$ cells. Drug intolerance and drug toxicity are the major drawbacks for all NRTIs used to treat HIV infection. Another sub-class, non-nucleoside reverse transcriptase inhibitors (NNRTIs) has also been developed to treat HIV infection. The first generation drugs in this sub-class include nevirapine, delavirdine, and efavirenz. Second generation drugs with less cross-resistance include diarylpyrimidines analogues etravirine and rilpivirine [21].

1.5.2 Protease inhibitors (PIs)

Proteases are enzymes that split the peptide bonds of larger proteins into smaller proteins. HIV protease is part of the precursor protein gp 160 and facilitates the maturation process. HIV protease autocleaves itself from the precursor protein gp 160. Following autocleavage, gpl60 is cleaved into the two glycoproteins (gp 120 and gp 41) of the viral coat. Then it promotes maturation of HIV by splitting retroviral precursor polyproteins into structurally essential glycoproteins and proteins. Thus, HIV protease allows immature, non-infectious virions to become mature, infectious virions.

Protease inhibitors (PIs) prevent maturation of newly formed virions by preventing the cleavage of HIV's polyproteins. Thus, protease inhibitors are effective against the spread of new infections and are integral part of the current therapy. The PIs approved by the USFDA are: saquinavir, ritonavir, indinavir, nelfinavir, amprenavir, atazanavir and lopinavir-ritonavir co-formulation [22].

Most of the PIs exhibit poor oral bioavailability due to high first pass metabolism and rapid clearance. Hence, protease inhibitors are often most effective at high doses, but adverse reactions to these toxic agents may limit their use. All of them may cause gastrointestinal symptoms, including nausea, vomiting, and diarrhea, lipodystrophy, impaired glucose intolerance, hepatotoxicity and paresthesias [23, 24].

1.5.3 Highly Active Antiretroviral Therapy (HAART)

Development of an effective drug delivery approach for the treatment of HIV/AIDS has been a global challenge. With better understanding of pathogenesis and replication processes of HIV, single agent antiretroviral therapy has been largely substituted by combination therapy. The primary rationale for using multiple agents is to disrupt HIV replication at multiple-points in the life cycle and avoid the emergence of resistance. Each of these "cocktail" regimens often comprises two nucleoside analogues and a PI to achieve a potential synergistic effect. Sometimes a secondary PI at low dose (typically ritonavir) is included to "boost" up the bioavailability of the primary PI. Because of their higher clinical efficacy in lowering the mortality and morbidity in HIV patients, these therapeutic combinations are referred as the Highly Active Antiretroviral Therapy (HAART). It is reported that combinations of reverse transcriptase inhibitors with PI have significantly increased the life span of the HIV/AIDS patient [25, 26].

1.6 Clinical challenges in AIDS therapy

Although, the HAART is an integral part of standard treatment; antiretroviral drugs show poor clinical outcome. Being a chronic therapy, patient non-compliance to the dosage regimen is a major problem that is commonly seen with the antiretroviral therapy. Further, failure to adhere to prescribed therapies threatens the emergence of resistance [24, 27]. Though, dosing regimens for antiretroviral therapy is complex, it is essential that patients adhere to the regimen for adequate and continued suppression of viremia. An adherence rate of 95% is required for optimal suppression of viremia [28].

Factors like heavy pill burden (due to poor bioavailability and rapid clearance), drug-induced side effects, frequent drug-drug interactions, and high cost of the therapy have been considered as the possible reasons for patient non-compliance with existing conventional formulations [29]. Moreover, the majority of the currently available antiretroviral drugs is unable to reach 'viral reservoirs'/HIV localization sites at an effective concentration for the necessary time duration leading to poorer clinical outcomes [30]. The overall consequence is that, upon discontinuation of therapy and upon the development of drug resistance, HIV is able to re-seed the systemic circulation and continue to propagate the infection [31, 32].

1.7 Nanotechnology-a revolution in drug delivery systems

The combination of controlled release technology and targeted drug delivery may provide a more efficient and less harmful solution to overcome the limitations present in HAART. Recent research has focused on developing nanoparticulate based drug delivery

systems capable of enhancing bioavailability and delivering therapeutic agents selectively to the target organs like lymphatic viral reservoirs [33]. In order to facilitate the distribution and control the release, a drug may be attached or encapsulated to the nanoparticles. Thus, nanoparticle offers a unique solution to the pharmacokinetic barriers for successful therapy such as P-gp efflux, first pass metabolism and rapid clearance [34].

In the recent past, the exponential growth of nanoscience and nanotechnology has surged into notable innovations in the field of pharmaceutical sciences with tremendous impact on therapeutics and diagnostics [35-37]. The advent of nanotechnology in pharmaceutical sciences has added a new dimension to the century old concept of targeted drug delivery systems [38-40].

Nanoparticle, the closest version of the 'magic bullet' proposed by Sir Paul Ehrlich, is now feasible to design and produce in the laboratory. The nanodrug delivery systems are in the limelight due to their outstanding potential to improve availability of drug at the physiological sites/organs where the pharmacological activity is desired [41, 42]. In comparison with their conventional counterpart, materials at nanoscale level exhibit significantly different quantum mechanical properties leading to a fundamental change in their physical, chemical and biological properties. Several researchers have demonstrated the possibility of manipulating the primary characteristics of the drugs such as melting point, magnetic properties without altering its chemical composition. This ability to manipulate and/or organize matter systematically at the nanometer scale is spurring a revolution in science, engineering, technology and inevitably drug delivery and therapeutics [43].

1.8 Nanotechnology in antiretroviral therapy: opportunities and challenges

Nanoparticulate drug delivery system offers unique advantages over conventional therapy. The nanometric size of these carriers allows for efficient crossing of biological barriers and cellular barriers and can enter most of the cells. As a result, these carriers can readily and rapidly interact with biomolecules on both the cell surface and within the cell without altering the inherent property of the molecule. Thus, nanoparticles exhibit a significant change in cellular interactions leading to noninvasive access to the interior of living cells and present the opportunity for unprecedented gains on clinical and basic research frontiers [41].

One of the major challenges in conventional dosage form of antiretroviral therapy is the poor drug bioavailability, off-target distribution and associated side effects [23]. Recent advances in nanotechnology have advocated that nanoparticles are effective in altering the

pharmacokinetics of drugs such as rapid and improved absorption, selective bio-distribution, reduced degradation and elimination [44-46]. Therefore, nanoparticles which have a size small enough to allow intra-capillary or trans-capillary passage and appropriate surface coating to avoid metabolism and efflux could provide an ideal solution for antiretroviral therapy. Moreover, controlled and targeted delivery of nanoparticles to the lymphatic system can also improve the therapeutic outcome of current antiretroviral therapy [33, 47].

1.8.1 Nanoparticles and physiological barriers

Intestinal mucosa acts as a major barrier for entry of orally delivered nanoparticles [48]. The luminal surface of the GI tract is entirely protected by a thick viscoelastic, negatively charged mucus layer. Consequently, mucus layer acts as a 'trap' for many sub-micron particles and particles having positive surface charge [49]. Several researchers have suggested that particles less than 200 nm can only diffuse through the mucus barrier [50]. On the contrary, few researchers have also demonstrated the nanoparticle uptake in to the body after oral administration with sizes larger than 200 nm [48].

The surface charge on the nanoparticles plays an important role in determining its fate after oral administration. In the past few years, extensive research has been done in the design and development of mucoadhesive nanoparticles using positively charged polymers including chitosan and its derivatives. Forces like hydrogen bonding, van der Waals force interactions, polymer chain interpenetration and electrostatic/ionic interactions between negatively charged mucin and positively charged polymer can cause mucoadhesion [51]. Smaller particles carrying strong positive charge readily bind to the mucosa and exhibit longer residence time in the GI tract. While, the negatively charged particles move 20-30 times faster towards the epithelium and display lesser retention time. In conclusion, for an effective oral delivery, a fine balance between mucoadhesion and mucus-penetration should be maintained [52].

1.8.2 Endocytic uptake mechanisms for nanoparticles from GI Tract

Different mechanisms exist for uptake of water-soluble and water-insoluble compounds through GI tract. The water-soluble small molecules passively diffuse through the intestinal barriers via water filled aqueous channels by a process known as paracellular diffusion. In humans, these aqueous channels are reported to be as small as 4 to 8 Å. These pores act as barriers for water insoluble molecules, macromolecules and other particulate matter (e.g. nanoparticles) [53].

The uptake of nanoparticles in GI tract can follow two routes: paracellular route and transcellular route. However, the tight junctions between the epithelial cells largely restrict

the entry of particles through the paracellular route, making the role of paracellular transport for nanoparticles trivial [54]. Transcellular transport is a major transport mechanism for uptake of orally administered nanoparticles. The steps involved in transcellular transport of nanoparticles via oral route are: (i) uptake of nanoparticle at the apical side of the cell (ii) transport through the epithelial cell and (iii) release of nanoparticle at the basolateral side of the epithelial cell [54].

Several mechanisms have been proposed for transcellular transport of nanoparticles across the intestinal barrier. These include, but not limited to, transcytosis, receptor-mediated uptake by enterocytes and microfold cells (M-cells) and, to a small extent, paracellular uptake. [55]. The M-cells, found in follicle associated epithelium of the Payer's patches, have a unique ability to deliver foreign materials by transepithelial transport from the lumen to organized mucosa-associated lymphoid tissues (O-MALT). The apical membrane of M-cells is designed to facilitate adherence and uptake of antigens and to efficiently deliver to the intra-epithelial pocket and underlying lymphoidal tissues [56]. Targeting M-cells could be a feasible option for orally delivered nanoparticles and vaccines. However, this type of uptake is limited because M-cells constitute of less than 1% of the total intestinal epithelial cell population. Further, after transport through M-cells, the entry of nanocarriers to systemic circulation is limited because the cargo often gets trapped in the local lymph nodes. Therefore, for drugs that need to reach the blood circulation for systemic action, this route is less suitable; it is more prudent to target these types of drugs to the absorptive epithelial cells (or the enterocytes) of the intestine [57, 58].

The uptake of nanoparticles through enterocytes can be described by several energy dependent processes. These include macropinocytosis, clathrin-mediated endocytosis, caveolae-mediated endocytosis and clathrin-and caveolae-independent endocytosis [59, 60]. Different endocytic pathways for nanoparticle uptake through enterocytes are illustrated in Fig. 1.3 and Fig 1.4.

The clathrin mediated endocytosis (CME) is a "classical route" of access for particulate materials into the cell. It is a common route for uptake of physiologically important molecules (cholesterol and iron) and is present in all mammalian cells. The CME can occur as specific ligand-receptor interaction or via non-specific endocytosis [61].

The specific CME involves concentration of high-affinity transmembrane receptors and their bound ligands into "coated pits" on the plasma membrane [62].The assembly of clathrin molecules on the coated pit induces an invagination of the membrane and forms a clathrin-coated vesicle (100 to 120 nm). The cargo containing invagination is then pinched-

off from the cell membrane to form vesicles that are further degraded by acidified early and late endosomes (Fig. 1.4) [61, 63].

On the other hand, caveolae-mediated endocytosis is a highly regulated process involving complex signaling pathways. It is associated with cholesterol and sphingolipid-rich microdomains of the cell membrane. Caveolae are flask-shaped invaginations on the plasma membrane that can 'engulf' cargo molecules or carriers binding to their surface. These invaginations are static structures with a size of 50 to 100 nm on plasma membrane [64, 65].

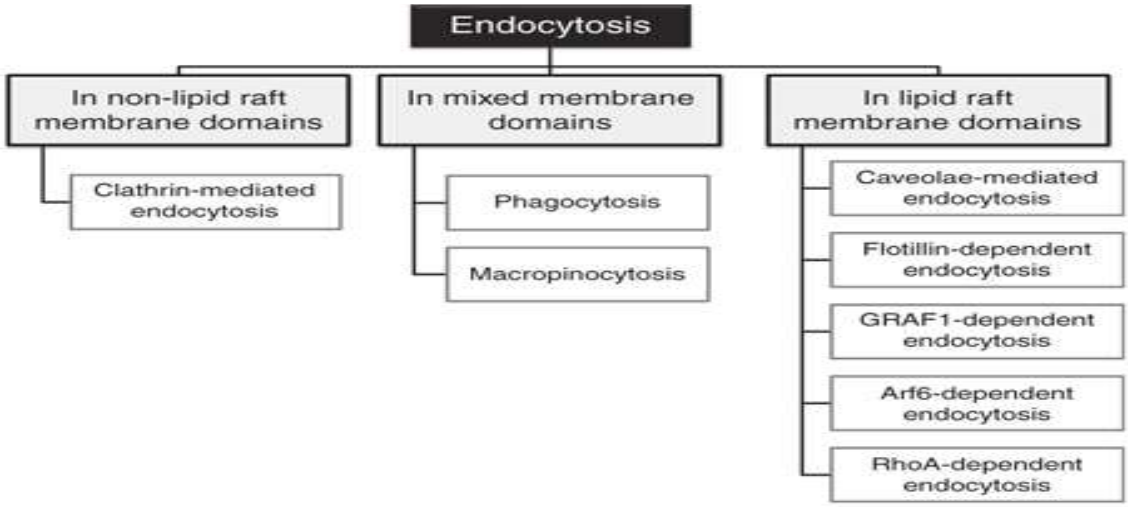

Fig. 1.3: Classification of endocytic pathways. Fig. source: El-Sayed A, Harashima H. Endocytosis of gene delivery vectors: from clathrin-dependent to lipid raft-mediated endocytosis. Mol Ther. 2013; 21: 1118-1130.

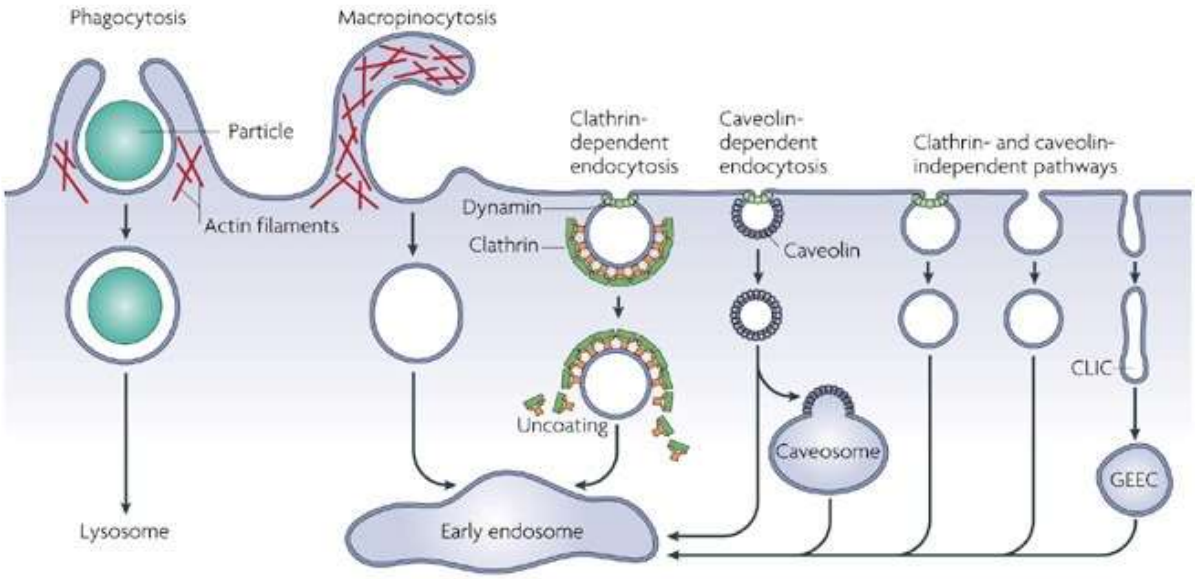

Fig. 1.4: An overview of endocytic uptake pathways and the fate of cargo after uptake. Fig. source: Parton R G, Simons K. The multiple faces of caveolae. Nat Rev Mol Cell Biol. 2007; 8: 185-194.
CLIC - clathrin- and dynamin-independent carriers; GEEC - glycosyl phosphatidylinositol-anchored protein-enriched early endosomal compartments.

Few researchers have also reported that the cellular entry of particulate matter can occur via caveolae- and clathrin-independent pathways in the cells devoid of both CME and caveolin-1 [61]. The caveolae- and clathrin-independent pathways have been classified as: Arf6-dependent, flotillin-dependent, Cdc42-dependent and RhoA-dependent pathways [66]. All these pathways generally require some specific lipid compositions and are mostly dependent on cholesterol [67]. However, not many nanocarriers have been reported to utilize different sub-types of the clathrin- and caveolae-independent endocytosis [68].

The macropinocytosis is clathrin-, caveolae- and dynamin-independent non-specific transport mechanism driven by Rho-family GTPases [69]. The macropinocytosis is initiated by transient activation of receptor tyrosine kinases by growth factors. Here, a large (0.5 to 2 μm) heterogeneous, dynamic, vesicular structures at the cell surface called, macropinosome is formed; particles smaller than 2 μm can be internalized into enterocytes by this mechanism [70].

Apart from pinocytosis, nanoparticles can also be taken up by phagocytosis mechanism. Phagocytosis is an endocytic mechanism that occur primarily in phagocytic cells like macrophages, monocytes, neutrophils and dendritic cells [71]. Process of phagocytosis involves opsonization of nanoparticles (by activation of complementary system) followed by ingestion of the particle by the cells. Opsonization process aids in identification of foreign material present in the blood to antigen presenting cells by adsorption of protein, such as immunoglubulins (IgG and IgM), complement components (C3, C4, C5) and blood serum proteins (including laminin, fibronectin). The size of the phagosome formed can vary greatly depending on the size of the cargo. It can range from few hundred nanometers to dozens of microns [72].

1.8.3 Oral uptake mechanisms for lipid-based nanoparticles

Following oral administration, lipid based nanocarriers can access the blood/lymphatic circulation system by various mechanisms that includes M-cells and GALT, stimulating chylomicron production, transport via triglyceride-rich lipoproteins and digestion of lipid by lipases and formation of vesicles/micelles [73].

Following the action of lipases, the products of lipid metabolism - monoglyceride and fatty acid are taken up into the enterocytes (Fig 1.5). Once inside, these products of lipid metabolism are re-joined to form triglycerides in the smooth endoplasmic reticulum. Subsequently, they get assembled into triglyceride-rich lipoproteins (TG-LPs) [74]. These TG-LPs are then exocytosed into the lamina propria where the tight-junctions and presence of an underlying basement membrane prevent their easy access into blood capillaries [75].

Therefore, the TG-LPs then selectively access the lymphatic systems where the adjacent cells are arranged in an overlapping manner resulting in 'gaps' between the cells. Colloidal species like TG-LPs can sneak through these 'gaps' thus gaining entry into the lymphatic system and bypassing the portal hepatic circulation [74, 75].

Lipid based nanocarrier system can affect drug disposition in three ways: (a) by enhancing solubility of hydrophobic drugs in the intestinal milieu through alterations to the composition and character of the colloidal environment; (b) by preventing enterocyte-based drug efflux and metabolic processes and (c) altering the pathway (portal vein versus the intestinal lymphatic system) of drug transport to the systemic circulation [76].

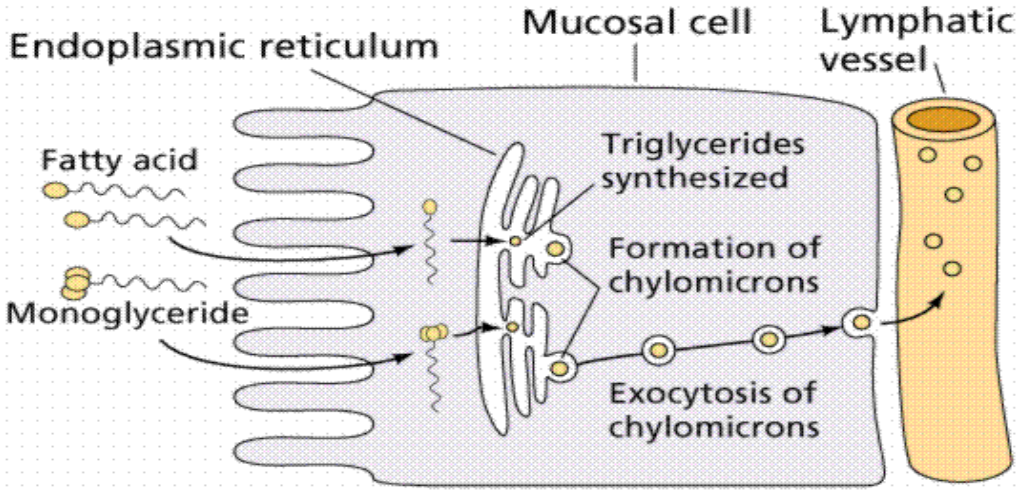

Fig. 1.5: Schematic representation of lipid transport by the mesenteric lymph or portal blood upon oral delivery. Fig. source: http://www2.estrellamountain.edu/faculty/farabee/BIOBK/biobookdigest.html. Accessed July 28, 2014.

1.8.4 Fate of nanocarriers after oral delivery

The *in vivo* fate of a drug after oral administration is determined by combination of several processes such as absorption, distribution, metabolism and excretion. Irrespective of the mechanism involved, these pharmacokinetic processes are in many ways dependent on the physico-chemical properties of the drug. In past few years, extensive research work has been carried out for the development of delivery systems which can modulate the *in vivo* fate of drugs for the improvement of the final therapeutic outcome [77-79]. Although, nanoparticles are reported to act mainly on the drug distribution process in the body, they also have potential to modify the absorption, metabolism and excretion processes of the loaded drug. The potential advantage of nanoparticles over naked drug are: enhancement of oral bioavailability, controlled release of drug from the carrier matrix, site specific drug delivery and reduced gastric complications (achieved by overcoming one or more physical

problems such as low solubility, poor permeability, gut-wall metabolism, first-pass effect and physical and chemical instability) [80, 81].

As discussed in the previous sections of this chapter, several mechanisms contribute to uptake of orally administered nanoparticles. The lymphatic absorption of nanoparticles through GALT and chylomicron transport bypasses the portal blood circulation to the liver and thus the entrapped drug is protected from pre-systemic metabolism [57, 58, 76].

Moreover, after oral administration, nanoparticles provide extended physical protection to the entrapped drug from hostile gastrointestinal tract environment including gut metabolizing enzymes and harsh pH conditions. However, composition of nanoparticles plays a significant role in its stability (in the GI tract). Nanoparticles comprising insoluble polymers or high-carbon chain length lipids are more useful, because, they are neither immediately degraded nor do they release the entrapped drug rapidly in GI tract [82].

Upon reaching systemic circulation, nanoparticles come in contact with various blood components such as plasma proteins and blood cells. Like other xenobiotic entering into vascular compartment, most nanoparticles evoke body immune responses which in turn activate a cascade of immune activity with a sole purpose of exterminating the nanoparticles from the body. Several researchers have reported that, irrespective of their chemical composition, nanoparticles are cleared immediately after systemic administration. Short half-life is consistently observed with nanoparticles manufactured using polymers like: poly styrene, poly(lactic acid), albumin, poly(lactic acid-co-glycolic acid), poly(alkyl cyanocrylate) and poly(aryl starch) [83-85]. Recognition of nanoparticulate DDS by macrophage cells of reticulo-endothelial system (RES) is the primary mechanism for detection and elimination. It is now known that particle phagocytosis principally depends on the rate of particle opsonisation [86-88]. Rapid uptake of nanoparticles by the RES cells poses a significant challenge in drug targeting. Saba et al. have reported that the Kupffer cells of the liver contribute to 85-95% of the body's total elimination capacity of nanoparticles. This scavenging mechanism also exists in the spleen and bone marrow and is also found to play a pivotal role in the elimination of nanoparticles [86-88].

It has been demonstrated that the particle size and particle charge have a significant impact on bio-distribution and systemic elimination of nanoparticles [89]. It is reported that larger particles have a greater tendency to aggregate and accumulate in the liver and are cleared rapidly than smaller nanoparticles. Nanoparticles larger than 200 nm are selectively screened by monocytes and macrophages of the liver and spleen [89]. Hence, their distributions to these organs are commonly observed following oral administration.

The particle charge also has a significant impact on the pharmacokinetics of nanoparticles. Levchenko et al. have reported that strong negatively charged nanoparticles are taken up to a greater extent by macrophages in the liver that contributes to faster elimination from the body [90]. On the other hand, positively charged particles tend to aggregate in presence of serum proteins. Strong positively charged nanoparticles (ζ-potential of ~ +40 mV) also exhibit rapid clearance from plasma and tend to accumulate in liver and lungs [91].

Therefore, it is critical to strike a balance between particle size and particle charge when designing long-acting nanoparticulate DDS for systemic drug delivery.

1.9 Preparation of nanoparticles

Although several methods are reported in the literature for the preparation of nanoparticles, principally these methods are classified into two broad categories as a) top-down approach and b) bottom-up approach.

a) Top-down approach

Most of the top down approaches use conventional size reduction method to produce the desired size of nanoparticles including comminuting, milling or grinding. The processing of these macroscopic materials is externally well-controlled. However, application of this technique in nanoparticulate drug delivery system is limited as the energy requirement is significantly high. Moreover, this technique is not suitable for heat and pressure sensitive materials such as proteins, peptides, and several other small molecule drugs [92].

b) Bottom-up approach

In bottom up technique, the raw material is taken in a pre-miniaturized form (molecular/atomic level) and later either allowed to self-assemble into nanomaterial or assembly is facilitated by the addition of other catalysts. During the assembly process, other molecules of interest can be incorporated into the nanomaterial to finally get a composite nanoproduct. Although, this technique requires a small amount of energy, controlling the process of nanoparticle formation is a challenging task for the formulation scientists.

In the recent past, bottom up approaches have been extensively investigated and have become an integral part in manufacturing nanoparticulate DDS. This technique offers the advantage of selecting suitable chemical reagents and solvents for sensitive drugs such as peptides, vaccines and genes [93]. Since these fine nanoparticles demonstrate a tendency to aggregate upon storage, the stabilization of prepared nanoparticles is a challenging task.

Bottom-up approach can be further classified as (i) two steps procedures and (ii) single step procedures. The two steps procedure involves (a) preparation of the emulsified system and (b) formation of polymer nanoparticles from an emulsion. The preparation steps involved in both these methods are summarized in Fig. 1.6.

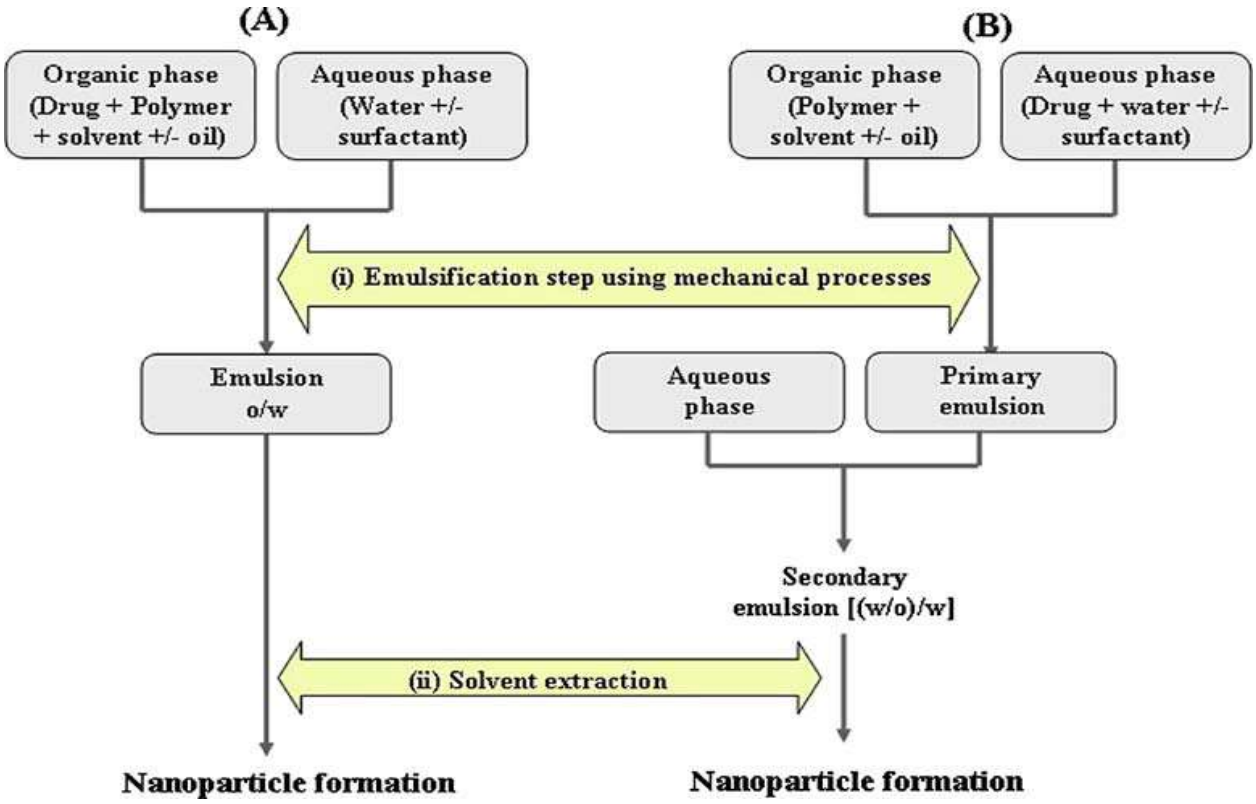

Fig. 1.6: Schematic representations of single (A) and double (B) emulsion techniques for nanoparticle preparation. Fig. source: Vauthier C, Bouchemal K.Methods for the preparation and manufacture of polymeric nanoparticles. Pharm Res. 2009; 26: 1025-58.

1.9. 1 Two steps procedure: preparation of the emulsified system

All these methods require two immiscible phases and a surface active agent to produce nanoparticles. However, the methods used to achieve the dispersion of one phase in the other to obtain nanoparticles is diversified. Most of these methods are based on mechanical processes and are related to the high-energy emulsification techniques [94]. They allow for the preparation of emulsions uniform sized droplets that can easily be scaled up wherever necessary [95]. A good example here is the colloidal mill. In some methods, extrusion process is used to obtain fine emulsion. In these types of machines, the dispersed phase is forced to penetrate a micro-filtration device that results in pre-determined droplet size of dispersed phase. This dispersed phase is later introduced into the continuous phase to complete the emulsion formation [96].

1.9.2 Two steps procedure: formation of polymer nanoparticles from an emulsion

1.9.2.1 Inducing polymer precipitation by solvent removal

There are many ways to provoke polymer precipitation in the emulsion droplets by removing the solvent. Solvent can be extracted from the organic phase by different methods such as solvent evaporation, fast diffusion after dilution or salting out. These methods lead to production of "nanospheres" when formed from oil-in-water emulsion [97]. Liquid core containing "nanocapsules" can be obtained by adding oil in the polymer solution composing the emulsion droplets. Water containing nanocapsules can be produced by multiple emulsion method (e.g w/o/w emulsion). In general, nanocapsules formulated by multiple emulsion method are much larger in size than the oil-containing nanocapsules obtained by simple emulsions [98].

A) Obtaining nanoparticles by emulsification–solvent evaporation

This is one of the earliest methods for formation of nanoparticles. In this method, emulsions are formulated with polymer solutions prepared in volatile solvents. Dichloromethane and chloroform were widely used in the past but are now replaced by ethyl acetate which displays a better toxicological profile. Conversion of the emulsion into a nanoparticle suspension occurs by the evaporation of the solvent which is allowed to diffuse through the continuous phase of the emulsion. This is a slow process and usually carried out under vacuum. The process of solvent evaporation is biphasic–initial rapid evaporation phase where ~90% of solvent is evaporated, followed by a slower evaporation phase for the remaining 10% solvent [99].

In the first phase, the size of the particle rapidly decreases and reaches a critical lower value. However, in the second evaporation phase, the particle size again increases due to coalescence. The emulsification–solvent evaporation method has been widely applied to prepare nanoparticles composed of PLA, PLGA and PCL using pluronic F68 as stabilizing agent [100, 101].

B) Obtaining nanoparticles by emulsification–solvent diffusion

The emulsification–diffusion solvent method is also called emulsification–solvent displacement method. It has been successfully employed to prepare biodegradable nanoparticles in an efficient and reproducible manner [102]. For this method to be successful, the solvent used to prepare the emulsion must be partly soluble in water. The emulsion is prepared by saturating each phase with the other. Mutual saturation of both phases is obtained by mixing the two liquids in equal volume and waiting for phase separation to collect the saturated phases. Once the oil-in-water emulsion is obtained, it is

diluted with excess of pure water. This aids in diffusion of solvent into the bulk of the aqueous phase leading to precipitation of the polymer. Suitable solvents include benzyl alcohol, propylene carbonate, ethyl acetate, isopropyl aceatate, methyl acetate, methyl ethyl ketone, benzyl alcohol, benzyl lactate and isovaleric acid. Surfactants like pluronic F68, PVA and sodium taurodeoxycholate are generally added as stabilizers to the aqueous phase. Polymers suitable for this method are: PLA, PLGA, PCL and Eudragit® E [103-106].

In general, diameter of the particles produced by this method is around 150 nm [107]. During initial stages, the particle size is reduced because of solvent extraction. Unlike the solvent evaporation process, the solvent extraction process takes milli seconds. Thus, drop in the particle size is abrupt. With increase in miscibility of the solvent with water, the mean diameter of the particles is significantly lowered. Size can also be reduced by increasing the rate of stirring and increasing the concentration of stabilizing agent. Increase in polymer concentration leads to increase in particle size [108, 109].

C) Obtaining nanoparticles by emulsification–reverse salting out

The main difference between this and the previous method is in the composition of the emulsion. The emulsion is formulated with a polymer solvent which is normally totally miscible with water, e.g. acetone. This method consists in dissolving high concentration of salt or sucrose (several mol/l) chosen for their strong salting out effect in the aqueous phase. Examples of suitable electrolytes are magnesium chloride, calcium chloride, and magnesium acetate. These hydrophilic molecules retain water for their own solubility. Thus, they modify the miscibility of water with other solvents such as acetone. The polymer dissolved in acetone is precipitated out resulting in formation of nanoparticles [110, 111].

1.9.2.2 Obtaining nanoparticles by gelation of the emulsion droplets

In this method, nanoparticles are obtained from the emulsion by gelifying the dissolved polymer. This method is limited to polymers that show gelifying behavior. Gelification of polymer can be achieved by means like change in temperature, change in pH. When these methods are used for water soluble polymers, hydrogel nanoparticles are obtained [112].

1.9.2.3 Inducing nanoparticle formation by *in situ* polymerization

To produce nanoparticles by *in situ* polymerization, first a monomer is added in the emulsion instead of a polymer solution and the polymer is formed *in situ* by polymerization to give nanoparticles. Poly(alkylcyanoacrylate) is the most commonly used polymer in this method [113].

1.9.3 One step procedure: obtaining nanospheres by methods based on nanoprecipitation of a polymer

The nanoprecipitation method, also called solvent displacement was developed by Fessi et al [114]. It is one of the easiest methods to prepare nanospheres. The basic principle of this technique is close to the one described earlier for the preparation of emulsions by spontaneous emulsification. For this method, the system should contain following three components: polymer, the polymer solvent and the non-solvent of the polymer. Solvents that are miscible with water but are also easily removed (e.g alcohol and acetone) are used to prepare the nanoparticles. The nanoparticles form instantaneously during the rapid diffusion of the polymer solution in the non-solvent. The resulting colloidal suspension contains polymer particles with well-defined size (typically below 200 nm in diameter) and is characterized by a narrow distribution [115, 116].

1.9.4 One step procedure: methods based on ionic gelation

These types of nanoparticles are synthesized completely in aqueous media. Ionic nanogels are obtained when aqueous solutions of charged polysaccharides are treated with oppositely charged ions. This process has to be performed at low dilution levels using concentration of polysaccharide below its gelling point. Clusters formed in the pre-gel phase are stabilized by forming complex with opposite charged polyelectrolytes e.g. sodium alginate-calcium salts. Chitosan is another gelling polysaccharide which has been used to produce nanoparticles through a gelling process. Ionic gels can form by adding small polyphosphates ions like tri-polyphosphates. Poly(ethyleneglycol) and Poly(propyleneglycol) and pluronic can be used as co-polymer to icrease stability. Change of pH from acid to basic pH can cause shrinkage of nanoparticles because the intra-molecular electric repulsions inside the particle mesh are reduced. Ionic strength variations also result in structural changes in nanoparticles. In presence of KCl, the chitosan-TPP nanoparticle swells which may result in disintegration of the nanoparticles [117, 118].

1.10 Lipid based nanoparticles – Solid lipid nanoparticles

Solid lipid nanoparticles (SLNs) have been developed as an alternative to emulsions, liposomes, polymeric micro and nanoparticles. SLNs consist of a solid lipid matrix that is in solid state at both room and body temperatures. High carbon chain fatty acids, fatty acid esters and waxes are used as solid lipids in the preparation of SLNs. Typically, the SLNs particle size ranges from 80 to 1000 nm [119, 120]. The SLNs can alter the inherent properties of the drug incorporated in them. They act by enhancing the dissolution rate (thus, improving oral bioavailability of many drugs), improving tissue

distribution, targeting organs and protecting the drug from *in vivo* processes like metabolism in the gut/liver [121, 122].Numerous factors like solubility of the drug in the lipid matrix, physicochemical properties of the drug, nature of the lipid and surfactant used and manufacturing method play an important role in determining the amount of drug loaded into the SLNs [123]. A systemic classification of lipid-based formulation for oral delivery, as proposed by Pouton [123], is presented in Fig. 1.7.

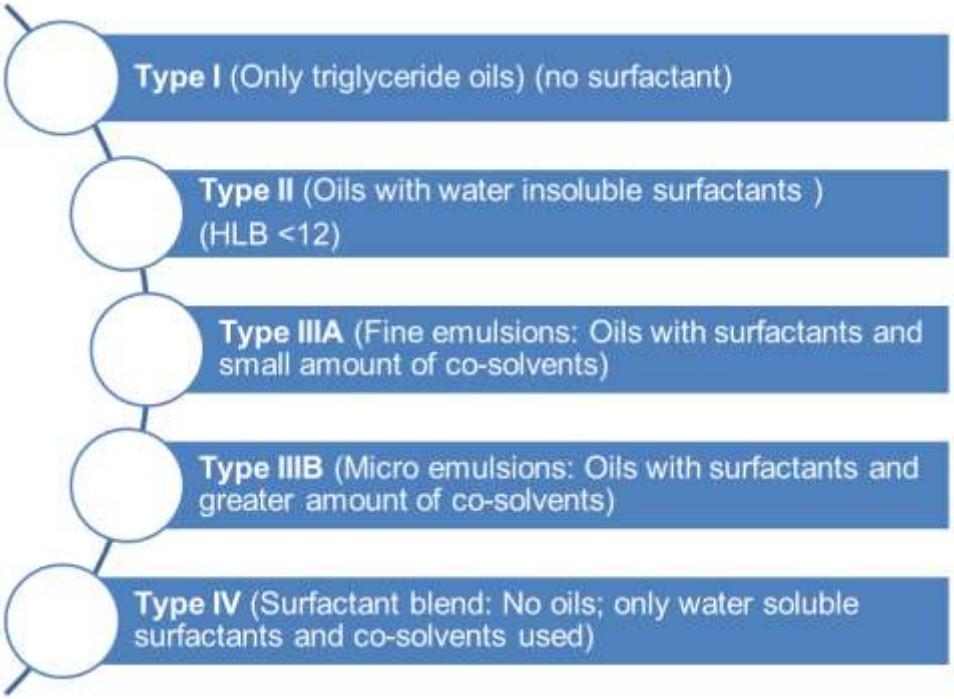

Fig. 1.7: Pouton's classification of lipid-based formulations for oral delivery. Fig. source: Pouton CW. Formulation of poorly water-soluble drugs for oral administration: Physicochemical and physiological issues and the lipid formulation classification system. Eur J Pharm Sci. 2006; 29: 278-287.

1.10.1 Production methods for lipid nanoparticles

a) High pressure homogenization

The high pressure homogenization method can be further divided as i) hot homogenization and ii) cold homogenization method.

i) Hot homogenization method

The hot homogenization method involves homogenization of drug containing molten lipid, dispersed into a hot aqueous surfactant solution using a high-speed stirrer at an elevated temperature (above the melting range of the lipid). This results in the formation of a coarse pre-emulsion which is further subjected to high pressure homogenization to get nanosized dispersion of lipid droplets. In a typical formulation, one to three homogenization cycles are used. The nanoemulsion is then cooled to room temperature that causes lipids to

crystallize and finally results in the formation of SLNs. This method is primarily useful to encapsulate lipophilic and thermostable drugs [124-126].

To improve loading efficiency, few modifications have been reported to hot homogenization technique such as preparation of lipid nanoparticles via o/w micro-emulsion technique. In this, lipid micro emulsion is rapidly quenched using cold aqueous medium (below 5 ºC) under mechanical stirring. This method is more suited for fatty acids and lipids (e.g. stearic acid, glyceryl monostearate and glyceryl behenate) with low melting point (50 to 70 ºC). The major disadvantage of this method is the removal of excess water and surfactant/co-surfactant from the final formulation [127].

Cold homogenization technique is yet another modification of hot homogenization technique in order to encapsulate temperature sensitive drugs and to improve loading efficiency of the formulation [124].

b) Preparation by solvent emulsification-evaporation/diffusion

In this method, the lipid is dissolved in an organic solvent and is then emulsified with an aqueous phase containing surfactant/co-surfactant mixture. Stirring ensures formation of an o/w type emulsion while an ambient temperature is maintained. The solvent is removed under reduced pressure to precipitate the lipids and yield nanoparticles. Depending on the lipid type and surfactant, the particle size of nanoparticles formed by this method varies from 30 to 100 nm. The most important advantage of this method is the avoidance of high temperatures to melt the lipids [128, 129].

Several modifications of the method have led to improved product performance such as double emulsion method (w/o/w) [130, 131] and use of high pressure homogenization and preparation of solvent free nanoparticles [132]. The double emulsion method has potential to encapsulate, wide variety of molecules such as hydrophilic and macromolecules.

1.11 Characterization of nanoparticles

A unique therapeutic benefit of nanoparticulate drug delivery principally originates from their changed physico-chemical properties. The evaluation of properties aids in enhancing the theoretic performance of nanoparticulate DDS. Like all other pharmaceutical formulations, *in vivo* performance of nanoparticulate formulations can be correlated with the critical product attributes such as particle size, size distribution, surface morphology and properties, drug loading efficiency, in vitro drug release behavior. Although, FDA has not released specific guidelines for characterization of nanoparticulate DDS, most of the methods currently employed are of similar nature as that of their sub-micronic colloidal associates such as micelles, liposomes, emulsion. Several unique properties of

nanoparticulate DDS offer distinct advantages as compared to conventional DDS, which are extensively investigated during their characterization.

1.11.1 Particle size and polydispersity index

Most of the advantages offered by nanoparticles are based on the assumption that they exist in a sub-micronic range. As discussed earlier, the particle size offers a unique advantage to this drug delivery system. Hence, particle size and polydispersity index (PDI) are the most important parameters for the characterization of nanoparticles. However, owing to the small size of nanoparticles and their sensitivity to the immediate environment, there is a significant analytical challenge in determination of accurate particle size. Moreover, size of nanoparticles may exist in a homogeneous (mono-dispersed) or heterogeneous (poly-dispersed) form imposing additional challenges [133, 134].

PDI is a measure of the width of particle size distribution with the sample. A small value of PDI is highly desirable that indicates narrow size distribution of nanoparticles. A colloidal system is considered to have a narrow size distribution if the values of PDI lie in the range of 0.1 to 0.2 (monodisperse). PDI values of 0.2 to 0.5 are indicative of a polydisperse colloidal system [135].

Most commonly used methods for the determination of particle size and size distribution are based on light scattering (static or dynamic) and imaging (electron microscopy) techniques [136]. The former class represents the advanced spectroscopic techniques such as photon correlation spectroscopy (PCS), quasi-elastic light scattering (QELS); while, the latter methods represent advanced imaging techniques such as scanning electron microscopy (SEM), transmission electron microscopy (TEM), scanning tunneling electron microscopy (STEM), atomic force microscopy (AFM).

a) Dynamic light scattering

Dynamic light scattering (DLS) based instruments, records the variation in the intensity of scattered light, resulting from the interference of light scattered by individual particles due to Brownian motion, on time scale (μS). The intensity of fluctuation is then transmitted to an autocorrelation function, $G(\tau)$, that decays exponentially. The microprocessor in the PCS calculates the diffusion coefficient (D) of the particles in the given dispersion media (at given temperature and viscosity). The value of D is then related to particle size by Stokes-Einstein equation. Stokes-Einstein equation to determine particle size:

$$D = \frac{kT}{3\pi\eta d}$$

Where,

$D =$ *Diffusion coefficient of the particles*

$k =$ *Boltzmann's constant* ($1.3806488 \times 10^{-23}\ m^2\ kg\ s^{-2}\ K^{-1}$)

$T =$ *Absolute temperature* ($\mathrm{K} = {}^{\circ}\mathrm{C} + 273.15$)

$\eta =$ *Viscosity of the dispersion medium*

$d =$ *Diameter of a spherical particles*

PCS represents the most frequently used technique for accurate estimation of the particle size and size distribution based on DLS [137].

b) Electron microscopy

SEM offers advantages of morphological examination with direct visualization of particulate surface. In this, a high-energy electron beam is targeted at the sample and a three dimensional image of the sample is obtained on the screen. The sample is observed at various zoom levels and finally, the image is captured using the software attached to the SEM instrument. TEM operates at relatively smaller particle size and it provides structural information using electron diffraction [138, 139]. However, in contrast to SEM, the TEM generates two dimensional images of the sample. TEM permits differentiation among nanocapsules, nanospheres, liposomes and emulsions. Techniques based on electron microscopy offer several advantages in morphological and sizing analysis; however, they provide limited information about the size distribution and true population average. Moreover, these techniques are time consuming, costly and frequently need complementary information about sizing distribution.

c) Atomic force microscopy

AFM offers ultra-high resolution in particle size measurement and is based on a physical scanning of samples at a sub-micron level using a probe tip of atomic scale. The instrument provides a topographical map of the sample based on forces between the tip and the sample surface. Samples are usually scanned in contact or non-contact depending on their properties. AFM provides the most accurate description of particle size and size distribution and requires no mathematical treatment [140, 141].

1.11.2 Surface properties

Surface properties of nanoparticulate DDSs are critical in determining their drug delivery potential, as these properties govern the overall *in vivo* performance of the DDS. These properties also modulate the *in vitro* performance, such as stability, stability drug entrapment and drug release kinetics. The specific surface area, surface charge and surface hydrophobicity are important properties of nanoparticles as these govern the physico-chemical and electrostatic interactions with biological components and overall distribution of loaded nanoparticles.

a) Surface charge

Surface charge of the colloidal drug carriers can be determined by electrophoretic mobility of nanoparticles. The surface charge is represented as the zeta potential, which can be derived from the electrophoretic mobility by using Helmholtz-Smoluchowski equation. The value of zeta potential is usually considered important to the stability of a colloidal dispersion. It is used as a predictive tool for stability of nanoparticles upon storage. Additionally, this information may be useful in predicting the effectiveness of the barrier function against opsonization under *in vivo* conditions after surface modification or treatment.

Zeta potential with values of less than -30 mV or more than +30 mV is considered suitable for the stability of colloidal dispersions [142, 143]. This is true only in case of colloidal dispersions purely stabilized by electrostatic forces.

b) Surface hydrophobicity

Surface hydrophobicity can be determined by several techniques such as hydrophobic interaction chromatography, biphasic partitioning, adsorption of probes, contact angle measurements. Frequently, nanoparticles are surface engineered to decrease surface hydrophobicity as it leads to opsonization. In the recent past, several sophisticated techniques have been reported in literature for surface analysis of nanoparticles. X-ray photon correlation spectroscopy permits the identification of specific chemical groups on the surface of nanoparticles [144].

c) Specific surface area and other properties

Specific surface area of dried nanoparticles can be measured by sorptometric techniques. Together with density measurements, these data provide critical information about the porosity, density distribution within the particle, and structural properties (smoothness, imperfection).The latter studies can be carried out by gas Pycnometer as described by Kreuter [145].

1.11.3 Bulk properties

Most of the bulk properties indicate the ability of nanoparticles to efficiently deliver the drug to the site of action. However, the ultimate *in vivo* performance of the nanoparticulate systems govern the gross product performance, including drug loading and entrapment efficiency, drug release kinetics, drug stability and compatibility. *In vitro* evaluation of these properties provides a better understanding of various pharmaceutical considerations, which may aid in the development and optimization of the product.

a) Drug loading and entrapment efficiency

Therapeutic success of nanoparticulate DDS is attributed to its ability to release the drug within the vicinity of the site of action at the required rate over the extended duration. A drug associated with nanoparticles offer unique advantages, which are not available with free drug. Thus, the extent of incorporation of the drug to nanoparticles (drug loading capacity) is the most critical factor in determining *in vivo* efficacy. The loading capacity of a formulation is expressed as the amount of drug loaded (or encapsulated) in the nanoparticles to the total amount of matrix forming material used. The loading capacity depends on factors like relative solubility of drug and matrix forming material in a given solvent (for polymeric nanoparticles), solubility of the drug in the matrix forming material (for SLNs and NLCs) and polymorphic nature of the matrix forming material and method used for the manufacture of nanoparticles [104]. The loading capacity (LC%) is given by the following formula:

$$\mathrm{LC}(\%) = \frac{(\text{Total amount of drug}) - (\text{Amount of free drug})}{\text{Total amount of nanoparticles}} \text{ X } 100$$

The ability of manufacturing process and components to incorporate or associate the drug efficiently in nanoparticles is represented as drug entrapment efficiency (EE), which can be conveniently determined by analyzing the free drug and entrapped drug or total drug. The EE is calculated using the following formula:

$$\mathrm{EE}(\%) = \frac{(\text{Total amount of drug}) - (\text{Amount of free drug})}{\text{Total amount of drug}} \text{X } 100$$

Within the formulation the drug can either be entrapped within the reservoir (nanocapsules) or uniformly dispersed within the matrix (nanospheres) and or it may be associated with the surface of nanoparticles. Loosely associated and adsorbed drugs can be

separated by mild washing treatment with suitable solvent media. The overall efficiency of the manufacturing process is represented as a recovery of the product obtained.

b) *In vitro* drug release kinetics

In a conventional DDS, the drug is released from the formulation at the site of administration or absorption and released drug migrate across various biological barriers reaching the desired site of action. The mathematical model for the release studies are based on the premise that the rate and extent of drug available at the site of action is a function of free drug released at the site of absorption or administration.

Unlike the conventional DDS, the nanoparticulate systems have ability to cross various biological barriers as they permeate inside the systemic circulation and other tissues with differential affinity. Therefore, mathematical model used in modeling of release data from conventional DDS may not be suitable for nanoparticulate DDS.

In line with this, Polakovic et al. have made significant contributions in explaining the release behavior of drugs from the nanoparticulate DDS [146]. Many previous attempts to model diffusion-controlled drug delivery from nanoparticulate DDS are largely based on the empirically determined diffusion coefficient. In this, the release kinetics of the drug can be explained by Fickian kinetics, if the drug is in dissolved state or by the Higuchi's square-root kinetics, if the drug is uniformly dispersed in the polymer matrix.

For the first time, Polakovic et al. have suggested two main possible models to investigate the release rate of the drug from the polymeric nanoparticulate DDS and these are based on the diffusion and the dissolution phenomenon.

Recently, Jo et al. have reported a revised mathematical expression for diffusion models based on Fick's second law for diffusion phenomenon [147]. Further, coefficient reported by Jo et al. is significantly different than that of Polakovic et al. and gives more accurate mathematical expression. Unlike conventional models, these mathematical models are applicable to nanoparticulate DDS and can explain the controlled-release behavior during circulation in the blood stream and localization on the target site.

Further, Jalil et al. have suggested that the various formulation factors such as diffusion through particle pores, intact polymers, water swollen polymers and surface desorption along with the surface or bulk erosion of the polymeric matrix influence the release mechanism of the drug from spherical DDS. Often, one or more such mechanisms contribute in the process of drug release. To some extent, polymer matrix erosion contributes in drug release, while the other factors indirectly influence the rate of drug release through diffusion mechanisms as they affect the particle morphology. In addition,

swelling of polymer network and solid drug dissolution are also reported to play significant role in modulation of drug release from nanoparticulate DDS [148, 149].

Drug release from lipid based nanoparticles (SLNs) depends on various parameters such as particle size, composition of formulation (such as surfactant/surfactant mixture, amount of drug incorporated, structural properties of lipid and drug), production methods and conditions (such as time, production temperature, equipment, sterilization and lyophilization).

The drug incorporation model of SLNs is crucial to the drug release pattern. In the case of SLNs production by cold homogenization technique, the drug-loaded lipid phase remains mainly in the solid state. Since, mobility of the drug molecularly dispersed in colloidal particles is very limited: drug release is prolonged over several weeks [130].

On contrary to this, fast initial drug release (burst effect) is commonly observed in the drug-enriched shell model (ie, about 100% within <5 min) due to the large surface area of drug depositon on the particle surface. Higher surface area due to smaller particle size in the nanometer range gives higher drug release. Further, crystallization behavior of the lipid carrier and high mobility of the drug lead to fast drug release [150]. Muller et al. have established that drug release from nanoparticles with drug-enriched core follows Fick law diffusion [119].

Significance of the individual mechanism of drug release from nanoparticles varies with factors such as molecular weight of the polymer, composition, crystallinity, the loading amounts of the drug, interaction between polymer and drug. These factors can be adjusted in a formulation design to achieve the desired release profile of the drug.

The accurate mathematical modeling of the drug release rate is a key input in the design and development of nanoparticulate DDS. Most commonly employed mathematical modeling to determine drug release kinetics from nanoparticles are:

1. Zero order model: $F = k_0 t$,
2. First order model: $\ln(1 - F) = -k_f\, t$,
3. Higuchi model: $F = k_H \sqrt{t}$,
4. Reciprocal powered time model: $(1/F - 1) = \mathrm{m/t^b}$

Where, F is fraction of drug released up to time t; k_0, k_f, k_H, m and b are model parameters.

1.11.4 Drug stability and other properties

Nanoparticulate DDS provides extendable protection to the entrapped drug by reducing interaction with external factors such as enzymatic, proteolytic and oxidative stress. The protective function of nanoparticulate DDS is assessed by the in vitro characterization for stability of free drug and encapsulated drug. Like conventional DDS, the preparation of nanoparticles involve several processing steps, wherein, the drug is exposed to various stressed conditions such as solvents, homogenization, high speed shear, heat treatment, freeze-drying etc. Stability of drug during and after preparation is analyzed in a similar way to that of a conventional DDS.

a) Thermal properties and crystallinity

Nanopaticulate materials provide significantly different properties as compared to free drugs. Thermal properties provide a good understanding about the materials such as the physicochemical properties of polymer, drug, stabilizer, and other excipients and their compatibility with each other. Moreover, the measurement of thermal properties such as glass transition temperature, melting temperature and their associate enthalpies offer unique advantages, which can be used to determine the nature and speciation of crystallinity within the nanoparticles [151]. These techniques always provide complement information to X-ray diffraction analysis and it can be used to determine the relative extent of multiple phases in the nanomaterial and their possible interaction. Differential scanning calorimetry (DSC) represents the most frequently used analytical tool for thermal analysis of samples. The information obtained from a DSC thermogram is illustrated in Fig. 1.8.

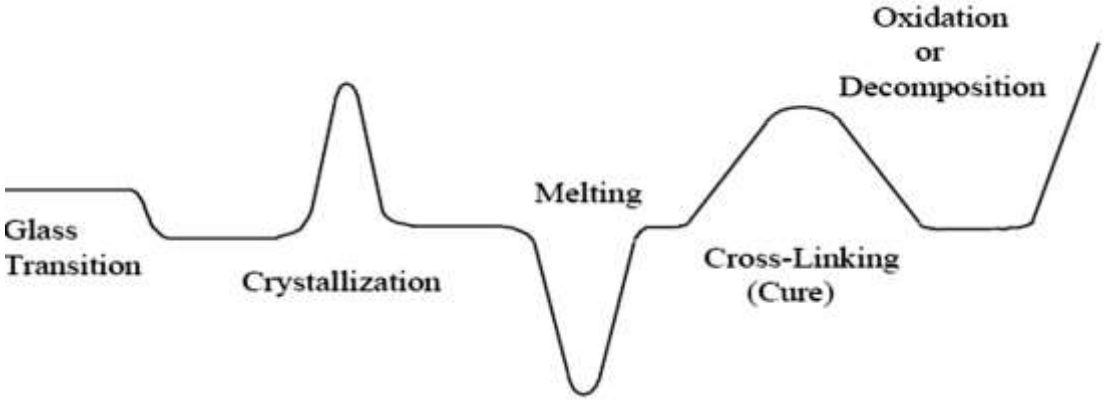

Fig. 1.8: Various phase transitions in a typical DSC thermogram.

b) Wide angle X-ray diffraction (WAXS)

Wide angle X-ray diffraction (WAXS) is a rapid analytical technique primarily used for phase identification of a crystalline material (polymorphism and degree of crystallinity) and can provide useful information on unit cell dimensions. This technique refers to the analysis of Bragg peaks scattered to wide angles. Principally, crystalline materials give rise to sharp diffraction peaks whereas, amorphous material produce broad, diffuse scattering of X-rays. WAXS uses information about the position, intensity, width, and shape of diffraction peaks in a pattern from a polycrystalline sample. Together with DSC, WAXS provides valuable information to elucidate the crystallinity and polymorphic nature of polymer/nanocomposite [151]. In many cases, the nature of API (bulk and entrapped API) can be ascertained with the use of these techniques.

1. 12 Drug information

Lopinavir is a potent HIV protease inhibitor (PI) and an integral part of Highly Active Anti Retroviral Therapy (HAART) program. It (Fig. 1.9) is chemically designated as (2S)-N-[(1S,3S,4S)-1-benzyl-4-{[(2,6-dimethylphenoxy)acetyl]amino}-3-hydroxy-5 phenyl pentyl]-3-methyl-2-(2 oxotetrahydropyrimidin1(2H)-yl) butanamide.

It is used against HIV infections as a fixed-dose combination with ritonavir under the trade name of Kaletra® and Aluvia® [152]. Detailed information about lopinavir is given in Table 1.1.

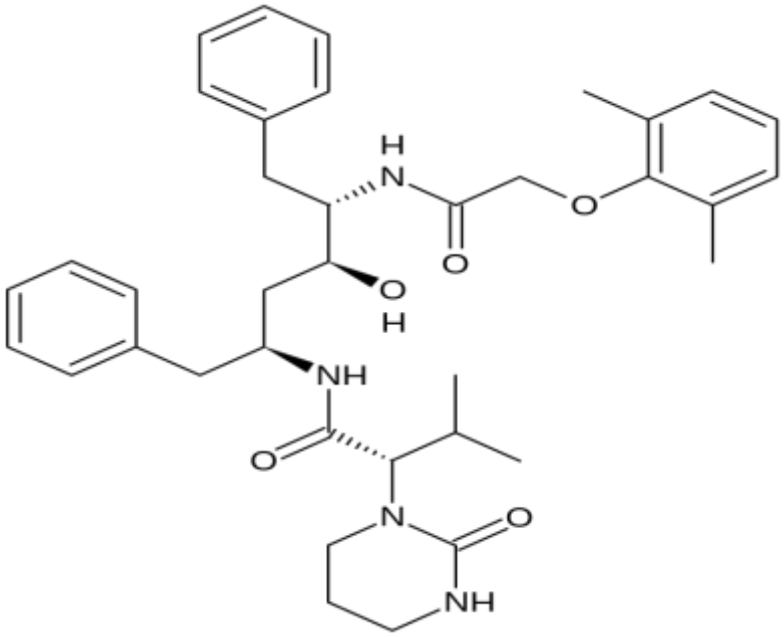

Fig. 1.9: Chemical structure of lopinavir.

Table 1.1: Drug information.

Parameters	Description
Drug Name	Lopinavir
Category	Antiretroviral
Therapeutic class	HIV Protease Inhibitor
Chemical formula	$C_{37}H_{48}N_6O_5S_2$
Generic name	Lopinavir
Proprietary name	Kaletra® and Aluvia®
Proprietor	Abbott Laboratories
CAS registry number	192725-17-0
Melting point	124-127
Molecular weight	628.80
Water solubility	1.9 µg/ml
Physical state	White crystalline solid
Hydrophobicity	clog P 4.69
Ionization constant (pKa)	13.39
Physical stability	Hygroscopic; -20^{o}C freezer

1.12.1 Clinical Pharmacology

a) Mechanism of action

HIV protease plays a crucial role in the viral life cycle. It is a homodimeric aspartic protease; involved in the post-translational processing of the HIV gag-pol polyprotein. Protease produces mature infectious virus particles through cleavage of the viral gag and gag-pol precursor proteins. The gag precursor protein encodes for all the structural viral proteins, matrix (p17, MA), capsid (p24, CA) and nucleocapsid (p7, NC) and the viral enzymes: protease, reverse transcriptase and integrase [153, 154]. Lopinavir is a highly potent and specific peptidomimetic inhibitor of the HIV-1 protease. Therefore, the main antiviral mechanism of lopinavir is to prevent further infection of susceptible cells [155].

b) Spectrum of activity and resistance profile

Lopinavir has demonstrated significant antiretroviral activity against laboratory strains and clinical isolates of HIV-l [156]. In MT4 cell lines, the concentration of lopinavir required to reduce 50 % cellular activity (EC50%; replication) of HIV-l ranges between 10-27 nM against laboratory strains and 4-11 nM against several HIV-1 subtype B clinical isolates. However, the presence of human serum (50% HS) attenuates the anti-viral activity of lopinavir. In this case, the mean EC50 values of lopinavir against HIV-1 laboratory strains ranges from 65-289 nM [157].

Several *in vitro* studies were performed to elucidate the resistance profile of lopinavir. After sequential *in vitro* passages in the presence of lopinavir and ritonavir,

mutations were mainly observed at positions 32 (V32I), 46 (M46I) and 84 (I84V). These mutations are often associated with resistance to other protease inhibitors. In clinical isolates from patients who had failed therapy to ritonavir, a reduced susceptibility to lopinavir was demonstrated [158].

c) ADME of lopinavir

Lopinavir was developed by Abbott in an attempt to improve on the HIV resistance and serum protein-binding properties of the company's earlier protease inhibitor, ritonavir. However, like other PIs, lopinavir suffers from several pharmacokinetics problems. It exhibits low plasma profile and short half-life with wide inter-individual variability both in rats and humans when administered alone [159, 160]. The absolute bioavailability of lopinavir in humans has not been established. However, in rats following single dose administration the oral bioavailability of lopinavir was ~ 25% [156, 161].

Similarly, in humans, following oral administration of a single 400-mg dose, lopinavir shows rapid absorption with C_{max} of less than 1µg/ml [156]. One of the primary reasons for the low bioavailability of lopinavir in humans is attributed to extensive first pass metabolism and poor aqueous solubility [160, 161].

Several *in vitro* metabolism studies reveal that lopinavir is extensively metabolized by the gut and hepatic cytochrome P450 system, almost exclusively by the CYP3A isozyme. Studies conducted with human hepatic microsomes reveal that lopinavir primarily undergoes oxidative metabolism and at least 13 lopinavir oxidative metabolites have been identified in humans [159, 162].

Additionally, it is also a substrate for efflux transporters such as P-gp and Multidrug Resistance Protein (MRP2) [163, 164]. Recent studies demonstrate that these efflux transporters play an important role in limiting the oral bioavailability of lopinavir by an active secretion process. Co-interplay between CYP3A4 and P-gp at absorption site is thought to dramatically reduce the oral bioavailability of lopinavir in humans [164].

P-gp is an important protein of the cell membrane that pumps many foreign substances out of cells and thus, plays an important role in drug distribution and disposition process [165]. Wide distribution and strategic locations of P-gp including the mucosal surface of gastrointestinal tract (enterocytes), biliary and renal canaliculi cells, blood brain barrier and immune cells leads to significant reduction in the intracellular accumulation of lopinavir at target reservoir sites [166, 167]. As a result, when given alone in conventional formulation, it fails to achieve therapeutic concentration in blood and target viral reservoirs leading to a poor clinical outcome of the therapy [168-170].

d) Kaletra® (lopinavir/ritonavir)

Several pre-clinical and clinical studies demonstrate that low dose of ritonavir co-administration drastically improves the oral plasma exposure of lopinavir by reducing its first-pass metabolism and rapid clearance. After single oral dose administration of lopinavir/ritonavir (2:1) in rats (10 mg/kg lopinavir) and humans (5.7 mg/kg), there was a 2-fold increase in C_{max} and a 6-fold increase in AUC for the rat and a 44-fold increase in C_{max} and a 182-fold increase in AUC in humans respectively [156, 171]. It is reported that ritonavir inhibits the microsomal activity of hepatic and gut CYP 3A4/5 in a concentration dependent-manner resulting in increased plasma lopinavir concentrations [171].

Therefore, in order to improve the bioavailability and effectiveness of lopinavir, Abbott pursued a strategy of co-administering lopinavir with sub-therapeutic doses of ritonavir, a potent CYP P450 3A4 inhibitor. The combination is marketed by Abbott Laboratories as Kaletra® (high-income countries) and Aluvia® (low-income countries). Thus, co-formulation of lopinavir/ritonavir (Kaletra®) was the first combination pill to contain a drug (lopinavir) not available separately. Kaletra® received accelerated FDA approval in the year 2000 for the treatment of HIV infection [152].

e) ADME of lopinavir in Kaletra®

Following oral administration of Kaletra® (400 mg lopinavir/100 mg ritonavir), lopinavir shows fairly rapid absorption with C_{max} being observed within 4.0 h [171]. The absolute bioavailability of lopinavir in humans is unknown due to the lack of an adequate intravenous formulation. However, after oral administration, lopinavir in combination with ritonavir is well absorbed and the relative bioavailability of lopinavir increases by 77-fold.

From a radio-labeled study, the amount of ^{14}C lopinavir unchanged recovered in the feces accounted for approximately 20%, indicating extensive absorption of lopinavir. Further, no significant effect of food on oral absorption of Kaletra® tablets has been established [156, 152].

As discussed earlier, lopinavir is eliminated mainly through oxidative metabolism via CYP3A. Ritonavir is a very potent inhibitor of the metabolism of lopinavir (Ki equal to 0.013 μM (0.009 μg/ml)). Further, other than CYP3A4, ritonavir is also known to inhibit CYP2D6 and to a lesser extent CYP2C9/10 and CYP2C19 [156]. The primary route of drug elimination is hepato-biliary secretion and it is excreted via the feces (>80% of the dose). From a study conducted in human volunteers (n=19), following a 400/100 mg labeled-lopinavir/ritonavir dose, the apparent oral clearance (CL/F) and half-life of lopinavir was 5.98 ± 5.75 l/h (mean ± SD,) and 5 h (4-6 h) respectively. Such a low clearance of lopinavir

argues well with the fact that metabolism of lopinavir is decreased in the presence of ritonavir. As no intravenous formulation is available, the total volume of distribution (V_d) of lopinavir in Kaletra® is unknown. However, the apparent distribution volume in man was estimated to be around 40 l [156, 152]. Low V_d of lopinavir (with high log P) indicates the significant role of P-gp in limiting the drug distribution process in tissues.

f) Indications

Kaletra® (lopinavir/ritonavir co-formulation) is indicated for the management of advanced HIV infection in adults and pediatric patients older than 14 days, in combination with other antiretroviral agents [152].

g) Dosage and administration

Kaletra® is currently available as film coated tablets in two strengths: 200-mg lopinavir/50-mg ritonavir per tablet and 100-mg lopinavir/25-mg ritonavir per tablet and as oral solution containing 80 mg lopinavir and 20 mg ritonavir per ml. The recommended daily dose for Kaletra® tablets in adult patients is 400 mg/100 mg (given as two 200/50 mg tablets) by mouth b.i.d with or without food. Tablets may be administered to adult patients as once (800 mg/200 mg; given as four 200/50 mg tablets) daily regimen, but latter approach is preferable as high evidence of diarrhea, nausea and vomiting is associated with once daily regimen [152].

h) Adverse effect

Clinical studies have shown that adverse effects observed during Kaletra® therapy frequently occur in patients that present an advanced HIV infection than in HIV–naïve patients. Diarrhea, vomiting and asthenia are the most common dose-related adverse reactions of Kaletra® in both adult and pediatric patients. However, these side effects are usually reversible on discontinuation of therapy. Pancreatitis, hepatotoxicity and QT prolongation have also been reported as potentially life-threatening side effects during post-marketing surveillance in HIV-1 infected patients

Other adverse effects that have been associated with therapy include diabetes mellitus/hyperglycemia, immune reconstitution syndrome, fat redistribution and hyperlipidemia [23, 172,173].

1.13 Summary

Despite the enormous development in molecular understanding of HIV, even the rationally designed therapeutic approaches suffer from major problems such as poor physicochemical properties (drug instability and poor bioavailability); non-specific distribution; emergence of inherent and acquired resistance by pathogens; intra and inter subject pharmacokinetic variations; sub-optimum drug levels due to activated efflux systems and recurrence of the disease [4, 32]. Most of these reasons are interlinked but they need to be addressed individually. In order to translate new techniques into clinical practice; various aspects of this disease will remain as a formidable challenge in drug delivery for the ultimate success of the therapy.

On the other hand, nanotechnology and nanoscience are becoming increasingly important for various drug delivery applications in several therapeutic and diagnostic segments. Considering the fact that the diameter of smallest blood capillaries is 4 μm, the US-FDA has approved the use of nanoparticles of less than 1 μm for intravenous application. Similar requirements are also applicable for intra-muscular and subcutaneous application of nanoparticulate DDS in order to reduce the possible irritation reaction.

1.14 Problem definition and research objectives

It is reported that though lopinavir is a potent PI against HIV-1, when given alone, it fails to achieve therapeutic concentration in blood and target viral reservoirs [168, 169]. In order to re-establish anti-HIV activity of lopinavir, ritonavir, a known CYP inhibitor, is co-formulated in low dose as a pharmacokinetic booster for lopinavir. Lopinavir/ritonavir is a fixed dose combination drug for the treatment of HIV infection and is currently marketed by Abbott as Kaletra®.

Though, the co-formulation of ritonavir has significantly improved the plasma exposure of lopinavir; a desired therapeutic concentration of lopinavir at viral reservoir sites can not be achieved for the necessary time duration [174]. This is attributed to off-target distribution and the inability of the drug molecule to permeate into viral reservoirs from the blood [30]. Consequently, HIV remains viable in these viral reservoirs even when sufficient concentration of lopinavir is available in the blood leaving patients susceptible to re-infection upon discontinuation of the therapy [175-177]. Moreover, like classical chemotherapy, lopinavir requires continuous treatment regimen extending over a time demanding frequent administration [152].

Additionally, researchers have also raised several concerns over the use of ritonavir in the Kaletra® formulation. Several researchers have reported a significant contribution of

ritonavir in synergizing the side effects of Kaletra® formulation [173]. Life threatening serious side effects of Kaletra® treatment, as mentioned in the previous section, is reported to be one of the major reasons for patient non-compliance with anti-HIV therapy. In addition to this, dose-dependent severe GI intolerance is a cause of frequent lopinavir/ritonavir therapy modification or interruption [152, 172].

Moreover, owing to the presence of ritonavir, Kaletra® formulation behaves like potent CYP3A inhibitor [152, 178]. Therefore, initiating treatment with Kaletra® in patients receiving medications metabolized by CYP3A or initiating medications metabolized by CYP3A in patients already maintained on Kaletra® may result in increased plasma concentrations of concomitantly administered medications. Higher plasma exposure of concomitant medications can result in increased or prolonged therapeutic or adverse effects, potentially leading to severe, life-threatening or fatal events. Thus, there is a need of ritonavir-free strategy for improving lopinavir oral bioavailability and also to achieve optimum lopinavir concentration to HIV localization sites in the body.

The poor clinical outcome of Kaletra® formulation has triggered several researchers to look for a safe and effective alternative of ritonavir in lopinavir/ritonavir combination. In the recent past, many researchers have attempted to improve therapeutic efficacy of lopinavir without combining it with ritonavir [163, 179-174]. Various strategies including chemical modification [179], pharmacokinetic [163] and formulation design [180-184] have been explored.

In an approach to evade the first-pass metabolism and efflux of lopinavir, Agarwal et al have synthesized peptide pro-drugs of lopinavir [valine-valine-lopinavir (VVL) and glycine-valine-lopinavir (GVL)]. *In vitro* studies demonstrate the potential of pro-drug approach to improve permeability and microsomal stability of lopinavir [179].

In pharmacokinetic approach, du Plooy et al. have investigated the effects of verapamil, a P-gp inhibitor on the oral bioavailability of lopinavir. The results demonstrate a significant role of P-gp in limiting oral bioavailability of lopinavir and also indicate a significant improvement of plasma exposure by blocking the efflux mechanism [163].

On the other hand, few researchers have also explored the formulation strategy to overcome the problems associated with the current conventional formulation including melt-extruded lopinavir tablet formulation [180] and surface stabilized lopinavir nanocrystals [181]. In both these cases, improvement in oral bioavailability was observed due to enhanced solubility and dissolution rate of lopinavir.

Though, all the approaches showed significant improvement in plasma exposure of drug: no efforts have been made to improve selective distribution of the drug towards viral reservoir sites. There is a clinical need to achieve therapeutically effective concentration in the viral reservoir sites which can be achieved by targeting drug to these sites. Moreover, controlled drug release at the target site for extended duration is key to successful HIV therapy.

To achieve better anti-HIV effect by improving bioavailability and enhancing selective distribution of the drug towards viral localization sites, researchers have also explored nanoparticulate DDSs. In line with this, Destache et al. have successfully demonstrated the use of PLGA based nanoparticles in delivering combination of antiretroviral drugs (ritonavir, lopinavir and efaverinz) to peripheral blood mononuclear cells [184].

In the present work, we hypothesized that by increasing concentration of lopinavir in blood and viral reservoir sites (with the use of nanoparticles), we can improve the therapeutic outcome of drug. Moreover, reframing ritonavir from the current co-formulation would further reduce the drug associated side effects and improve the patient compliance.

Thus, the primary objective of the present work was to:

I. Design and develop nanocarriers for lopinavir.

II. Investigate *in vitro*/*in vivo* performance of optimized nanocarriers of lopinavir in comparison with marketed formulation (Kaletra®).

To achieve this broad objective, following specific studies were carried out in the present work:

- Quality parameters of the drug product were evaluated by well-established methods and protocols.
- Suitable analytical and bioanalytical methods were developed using liquid chromatography for determination of lopinavir in formulation and biological matrices.
- For the efficient product development, the pre-formulation studies were performed to establish necessary physico-chemical data of lopinavir prior to formulation development. Studies were performed to address the product specific questions related to drug solubility, stability, drug-excipient compatibility.
- Formulation development was carried out by identifying and optimizing the critical factors in the design and the process using optimization techniques (DoE). The prepared

nanoparticles were extensively characterized for surface morphology and shape, particle size and size distribution, drug content (loading and entrapment efficiency) and *in vitro* drug release. Further, optimized formulations were studied for the drug product stability and reproducibility.

- Pharmacokinetic studies were performed to investigate the *in vivo* performance of the prepared nanoparticles in the healthy rat model. Microsomal stability studies were conducted to investigate the extent of metabolic protection offered by nanoparticles to loaded drug. *In vitro* rat intestinal permeability studies were carried out to investigate the mechanism of nanoparticle uptake. *In vivo* lymph transport inhibition studies were conducted to understand the contribution of lymphatic system in the uptake and transport of nanoparticles.
- Tissue distribution studies were conducted to study the comparative distribution pattern of free lopinavir and lopinavir upon loading into nanocarriers towards the selective organs like lymph nodes, spleen, and liver after oral administration.
- The *in vivo* bio-distribution behaviour of lopinavir loaded nanoparticles after oral and intra venous administration was studied in comparison with the pure drug.

References

1. Freed EO. HIV-1 Replication. Somat Cell Mol Genet. 2001; 26: 13-33.
2. Cohen MS, Hellmann N, Levy JA, DeCock K, Lange J. The spread, treatment, and prevention of HIV-1: evolution of a global pandemic. J Clin Invest. 2008; 118: 1244-1254.
3. Pomerantz RJ. Reservoirs of human immunodeficiency virus type 1: The main obstacles to viral eradication. Clin Infect Dis. 2002; 34: 91-7.
4. Pierson T, McArthur J, Siliciano RF. Reservoirs for HIV-1: Mechanisms for viral persistence in the presence of antiviral immune responses and antireteroviral therapy. Annu Rev Immunol. 2000; 18: 665-708.
5. Haase AT. Population biology of HIV-1 infection: viral and CD4+ T cell demographics and dynamics in lymphatic tissues. Annu Rev Immunol. 1999;17: 625-56.
6. Global report. UNAIDS report on the global AIDS epidemic 2013. Available at: http://www.unaids.org/en/media/unaids/contentassets/documents/epidemiology/2013/gr2013/unaids_global_report_2013_en.pdf. Accessed July 28, 2014.

7. Statement containing brief activities of the department of AIDS control in 2013. Department of AIDS Control, Ministry of Health and Family Welfare, Government of India. Available at: http://www.unaids.org/en/dataanalysis/knowyourresponse/countryprogressreports/2014countries/IND_narrative_report_2014.pdf. Accessed July 28, 2014.
8. Joint United Nations Programme on HIV/AIDS (UNAIDS) and World Health Organization (WHO). AIDS epidemic update 2009. Geneva: UNAIDS Available at: http://data.unaids.org/pub/Report/2009/JC1700_Epi_Update_2009_en.pdf. Accessed July 28, 2014.
9. Sierra S, Kupfer B, Kaiser R. Basics of the virology of HIV-1 and its replication. J Clin Virol. 2005; 34: 233-244.
10. Sundquist W, Kräusslich H-G. HIV-1 Assembly, Budding, and Maturation. Cold Spring Harb Perspect Med. 2012; 2: a006924.
11. Greene WC. AIDS and the immune system. Sci Am. 1993; 269: 98-105.
12. Blocker ME, Cohen MS. Biologic approaches to the prevention of sexual transmission of human immunodeficiency virus. Infect Dis Clin North Am. 2000; 14: 983-999.
13. Ziegler-Heitbrock L, Ancuta P, Crowe S, Dalod M, Grau V, Hart DN, et al. Nomenclature of monocytes and dendritic cells in blood. Blood. 2010; 116: e74-80.
14. Levy JA. HIV pathogenesis: 25 years of progress and persistent challenges. AIDS. 2009; 23: 147-160.
15. Tugizov SM, Herrera R, Veluppillai P, Greenspan D, Soros V, Greene WC, et al. Differential transmission of HIV traversing fetal oral/intestinal epithelia and adult oral epithelia. J Virol. 2012; 86: 2556-2570.
16. Bobardt MD, Chatterji U, Selvarajah S, Van der Schueren B, David G, Kahn B, et al. Cell-free human immunodeficiency virus type 1 transcytosis through primary genital epithelial cells. J Virol. 2007; 81: 395-405.
17. Bobardt MD, Saphire AC, Hung HC, Yu X, Van der Schueren B, Zhang Z, et al. Syndecan captures, protects, and transmits HIV to T lymphocytes. Immunity. 2003; 18: 27-39.
18. Stebbing J, Gazzard B, Douek DC. Mechanisms of disease: where does HIV live? N Engl J Med. 2004; 350: 1872-1880.
19. Pantaleo G, Graziosi C, Demarest JF, Butini L, Montroni M, Fox CH, et al. HIV infection is active and progressive in lymphoid tissue during the clinically latent stage of disease. Nature. 1993; 362: 355-358.

20. Cohen MS, Hellmann N, Levy JA, DeCock K, Lange J. The spread, treatment, and prevention of HIV-1: evolution of a global pandemic. J Clin Invest. 2008; 118: 1244-1254.
21. Lert F. Advances in HIV treatment and prevention: should treatment optimism lead to prevention pessimism? AIDS Care. 2000; 12: 745-755.
22. Phillips KD. Protease Inhibitors: A new weapon and a new strategy against HIV. J Assoc Nurses AIDS Care. 1996; 7: 57-71.
23. Neuman MG, Schneider M, Nanau RM, Parry C. HIV-antiretroviral therapy induced liver, gastrointestinal, and pancreatic injury. Int J Hepatol. 2012; 2012: 760706.
24. Wensing AM, van Maarseveen NM, Nijhuis M. Fifteen years of HIV Protease Inhibitors: raising the barrier to resistance. Antiviral Res. 2010; 85: 59-74.
25. Temesgen Z, Warnke D, Kasten MJ. Current status of antiretroviral therapy. Expert Opin Pharmacother. 2006; 7: 1541-54.
26. The-Antiretroviral-Therapy-Cohort-Collaboration. Life expectancy of individuals on combination antiretroviral therapy in high-income countries: A collaborative analysis of 14 cohort studies. Lancet. 2008; 372, 293-299.
27. Perno CF, Moyle G, Tsoukas C, Ratanasuwan W, Gatell J, Schechter M. Overcoming resistance to existing therapies in HIV-infected patients: the role of new antiretroviral drugs. J Med Virol. 2008; 80: 565-576.
28. Thompson MA, Aberg JA, Cahn P, Montaner JS, Rizzardini G, Telenti A, et al. International AIDS Society-USA. Antiretroviral treatment of adult HIV infection: 2010 recommendations of the International AIDS Society-USA panel. *JAMA*. 2010; 304: 321-333.
29. Bozzette SA, Joyce G, McCaffrey DF, Leibowitz AA, Morton SC, Berry SH, et al. Expenditures for the care of HIV-infected patients in the era of highly active antiretroviral therapy. N Engl J Med. 2001; 344: 817823.
30. Vyas TK, Shah L, Amiiji MM. Nanoparticulate drug carriers for delivery of HIV/AIDS therapy to viral reservoir sites. Expert Opin Drug Deliv. 2006; 3: 613-28.
31. Bell SK, Little SJ, Rosenberg ES. Clinical management of acute HIV infection: best practice remains unknown. J Infect Dis. 2010; 202: S278-288.
32. Ojewole E, Mackraj I, Naidoo P, Govender T. Exploring the use of novel drug delivery systems for antiretroviral drugs. Eur J Pharm Biopharm. 2008; 70: 697-710.
33. Cai S, Yang Q, Bagby TR, Forrest ML. Lymphatic drug delivery using engineered liposomes and solid lipid nanoparticles. Adv Drug Deliv Rev. 2011; 63: 901-908.

34. Kingsley JD, Dou H, Morehead J, Rabinow B, Gendelman HE, Destache CJ. Nanotechnology: a focus on nanoparticles as a drug delivery system. J Neuroimmune Pharmacol. 2006; 1: 340-50.
35. Allen TM, Cullis PR. Drug delivery systems: entering the mainstream. Science. 2004; 303: 1818-22.
36. Kostarelos K. Rational design and engineering of delivery systems for therapeutics: biomedical exercises in colloid and surface science. Adv Colloid Interface Sci. 2003; 106: 147-68.
37. Moghimi SM, Kissel T. Particulate nanomedicines. Adv Drug Deliv Rev. 2006; 58: 1451-5.
38. Salata O. Applications of nanoparticles in biology and medicine. J Nanobiotechnology. 2004; 2: 3.
39. Kocbek P, Kralj S, Kreft ME, Kristl J.Targeting intracellular compartments by magnetic polymeric nanoparticles. Eur J Pharm Sci. 2013; 50: 130-8.
40. Schroeter A, Engelbrecht T, Neubert RH, Goebel AS. New nanosized technologies for dermal and transdermal drug delivery. A review. J Biomed Nanotechnol. 2010; 6: 511-28.
41. Park K. Nanotechnology: what it can do for drug delivery. J Control Release. 2007; 120: 1-3.
42. Florence AT. Pharmaceutical nanotechnology: more than size. Ten topics for research. Int J Pharm. 2007; 339: 1-2.
43. Farokhzad OC, Langer R. Nanomedicine: developing smarter therapeutic and diagnostic modalities. Adv Drug Deliv Rev. 2006; 58: 1456-9.
44. Cooper DL, Conder CM, Harirforoosh S. Nanoparticles in drug delivery: mechanism of action, formulation and clinical application towards reduction in drug-associated nephrotoxicity. Expert Opin Drug Deliv. 2014; 23:1-20.
45. Shilakari Asthana G, Asthana A, Kohli DV, Vyas SP. Mannosylated chitosan nanoparticles for delivery of antisense oligonucleotides for macrophage targeting. Biomed Res Int. 2014; 2014: 526391.
46. Fan T, Chen C, Guo H, Xu J, Zhang J, Zhu X, et al. Design and evaluation of solid lipid nanoparticles modified with peptide ligand for oral delivery of protein drugs. Eur J Pharm Biopharm. 2014. pii: S0939-6411(14)00203-3.

47. Gu G, Hu Q, Feng X, Gao X, Menglin J, Kang T, et al. PEG-PLA nanoparticles modified with APTEDB peptide for enhanced anti-angiogenic and anti-glioma therapy. Biomaterials. 2014; 35: 8215-26.
48. Tang BC, Dawson M, Lai SK, Wang YY, Suk JS, Yang M, et al. Biodegradable polymer nanoparticles that rapidly penetrate the human mucus barrier. Proc Natl Acad Sci, 2009; 106: 19268-73.
49. Cone RA. Barrier properties of mucus. Adv Drug Deliv Rev. 2009; 61: 75-85.
50. Crater JS, Carrier RL. Barrier properties of gastrointestinal mucus to nanoparticle transport. Macromol Biosci. 2010; 10: 1473-83.
51. Lai SK, Wang YY, Hanes J. Mucus-penetrating nanoparticles for drug and gene delivery to mucosal tissues. Adv Drug Deliver Rev. 2009; 61: 158-171.
52. Huang Y, Leobandung W, Foss A, Peppas NA. Molecular aspects of muco- and bioadhesion: tethered structures and site-specific surfaces. J Control Release. 2000; 65: 63-71.
53. Lehr CM. Lectin-mediated drug delivery: the second generation of bioadhesives. J Control Release. 2000; 65: 19-29.
54. O'Hagan DT. Intestinal translocation of particulates-implications for drug and antigen delivery. Adv Drug Deliver Rev.1990; **5**: 265-285.
55. Kreuter J. Peroral administration of nanoparticles. Adv Drug Deliver Rev. 1991; **7**: 71-86.
56. Gebert A, Rothkötter HJ, Pabst R. M cells in peyer's patches of the intestine. Int Rev Cytol. Kwang WJ, Editor. 1996. Academic Press. p. 91-159.
57. Plapied L , Duhem N, des Rieux A, Préat V. Fate of polymeric nanocarriers for oral drug delivery. Curr Opin Colloid Interface Sci. 2011; 16: 228-237.
58. Roger E, Lagarce F, Garcion E, Benoit JP. Biopharmaceutical parameters to consider in order to alter the fate of nanocarriers after oral delivery. Nanomedicine (Lond). 2010; 5: 287-306.
59. Conner SD, Schmid SL. Regulated portals of entry into the cell. Nature. 2003; 422: 37-44.
60. Snoeck V, Goddeeris B, Cox E. The role of enterocytes in the intestinal barrier function and antigen uptake. Microbes Infect. 2005; **7**: 997-1004.
61. Sahay G, Alakhova DY, Kabanov AV. Endocytosis of nanomedicines. J Control Release. 2010; 145: 182-95.

62. Brodsky FM, Chen CY, Knuehl C, Towler MC, Wakeham DE. Biological basket weaving: formation and function of clathrin-coated vesicles. Annu Rev Cell Dev Biol. 2001; 17: 517-68.
63. Bareford LM, Swaan PW. Endocytic mechanisms for targeted drug delivery. Adv Drug Deliv Rev. 2007; 59: 748-58.
64. Mayor S, Pagano RE. Pathways of clathrin-independent endocytosis. Nat Rev Mol Cell Biol. 2007, **8**: 603-12.
65. Hillaireau H, Couvreur P. Nanocarriers' entry into the cell: relevance to drug delivery. Cell Mol Life Sci. 2009. 66: 2873-2896.
66. Sandvig K, Pust S, Skotland T, van Deurs B. Clathrin-independent endocytosis: mechanisms and function. Curr Opin Cell Biol. 2011; 23: 413-20.
67. Doherty GJ, McMahon HT. Mechanisms of endocytosis. Annu Rev Biochem. 2009; 78: 857-902.
68. Lu Y, Low PS. Folate-mediated delivery of macromolecular anticancer therapeutic agents. Adv Drug Deliv Rev. 2002; 54: 675-93.
69. Kerr MC, Teasdale RD. Defining macropinocytosis. Traffic. 2009; 10: 364-71.
70. Jones AT. Macropinocytosis: searching for an endocytic identity and role in the uptake of cell penetrating peptides. J Cell Mol Med. 2007; 11: 670-84.
71. Rabinovitch M. Professional and non-professional phagocytes: an introduction. Trends Cell Biol. 1995; **5**: 85-7.
72. Aderem A, Underhill DM. Mechanisms of phagocytosis in macrophages. Annu Rev Immunol. 1999; 17: 593-623.
73. Porter CJH, Trevaskis NL, Charman WN. Lipids and lipid-based formulations: optimizing the oral delivery of lipophilic drugs. Nat Rev Drug Discov. 2007; 6: 231-248.
74. Lehner R, Kuksis A. Biosynthesis of triacylglycerols. Prog Lipid Res. 1996; 35: 169-201.
75. Hussain N, Jaitley V, Florence AT. Recent advances in the understanding of uptake of microparticulates across the gastrointestinal lymphatics. Adv Drug Deliver Rev. 2001; 50: 107-142.
76. Phan CT, Tso P. Intestinal lipid absorption and transport. Front Biosci. 2001; 6: D299-319.
77. Jain K, Jain NK. Surface engineered dendrimers as antiangiogenic agent and carrier for anticancer drug: dual attack on cancer. J Nanosci Nanotechnol. 2014; 14: 5075-87.

78. Dimer FA, Ortiz M, Pase CS, Roversi K, Friedrich RB, Pohlmann AR, et al. Nanoencapsulation of olanzapine increases its efficacy in antipsychotic treatment and reduces adverse effects. J Biomed Nanotechnol. 2014; 10: 1137-45.
79. Karavana SY, Gökçe EH, Rençber S, Özbal S, Pekçetin C, Güneri P, et al. A new approach to the treatment of recurrent aphthous stomatitis with bioadhesive gels containing cyclosporine A solid lipid nanoparticles: in vivo/in vitro examinations. Int J Nanomedicine. 2012; 7: 5693-704.
80. Dwivedi P, Khatik R, Khandelwal K, Taneja I, Raju KS, Wahajuddin, et al. Pharmacokinetics study of arteether loaded solid lipid nanoparticles: an improved oral bioavailability in rats. Int J Pharm. 2014; 466: 321-7.
81. Cho HJ, Park JW, Yoon IS, Kim DD. Surface-modified solid lipid nanoparticles for oral delivery of docetaxel: enhanced intestinal absorption and lymphatic uptake. Int J Nanomedicine. 2014; 9: 495-504.
82. Singh R, Lillard JW. Nanoparticle-based targeted drug delivery. Expt Mol Patho. 2009. 86: 215-223.
83. Illum L, Davis SS, Müller RH, Mak E, West P.The organ distribution and circulation time of intravenously injected colloidal carriers sterically stabilized with a block copolymer--poloxamine 908. Life Sci. 1987; 40: 367-74.
84. Bazile DV, Ropert C, Huve P, Verrecchia T, Marlard M, Frydman A, et al. Body distribution of fully biodegradable [14C]-poly(lactic acid) nanoparticles coated with albumin after parenteral administration to rats. Biomaterials. 1992; 13: 1093-102.
85. Williams J, Lansdown R, Sweitzer R, Romanowski M, LaBell R, Ramaswami R, et al. Nanoparticle drug delivery system for intravenous delivery of topoisomerase inhibitors. J Control Release. 2003; 91: 167-72.
86. Saba TM. Physiology and pathophysiology of the reticuloendothelial system. Arch Interm Med. 1970; 126: 1031-1052.
87. Allen TM, Hansen C, Rutledge J. Liposomes with prolonged circulation times: factors affecting uptake by reticuloendothelial and other tissues. Biochim Biophys Acta. 1989 ; 981: 27-35.
88. Moghimi SM, Patel HM. Differential properties of organ-specific serum opsonins for liver and spleen macrophages. Biochim Biophys Acta. 1989; 984: 379-83.
89. Nagayama S, Ogawara K, Fukuoka Y, Higaki K, Kimura T. Time-dependent changes in opsonin amount associated on nanoparticles alter their hepatic uptake characteristics. Int J Pharm. 2007; 342: 215-221.

90. Levchenko TS, Rammohan R, Lukyanov AN, Whiteman KR, Torchilin VP. Liposome clearance in mice: the effect of a separate and combined presence of surface charge and polymer coating. Int J Pharm. 2002; 240: 95-102.
91. Zhang JS, Liu F, Huang L. Implications of pharmacokinetic behavior of lipoplex for its inflammatory toxicity. Adv Drug Deliv Rev. 2005; 57: 689-98.
92. Introduction to nanoparticles, in microwaves in nanoparticle synthesis: fundamentals and applications. Horikoshi SS, Serpone N Editor. 2013, Wiley-VCH Verlag GmbH & Co. KGaA: Wiley-VCH Verlag GmbH & Co. KGaA. p. 8-10.
93. Peek LJ, Middaugh CR, Berkland C. Nanotechnology in vaccine delivery. Adv Drug Deliv Rev. 2008; 60: 915-28.
94. Stork M, Tousain RL, Wieringa JA, Bosgra OH. A MILP approach to the optimization of the operation procedure of a fed-batch emulsification process in a stirred vessel. Comp Chem Eng. 2003; 27: 1681–1691.
95. Mabille C, Leal-Calderon F, Bibette J, Schmitt V. Monodisperse fragmentation in emulsions: Mechanisms and kinetics. Europhys Lett. 2003; 61: 708–714.
96. Allémann E, R. Gurny, and E. Doelker. Preparation of aqueous polymeric nanodispersions by a reversible salting-out process: influence of process parameters on particle size. Int. J. Pharm. 87(1–3):247–253 (1992).
97. Dong WY, Körber M, López EV, Bodmeier R. Stability of poly(D,L-lactide-co-glycolide) and leuprolide acetate in in-situ forming drug delivery systems. J Control Release. 2006; 115: 158-167.
98. Bilati U, Allémann E, Doelker E. Poly(D,L-lactide-coglycolide) protein-loaded nanoparticles prepared by the double emulsion method−processing and formulation issues for enhanced entrapment efficiency. J Microencapsul. 2005; 22: 205-214.
99. Allémann E, Gurny R, Doelker E. Drug loaded nanoparticles. Preparation, methods and drug targeting issues. Eur J Pharm Biopharm. 1993; 39: 173-191.
100. Anton N, Benoit JP, Saulnier P. Design and production of nanoparticles formulated from nano-emulsion templates-A review. J Control Release. 2008; 128: 185-199.
101. Mundargi RC, Babu VR, Rangaswamy V, Patel P, Aminabhavi TM. Nano/micro technologies for delivering macromolecular therapeutics using poly(D,L-lactide-co-glycolide) and its derivatives. J Control Release. 2008; 125: 193-209.
102. Moinard-Chécot D., Chevalier Y, Briançon S, Fessi H, Guinebretière S. Nanoparticles for drug delivery: review of the formulation and process difficulties illustrated by the emulsiondiffusion process. J Nanosci Nanotechnol. 2006; 6: 2664-2681.

103. Battaglia L, Trotta M, Gallarate M, Carlotti ME, Zara GP, Bargoni A. Solid lipid nanoparticles formed by solvent-inwater emulsion–diffusion technique: Development and influence on insulin stability. J Microencapsul. 2007; 24: 672-684.
104. Leroux JC, Allemann E, Doelker E, Gurny R. New approach for the preparation of nanoparticles by an emulsification–diffusion method. Eur J Pharm Biopharm. 1995; 41: 14-18.
105. Vauthier C, Bouchemal K.Methods for the preparation and manufacture of polymeric nanoparticles. Pharm Res. 2009; 26: 1025-58.
106. Avgoustakis K. Pegylated poly(lactide) and poly(lactide-coglycolide) nanoparticles: preparation, properties and possible applications in drug delivery. Curr Drug Deliv. 2004; 1: 321-333.
107. Quintanar-Guerrero D, Ganem-Quintanar A, Allemann E, Fessi H, Doelker E. Influence of the stabilizer coating layer on the purification and freeze-drying of poly(D,L-lactic acid) nanoparticles prepared by an emulsion–diffusion technique. J Microencapsul. 1998;15: 107-119.
108. Moinard-Chécot D, Chevalier Y, Briançon S, Beney L, Fessi H. Mechanism of nanocapsules formation by the emulsion–diffusion process. J Colloid Interface Sci. 2008; 317: 458-468.
109. Trotta M, Debernardi F, Caputo O. Preparation of solid lipid nanoparticles by a solvent emulsification‑diffusion technique. Int J Pharm. 2003; 257: 153-160.
110. Ibrahim H, Bindschaedler C, Doelker E, Buri P, Gurny R. Aqueous nanodispersions prepared by a salting-out process. Int J Pharm. 1992; 87: 239-246.
111. Allémann E, Gurny R, Doelker E. Preparation of aqueous polymeric nanodispersions by a reversible salting-out process: influence of process parameters on particle size. Int J Pharm. 1992; 87: 247-253.
112. Wang N, Wu XS. Preparation and characterization of agarose hydrogel nanoparticles for protein and peptide drug delivery. Pharm Dev Technol. 1997; 2: 135-142.
113. Vauthier C, Labarre D, Ponchel G. Design aspects of poly (alkylcyanoacrylate) nanoparticles for drug delivery. J Drug Targeting. 2007; 15: 641-663
114. Fessi H, Puisieux F, Devissaguet JP, Ammoury N, Benita S. Nanocapsule formation by interfacial deposition following solvent displacement. Int J Pharm. 1989; 55: R1–R4.
115. Thioune O, Fessi H, Devissaguet JP, Puisieux F. Preparation of pseudolatex by nanoprecipitation: Influence of the solvent nature on intrinsic viscosity and interaction constant. Int J Pharm. 1997; 146: 233-238.

116. Legrand P, Lesieur S, Bochot A, Gref R, Raatjes W, Barratt G, et al. Influence of polymer behaviour in organic solution on the production of polylactide nanoparticles by nanoprecipitation. Int J Pharm. 2007; 344: 33-43.
117. Calvo P, Remuñan-Lopez C, Vila-Jato JL, Alonso MJ. Novel hydrophilic chitosan-polyethylene ocide nanoparticles as protein carriers. J Appl Polym Sci. 1997; 63: 125-132.
118. López-León T, Carvalho EL, Seijo B, Ortega-Vinuesa JL, Bastos-González D. Physicochemical characterization of chitosan nanoparticles: electrokinetic and stability behavior. J Colloid Interf Sci. 2005; 283: 344-351.
119. Müller RH, Mäder K, Gohla S. Solid lipid nanoparticles (SLN) for controlled drug delivery – a review of the state of the art. Eur J Pharm Biopharm. 2000; 50: 161-177.
120. Müller RH, Radtke M, Wissing SA. Solid lipid nanoparticles (SLN) and nanostructured lipid carriers (NLC) in cosmetic and dermatological preparations. Adv Drug Deliver Rev. 2002; 54: S131-S155.
121. Qi J, Lu Y, Wu W. Absorption, disposition and pharmacokinetics of solid lipid nanoparticles. Curr Drug Metab. 2012; 13: 418-28.
122. Wang J, Chen J, Ye N, Luo Z, Lai W, Cai X, et al. Absorption, pharmacokinetics and disposition properties of solid lipid nanoparticles (SLNs). Curr Drug Metab. 2012; 13: 447-56.
123. Pouton CW. Formulation of poorly water-soluble drugs for oral administration: Physicochemical and physiological issues and the lipid formulation classification system. Eur J Pharm Sci. 2006; 29: 278-287.
124. Mehnert W, Mäder K. Solid lipid nanoparticles: Production, characterization and applications. Adv Drug Deliver Rev. 2001; 47: 165-196.
125. Souto EB, Muller RH. Lipid nanoparticles (SLN and NLC) for drug delivery, in Nanoparticles for Pharmaceutical Applications, Domb YTAJ, Kumar MNVR, Farber S, Editor. 2007, American Scientific Publishers: Stevenson Ranch, California. p. 102-122.
126. Igartua M, Saulnier P, Heurtault B, Pech B, Proust JE, Pedraz JL, et al. Development and characterization of solid lipid nanoparticles loaded with magnetite. Int J Pharm. 2002; 233: 149-57.
127. Gasco MR. Solid lipid nanospheres from warm micro-emulsions. Pharm Technol Eur. 1997; 9: 52-58.

128. Singh B, Vuddanda PR, M RV, Kumar V, Saxena PS, Singh S. Cefuroxime axetil loaded solid lipid nanoparticles for enhanced activity against S. aureus biofilm. Colloids Surf B Biointerfaces. 2014; 121C: 92-98.
129. Siekmann B, Westesen K. Investigations on solid lipid nanoparticles prepared by precipitation in o/w emulsions. Eur J Pharm Biopharm. 1996, 43: 104-109.
130. Morel S, Ugazio E, Cavalli R, Gasco M R. Thymopentin in solid lipid nanoparticles. Int J Pharm. 1996, 132: 259-261.
131. Cortesi R, Esposjto E, Luca G, Nastruzzi C. Production of lipospheres as carriers for bioactive compounds. Biomaterials. 2002; 23: 2283-2294.
132. Mei Z, Chen H, Weng T, Yang Y, Yang X. Solid lipid nanoparticle and microemulsion for topical delivery of triptolide. Eur J Pharm Biopharm. 2003; 56: 189-96.
133. Gaumet M, Vargas A, Gurny R, Delie F. Nanoparticles for drug delivery: the need for precision in reporting particle size parameters. Eur J Pharm Biopharm. 2008; 69: 1-9.
134. Champion JA, Katare YK, Mitragotri S. Particle shape: a new design parameter for micro- and nanoscale drug delivery carriers. J Control Release. 2007; 121: 3-9.
135. Hassan PA, Rana S, Verma G. Making sense of brownian motion: colloid characterization by dynamic light scattering. Langmuir. 2014 [Epub ahead of print].
136. Villari V, Micali N. Light scattering as spectroscopic tool for the study of disperse systems useful in pharmaceutical sciences. J Pharm Sci. 2008;97: 1703-30.
137. Jores K, Mehnert W, Drechsler M, Bunjes H, Johann C, Mäder K. Investigations on the structure of solid lipid nanoparticles (SLN) and oil-loaded solid lipid nanoparticles by photon correlation spectroscopy, field-flow fractionation and transmission electron microscopy. J Control Release. 2004; 95: 217-27.
138. Dubes A, Parrot-Lopez H, Abdelwahed W, Degobert G, Fessi H, Shahgaldian P, et al. Scanning electron microscopy and atomic force microscopy imaging of solid lipid nanoparticles derived from amphiphilic cyclodextrins. Eur J Pharm Biopharm. 2003; 55: 279-282.
139. Buhr E, Senftleben N, Klein T, Bergmann D, Gnieser D, Frase CG, et al. Characterization of nanoparticles by scanning electron microscopy in transmission mode. Meas Sci Technol. 2009; 20: 084025.
140. Montasser I, Fessi H, Coleman AW. Atomic force microscopy imaging of novel type of polymeric colloidal nanostructures. Eur J Pharm Biopharm. 2002; 54: 281-4.

141. Shi HG, Farber L, Michaels JN, Dickey A, Thompson KC, Shelukar SD, et al. Characterization of crystalline drug nanoparticles using atomic force microscopy and complementary techniques. Pharm Res. 2003; 20: 479-84.
142. Radomska-Soukharev A. Stability of lipid excipients in solid lipid nanoparticles. Adv Drug Deliv Rev. 2007; 59: 411-8.
143. Kuo YC, Lin TW. Electrophoretic mobility, zeta potential, and fixed charge density of bovine knee chondrocytes, methyl methacrylate-sulfopropyl methacrylate, polybutyl-cyanoacrylate, and solid lipid nanoparticles. J Phys Chem B. 2006; 110: 2202-2208.
144. Scholes PD, Coombes AG, Illum L, Davis SS, Watts JF, Ustariz C, et al. Detection and determination of surface levels of poloxamer and PVA surfactant on biodegradable nanospheres using SSIMS and XPS. J Control Release. 1999; 59: 261-78.
145. Kreuter J. Evaluation of nanoparticles as drug-delivery systems. III: materials, stability, toxicity, possibilities of targeting, and use. Pharm Acta Helv. 1983; 58: 242-50.
146. Polakovic M, Görner T, Gref R, Dellacherie E. Lidocaine loaded biodegradable nanospheres. II. Modelling of drug release. J Control Release. 1999; 60: 169-77.
147. Jo YS, Kim MC, Kim DK, Kim CJ, Jeong YK, Kim KJ, et al. Mathematical modelling on the controlled-release of indomethacin-encapsulated poly(lactic acid-co-ethylene oxide) nanospheres. Nanotechnology. 2004; 15: 1186.
148. Jalil R, Nixon JR. Microencapsulation using poly(DL-lactic acid). III: Effect of polymer molecular weight on the release kinetics. J Microencapsul. 1990; 7: 357-74.
149. Jalil R, Nixon JR. Biodegradable poly(lactic acid) and poly(lactide-co-glycolide) microcapsules: problems associated with preparative techniques and release properties. J Microencapsul. 1990; 7: 297-325.
150. zur Mühlen A, Schwarz C, Mehnert W. Solid lipid nanoparticles (SLN) for controlled drug delivery-drug release and release mechanism. Eur J Pharm Biopharm. 1998; 45: 149-55.
151. Higami M, Ueno S, Segawa T, Iwanami K, Sato K.Simultaneous synchrotron radiation X-ray diffraction-DSC analysis of melting and crystallization behavior of trilauroylglycerol in nanoparticles of oil-in-water emulsion. J Am Oil Chem Soc. 2003; 80: 731-739.
152. Abbott Laboratories. Kaletra (lopinavir-ritonavir) package insert. North Chicago, IL; 2000.
153. Weiss RA. Special anniversary review: twenty-five years of human immunodeficiency virus research: successes and challenges. Clin Exp Immunol. 2008; 152: 201-210.

154. Gomez C, Hope TJ. The ins and outs of HIV replication. Cell Microbiol. 2005; 7: 621-626.
155. Vandegraaff N, Engelman A. Molecular mechanisms of HIV integration and therapeutic intervention. Expert Rev Mol Med. 2007; 9: 1-19.
156. Sham HL, Kempf DJ, Molla A, Marsh KC, Kumar GN, Chen CM, et al. ABT-378, a highly potent inhibitor of the human immunodeficiency virus protease. Antimicrob Agents Chemother. 1998; 42: 3218-24.
157. Molla A, Vasavanonda S, Kumar G, Sham HL, Johnson M, Grabowski B**.** Human serum attenuates the activity of protease inhibitors toward wild type and mutant humanimmunodeficiency virus. Virology. 1998; 250: 255-62.
158. Molla A, Korneyeva M, Gao Q, Vasavanonda S, Schipper PJ, Mo HM, et al. Ordered accumulation of mutations in HIV protease confers resistance to ritonavir. Nat Med. 1996; 2: 760-766.
159. Kumar GN, Dykstra J, Roberts EM, Jayanti VK, Hickman D, Uchic J, et al. Potent inhibition of the cytochrome P-450 3A-mediated human liver microsomal metabolism of a novel HIV protease inhibitor by ritonavir: a positive drug-drug interaction. Drug Metab Dispos. 1999; 27: 902-8.
160. Qazi NA, Morlese JF, Pozniak AL. Lopinavir/ritonavir (ABT-378/r). Expert Opin Pharmacother. 2002; 3: 315-27.
161. King JR, Wynn H, Brundage R, Acosta EP. Pharmacokinetic enhancement of protease inhibitor therapy. Clin Pharmacokinet. 2004; 43: 291–310.
162. Kumar GN, Jayanti V, Lee RD, Whittern DN, Uchic J, Thomas S, et al. In vitro metabolism of the HIV-1 protease inhibitor ABT-378: species comparison and metabolite identification. Drug Metab and Dispos. 1999; 27: 86-91.
163. du Plooy M, Viljoen M, Rheeders M. Evidence for time dependent interactions between ritonavir and lopinavir/ritonavir plasma levels following P-glycoprotein inhibition in Sprague-Dawley rats. Biol Pharm Bull. 2011; 34: 66-70.
164. Agarwal S, Pal D, Mitra AK. Both P-gp and MRP2 mediate transport of lopinavir, a protease inhibitor. Int J Pharm. 2007; 339: 139-47.
165. van Waterschoot RAB, ter Heine R, Wagenaar E, van der Kruijssen CMM, Rooswinkel RW, Huitema ADR. Effects of cytochrome P450 3A (CYP3A) and the drug transporters P-glycoprotein (MDR1/ABCB1) and MRP2 (ABCC2) on the pharmacokinetics of lopinavir. J Pharmacol. 2010; 160: 1224-1233.

166. Griffin LT, Annaert P, Brouwer K. Influence of drug transport proteins on pharmacokinetics and drug interactions of HIV protease inhibitors. J Pharm Sci. 2011; 100: 3636-3654.
167. Zha W, Zha BS, Zhou F, Zhou H, Wang G. The cellular pharmacokinetics of HIV protease inhibitors: current knowledge and future perspectives. Curr Drug Metab. 2012 ; 13: 1174-83.
168. Wong HL, Chattopadhyay N, Wu XY, Bendayan R. Nanotechnology applications for improved delivery of antiretroviral drugs to the brain. Adv Drug Del Rev 2010; 62: 503-515.
169. Chandwani1 A, Shuter J. Lopinavir/ritonavir in the treatment of HIV-1 infection: a review. Ther Clin Risk Manag. 2008; 4; 1023-1033.
170. Pierson T, McArthur J, Siliciano RF. Reservoirs for HIV-1: Mechanisms for viral persistence in the presence of antiviral immune responses and antireteroviral therapy. Annu Rev Immunol. 2000; 18: 665-708.
171. Kumar GN, Jayanti VK, Johnson MK, Uchic J, Thomas S, Lee RD, et al. Metabolism and disposition of the HIV-1 protease inhibitor lopinavir (ABT 378) given in combination with ritonavir in rats, dogs, and humans. Pharm Res. 2004; 21: 1622-30.
172. Hoetelmans RM. Pharmacology of antiretroviral drugs. Antiviral Ther. 1999; 3: 29-41.
173. Yanovski JA, Miller KD, Kino T, Friedman TC, Chrousos GP, Tsigos C, Falloon J.Endocrine and metabolic evaluation of human immunodeficiency virus-infected patients with evidence of protease inhibitor-associated lipodystrophy. J Clin Endocrinol Metab. 1999; 84: 1925-1931.
174. Schrager LK, D'Souza MP. Cellular and anatomical reservoirs of HIV-1 in patients receiving potent antiretroviral combination therapy. JAMA. 1998; 280: 67-71.
175. Lanao JM, Briones E, Colino CI. Recent advances in delivery systems for anti-HIV1 therapy. J Drug Target. 2007; 15: 21-36.
176. Yong HL, Patrick JS. Preface- Delivery of antiretroviral drugs. Adv Drug Del Rev. 1999; 39; 1-3.
177. Wong HL, Chattopadhyay N, Wu XY, Bendayan R. Nanotechnology applications for improved delivery of antiretroviral drugs to the brain. Adv Drug Del Rev. 2010; 62: 503-515.
178. Foy M, Sperati CJ, Lucas GM, Estrella MM. Drug interactions and antiretroviral drug monitoring. Curr HIV/AIDS Rep. 2014; 11: 212-22.

179. Agarwal S, Boddu SH, Jain R, Samanta S, Pal D, Mitra A. Peptide prodrugs: Improved oral absorption of lopinavir, a HIV protease inhibitor. Int J Pharm. 2008; 359: 7-14.
180. Else LJ, Douglas M, Dickinson L, Back DJ, Khoo SH, Taylor GP. Improved oral bioavailability of lopinavir in melt-extruded tablet formulation reduces impact of third trimester on lopinavir plasma concentrations. Antimicrob Agents Chemother. 2012; 56: 816-24.
181. Jain S, Sharma JM, Jain AK, Mahajan RR. Surface-stabilized lopinavir nanoparticles enhance oral bioavailability without co-administration of ritonavir. Nanomedicine (Lond). 2013; 8: 1639-55.
182. Gunaseelan S, Gunaseelan G, Deshmukh M, Zhang X, Sinko PJ. Surface modifications of nanocarriers for effective intracellular delivery of antiretroviral drugs. Adv Drug Deliv Rev. 2010; 62: 518-531.
183. Sharma P, Garg S. Pure drug and polymer based nanotechnologies for the improved solubility, stability, bioavailability and targeting of anti-HIV drugs. Adv Drug Deliv Rev. 2010; 62: 491-502.
184. Destache CJ, Todd B, Christensen K, Shibata A, Sharma A, Dash A. Combination antiretroviral drugs in PLGA nanoparticles for HIV-1. BMC Infect Dis. 2009; 9; 198.

Chapter 2

Analytical and Bioanalytical Methods

2.1 Introduction

Bioanalytical chemistry is the qualitative and quantitative analysis of drug substances in biological fluids (mainly plasma and urine) or tissue. It plays a significant role in the evaluation and interpretation of bioavailability, bioequivalence and pharmacokinetic data [1]. The main analytical phases that comprise analytical and bioanalytical services are method development, method validation and sample analysis (method application). Owing to increased interdependence among countries in recent times, it has become necessary for results of many analytical methods to be accepted internationally. Consequently, to assure a common level of quality, the need for and use of validated methods has increased [2]. Pharmacokinetic and bio-equivalency studies require very precise and accurate assay methods that are well validated to quantify drugs in biological samples. The assay methods have to be sensitive enough to determine the biological sample concentration of the drug and/or its metabolite(s) for a period of about five elimination half-lives after dosage of the drug [3]. The assay methods also have to be very selective to ensure reliable data, free from interference of endogenous compounds and possible metabolites in the biological samples.

An insensitive and inaccurate analytical method results in erroneous conclusions about the drug product. As an antecedent to formulation development, analytical method development and validation was undertaken. Though, there are several methods described in the literature for the analysis of lopinavir in drug products and bulk formulations [4, 5]. We developed and validated in-house analytical method that was customized to suit our needs. For analysis of lopinavir in aqueous samples, high performance liquid chromatography (HPLC) method has been developed and validated in the present work.

Several simultaneous bioanalytical methods, using liquid chromatography tandem mass spectrometry (LC-MS), have been reported for estimation of lopinavir in human plasma and/or other biological matrices [6-13]. Extensive literature survey reveals that few bio-analytical methods [14-17] employing high-performance liquid chromatography (HPLC) have also been developed for estimation of lopinavir in plasma matrix. Although, it is indisputable that some of the earlier reported methods are sensitive and accurate, they mostly rely on the use of LC-MS technique that makes them expensive and involves many steps for sample preparation and processing. Moreover, most of these methods were aimed for simultaneous estimation of lopinavir with other protease inhibitors in human plasma thus, were not suitable for animal

studies. Extensive literature survey did not reveal any bioanalytical method for estimation of lopinavir in rat plasma which can be useful for *in vivo* pharmacokinetic evaluation of drug delivery systems containing lopinavir in rat models. Therefore, it was envisaged to develop a simple, rapid, sensitive, accurate and reliable HPLC method for estimation of lopinavir in rat plasma.

2.2 Analytical method development and validation using HPLC

2.2.1 Instruments

The liquid chromatography system employed was Shimadzu HPLC (Shimadzu, Japan) with solvent delivery system from binary pumps (Model LC-20AD, Prominence Liquid Chromatograph, Shimadzu, Japan), auto injector (Model SIL-20A HT, Prominence Auto Sampler, Shimadzu, Japan) and photo diode array (PDA) UV detector (Model SPD-M20A, Prominence UV Detector, Shimadzu, Japan). Data collection and integration was accomplished using LC Solutions, 1.25 version software.

Other instruments used in the method development and validation include vortex mixer (Model VX-200, Labnet International Inc., USA), sonicator (Model SONICA® 2200 MH, Soltec, Italy), refrigerated centrifuge (Model C-24 BL, Remi, India) and deep freezer (Model BFS-345-S, Celfrost Innovations Pvt Ltd., India). pH meter (Model pHTestr 30, Eutech Instruments, Singapore) was used for measuring pH of all buffer systems used. Membrane filters of 0.22 µm (Millipore, USA) were used for filtration of aqueous phase of mobile phase system.

The HPLC system was stabilized for 1 h at 1 ml/min flow rate, through baseline monitoring prior to actual analysis. Lopinavir was monitored at a wavelength of 210 nm.

2.2.2 Chemicals and Reagents

Lopinavir was obtained as a gift sample from Mylan Laboratories, India. Acetonitrile (HPLC grade), methanol (HPLC grade) and ammonium acetate (LiChropur®) were purchased from Merck laboratories, India. Ethanol and polyethylene glycol (PEG) 400 were purchased from S.D. Fine Chem. Ltd., India. Milli-Q water purification system (Millipore, USA) was used for obtaining high quality HPLC grade water.

2.2.3 Sample preparation

The primary stock solution of 1 mg/ml of lopinavir was prepared in methanol. From the primary stock solution, working stock solution was prepared to get the concentration of 100

μg/ml of lopinavir. Appropriate dilutions of the working stock solution were carried out in methanol to get different concentrations of aqueous standards of lopinavir.

2.2.4 Method development

In the analytical method development, various combinations of mobile phases (with different strengths, compositions and pH conditions) and stationary phases (columns) were explored to produce quality chromatogram of lopinavir. Quality parameters such as peak shape, tailing factor, retention time (RT) and height equivalent to theoretical plates (HETP) were considered for the optimization of chromatography conditions.

2.2.5 Method validation

The validation was performed as per ICH guidelines. The developed HPLC method was validated with respect to the following parameters [18].

a) Specificity

To determine the specificity of the developed method in the presence of excipients, the drug was spiked with the excipient used for the preparation of nanoformulation. The drug was extracted from these excipient by sonication in DCM and methanol pre-mixture (50:50 v/v) for 5 min followed by centrifugation at 10,000 rpm for 15 min. The supernatant solution was diluted with the methanol and injected into the HPLC. A placebo formulation was processed separately as mentioned above and injected into the HPLC system followed by the standard lopinavir solution (1000 ng/ml). The developed chromatograms were also analysed by HPLC-PDA detector to check the peak integrity as peak purity. The chromatograms of placebo formulation and standard lopinavir were compared to monitor interferences from excipients at the retention time of lopinavir.

b) Linearity and range

The linearity plot was constructed for lopinavir in the range of 125 to 8000 ng/ml. The primary stock solution of 1 mg/ml of lopinavir was prepared in methanol. From the primary stock solution, secondary stock solution of 100 μg/ml lopinavir was prepared. Appropriate dilution of the primary and secondary stock solutions were carried in methanol to get calibration standards (125, 250, 500, 1000, 2000, 4000 and 8000 ng/ml) and analytical quality control samples (LQC = 375, MQC = 1500 and MQC = 6000 ng/ml) of lopinavir. The calibration curve was plotted as concentration of the respective drug solutions versus the peak

area at each level for six days. The coefficient of regression (r^2), slope and intercept values were determined and statistically evaluated.

c) Precision

Precision reflects the random errors which occur in a method. Precision is usually measured as the coefficient of variation or relative standard deviation (RSD) of analytical results acquired from independently prepared quality control standards. The precision of the method was determined at quality control levels covering entire range of linearity. The intraday precision was evaluated by analysing six sample solutions (n=6) at each level in two different sets in a day. Similarly, the inter-day precision was evaluated in three consecutive days (n=18). The lopinavir concentrations were determined and the relative standard deviations (RSD) were calculated.

d) Accuracy and recovery

In order to evaluate the accuracy of the proposed method, a recovery test was performed by adding a known amount of standard solutions to the placebo formulation before extraction, followed by analysis using the proposed method. The recovery studies were done in the three different levels at 80%, 100%, and 120% of assay concentration using the standard spiking method. The placebo formulation was spiked with 800, 1000, and 1200 ng/ml of standard lopinavir. The prepared samples were analysed using proposed chromatographic conditions. The amount recovered was using the linearity curve. The percentage of recovery was calculated according to the following formula:

$$\textbf{Recovery}\ (\%) = \frac{\textbf{(Amount found in spiked placebo sample)}}{\textbf{Spiked amount}}\ \text{X}\ 100$$

e) Sensitivity

The sensitivity of the method was assessed by using seven calibration standards and was expressed as a limit of detection (LOD) and limit of quantification (LOQ) for lopinavir. The LOD and LOQ were determined using standard deviation of intercept (σ) and slope (s) of the calibration curve. Following equations were used to determine LOD and LOQ values:

$$(1)\quad \textbf{LOD} = \frac{\textbf{3.3}\sigma}{\textbf{s}} \qquad (2)\quad \textbf{LOQ} = \frac{\textbf{10}\sigma}{\textbf{s}}$$

f) Stock solution stability

The solution stability of lopinavir was carried out at bench top, refrigerated condition and in auto-sampler. A stock solution of 100 µg/ml of lopinavir was prepared in methanol. The solution was further diluted to get the lopinavir concentration of 1000 ng/ml and subjected to

bench top and auto-sampler stability conditions. The stock solution was subjected to the refrigerated stability condition and monitored for 30 days as long-term stability. The samples after being subjecting to various stability conditions were injected into the HPLC system. The concentration was determined at pre-determined time interval using freshly prepared calibration curve.

g) System Suitability

The purpose of the system suitability test is to ensure that the complete testing system (including instrument, reagents, columns, and analysts) is suitable for the intended application. System suitability testing is an integral part of liquid chromatographic methods which is used to verify the reproducibility of the chromatographic system for the analysis to be done. The tests are based on the concept that the equipment, electronics, analytical operations, and samples to be analysed constitute an integral system that can be evaluated as such. In the current USFDA guidelines on "validation of chromatographic methods," the following acceptance limits are proposed as initial criteria.

For the present study, 1000 ng/ml of lopinavir was injected six times to record the system suitability parameters. From results, it is evident that tested parameters are well within the acceptable limits. Results are presented in Table 2.5.

h) Sample preparation and method application

Validated method was successfully employed for estimation of lopinavir in various samples. For encapsulation efficiency, 1 ml of nanosuspension was added to 5 ml DCM and methanol pre-mixture (50:50, v/v) to dissolve the polymer matrix and release the free drug. Samples were then subjected to ultra-sonication using a probe sonicator (Vibra cell, Sonics, USA) for 5 min at a fixed amplitude (30 W output) followed by centrifugation for 15 min at 10,000 rpm, 4 ^{o}C. A clear supernatant was obtained in each case; 1 ml of the supernatant was transferred to 10 ml calibrated volumetric flasks and the volume was made with the methanol.

For solid sample analysis, a quantity of the product, powdered tablets (Lopimune® 200 mg tablets) or nanoparticles equivalent to 5 mg lopinavir were weighed and taken into a 10 ml volumetric flask. In all the cases, the volume was made up to 10 ml with the solvent system (DCM: Methanol 50:50, v/v), sonicated for 5 min and centrifuged (Remi, Mumbai, India) at 10, 000 rpm for 15 min. A clear supernatant was obtained in each case; 1 ml of the supernatant was transferred to 10 ml calibrated volumetric flasks and the volume was made with the methanol.

2.2.6 Results and discussion

2.2.6.1 Method development

To optimize the RP-HPLC parameters, several mobile phase compositions were tried in combination with different columns and pH conditions. A satisfactory separation and good peak symmetry for lopinavir was obtained using Phenomenex column (250 x 4.6 mm; 5 µm particle size) with isocratic mobile phase ammonium acetate: ACN (20:80 v/v) at a flow rate of 1.0 ml/min. Lopinavir was monitored at a wavelength of 210 nm.

Initial trials of chromatographic separations were tried with ammonium acetate buffer in combination of organic phases like methanol and acetonitrile. After a series of screening experiments, it was concluded that acetonitrile gave better peak shapes than methanol. The chromatographic conditions were further optimized by using different compositions of acetonitrile in the mobile phase. From trials, a significant effect of acetonitrile compositions on quality of chromatogram was observed. A longer retention time of more than 18.0 min and broad peak of lopinavir was obtained with low acetonitrile (45 %) composition in mobile phase. Also, the peak tailing of lopinavir was more than 2.To reduce the peak tailing and total elution time of lopinavir, it was decided to increase the organic phase of the mobile phase up to 80%. High amount of ACN significantly reduced the elution time of lopinavir to 7.10 with tailing factor less than 2.

To determine the effect of mobile phase pH on quality of chromatogram, optimization trials for mobile phase pH were also conducted at three different pH levels. By attempting the various pH of the mobile phase (pH 4.5, unadjusted, and 9.5), it was observed that the retention time for lopinavir was found to be around 7.20 min in all the above mentioned pH and there was no significant effect of pH on the retention time. The peak shape was found to be good across the pH range. This can be explained on the fact that analyte (lopinavir) is a weakly ionized hydrophobic compound. Hence, for the present method no pH adjustment for ammonium acetate was made.

For the selection of stationary phase, chromatographic separation was performed in Waters Symmetry and Luna Phenomenex columns. The retention time of lopinavir on Waters Symmetry C18 (250 × 4.6 mm, 5 μm) was relatively longer as compared to Phenomenex (250 × 4.6 mm, 5 μm). The peak was broader and column efficiency was less in case of Waters

Symmetry column leaving it unconsidered for the present study. Data obtained from optimization trials are summarized in Table 2.1.

Table 2.1. Optimization trials for chromatographic conditions.

Parameters	**Effect of organic phase (% ACN)**			**Effect of mobile phase pH (with fixed 80 % ACN)**			**Effect of stationary phase**	
							Luna Phenomenex	**Waters Symmetry**
	45	**65**	**80**	**4.5**	**6.8**	**9.5**	**Unadjusted pH & 80% ACN**	
R_t	18.40	13.50	7.10	7.10	7.30	7.30	7.30	8.10
T	2.50	1.28	1.04	1.05	1.09	1.09	1.09	2.01
K	1.95	2.01	2.21	2.09	2.01	2.01	2.01	1.98
N	8060.50	9345.40	10005.20	99901.91	99005.60	98805.20	99005.60	88564.40

2.2.6.2 Method validation

a) Specificity

The present method was found to be highly specific as there was no interference at retention time of the lopinavir from the placebo formulation. The specificity of the method was also investigated by conducting a photodiode-array analysis to investigate the integrity of the drug peaks and to clarify the purity of the peaks. The total peak purity was monitored for lopinavir. The peak purity was found to be greater than the peak purity threshold which indicated that the peak of lopinavir was pure and there was no interference from excipients.The specificity of the method is illustrated in Fig. 2.1.

b) Linearity and range

The response for the detector was determined to be linear over the range of 125 to 8000 ng/ml for lopinavir. The calibration curve was plotted as concentration of the drug versus the response (area of the drug peak) at each level (Table 2.2). The proposed method was evaluated by its coefficient of determination and intercept value calculated in the statistical study (n=6). From a linear regression analysis, the slope (± standard error) and intercept (± standard error) were found to be 85.5 (± 0.82) and 2916.82 (± 323.06) respectively with a regression coefficient value of 0.9995.

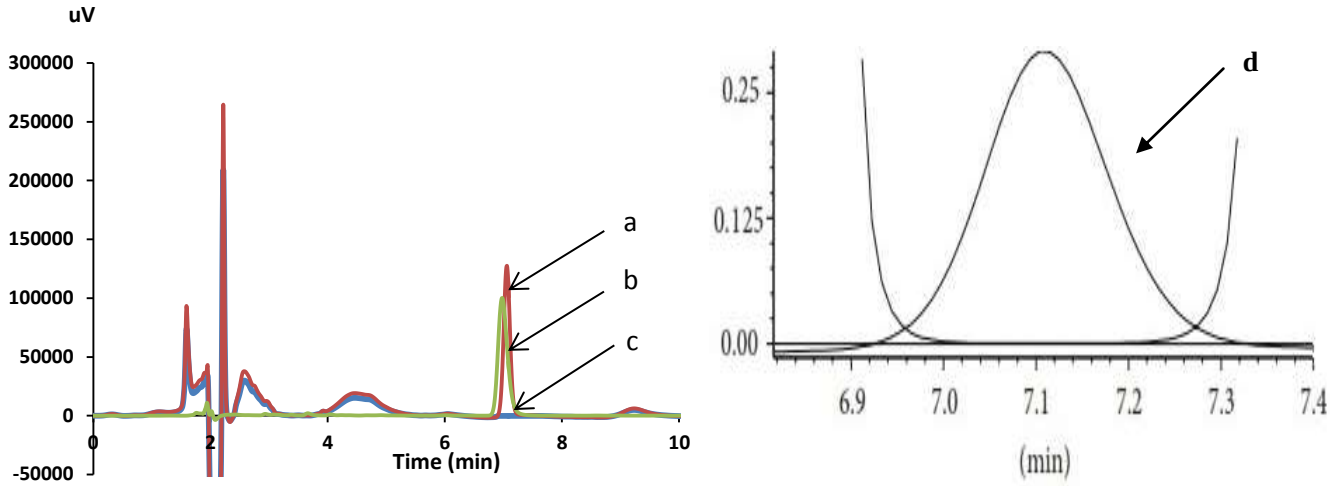

Fig.2.1: Representative chromatograms of **a)** pure lopinavir (1000 ng/ml); **b)** extracted lopinavir (1000 ng/ml) from nanoformulation; **c)** extracted blank nanoformulation; and **d)** purity graph of extracted lopinavir.

c) Precision

The precision was carried out at three different concentrations of lopinavir over the linearity range. The % RSD of inter-day and intra-day precision obtained was less than 5% for lopinavir. The intra-day and inter-day precision of lopinavir was in the range of 0.93–1.32 and 2.57–4.58, respectively (Table 2.3). From the data obtained, the developed HPLC method was found to be highly precise.

d) Accuracy and recovery

The assay concentration for lopinavir was considered to be 1000 ng/ml. The recovery was calculated using the placebo spiking method at three levels of 80–120% of the assay concentration. The mean absolute recovery ranged from 97.19–102.02%. With the proposed HPLC method, lopinavir showed consistent and high absolute recoveries at all the tested concentration levels. The recovery data for the lopinavir is shown in Table 2.4.

e) Sensitivity

In the proposed method, the LOD and LOQ of lopinavir were calculated as 27.79 and 92.54 ng/ml respectively. For practical purpose, the LLOQ was considered as 125 ng/ml.

f) Solution stability

While determining the solution stability of lopinavir, it was observed that the methanolic solution of lopinavir is stable at bench top and auto-sampler for 12 h and 24 h, respectively. Also lopinavir was stable at refrigerated condition for 30 days.

Table 2.2. Linearity and range of lopinavir.

Nominal concentrations (ng/ml)	**Back[a] calculated concentrations (ng/ml)±SD**	**RSD[b] (%)**	**Accuracy[c] (%)**	**RE[d] (%)**
125	131.10 ± 5.90	4.50	104.88	4.88
250	252.20 ± 10.81	4.28	100.88	0.88
500	507.61 ± 19.10	3.76	101.52	1.52
1000	1002.21 ± 32.01	3.10	102.20	2.20
2000	1940.42 ± 46.22	2.38	97.01	-2.99
4000	3910.11 ± 34.80	0.89	97.75	-2.25
8000	8050.33 ± 30.40	0.38	100.62	0.62

[a]Each value represents the average of six independent determinations (n = 6).

[b] $\mathbf{RSD}\ (\%) = \frac{\mathbf{SD}}{\mathbf{Mean}}\mathbf{x\ 100}$; [c] $\mathbf{Accuracy} = \frac{\mathbf{Back\ calculated\ conc}}{\mathbf{Nominal\ conc}}\mathbf{x\ 100}$

[d] $\mathbf{RE}\ (\%) = \frac{\mathbf{Back\ calculated\ conc - Nominal\ conc}}{\mathbf{Nominal\ conc}}\mathbf{x\ 100}$

Table 2.3. The precision data of lopinavir by the proposed HPLC method.

QC levels (ng/ml)	**Intra-day (n = 12)**		**Inter-day (n = 18)**	
	Mean±SD	**RSD (%)**	**Mean±SD**	**RSD (%)**
LQC (375)	381.11± 5.41	1.41	377.11 ± 18.50	4.90
MQC (1500)	1480.01 ± 28.50	1.92	1490.08 ± 36.91	2.47
HQC (6000)	6170.20 ± 38.01	0.61	5930.06 ± 55.67	0.90

Table 2.4. Recovery studies by placebo-spiking method.

Drug products	Spiked level (%)	Amount added (ng/ml)	Mean absolute[a] recovery[b] ± SD (%)	RE[c] (%)
Tablets	80	800	101.98 ± 3.05	1.98
	100	1000	97.19 ± 2.94	-2.81
	120	1200	98.08 ± 2.67	1.92
NPs	80	800	102.01 ± 3.02	2.01
	100	1000	99.06 ± 3.66	-0.94
	120	1200	98.79 ± 2.44	-1.21

[a]Each value represents the average of six independent determinations (n = 6).

[b] $\mathbf{Recovery} = \frac{\mathbf{Amount\ recovered}}{\mathbf{Amount\ added}}\ \mathbf{x\ 100}$; [c] $\mathbf{RE} = \frac{\mathbf{Back\ calculated\ conc - Nominal\ conc}}{\mathbf{Nominal\ conc}}\ \mathbf{x\ 100}$

Table 2.5: System suitability parameters.

Parameter	Limit	Observed value
Capacity factor	K' > 2	2.208 ± 0.002
Injection precision	RSD < 1% for n > 6	0.23
Tailing factor	T < 2	1.04 ± 0.13
Theoretical plates/meter	N > 2000	10013.41± 120.50

2.3 Bioanalytical method development and validation

2.3.1 Method development

In the process of analytical method development for lopinavir, mobile phase optimization was done by trying different aqueous phase and non-aqueous phase combinations. Various buffers with different pH and in varying compositions with acetonitrile and/or methanol were investigated. Based on analytical method, composition of mobile phase was further fine-tuned to produce good quality chromatogram of lopinavir in plasma matrix. Mobile phase was selected based on the criteria of peak properties (retention time and asymmetric factor), sensitivity (height and area), ease of preparation and applicability of the method for *in vivo* studies in rats.

2.3.2 Stock solution preparation and calibration range

Primary stock solution of lopinavir (1 mg/ml) was prepared in volumetric flask by dissolving accurately weighed amount of lopinavir in methanol. Secondary stock solutions (10X) of lopinavir were prepared by making appropriate dilutions in methanol**.**

Plasma calibration standards and plasma quality control samples were prepared by spiking 10 µl of appropriate standard solutions of lopinavir in 90 µl of drug-free rat plasma to obtain final concentrations of 250, 500, 1000, 1500, 2000, 2500, 3000, 4000 ng/ml for calibration curve and 800, 1600 and 3200 ng/ml for lower quality control (LQC), medium quality control (MQC) and higher quality control (HQC) samples respectively. Blank sample was prepared by spiking 10 µl of methanol (drug diluent) in 90 µl of blank plasma. All solutions were stored at 4 ^{o}C till further use.

2.3.3 Extraction technique

A simple, single-step protein precipitation method was followed for extraction of lopinavir from wistar rat plasma. A 100 µl of the drug spiked plasma sample was pipetted into a RIA vial and 350 µl of acetonitrile (protein precipitating solvent) was added to it and vortex mixed for 2 min. Samples were then centrifuged at 9000 rpm at 4 ^{o}C for 20 min. From the centrifuged samples, 300 µl of supernatant was transferred to a sample loading vial and injected into the HPLC system.

2.3.4 Bioanalytical method validation

The developed method was validated statistically as per the guidelines given by International Conference on Harmonization [18] and United States Pharmacopoeia (USP 2003) [19]. Steps involved in bioanalytical method validation are summarized in Fig 2.2.

a) Selectivity

Selectivity of the method can be defined as non-interference by the proteins and other impurities present in the bio-matrix at the retention time shown by lopinavir. Six different lots of drug-free rat plasma samples were extracted and analyzed for assessment of specificity and selectivity. Overlaid chromatograms of blank plasma, plasma standard (1500 ng/ml) and *in vivo* test sample are shown in Fig. 2.3.

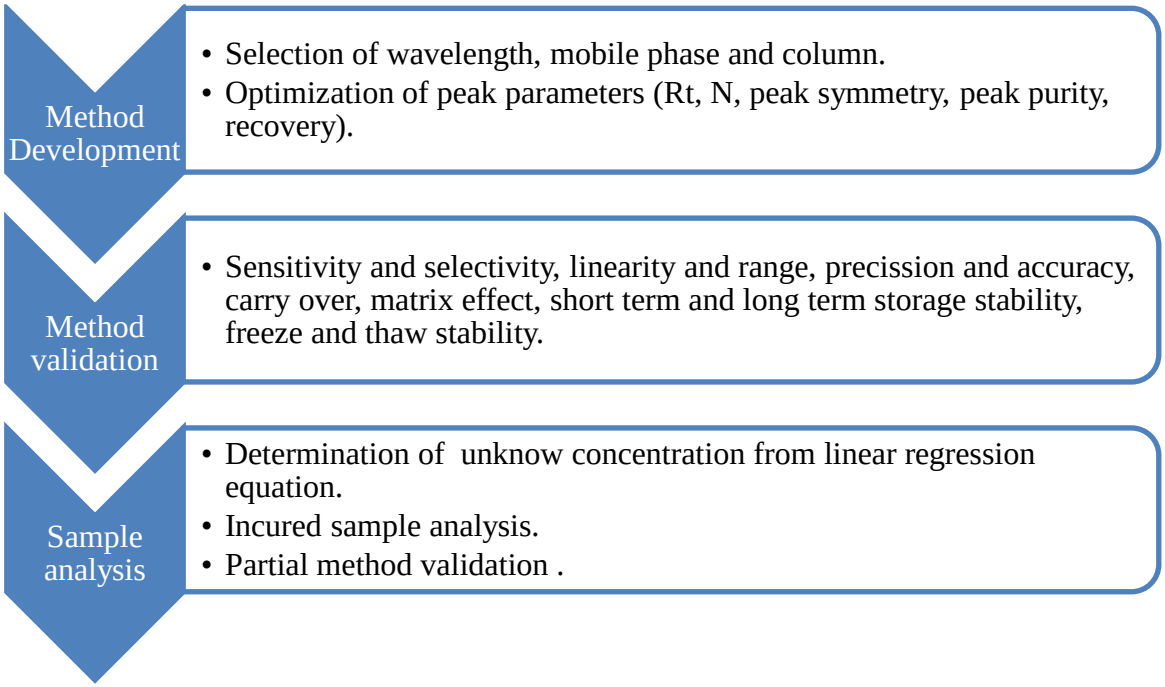

Fig. 2.2: Steps involved in the bioanalytical method development and validation.

b) Linearity

Plasma calibration standards were prepared and analyzed in five independent runs. Individual standard curves were constructed using the observed peak area to that of nominal concentration. A calibration curve was constructed from a blank sample (plasma sample processed without drug) and eight non-zero concentrations ranging from 250 ng/ml to 4000 ng/ml. The data are presented in Table 2.6.

c) Accuracy

For determining the accuracy of the proposed method, different quality control (QC) levels of lopinavir in plasma (LQC = 800 ng/ml, MQC = 1600 ng/ml and HQC = 3200 ng/ml) were prepared independently and analyzed (n = 6). The data are presented in Table 2.7.

d) Precision

Repeatability was determined by analyzing all three QC levels of drug concentrations. Inter-day and intra-day variation and analyst variations were studied to determine the intermediate precision of the proposed method. Three QC levels of drug concentrations in triplicates were prepared twice in a day and studied for intra-day variation (n = 6). The same protocol was followed for three different days to study inter-day variation (n = 18).The percent relative standard deviation (%RSD) was calculated from the predicted concentrations obtained by the regression equation. The data are presented in Table 2.8.

e) Sensitivity

Limit of quantification (LOQ) is defined as the minimum concentration of lopinavir in plasma sample that can be quantified with less than 20% RSD [18, 19]. In order to determine LOQ, six independent plasma samples containing 250 ng/ml of lopinavir were prepared and analyzed using a developed method. The peaks were integrated and concentrations were calculated using calibration equation. Mean concentration and %RSD for these six values were determined.

The LOD and LOQ were also determined using standard deviation of intercept (σ) and slope (s) of the calibration curve. Following equations were used to determine LOD and LOQ values:

$$(1) \quad \mathbf{LOD} = \frac{3.3\sigma}{s} \qquad (2) \quad \mathbf{LOQ} = \frac{10\sigma}{s}$$

f) Recovery

Recovery of the drug was determined by comparing the area obtained from plasma (extracted) samples with analytical standard (un-extracted) samples. For the recovery experiment, plasma extracted samples were prepared by spiking lopinavir at three different concentration levels (LQC, MQC and HQC) in triplicate. Precision of lopinavir recovery at each level (n = 3) was determined and is presented in Table 2.9.

g) Stability

Freeze thaw stability of lopinavir in rat plasma was determined using three QC (LQC, MQC and HQC) samples for three freeze-thaw cycles. Total of four sets were prepared in triplicates and one set of the prepared concentrations was analyzed on the day of preparation (no freeze thaw cycle) and the remaining three sets were frozen at –20 ^{o}C for 24 h. Frozen samples were thawed by keeping the sealed tubes at room temperature for at least 1 h. One set in triplicate was analyzed and the remaining two sets were kept at –20 ^{o}C for freezing and were analyzed after two and three freeze thaw cycles. The percentage deviation from the mean concentrations observed on the day of preparation was calculated and is presented in Fig. 2.4a.

Post extraction stability of the processed samples of lopinavir in rat plasma was investigated by preparing five sets of QC samples (LQC, MQC and HQC) in triplicates. Processed samples were kept in the sample rack of auto sampler and samples were analyzed in triplicates every 6 h for 24 h period on the day of preparation. The percentage deviation from

the mean concentrations observed at zero time was calculated. Results obtained are shown in Fig. 2.4b.

Long-term stability of lopinavir in rat plasma was determined by preparing three QC samples (LQC, MQC and HQC). Total of four sets were prepared in triplicates and one set of the prepared concentrations was analyzed on the day of preparation. The remaining three sets were frozen at –20 ^{o}C. One set each of stored samples was analyzed after 3, 7 and 15 days of sample preparation by thawing them at room temperature. The percentage deviation from the mean concentrations observed on day of preparation was calculated and the values obtained are shown in Fig. 2.4c.

2.3.5 Pharmacokinetic Study

Lopinavir formulation for intravenous (IV) bolus administration was prepared by dissolving the drug in a solvent mixture of PEG 400, ethanol and water (10:40:50) just before the commencement of study. The formulation was administered through tail vein in male wistar rats (n = 6), weighing 180 to 220 g, at a dose of 5 mg/kg. Blood samples were drawn from retro-orbital plexus of wistar rats at 0.083, 0.17, 0.25, 0.50, 1.0, 2.0, 3.0, 4.0, 6.0, 8.0, 12.0 and 24 h post dose in microfuge tube pretreated with sodium citrate solution (3.8% *w/v*). Clear supernatant plasma was separated from the blood after the centrifugation at 3400 rpm, 4 ^{o}C, for 10 min. Samples were kept at –20 ^{o}C till further analysis. A baseline blank plasma sample was drawn from each animal before drug administration. All samples were processed according to the procedure described earlier and analyzed using the validated HPLC method.

Various pharmacokinetic parameters were calculated from measured lopinavir plasma concentrations verses time profiles after IV bolus administration using non-compartmental model and compartmental models in WinNonlin Professional software (Version 4.0, Pharsight Corporation, USA).

2.3.6 Results and discussions

2.3.6.1 Method development

Optimization of mobile phase consisting of aqueous phase (10 mM ammonium acetate) and acetonitrile (35:65 *v/v*) was based on peak properties (retention time and asymmetric factor) and sensitivity (height and area). With optimized mobile phase, retention time of lopinavir was found to be 13.51 ± 0.15 min with an asymmetric factor of 1.21 ± 0.10. Mobile phase had significant impact on elution time of lopinavir. The retention time of lopinavir was increased up to 21.02 min with decreasing acetonitrile composition from 65% to 50% *v/v*; whereas, same

composition of methanol (65% *v/v*) produced a broad peak of lopinavir with longer elution time. No significant effect of mobile phase pH on retention time and quality of chromatogram was observed. Hence, an isocratic mixture of 10 mM ammonium acetate (without pH adjustment) and acetonitrile in the ratio of 35:65 *v/v* was finally selected as mobile phase. The total chromatographic run time was 17 min and elution of lopinavir occurred at 13.51 min.

2.3.6.2 Method validation

a) Selectivity

Simple and efficient one-step precipitation technique was used to separate lopinavir from rat plasma. The technique was found to be suitable for estimation of lopinavir from bio-matrix with no interference from endogenous protein impurities. No interference was observed in processed test samples. Blank plasma sample also showed absence of any interference at retention time of the drug as shown in Fig. 2.3. Thus, the proposed method was found to be specific and selective for the estimation of lopinavir in rat plasma.

b) Linearity

Different concentrations and their corresponding areas are shown in Table 2.6. At all the concentration levels, %RSD did not exceed 5.93. Linearity was studied over a concentration range of 250 ng/ml to 4000 ng/ml. The calibration curve in rat plasma was linear in the selected calibration range. According to linear regression analysis, the slope (± standard error) and intercept (± standard error) were found to be 90.34 (± 0.87) and 2475.66 (± 532.97) respectively with a regression coefficient value of 0.996. Lower values of standard error of estimate (5.63) and MSSR (1.95×10^{-4}) indicates high precision of the developed method. Lower F_{cal} value of 0.039 in comparison to F_{crit} (5, 35) value of 2.48 at $p < 0.05$, further confirmed precision of the proposed method.

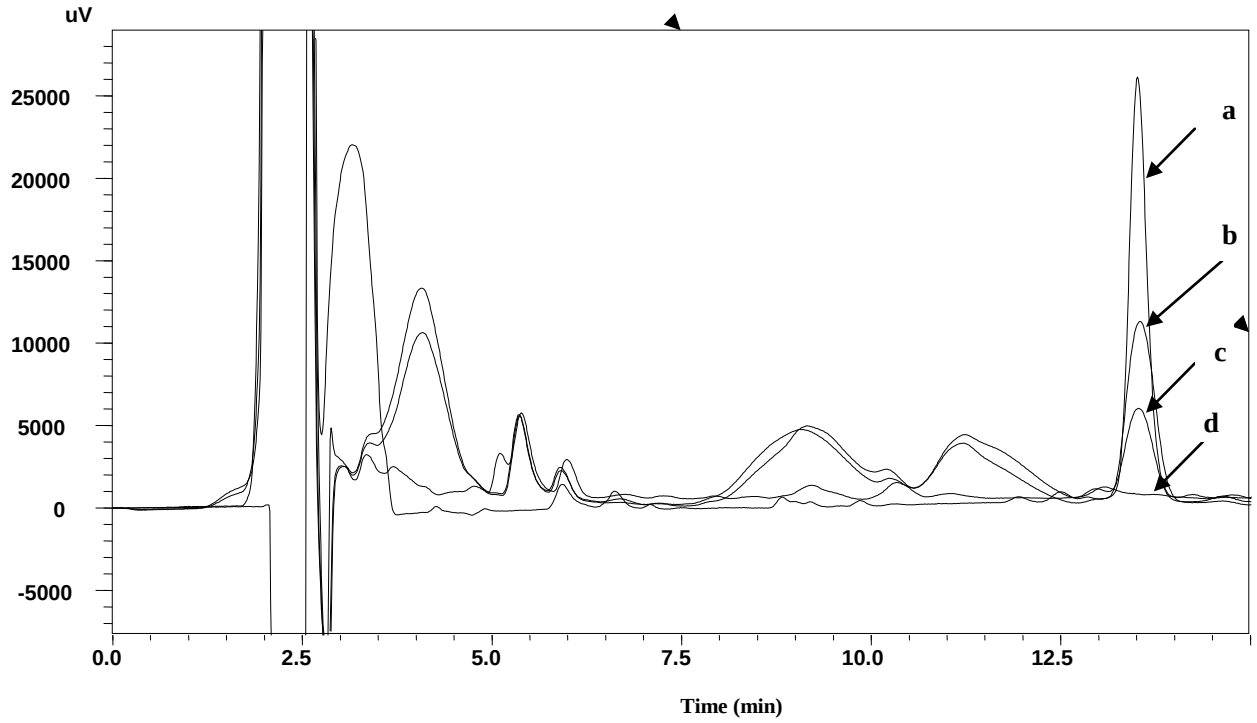

Fig. 2.3: Overlaid chromatograms of **a)** pure lopinavir (3200 ng/ml); **b)** plasma calibration standard (1500 ng/ml); **c)** *in vivo* test sample; and **d)** blank plasma.

Table 2.6. Calibration data of lopinavir in wistar rat plasma.

Nominal concentrations (ng/ml)	Back[a] calculated concentrations (ng/ml) ± SD[b]	RSD[b] (%)	Accuracy[c] (%)	RE[d] (%)
250	256.80 ± 12.61	4.91	102.72	2.72
500	490.49 ± 19.69	4.01	98.11	-1.89
1000	980.29 ± 40.60	4.14	98.29	-1.71
1500	1471.41 ± 45.45	3.09	98.10	-1.90
2000	1990.40 ± 55.60	2.79	99.49	-0.51
2500	2475.08 ± 60.69	2.45	99.10	-0.90
3000	2940.61 ± 64.56	2.19	98.11	-1.89
4000	3940.11 ± 75.70	1.92	98.45	-1.55

[a]Each value represents the average of five independent determinations (n = 5).

[b] $\mathbf{RSD}\ (\%) = \frac{\mathbf{SD}}{\mathbf{Mean}} \mathbf{x\ 100}$; $\mathbf{Accuracy} = \frac{\mathbf{Back\ calculated\ conc}}{\mathbf{Nominal\ conc}} \mathbf{x\ 100}$;

[d] $\mathbf{RE}\ (\%) = \frac{\mathbf{Back\ calculated\ conc - Nominal\ conc}}{\mathbf{Nominal\ conc}} \mathbf{x\ 100}$

c) Accuracy

All three quality control samples (LQC = 800 ng/ml, MQC = 1600 ng/ml and HQC = 3200 ng/ml) showed an accuracy ranging from –1.37% to 0.61% with maximum %RSD of 4.78 across all the QC levels, establishing the accuracy of the method (Table 2.7).

d) Precision

In repeatability study, %RSD ranged from 0.32 to 4.96 across all QC samples (Table 2.8). The %RSD values for intra-day variation were not more than 4.96 and for inter-day variation were less than 4.73. Acceptable %RSD values indicated the repeatability and intermediate precision of the method.

e) Sensitivity

The mean percentage accuracy of six independent samples of 250 ng/ml, calculated against calibration equation and was found to be 93.1 with a %RSD value of 4.88. Hence, the concentration of 250 ng/ml was considered as the lowest limit of quantification (LLOQ) for the proposed method. From the mean calibration curve (*n = 5*), LOD and LLOQ of lopinavir were calculated as 39.62 and 131.91 ng/ml respectively.

Table 2.7. Accuracy and precision data for the proposed method in wistar rat plasma.

Level	Predicted concentration[a] (ng/ml)			Mean accuracy[e] (%)
	Range	Mean[b] (±SD[c])	%RSD[d]	
LQC (800 ng/ml)	737 - 842	789.00 ± 37.74	4.78	-1.37
MQC (1600 ng/ml)	1608 - 1640	1623.46 ± 12.17	0.75	1.47
HQC (3200 ng/ml)	3168 - 3247	3219.54 ± 27.72	0.86	0.61

[a]Each value is mean of six independent determinations (*n* = 6); [b]Predicted concentration of lopinavir was calculated by linear regression equation; [c]Standard deviation; [d]Percentage relative standard deviation; [e]Accuracy is given in relative error % =[100 × (predicted concentration – nominal concentration)/nominal concentration.)].

Table 2.8. Results of intermediate precision study in wistar rat plasma.

Level	Intra-day repeatability (%RSD[a]) (*n*=3)			Inter-day repeatability (%RSD[a]) (*n*=18)
	Day-1	Day-2	Day-3	
LQC	4.37	3.30	4.34	4.73
	4.43	4.21	4.96	
MQC	0.32	2.17	1.89	1.44
	0.43	1.30	0.63	
HQC	1.03	0.69	0.60	1.57
	0.57	0.46	0.81	

[a]Percentage relative standard deviation.

f) Recovery

The absolute recovery of lopinavir from the spiked rat plasma samples, when compared with analytical standards of same concentration, was within 97.50% to 100.19% with %RSD less than 4.03 at each concentration level. The high (nearly 100%) mean percent recovery values (Table 2.9) which precludes the use of internal standard and low %RSD values (%RSD < 5.0) established the extraction efficiency of the selected solvent for precipitation and also robustness of the method.

Table 2.9. Absolute recovery of lopinavir from plasma samples following protein precipitation extraction method.

Nominal Concentrations (ng/ml)	% Mean recovery[a] (±SD[b])	%RSD[c]
LQC (800)	99.32 ± 4.01	4.03
MQC (1600)	97.50 ±1.32	1.35
HQC (3200)	100.19 ±1.44	1.44

[a]Percent drug recovery = [(Peak area of plasma standard/peak area of analytical standard of same concentration) ×100]; [b] Standard deviation; [c] Percentage relative standard deviation.

g) Stability

The stability of lopinavir in rat plasma was evaluated using QC samples under different stress conditions and the results obtained are shown in Fig. 2.4. In freeze thaw stability, no significant degradation of lopinavir was observed up to three cycles over a period of three days. The deviation from the zero time concentration was found to be less that 8.0% at the end of three freeze thaw cycles as shown in Fig. 2.4a. In post extraction stability study of the processed samples, lopinavir was found to be stable for 24 h, with a maximum deviation of less than 2.0% from the zero time concentration as shown in Fig. 2.4b

In long-term stability studies, lopinavir was found to be stable for 15 days when stored at –20 ^{o}C. The deviation in recoveries of lopinavir after analysis at 3, 7 and 15 days of sample preparation was found to be within acceptable limits (Fig. 2.4c). The results of this study indicated that storage temperature of –20 ^{o}C was adequate for storing the samples for at least 15 days.

2.3.7 Pharmacokinetic application

The developed and validated HPLC method for lopinavir estimation in rat plasma was applied to pharmacokinetic study of IV bolus administration of the drug in rats. The mean plasma concentration versus time profile of lopinavir following IV administration is given in Fig 2.5.

The time course of plasma drug concentration was found to follow a mono-exponential equation, concentration = 3168.7 $e^{-0.84t}$, with a good correlation coefficient (r^2 = 0.999) indicating that the drug follows one compartment open model in rats. The pharmacokinetic parameters obtained from the study using non-compartmental and compartmental analysis were area under the curve (AUC) = 3850.33 ± 263.87 h*ng/ml, area under the first-moment curve (AUMC) = 4403.07 ± 171.33 h^2*ng/ ml, mean retention time (MRT) = 1.15 ± 0.05 h, concentration at time zero (C_o) = 3168.68 ± 289.88 ng/ml, elimination half-life ($T_{½}$) = 0.82 ± 0.03 h and volume of distribution (V_{ss}) = 1592.09 ± 146.44 ml/kg.

Samples collected till 3 h (approximately equal to 4 times half-life of drug) post IV bolus administration of the drug were analyzed in the study indicating the sensitivity and the applicability of the *in vivo* pharmacokinetic studies of the drug in rats.

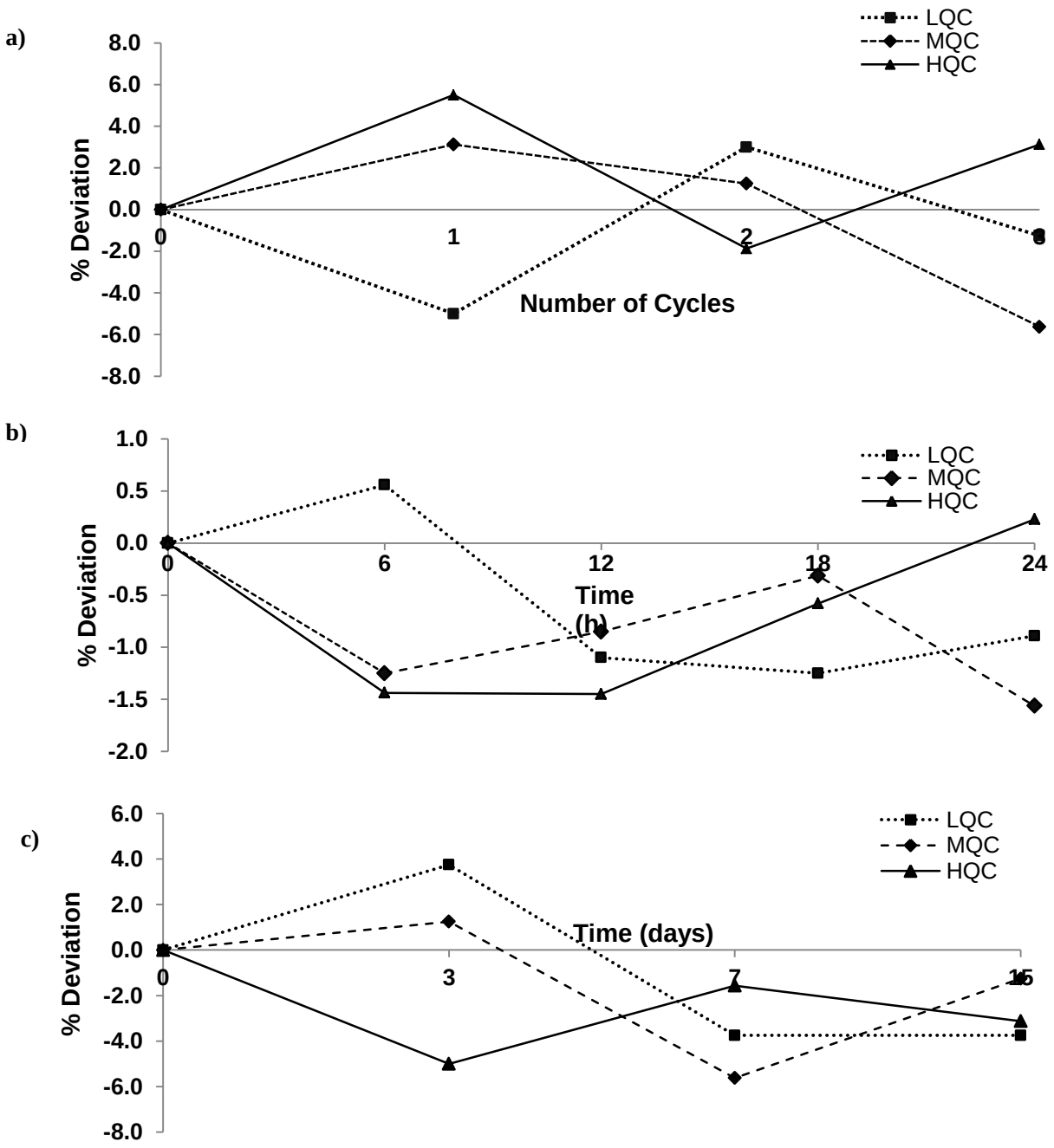

Fig. 2.4: Stability study of lopinavir in rat plasma **a)** freeze thaw stability; **b)** post extraction stability; **c)** long term stability. Each point represents mean of three independent determinations.

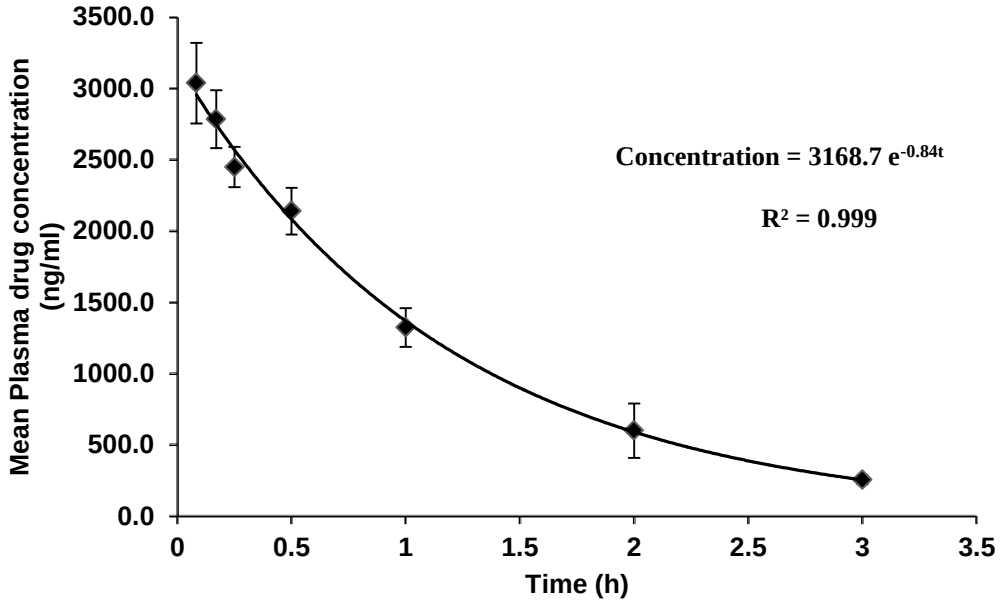

Fig. 2.5: The mean plasma concentration versus time profile of lopinavir in rats after intravenous bolus administration of the drug (5 mg/kg, *n* = 6).

2.4 Partial method validation for rat tissue samples

The proposed bioanalytical method was partially validated for analysis of lopinavir in tissue samples (liver, spleen and lymph node). Parameters for partial method validation were critically selected as per USFDA guidelines. Method was validated for recovery, sensitivity, selectivity, precision, accuracy, linearity, long term and short term stability.

2.4.1 Preparation of calibration curve and quality control samples

Tissue calibration standards and quality control samples were prepared by spiking 10 µl of appropriate standard solutions (10X) of lopinavir in 90 µl of blank tissue homogenate to obtain final concentrations of 200, 600, 1200, 1600, 3200, 6400 ng/ml for calibration curve and 800, 2000 and 4000 ng/ml for lower quality control (LQC), medium quality control (MQC) and higher quality control (HQC) samples respectively. Blank sample was prepared by spiking 10 µl of methanol in 90 µl of blank homogenate.

2.4.2 Sample preparation and extraction

After exsanguinations, tissues of interest (liver, spleen and mesenteric lymph nodes) were quickly removed, weighed and homogenized (25% w/v) in water: methanol (80:20) solution. Samples were stored at –70 ^{o}C until further analysis.

The plasma extraction protocol (section no 2.3.3) was followed with minor modification for recovery of drug from tissue samples. Briefly, in each aliquot (100 µl) of tissue homogenate

300 µl of acetonitrile (protein precipitating solvent) was added and vortex mixed for 2 min. Samples were then centrifuged (10,000 rpm; 4 ^{o}C) for 20 min and the resultant clean supernatant (75 µl) was injected into HPLC.

2.4.3 Validation parameters

To investigate the existence of potential chromatographic interferences from endogenous compounds (matrix effects) at the retention time of lopinavir, selectivity studies were conducted. Selectivity was evaluated by comparing the chromatograms generated after the analysis of blank samples (liver, spleen and lymph node homogenates) obtained from six different rats with those achieved from the corresponding spiked sample. Results are presented in Fig. 2.6.

Other parameters such as recovery, stability, precision and accuracy were conducted with quality control samples as discussed earlier.

2.4.4 Results and discussion

From 2.6, no significant interference was observed at the retention time of lopinavir, indicating specificity of the method.

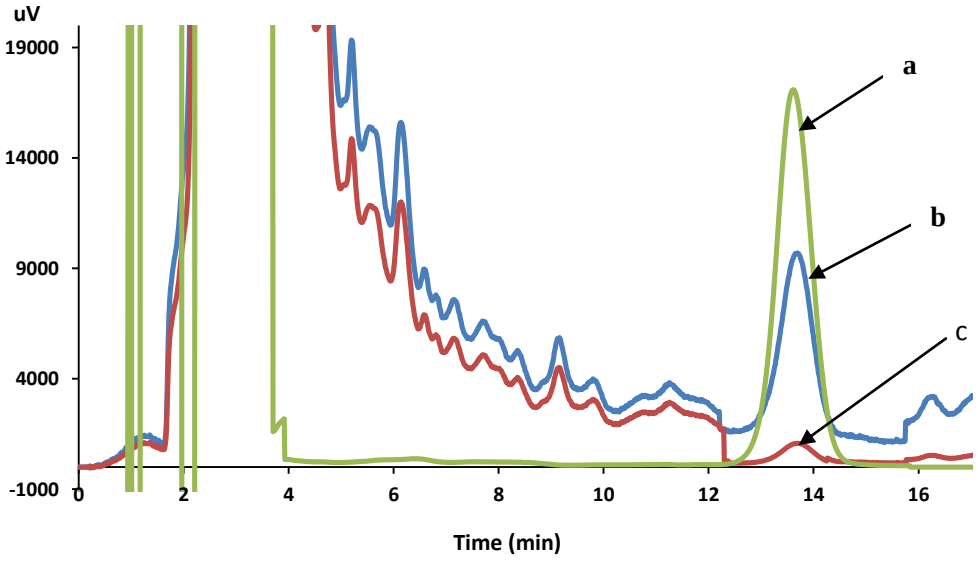

Fig. 2.6: Overlaid chromatograms of **a)** pure lopinavir solution (2000 ng/ml); **b)** spiked lopinavir (600 ng/ml) in liver tissue; and **c)** processed blank liver tissue.

The linearity of the analytical method was determined by developing a six point calibration curve in the range of 200 ng/ml to 6400 ng/ml; analyzed in three independent runs. Calibration curve was constructed by least-square linear regression of the peak area versus the

nominal concentrations of analyte spiked to drug-free tissue samples. The calibration curves were linear across the calibration range. The mean regression equations (n = 3) for calibration curves of lopinavir in various tissue matrices are summarized in Table 2.10.

Table 2.10: Calibration curve parameters for lopinavir tissue samples (n = 3).

Matrix type	**Calibration standards (ng/ml)**	**Slope (± SE)**	**Intercept (± SE)**	**r^2**
Liver	200, 600, 1200, 1600,3200, 6400	100.05 (± 1.65)	2834.20 (± 723.45)	0.996
spleen	200, 600, 1200, 1600,3200, 6400	99.07 (± 1.05)	2675.09 (± 598.12)	0.997
Lymph node	200, 600, 1200, 1600,3200, 6400	110.23 (± 1.47)	2910.8 (± 603.49)	0.995

Table 2.11 summarizes the intra- and inter-day precision and accuracy for lopinavir evaluated by assaying the QC samples. The results demonstrate that the values were within the acceptable range and the method was accurate and precise. Recovery of lopinavir from the spiked tissue samples, when compared with analytical standards of same concentration, across the QC levels tested was in the range of 93.78 % to 99.92% All recoveries had RSD less than 6.5% throughout the entire standard concentration ranges, showing robustness of extraction method.

From the stability data obtained in rat tissue (liver, spleen and lymph node) homogenates, no significant loss was observed for lopinavir when spiked QC samples were stored at room temperature for 4 h and at –70 ^{o}C for 30 days. The analyte was also demonstrated to be stable after three freeze-thaw cycles at –70 ^{o}C.

Table 2.11. Precision, accuracy and recovery for the analysis of lopinavir in rat tissues (n = 3 days, three replicates per day).

Analytes	Nominal concentration (ng/ml)	[a]Measured concentration (ng/ml); n=9	Intra-day RSD (%); n=3	Inter-day RSD (%); n=9	[b]RE (%)	Global recovery (%); n=9
Liver	200 (LLOQ)	190.51	8.90	12.80	-4.74	95.26
	800 (LQC)	780.79	5.91	9.91	-2.40	97.60
	1600 (MQC)	1560.69	4.60	8.70	-2.45	97.54
	3200 (HQC)	3009.10	3.90	6.31	-5.96	94.03
Spleen	200 (LLOQ	188.49	10.91	13.12	-5.75	94.25
	800 (LQC)	750.50	6.10	10.40	-6.23	93.78
	1600 (MQC)	1500.70	2.90	7.22	-6.21	93.79
	3200 (HQC)	3009.00	4.30	8.91	-5.97	94.03
Lymph node	200 (LLOQ	198.50	11.62	15.93	-0.75	99.25
	800 (LQC)	786.81	6.70	10.73	-1.45	98.55
	1600 (MQC)	1598.79	5.30	10.61	-0.08	99.92
	3200 (HQC)	3068.00	4.21	6.61	-4.13	95.87

[a]Mean of back calculated tissue concentrations. Measured concentration was calculated by linear regression equation; [b]Accuracy is given in RE (%) = [100 × (measured concentration–nominal concentration)/nominal concentration)]

2.5 Conclusions

The developed and validated methods for estimation of lopinavir in aqueous and biological samples (plasma and tissues) were found to be precise, specific, and reproducible. Recovery of lopinavir from various matrices by protein precipitation technique using acetonitrile was highly efficient (>90%). In addition, the drug was found to be stable under various processing and storage conditions. The method allows high sample throughput due to the simple procedure for sample preparation and relatively short run time. The method was successfully employed in determining drug content and pharmacokinetic parameters following IV bolus administration in rats.

References

1. Tiwari G, Tiwari R. Bioanalytical method validation: An updated review. Pharm Methods. 2010; 1: 25-38.
2. Kelley M, DeSilva B. Key elements of bioanalytical method validation for macromolecules. AAPS J. 2007; 9: E156-E163.
3. Whitmire M, Ammerman J, de Lisio P, Killmer J, Kyle D, Mainstone E, et al. LC-MS/MS bioanalysis method development, validation, and sample analysis: points to consider when conducting nonclinical and clinical studies in accordance with current regulatory guidances. J Anal Bioanal Tech. 2011; S4:001.
4. Patel KK, Kumar P, Thakkar HP. Formulation of niosomal gel for enhanced transdermal lopinavir delivery and its comparative evaluation with ethosomal gel AAPS PharmSciTech. 2012; 13: 1502-1510.
5. Seshachalam U, Haribabu B, Chandrasekhar KB. A novel validated LC method for quantitation of lopinavir in bulk drug and pharmaceutical formulation in the presence of its potential impurities and degradation products. Biomed Chromatogr. 2207; 21: 716-723.
6. Yadav M, Rao R, Kurani H, Singhal P, Goswami S, Shrivastav PS. Application of a rapid and selective method for the simultaneous determination of protease inhibitors, lopinavir and ritonavir in human plasma by UPLC–ESI-MS/MS for bioequivalence study in Indian subjects. J Pharm Biomed Anal. 2009; 49: 1115-1122.
7. Wang PG, Wei JS, Kim G, Chang M, El-Shourbagy T. Validation and application of a high-performance liquid chromatography–tandem mass spectrometric method for simultaneous quantification of lopinavir and ritonavir in human plasma using semi-automated 96-well liquid–liquid extraction. J Chromatogr A. 2006; 1130: 302-307.
8. Ehrhardt M, Mock M, Haefeli WE, Mikus G, Burhenne J. Monitoring of lopinavir and ritonavir in peripheral blood mononuclear cells, plasma, and ultrafiltrate using a selective and highly sensitive LC/MS/MS assay. J Chromatogr B. 2007; 850: 249-258.
9. Estrela RCE, Ribeiro FS, Seixas BV, Suarez-Kurtz G. Determination of lopinavir and ritonavir in blood plasma, seminal plasma, saliva and plasma ultra-filtrate by liquid chromatography/tandem mass spectrometry detection. Rapid Commun Mass Spectrom. 2008; 22: 657-664.
10. Myasein F, Kim E, Zhang J, Wu H, El- Shourbagy TA. Rapid, simultaneous determination of lopinavir and ritonavir in human plasma by stacking protein precipitations and salting-

out assisted liquid/liquid extraction, and ultrafast LC-MS/MS. Anal Chim Acta. 2009; 651: 112-116.

11. Tippabhotla SK, Thudi NR, Raghuvanshi R, Khuroo AH, Gurule S, Mishra S, Monif T, Lao VKC. A bioequivalence study comparing two formulations of lopinavir/ritonavir capsules. Int J Clin Pharmacol Ther. 2008; 46: 204-210.
12. Damaramadugu R, Inamadugu J, Kanneti R, Polagani S, Ponneri V. Simultaneous determination of ritonavir and lopinavir in human plasma after protein precipitation and LC-MS-MS. Chromatographia. 2010; 71: 815-824.
13. Gehring AK, Mikus G, Haefeli WE, Burhenne J. Electrospray tandem mass spectroscopic characterisation of 18 antiretroviral drugs and simultaneous quantification of 12 antiretrovirals in plasma. Rapid Commun Mass Spectrom. 2007; 21: 2704-2716.
14. Notari S, Bocedi A , Ippolito G , Narciso P , Pucillo LP, Tossini G, et al. Simultaneous determination of 16 anti-HIV drugs in human plasma by high-performance liquid chromatography. J Chromatogr B. 2006; 831: 258-266.
15. Usami Y, Oki T, Nakai M, Sagisaka M, Kanedat. A simple HPLC method for simultaneous determination of lopinavir, ritonavir and efavirenz. Chem Pharm Bull. 2003; 51: 715-718.
16. Faux J, Venisse N, Olivier JC, Bouquet. Rapid high-performance liquid chromatography determination of lopinavir, a novel HIV-1 protease inhibitor, in human plasma. Chromatographia. 2001; 54: 469-473.
17. Jayewardene AL, Zhu F, Aweeka FT, Gambertoglio JGJ. Rapid high-performance liquid chromatography determination of lopinavir, a novel HIV-1 protease inhibitor, in human plasma. Chromatogr B. 1998; 707: 203-211.
18. International Conference on Harmonization. Validation of Analytical Procedure. Text and Methodology Q2 (R1).ICH, IFPMA, Geneva, 2005.
    http://www.bcg-usa.com/regulatory/docs/ich/ICHQ2B.pdf. Accessed July 29, 2014.
19. United States Pharmacopoeia (USP), XXVI. Validation of compendial methods. United States Pharmacopoeial Convention Inc., Rockville, MD, USA, 2003.

Chapter 3

Preformulation Studies

3.1 Introduction

For a successful formulation design, the prior information of physicochemical and biological properties of the drug is vital to produce an effective, stable and marketable product. Frequently, this prior information reduces the efforts in later stages of product design and development by reducing cost and time to market [1]. Preformulation studies are designed to investigate specific drug characteristics which address identity, purity and strength of the substances and quality of the drug product. The data generated from the preformulation studies can be utilized to understand the behaviour of drug within and outside the body.

Classically, a standard pharmaceutical product development study includes comprehensive drug characterization such as determination of ionization constant, partition coefficient, solubility, polymorphism and hydrate, powder properties, thermal behaviour, molecular spectroscopic profile, drug excipient compatibility and stability [2, 3]. However, considering the scope of nanoparticulate formulations, methods were selected to investigate product specific questions, which offers a rational basis for nanotechnology based product design and the development strategies.

Physicochemical properties of lopinavir like aqueous solubility, dissociation constant and partition co-efficient have been reported in literature [4, 5]. However, it is prudent that we confirm these parameters again and also determine other parameters like melting point, purity, and stability under various processing conditions before delving into the actual formulation development. Moreover, as a part of preformulation studies, we also established the compatibility of lopinavir with various excipients that we planned to use in the formulation of nanoparticles.

3.2 Materials

3.2.1 Chemicals and reagents

Lopinavir was obtained as a gift sample from Mylan Laboratories Ltd. (Hyderabad, India). Poly-ε-caprolactone (PCL) and pullulan were purchased from Polysciences, Inc. (Warrington, USA). Poloxamer 407 (P407), poloxamer 188 (P188), poly vinyl alcohol (PVA) and mannitol (Pearlitorl SD) were procured form Signet Chemicals (Mumbai, India). Polyethylene glycol 400 (PEG 400), sodium lauryl sulfate (SLS), polysorbate 80 (Tween 80) were purchased from Merck Ltd. (Mumbai, India). The lipids– stearic acid, glyceryl monostearate, glyceryl distearate, glyceryl tristearate (Dynasan 118), and glyceryl tribehenate (Compritol ATO 888) were purchased from Himedia Pvt. Ltd. (Hyderabad, India). All other chemicals and reagents were of analytical grade.

3.2.2 Instruments

A digital pH meter equipped with a glass electrode and automatic thermal compensation probe (pH Tutor, Eutech Instruments, Singapore); calibrated digital analytical balance (Sartorius 2244S-CW, Goettingen, Germany); temperature controlled water bath with shaker (Remi, Mumbai, India); humidity and temperature controlled cabinet (Remi, Mumbai, India); rotary flash evaporator (Rotavapor R-215, Bucchi Labortechnik AG, Postfach, Switzerland); ultrasonicator (Vibracell, Sonics, Connecticut, USA); vortex mixer (Vortex 3, Ika India Pvt Ltd., Bengaluru, India) were used for these studies. All the analytical instruments were calibrated prior to use.

3.2.3 Methods

3.2.3.1 Preparation of reagents and buffers

Various buffers (0.1 M strength) ranging from pH 1.2 to 7.4 were prepared in accordance to procedures described in the United States Pharmacopeia [6]. Triple distilled water (TDW) was used as a solvent in all the cases.

3.2.3.2 Procedures and protocols

I. Bulk characterization

Following in-house tests were performed to establish identification and characterization of lopinavir.

a) FT-IR absorption spectrum of lopinavir

The FT-IR spectrum of pure lopinavir was recorded in solid state using KBr as a dispersion medium (1:10) using JASCO FT/IR-4200 (Jasco Inc., Maryland, USA) spectrometer in the range of 4000–400 cm^{-1}. An average of 40 scans was taken per sample.

b) Thermal analysis using DSC

Thermal analysis was carried out using DSC 60 (Shimadzu, Kyoto, Japan) instrument. For the study, accurately weighted samples were taken in aluminium pan and crimp sealed. In the DSC chamber, samples were allowed to equilibrate at 25 °C. Then, the samples were subjected to heating run over temperature range of 25 to 200 °C at a heating rate of 5 °C per min. DSC thermograms were directly obtained from the software supplied with the instrument.

c) Assay and purity assessment

For assessment of purity of the drug and to quantify the drug from the bulk sample, an in-house validated HPLC method (as described in Chapter 2) was used.

d) Molecular weight confirmation

To confirm the molecular weight of the drug, methanolic solution of lopinavir (1 µg/ml) was prepared and injected into LC-MS system (Shimadzu LCMS-2020, Shimadzu Corporation, Kyoto, Japan). Drug was scanned for base peak both in positive and negative polarity.

II. Determination of drug solubility

In the present work, the solubility study of lopinavir was carried out in selected aqueous media maintained at various pH conditions using the shake flask method. The pH range selected for aqueous solubility study was in accordance with the *in vivo* physiological conditions.

The saturation solubility of lopinavir was determined in buffered solutions with pH ranging from 1.2 to 7.4 at 37 ºC. In this, an excess amount of drug (10 mg) was added to 10 ml of buffered solutions. Samples were agitated in a water bath shaker maintained at 37 ºC. After 48 h, samples were centrifuged 5000 x g for 15 min to get a clear supernatant. The clear supernatant was then suitably diluted and analysed at 210 nm using a validated HPLC method against aqueous linearity as described in analytical section. Three replicates were taken for each sample and final values were expressed as mean ± S.D.

III. Partition coefficient

Partition coefficient is the ratio of concentrations of a compound in a mixture of two immiscible liquids at equilibrium. These coefficients indicate the preference of drug solubility in the two immiscible phases. Partition coefficient of lopinavir was determined by previously reported shake flask method using *n*-octanol-water system [7]. The *n*-octanol phase was pre-saturated for 24 h with water at room temperature (25 ± 2 ºC). Prior to start of the experiment, the *n*-octanol layer was separated by centrifugation (80 x g, 2 min) from the aqueous layer. To 10 ml of this water saturated organic phase, equal proportion of pre-saturated water (with *n*-octanol) was added. To 20 ml of the total mixture, 0.1 ml aliquot of 1 mg/ml lopinavir in methanol was added. The flasks were incubated on a rotary shaker (125 rpm), maintained at 25 ± 2 ºC for 24 h. After 24 h period, triplicate samples from each phase were collected from the flasks and analysed for drug content using validated HPLC method. The partition coefficient of lopinavir was calculated using the following formula:

$$P_{o/w} = C_{octanol} / C_{water}$$

Where, $C_{octanol}$ and C_{water} are the concentration of lopinavir in *n*-octanol and pure water respectively.

The saturation solubility of lopinavir in *n*-octanol was independently determined by incubating a known excess of lopinavir in *n*-octanol. The drug stability of lopinavir during experiment in *n*-octanol was confirmed by comparing the time zero concentration of drug with values obtained after 3 days of incubation at 25 ºC.

IV. Stability studies

The stability studies of lopinavir were performed in order to evaluate the integrity of drug molecules under various pH conditions during the product manufacturing and *in vivo* biological environment. If the drug is extensively degraded, it may substantially reduce the potency of the drug. Moreover, the degradation products of the drugs may be toxic to the consumer [8]. The stability studies were preformed both in liquid and solid states.

a) Liquid state stability studies

The liquid state stability for lopinavir was studied on various un-buffered and buffered pH solutions. Lopinavir stock solution (1 mg/ml) was prepared in methanol and appropriate volume of this stock was spiked into various buffered and un-buffered solutions with pH ranging from 1.2 to 10. The final concentration in each case was 1 µg/ml. Three sets of samples were also prepared in TDW.

The prepared solutions were placed on a temperature controlled water bath shaker (Remi, Mumbai, India) at fixed temperature of 25 ± 2 ºC. At pre-determined time points (0, 2, 4, 6, 12 and 24 h and 2, 4, 8, 15, 30, 45 and 60 days), an aliquot of sample was withdrawn and analysed for drug content using previously described validated HPLC method. The amount of drug remaining in the solution was plotted as a function of time. The order of degradation kinetics and the degradation rate constants were determined for respective solutions.

b) Solid state stability studies

For solid state stability**,** thermal stability studies were conducted while subjecting lopinavir to various thermal conditions with humidity. Procedure is discussed in detail under drug-excipient compatibility studies.

V. Drug-excipients compatibility studies

Excipients play an important role in determining the stability of the final formulation. It is common knowledge that formulation stability is affected by various factors such as chemical nature of excipient, moisture content, temperature, light, oxygen, relative humidity, packaging material, processing method and nature of packaging. Therefore, drug: excipient compatibility studies are integral part of preformulation studies. In the following section, the actual protocol followed for these studies is presented.

The purpose of this protocol is to describe the procedure for investigation of possible changes in the physicochemical characteristics and the purity of lopinavir in presence and/ or absence of excipients.

a) Sample details

Lopinavir manufactured by Mylan Laboratories Ltd. was used for the preformulation compatibility study. The details of lopinavir to be used for compatibility study are tabulated as shown in below Table 3.1.

Table 3.1: Details of the API used in drug: excipient compatibility studies.

Sr. No.	Name of the API	Batch No. / Lot No.	Mfg. by
1.	Lopinavir	LOP-0090410	Mylan

The details of individual excipients to be used in compatibility study are tabulated as shown below in Table-3.2. Individual excipient shall be sifted through # 40 ASTM SS sieve.

Table 3.2: Details of excipients used in drug: excipient compatibility studies.

Sr. No.	Excipient	General Function	Mfg. by
1.	Mannitol	Cryoprotectant	Roquette Pharma
2.	Sucrose	Cryoprotectant	Domino
3.	Tween 80	Non-ionic Surfactant	Sigma Aldrich
4.	Poloxamer 188 (P188)	Non-ionic Surfactant	Sigma Chemicals
5.	Poloxamer 407 (P407)	Non-ionic Surfactant	Sigma Chemicals
6.	Poly vinyl alcohol	Non-ionic Surfactant	Sigma Aldrich
7.	Poly-ε-caprolactone (PCL)	Polymer	Polysciences Inc.
8.	Pullulan acetate	Polymer	In-house
9.	Sodiul lauryl sulfate (SLS)	Anionic Surfactant	Sigma Aldrich
10.	Stearic acid	Lipid	Himedia
11.	Glyceryl monostearate	Lipid	Himedia
12.	Glyceryl tristearate (Dynasan 118)	Lipid	Himedia
13.	Glyceryl behenate (Compritol ATO 888)	Lipid	Himedia

b) Sample preparation

Solid state interactions between drug and various excipients were studied by subjecting physical admixtures of drug and excipient to different stress conditions (as mentioned in Table 3.3)**.** Samples were studied for physical observation (color, odor and physical state), drug content (assay), thermal (DSC) and spectroscopic analysis (FT-IR).

Drug and excipient were weighed accurately and mixed homogeneously by sieving (mesh #40) and blending process. Prepared admixtures were transferred to a set of glass vials with screw cap and wrapped with aluminium foil. Each vial was kept at a refrigerated (2-8 °C), ambient (room temperature; 25 °C/ 60%RH) or accelerated condition (AT; 40 °C/ 75%RH). Pure drug stability data obtained for each condition was treated as control.

At pre-determined time interval, samples were withdrawn in triplicate to perform physical inspection and drug content analysis. Drug content data were plotted against the time function and rate constant for each degradation curve was determined. In order to investigate possible physical and chemical interactions, at the end of stability period (6 months), thermal and spectroscopic analysis was performed. Sample description and storage conditions are presented in the Table given below.

Table 3.3: Details of different samples, drug: excipient ratios and test conditions used for drug: excipient compatibility studies.

Sample	**Drug: Excipient Ratio**		**Initial**	**25 ^{0}C/60%RH**	**40 °C/75%RH**
Lopinavir	1	**2-8° C (CONTROL SAMPLES)**	√	√	√
Mannitol	1		√	√	√
Sucrose	1		√	√	√
PCL	1		√	√	√
Pullulan acetate	1		√	√	√
Stearic acid	1		√	√	√
Glyceryl Monostearate	1		√	√	√
Tween 80	1		√	√	√
PVA	1		√	√	√
Lopinavir + Mannitol	1:9		√	√	√
Lopinavir + Sucrose	1:9		√	√	√
Lopinavir + PCL	1:9		√	√	√
Lopinavir + Pullulan Acetate	1:9		√	√	√
Lopinavir + Stearic acid	1:9		√	√	√
Lopinavir + Glyceryl Monostearate	1:9		√	√	√
Lopinavir+ Tween 80	1:1		√	√	√
Lopinavir + PVA	1:1		√	√	√
Lopinavir + PCL+ Tween 80	1:30:7		√	√	√
Lopinavir + Pullulan acetate + PVA	1:10:25		√	√	√
Lopinavir + Stearic acid+ PVA	1:45:12.5		√	√	√

3.3 Results and discussion

I. Identification and bulk characterization of lopinavir

a) FT-IR absorption spectrum

The infrared absorption spectrum of the lopinavir showed characteristic absorption peaks at 3358 (O-H stretching), 2954 (C-H stretching),1651(amide bond carbonyl stretching; -C=O),and 1528 (urea C=O stretching) which are in agreement with the reported values from the literature [9]. The FT-IR spectrum for bulk lopinavir is shown in Fig. 3.1.

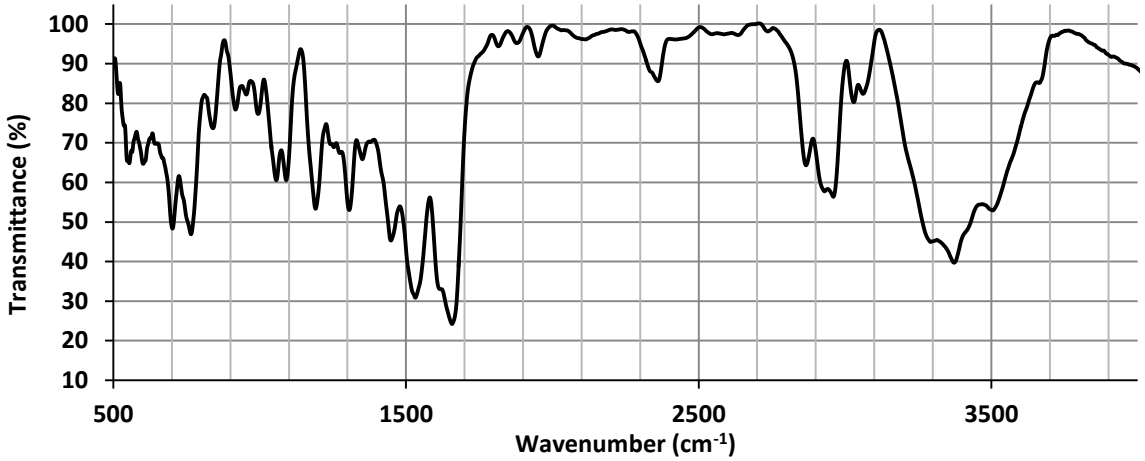

Fig. 3.1: FT-IR spectrum of lopinavir in bulk form.

b) Thermal analysis

The DSC thermogram of pure drug demonstrated a single sharp endothermic peak onset at 90.25 ºC and peak endset at 103.05 ºC. The average melting peak appeared at 97.38 ºC. The single strong endothermic peak indicates that the sample of lopinavir is crystalline in nature. The DSC thermogram data is presented in Fig. 3.2 below.

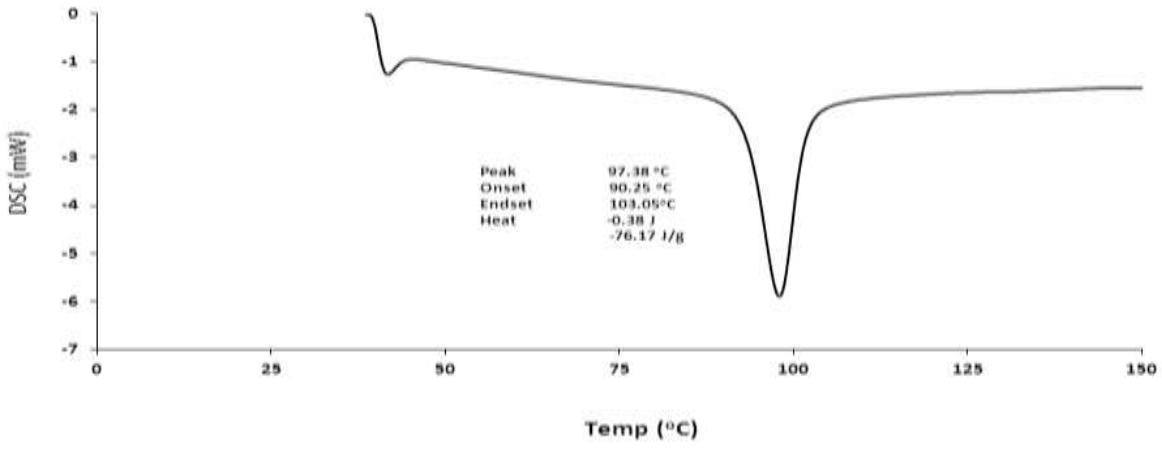

Fig. 3.2: DSC thermogram of pure lopinavir.

c) Molecular weight

In positive ionization mode, the protonated molecular ions $(M+H)^+$ are usually the dominant species. Sometimes, molecular ions can also be accompanied by salt adducts such as Na^+ (M+23) and K^+ (M+39). The mass spectrum for pure lopinavir in positive mode (M+H) showed two distinct peaks at m/z 629 and m/z 651. The two peaks obtained in our sample correspond to the sodium adduct of lopinavir (651 g/mol; (M+Na) and base form of lopinavir (629 g/mol). A strong peak at m/z 627 in negative scan further confirms the molecular weight of lopinavir as 628 g/mol, which is in close agreement with the reported values [10]. The data is represented in Fig. 3.3.

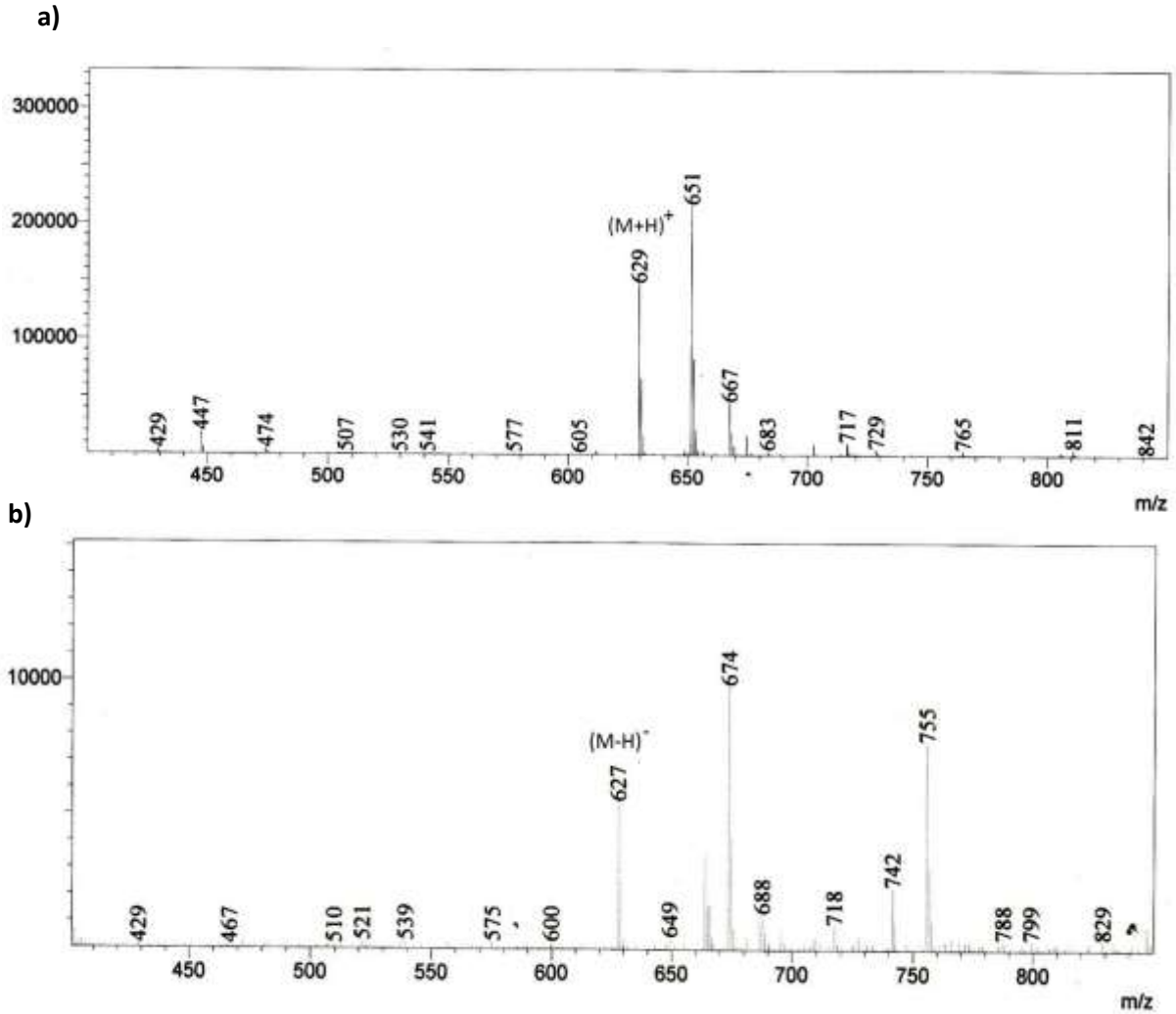

Fig. 3.3: Mass spectrum of lopinavir in **a)** positive and **b)** negative mode.

d) Assay and purity assessment

The assay results showed that the lopinavir used in the study has a purity of 98.91%.

II. Determination of drug solubility

The data from solubility studies in different pH conditions are presented in Fig. 3.4. The extent of solubility of lopinavir was found to be nearly same (~2.5 µg/ml) across the pH conditions (pH 1.5 to 7.4). Results indicate that solubility of lopinavir is pH independent. Lopinavir is reported to be a BCS class II drug with log p~4.7 (lipophilic) and pKa value of 13.69 (poor ionization property). Data are in close agreement with previously published reports [5].

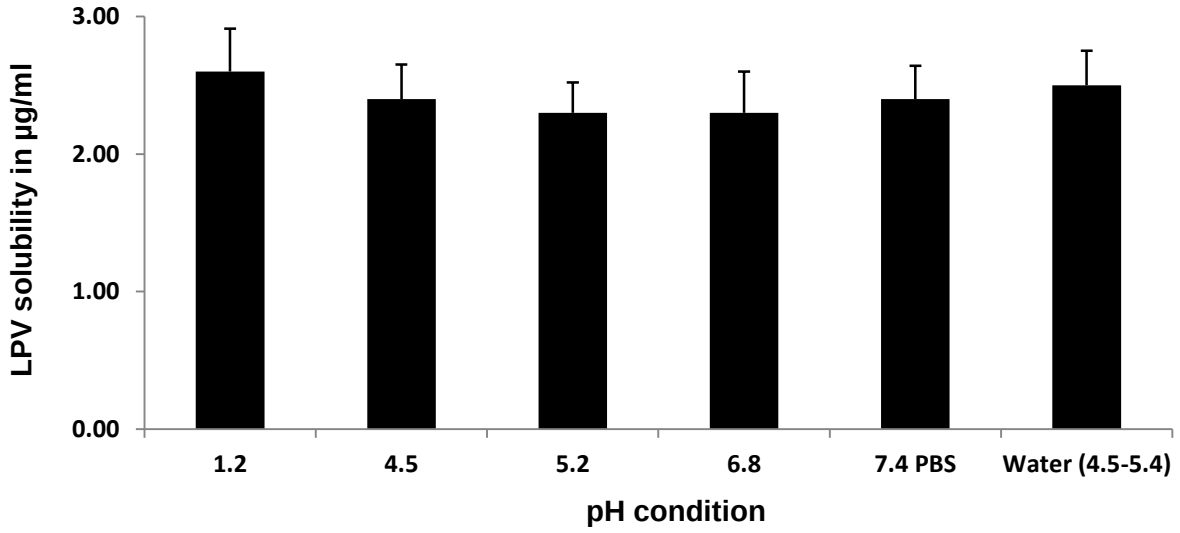

Fig. 3.4: Solubility profile of lopinavir (LPV) in different pH conditions and water. Each data represents mean ± SD (n = 3).

III. Partition coefficient

From experiment, the octanol-water partition coefficient ($P_{o/w}$) of lopinavir was found to be 40051 ± 1571 (mean ± SD, n = 3). The log $P_{o/w}$ value of the mean observation was calculated as 4.60 which is in close agreement with the reported value of 4.69 [5]. Moreover, findings of partition coefficient experiments correlate well with the solubility data.

Prior to experiment, the solubility studies of lopinavir in *n*-octanol and water were also carried out to ensure that, at equilibrium, the distribution of lopinavir in *n*-octanol and water was not limited by its solubility. The saturation solubility of lopinavir in *n*-octanol was found to be 1.5 ± 0.78 mg/ml by independent experiments.

IV. Stability studies

a) Liquid state stability studies

In order to estimate the stability of lopinavir in various pH conditions, the logarithm of percentage lopinavir unchanged was plotted as a function of time (Fig. 3.5) and slope of the curve was used to determine degradation rate constants (K_d) at the respective pH condition. From the result, it is evident that the degradation of lopinavir followed first-order rate kinetics with high correlation coefficient values (Table 3.4). Data indicates the lopinavir's sensitivity towards extreme pH conditions. The rate of degradation was relatively higher in both acidic condition and basic condition. Whereas, the degradation rate of lopinavir was minimal at neutral pH conditions with the first order degradation rate constant of 0.13×10^{-2} day^{-1}. Though, it is expected that while passing through GIT, lopinavir would be exposed to extreme acidic environment for a maximum period of 4 h; the fraction degradation during this period would be negligible. From these studies, it is suggested that lopinavir needs to be processed at neutral condition and prolonged exposure to extreme acidic and alkaline conditions must be avoided.

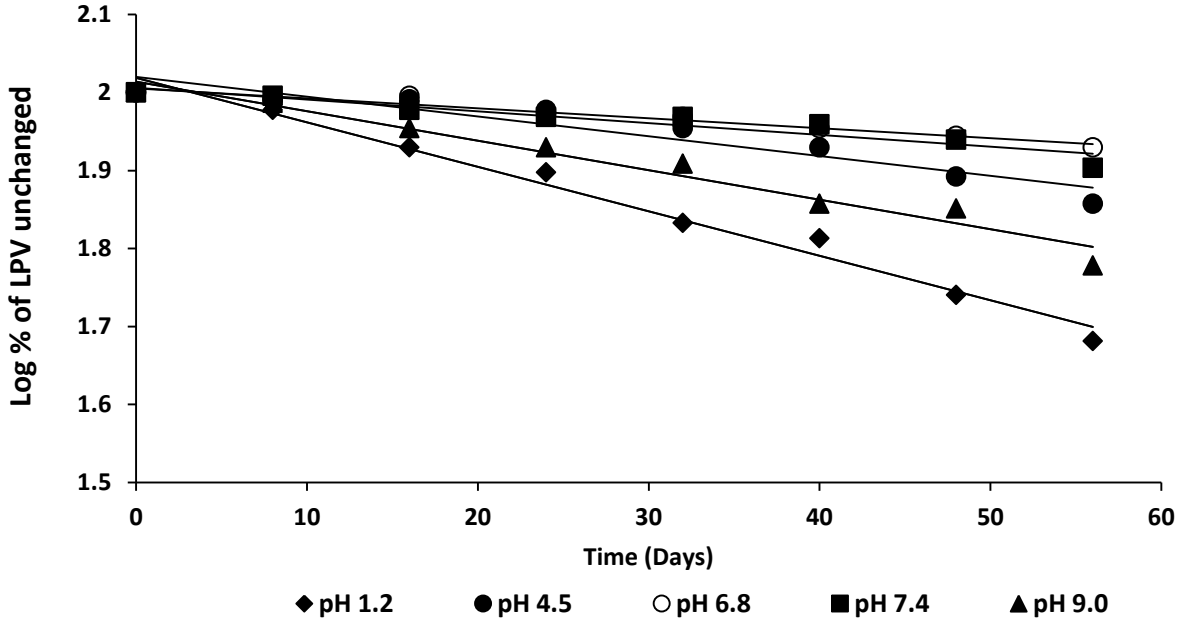

Fig 3.5: First-order plot of lopinavir (LPV) degradation in various pH conditions at 25 ºC.

Table 3.4: First-order degradation rate constants (K_d) and respective regression coefficients for lopinavir under different pH conditions.

pH condition	K_d x 10^2 (per day)	Regression co-efficient (r^2)
1.2	0.57	0.9833
4.5	0.25	0.9067
6.8	0.13	0.9569
7.4	0.15	0.9001
9.0	0.38	0.9638

V. Drug-excipient compatibility studies

The drug-excipient compatibility studies were conducted in various drug substance/excipient combinations. Excipients for the study were chosen based on their potential for use in preparation of lopinavir nanoparticles. The study indicated that lopinavir is stable in presence of all the tested excipients at both ambient and accelerated conditions. The drug was found to follow first order degradation kinetics in the mixture. Lopinavir showed good stability at controlled room temperature and accelerated temperature with the highest degradation rate constant of 0.52 x 10^{-5} day^{-1} and 0.76 x 10^{-5} day^{-1} respectively.

Drug content analysis showed high recovery of drug (> 95%) after 6 months of storage at different stress conditions, which further supports the stability of lopinavir in the physical mixture.

Furthermore, thermal analysis indicated no significant change in endothermic peak of the drug when stored in combination with various excipients; suggesting the physical compatibility of the drug with all studied excipients. In all the physical mixtures, drug showed nearly same melting point peak at 97.2 ^oC, without any additional thermal events. However in few cases, due to residual moisture in the sample, a broad interfering peak was observed ranging from 93 ^oC to 110 ^oC.

Further, these findings were supported by infrared absorption spectrum as it confirmed the absence of possible chemical interaction between drug and selected excipient.

The drug-excipient compatibility study did not reveal any physical and chemical interaction between drug and various selected excipients. Hence, compatibility study would support the rationale for selection of various excipients and justify the longevity of finished product. The data obtained from the study are presented in the Table 3.5.

Table 3.5: Compatibility analysis data of lopinavir with selected excipients.

Sample Name	Storage conditions	K_d x 10^5 (per day)	Assay (%) (mean ± SD, n = 3)	Thermal analysis Peak (ºC)
Lopinavir	Initial	-	100	97.3
	25°C /60%RH	0.32 ± 0.010	97.5 ± 1.8	96.7
	40°C /75%RH	0.56 ±0.012	96.5 ± 1.9	97.1
Lopinavir+Mannitol	Initial	-	98.5 ± 2.1	96.2
	25°C /60%RH	0.45 ± 0.012	97.8 ± 1.1	95.1
	40°C /75%RH	0.55 ± 0.011	96.0 ± 2.2	95.2
Lopinavir+PCL	Initial	-	98.2 ± 1.2	96.3
	25°C /60%RH	0.32 ± 0.013	97.1 ± 1.1	96.1
	40°C /75%RH	0.59 ± 0.012	96.4 ± 2.4	95.8
Lopinavir+Stearic acid	Initial	-	97.3 ± 2.0	95.2
	25°C /60%RH	0.48 ± 0.013	96.5 ± 1.9	93.8
	40°C /75%RH	0.63 ± 0.014	95.5 ± 2.6	93.6
Lpoinavir+Pullulan acetate	Initial	-	99.4 ± 1.1	97.1
	25°C /60%RH	0.31 ± 0.012	98.5 ± 1.2	96.5
	40°C /75%RH	0.58 ± 0.011	97.5 ± 1.5	96.8
Lopinavir+Tween 80	Initial	-	98.3 ± 2.0	97.3
	25°C /60%RH	0.48 ± 0.015	96.3 ± 1.9	96.7
	40°C /75%RH	0.76 ± 0.014	95.8 ± 3.0	95.4
Lopinavir+PVA	Initial	-	99.4 ± 1.0	96.4
	25°C /60%RH	0.34 ± 0.012	98.9 ± 1.2	96.5
	40°C /75%RH	0.53 ± 0.014	97.5 ± 1.6	97.1
Lopinavir+PCL+Tween 80	Initial	-	98.90 ± 1.7	96.5
	25°C /60%RH	0.52 ± 0.014	96.5 ± 1.9	97.1
	40°C /75%RH	0.69 ± 0.014	95.8 ± 2.1	96.7
Lopinavir+Stearic acid+PVA	Initial	-	98.86 ± 1.5	96.2
	25°C /60%RH	0.32 ± 0.011	96.9 ± 1.8	95.3
	40°C /75%RH	0.57 ± 0.013	95.8 ± 1.8	95.9
Lopinavir+ Pullulan acetate+PVA	Initial	-	98.9 ± 1.1	97.2
	25°C /60%RH	0.31 ± 0.013	97.1 ± 1.2	96.3
	40°C /75%RH	0.58 ± 0.011	96.9 ± 1.6	97.2

SD – Standard deviation; PCL – Poly (ε-caprolactone); PVA – Polyvinyl Alcohol.

References

1. Bharate SS, Vishwakarma RA. Impact of preformulation on drug development. Expert Opin Drug Deliv. 2013; 10: 1239-57.
2. Flanagan DR, Lach JL, Matheson LE. Preformulation and formultation investigational drugs, University of Iowa College of Pharmacy, 1990.
3. Ceresole R, Han YK, Rosasco MA, Orelli LR, Segall A. Drug-excipient compatibility studies in binary mixtures of avobenzone. J Cosmet Sci. 2013; 64: 317-28.

4. DeGoey DA, Grampovnik DJ, Flosi WJ, Marsh KC, Wang XC, Klein LL, et al. Water-soluble prodrugs of the human immunodeficiency virus protease inhibitors lopinavir and ritonavir. J Med Chem. 2009; 14; 52: 2964-70.
5. Alex A, Paul W, Chacko AJ, Sharma CP. Enhanced delivery of lopinavir to the CNS using Compritol-based solid lipid nanoparticles. Ther Deliv. 2011; 2: 25-35.
6. *US Pharmacopoeia XXX*. Vol. I. 2007, Rockville, MD: US Pharamcopoeial Convention.
7. Bruijn JD, Busser F, Seinen W, Hermens J. Determination of octanol/water partition coefficients for hydrophobic organic chemicals with the "slow-stirring" method. Environ Toxicol Chem. 1989; 8: 499-512.
8. Jiang S, Wang F, Zhu S, Zhang X, Guo Z, Li R, Xu Q. Preformulation study of methazolamide for topical ophthalmic delivery: physicochemical properties and degradation kinetics in aqueous solutions. Int J Pharm. 2013; 448: 390-3.
9. Lemmer HJ, Liebenberg W. Preparation and evaluation of metastable solid-state forms of lopinavir. Pharmazie. 2013; 68: 327-32.
10. Myasein F, Kim E, Zhang J, Wu H, El- Shourbagy TA. Rapid, simultaneous determination of lopinavir and ritonavir in human plasma by stacking protein precipitations and salting-out assisted liquid/liquid extraction, and ultrafast LC-MS/MS. Anal Chim Acta. 2009; 651: 112-116.

Chapter 4

Formulation Design and Pharmacokinetic Evaluation

Lipid based nanoparticles

4.1 Introduction

Solid lipid nanoparticles (SLNs) are unique lipid-based drug-delivery carriers for a number of reasons, including: i) feasibility to achieve particle in the size range of nanoscale after drug encapsulation; ii) availability of biocompatible and biodegradable lipids; iii) ease of preparation and scale up and economical to manufacture and iv) possibility to prepare nanoparticles without using any organic solvent systems [1, 2].

In comparison to other lipid based nanocarriers (nanoemulsion, liposome), SLNs offer controlled release of encapsulated drug attributed to its solid core which significantly reduces the drug mobility [3]. Additionally, SLNs in a powder form, when loaded into pellets, capsules, or tablets can further control the drug release over an extended period of time. However, the undesired particle growth by agglomeration or coagulation resulting in rapid "burst release" of the drug could limit the application of SLN formulation. Drug expulsion from SLNs during storage has also been reported as a major disadvantage of the present formulation. Several strategies have been investigated to improve stability of SLNs including the addition of a surfactant coating, and creating imperfection in the lipid matrix by adding chemically different solid lipid or lipid oils [3-5].

In preparation of nanoparticulate drug delivery system, the formulation parameters and the process variables can affect the particle size, shape, charge, and encapsulation efficiency of the nanoparticles which ultimately govern the therapeutic performance of the product. Therefore, preparation of SLNs is challenging with the influence of various formulation parameters such as nature and proportion of drug (lipophilicity and solubility), lipid (chain length and digestibility) and stabilizers (HLB value) and processing variables such as phase volume ratio, processing temperature, speed/intensity, time of mixing and rate of evaporation/cooling [6, 7].

It is reported that the nature of lipid has a significant impact on the particle size and loading capacity of nanoparticles. Irrespective of processing method used, lipids with higher melting point produce larger particle size. Further, the drug loading capacity of conventional SLNs is limited by the solubility of the drug in the lipid melt, the structure of the lipid matrix and the polymeric state of the lipid matrix. Drug solubulization in a lipid matrix ensures the greater partitioning of the drug towards the lipid core leading to high payload [8, 9]. Furthermore, researchers have demonstrated a significant correlation in *in vivo* performance of SLNs with the selection of lipids. It is reported that lipids with higher carbon chain length are resistant to the intestinal lipase and co-lipase system, resulting higher plasma concentrations and longer circulation time of the loaded drug [9, 10].

Selection of both appropriate surfactant and concentration are critical to produce stable SLNs with good entrapment efficiency. As discussed earlier, size and stability of SLNs depend on the stability of the primary o/w emulsion. Therefore, in order to produce stable nanoparticles, the primary emulsion system must contain emulsifier/surfactant with suitable HLB value in appropriate concentration. Upon addition, emulsifier gets distributed at o/w interface and stabilizes macro-emulsion for further processing. Surfactant stabilizes nanoparticles either by imparting charge or creating stearic hindrance. Thus, it prevents agglomeration of nanoparticles during storage [11, 12].

Another parameter that significantly affects the stability of SLNs is the rate of cooling of lipid. The pure solid lipids are crystalline in nature and prefer to exist in a low energy and a highly ordered state called the β-polymorphic state. During the preparation of SLNs, fast cooling creates an unstable and disordered amorphous α crystalline structure, which allows drug retention within lipid matrix. However, during the storage period, this α-crystalline form gets converted slowly to β-crystalline structure; a thermodynamically stable state of lipid. This change in crystallinity of lipid structure reduces the number of imperfections in the lipid matrix, leading to subsequent expulsion of drug in a phased manner [13]. Effect of ageing on drug expulsion in SLNs formulation is shown in Fig 4.1.

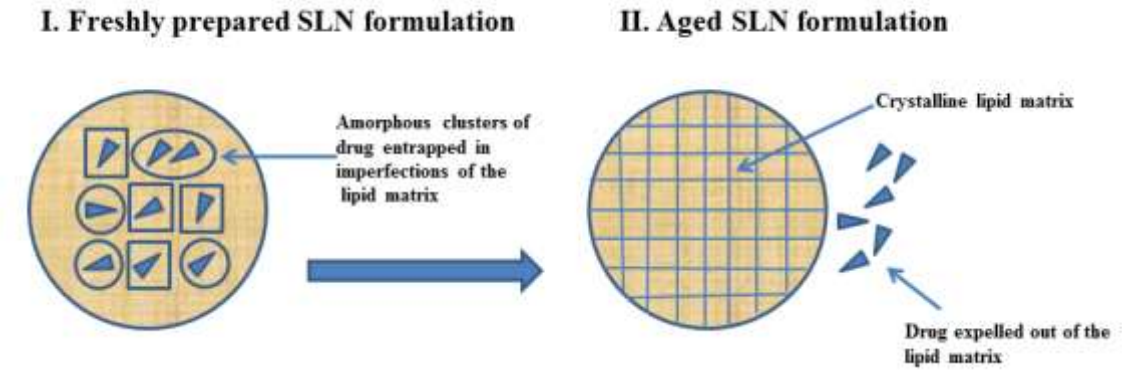

Fig. 4.1: Effect of ageing on drug expulsion in SLN formulation.

In the recent past, with the use of SLNs, several attempts have been made to improve the therapeutic effectiveness of antireteroviral drugs by targeting lymphatic system and enhancing oral bioavailability [14, 15]. Results from these studies demonstrate the potential of SLNs in the effective delivery of anti-HIV drugs.

The objective of the present work was to i) design and characterize lopinavir loaded SLNs and to ii) compare *in vivo* performance of the optimized formulation with the currently marketed lopinavir/ritonavir co-formulation.

SLNs were rationally designed and optimized using Plackett–Burman Design and Box–Behnken Design (BBD) and data were statistically analyzed using Design Expert software (Full version 8.0.7.1, Stat- Ease Inc., Minneapolis, MN). Processes involved in achieving optimum formulation of SLNs are shown in Fig. 4.2

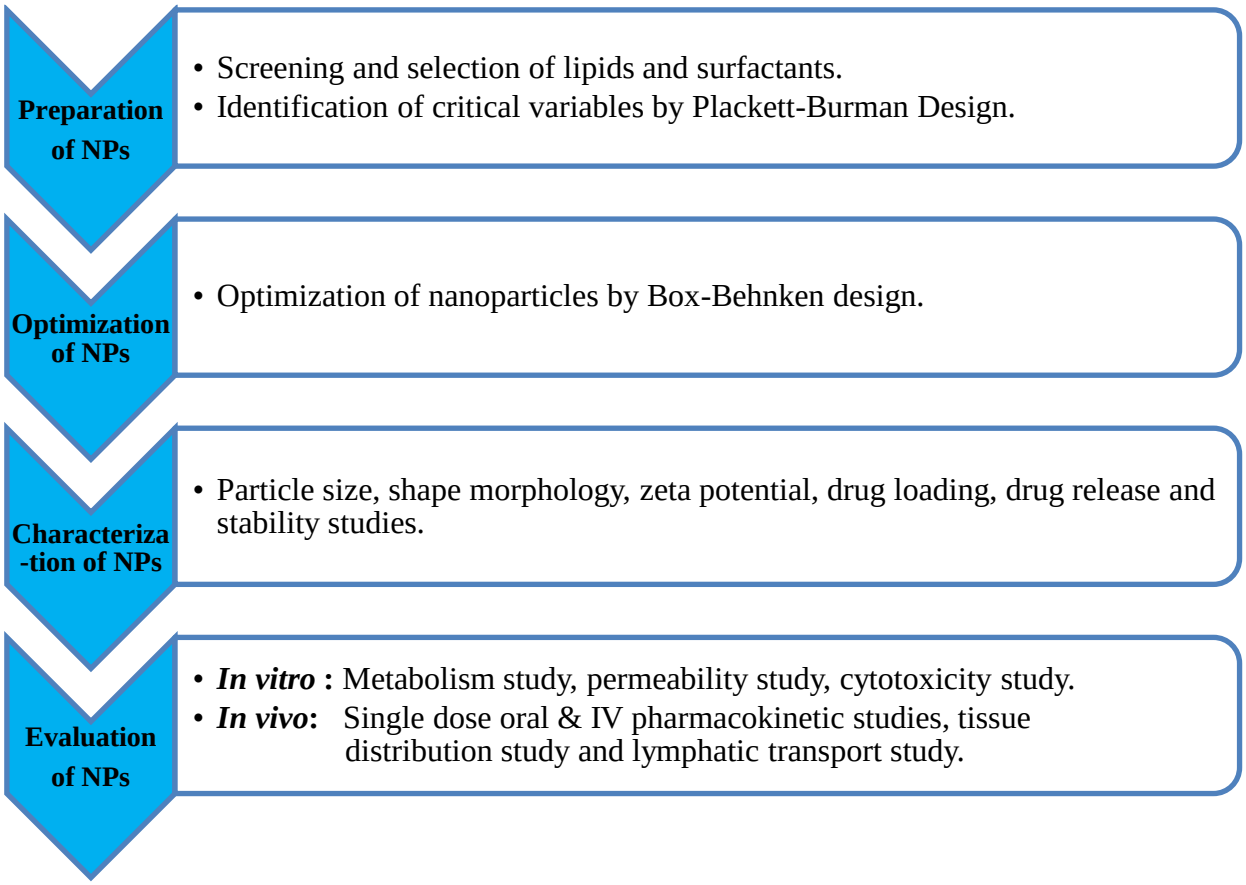

Fig. 4.2: Steps involved in the design, characterization and pharmacokinetic evaluation of SLN formulations.

4.2 Materials

Lopinavir (LPV) was obtained as a gift sample from Mylan Laboratories Ltd. Hyderabad, India. High purity lipids (stearic acid (SA; molecular weight, 284.4 g/mol), glyceryl monostearate (GMS), glyceryl distearate (GDS), glyceryl tristearate (GTS), and glyceryl behenate (GB) were purchased from M/s Himedia Pvt. Ltd. (Hyderabad, India). Poloxamer 407 (P407), Poloxamer 188 (P188), polysorbate 80 (Tween 80) and mannitol were procured form Signet Chemicals, Mumbai, India. All other chemicals used were of analytical grade and the solvents were of HPLC grade. Freshly collected Milli-Q water

(Millipore, Billerica, MA) was used in preparation of aqueous mobile phase of HPLC analysis.

4.3 Methodology

4.3.1 Screening and selection of lipid for preparation of SLNs

Selection of lipids for preparation of lopinavir loaded SLNs was based on the potential of lipid to encapsulate drug and its cost effectiveness. It is reported that in solid lipid nanoparticles, drug is either dissolved or dispersed in the lipid matrix. Therefore, extent of drug solubility in a lipid matrix is a good indicator of its encapsulation efficiency. In order to determine the maximum solubility of lopinavir in different lipid matrices, previously reported method with slight modification was followed [16]. Briefly, accurately weighed amount of lopinavir (10 mg) was added to a screw-capped glass vial. To this, individual lipids [stearic acid (SA), glyceryl monostearate (GMS), glyceryl distearate (GDS), glyceryl tristearate (GTS), or glyceryl behenate (GB)] were added in incremental amounts while maintaining the temperature of the vial 5-10 ºC above the melting point of the lipid. Drug solubility in lipid solution was visually monitored. Absence of any suspended particles in the molten lipid was considered as a visual endpoint for drug solubilisation.

Surfactants were carefully selected for the preparation of SLN formulations. For the initial trials, two distinct types of surfactants (polyvinyl alcohol and polysorbate 80 or tween 80) having different mechanisms of nanoparticle stabilization were selected. From the literature, it is evident that polyvinyl alcohol (PVA) is a widely used steric stabilizer for the preparation of nanoparticles. PVA absorbs on to the nanoparticle surface and creates repulsive barrier that prevents particle aggregation. On the other hand, being HLB value 16, tween 80 is a preferred surfactant for stabilizing o/w type emulsion. Hence, deemed suitable for preparation of SLN formulations [17, 18].

Solubility of lopinavir in various lipid matrices was established and data are presented in Fig. 4.3. From the study, the lowest amount of lipid required to dissolve 10 mg of lopinavir was determined. It is assumed that lipid having a higher solubility for lopinavir (lipid with lowest amount) will exhibit better drug loading in the SLNs.

The data from study reveals a significantly higher solubility of lopinavir in stearic acid than any other lipids chosen for the study. Stearic acid is an endogenous long-chain saturated fatty acid and a primary component of fats in both animal and plant sources, providing better biocompatibility and low toxicity. Therefore, stearic acid based nanoparticles is considered to be a potential drug carrier for oral delivery of lopinavir [19].

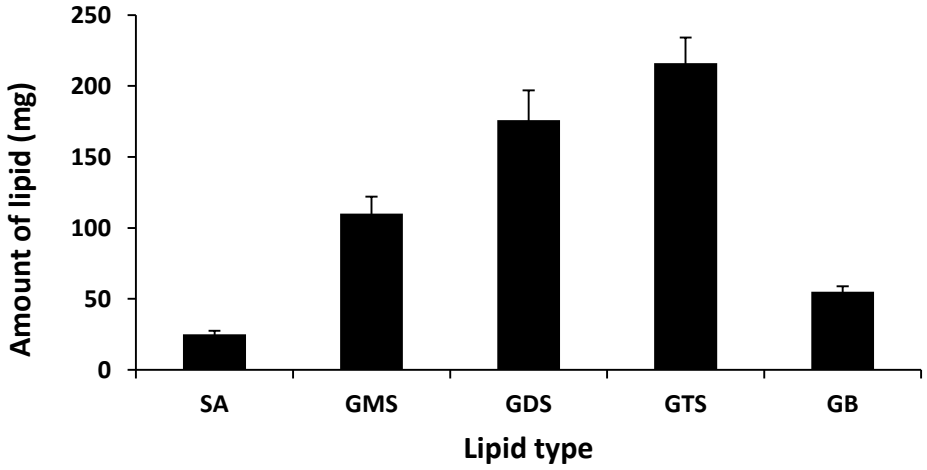

Fig 4.3: Solubility profile of lopinavir in different lipids in terms of amount of lipid required to dissolve 10 mg of lopinavir. Each value represents mean ± SD of three independent observations. SA – stearic acid, GMS – glyceryl monostearate; GDS – glyceryl distearate, GTS – glyceryl tristearate, GB – glyceryl behenate.

Considering the cost effectiveness, biodegradability, biocompatibility and extensive solubility of lopinavir, stearic acid was selected as a drug carrier for formulation of lopinavir loaded SLNs.

4.3.2 Experimental Design

The method for preparation of lopinavir SLNs involves several variables. To screen critical variables that affect quality attributes of SLNs, a low resolution Plackett-Burman Design (PBD) was used. Total of 11 variables were studied at two levels to determine their influence on two responses, viz. entrapment efficiency percentage (EE %) and particle size of loaded SLN formulations. The variables studied were: type of surfactant (PVA and tween 80), concentration of surfactant (0.5% and 1.5% w/v), temperature of surfactant solution (25 and 75 ^{o}C), volume of external phase (10 and 30 ml), speed of homogenization (7500 and 12500 rpm), time of homogenization (2 and 8 min), amount of lipid (400 and 1200 mg), time of ultra-sonication (5 and 15 min), amplitude of ultra-sonication (70% and 100%), ultra-sonication pulse (continuous and pulse mode) and temperature during homogenization (25 and 75 ^{o}C).

Based on the results obtained from PBD, three critical variables that significantly affect EE and particle size were identified (Table 4.1). These variables were further optimized using Box-Behnken Design (BBD). BBD, a sub-type of response surface methodology (RSM), was employed to develop quadratic models for optimization process

and to reduce the number of experimental trials. A 17-run, 3-factor, 3-level BBD was constructed to evaluate main effects, interaction effects and quadratic effects of identified initial factors. Non-linear quadratic model generated by BBD design was in the following form:

$$Y = b_0 + b_1X_1 + b_2X_2 + b_3X_3 + b_{12}X_1X_2 + b_{13}X_1X_3 + b_{23}X_2X_3 + b_{11}X_1^2 + b_{22}X_2^2 + b_{33}X_3^2$$

Where, Y is measured response associated with each factor level combination; b_0 - b_{33} are regression coefficients of respective factors and their interaction terms computed from observed experimental values of Y and X_1, X_2, X_3 are the coded levels of independent variables. The terms X_1X_2, X_2X_3, X_3X_1 and X_i^2 (i = 1, 2 or 3) represent the interaction and quadratic terms respectively. Dependent and independent variables selected are shown in Table 4.1. Critical variables evaluated in present study were surfactant concentration (X_1), lipid amount (X_2) and ultra-sonication time (X_3). Responses studied were particle size (Y_1) and EE (Y_2). Experiment design matrix generated by software is presented in Table 4.2.

Table 4.1 Variables and their levels in Box-Behnken Design (BBD).

Factor	Levels used		
	Low (-1)	**Medium (0)**	**High (+1)**
Independent variables			
X_1 = Surfactant concentration (% w/v)	0.5	1	1.5
X_2 = Lipid amount (mg)	400	800	1200
X_3 = Ultra-sonication time (min)	5	10	15
Dependent variables		**Constraints**	
Y_1= Particle size (nm)		Minimum	
Y_2 = Entrapment efficiency (%)		Maximize	

4.3.3 Preparation of solid lipid nanoparticles (SLNs)

Lopinavir SLNs were prepared by previously reported warm oil-in-water micro-emulsion dispersion technique [20]. Briefly, stearic acid (quantity varied as per experimental design) was held in a molten state at 75 ± 0.5 ^oC and accurately weighed quantity of lopinavir (20 mg) was dispersed thoroughly in it to form a homogenous dispersion. Aqueous phase (25 ml) was prepared by dissolving PVA (quantity varied as per experimental design) into high purity water which was then heated. When temperatures of both the phases became isothermal, hot surfactant solution was added to molten lipid phase under homogenization (Polytron PT 3100D, Kinematica, Switzerland) at 10000 rpm for 3 min while maintaining the temperature at 75 ± 0.5 ^oC. The obtained microemulsion was quickly ultra-sonicated using a probe sonicator (Vibra cell, Sonics, USA) for a specific time

period at a constant amplitude (80 W output). The obtained o/w nanoemulsion was then cooled down in an ice-bath to form SLNs and the volume was finally adjusted to 75 ml with high purity cold water. Resultant colloidal preparation was centrifuged at 20,000 × g for 45 min to obtain lopinavir loaded SLNs. Prepared nanoparticles were washed three times with water to remove adherent free drug from the outer surface of nanoparticles. Washed nanoparticles were re-suspended in water and subjected to pre-freezing at –80 ^{o}C for 6 h. Further, freeze-drying was carried for 12 h at –110 ^{o}C in a lyophilizer (Coolsafe 110-4, Scanvac, Denmark). Five percent mannitol was used as a cryoprotectant. This lyophilized powder was stored in sealed glass containers at room temperature till further use. The scheme of preparation is illustrated in Fig. 4.4 below.

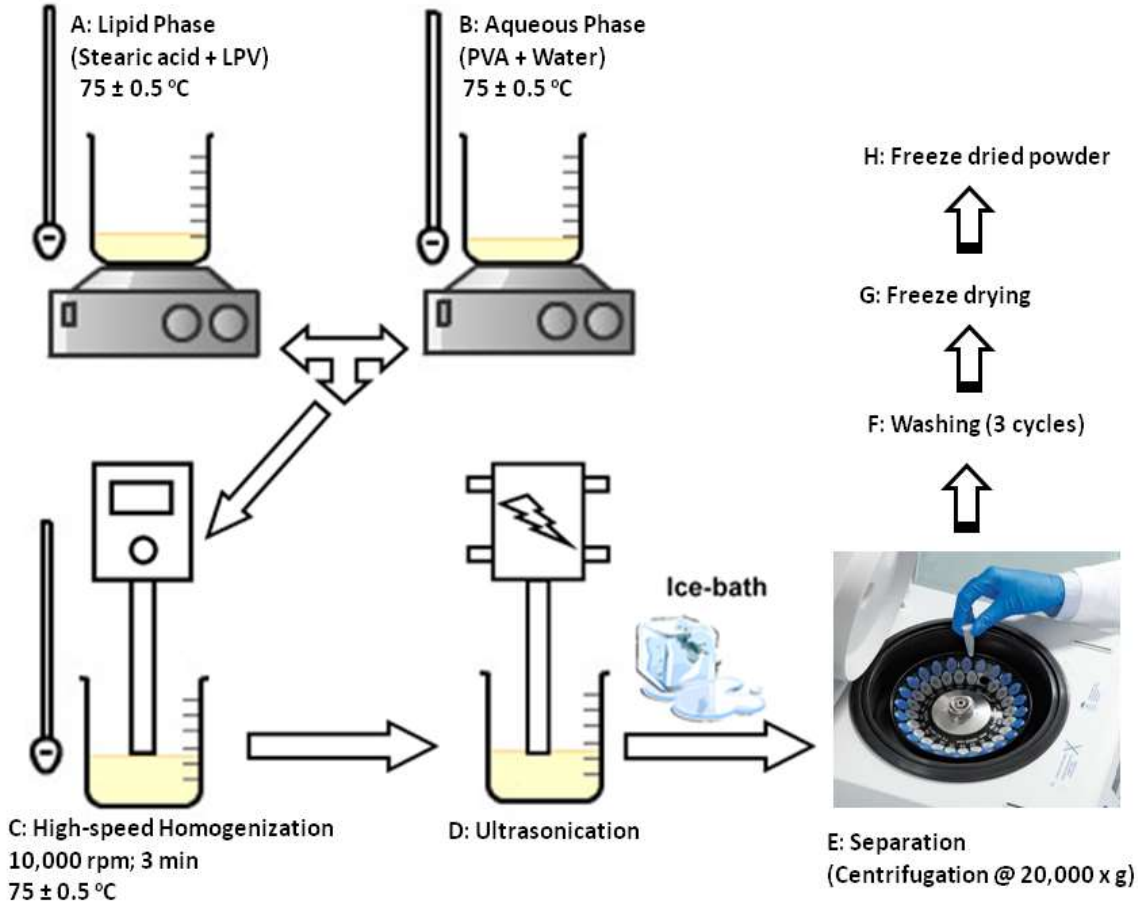

Fig. 4.4: Schematic representation of preparation of lopinavir SLNs by o/w micro-emulsion dispersion technique.

4.3.4 Analysis of lopinavir

The concentration of lopinavir present in different matrices was determined by RP-HPLC method as described in earlier section no. 2.2.

4.3.5 Nanoparticles characterization

a) Particle size and zeta potential analysis

Particle size, size distribution and zeta potential of the prepared NP dispersions were measured by Zetasizer (Nano ZS, Malvern Instruments Ltd., Worcestershire, UK). All the samples were suitably diluted with double distilled water before measurement. Backscattering was measured by a detector at an angle of 173^{o}. Instrument temperature was set at the 37 ^{o}C during the measurement.

b) Scanning electron microscopy (SEM) analysis

The surface morphology of optimized SLN formulation was examined under scanning electron microscope (JSM-6360LV Scanning Microscope; Jeol, Tokyo, Japan). Before analysis, 100 µl of SLN dispersion was placed on an aluminum stub and dried overnight under vacuum. This was then sputter-coated using a thin gold-palladium layer under an argon atmosphere using a gold sputter module in a high-vacuum evaporator (JFC-1100 fine coat ion sputter; Jeol, Tokyo, Japan). These coated samples were then scanned and photomicrographs were taken at an acceleration voltage of 15 kV.

c) Differential scanning calorimetry (DSC)

DSC analysis was carried out using DSC 60 (Shimadzu, Kyoto, Japan) instrument. Accurately weighted samples were taken in an aluminium pan and crimp sealed. Samples were equilibrated at 25 ^{o}C in DSC chamber. After sufficient equilibration time, samples were heated over a temperature range of 25 to 200 ^{o}C with constant heating rate of 5 ^{o}C/min during analysis.

d) Entrapment efficiency (EE) and drug loading determination

Drug EE was determined by previously reported ultra-filtration method [21] with slight modification using microfilters (Amicon Ultra; MWCO; 10 KDa). Briefly, microfilters containing 0.5 ml of SLN dispersion (suspended in water) were centrifuged at 6000 × g for 30 min to separate un-entrapped drug (free drug, $W_{free\ lopinavir}$) from the total drug ($W_{total\ lopinavir}$) added to the formulation. Un-entrapped drug (drug diffused through the membrane) was quantified by validated RP-HPLC method as described in an earlier section. Drug EE was calculated by following equation:

$$EE\ (\%) = \left[\frac{W_{total\ lopinavir} - W_{free\ lopinavir}}{W_{total\ lopinavir}} \right] x\ 100$$

Absence of membrane adsorption (non-specific binding) of lopinavir was confirmed by filtering lopinavir solution (1.5 µg/ml) prepared in phosphate buffer saline through microfilters. Recovery studies confirmed minimal adsorption of lopinavir (< 1%).

e) *In vitro* release study

In vitro drug release study of lopinavir nanoparticles was performed using the dialysis bag method [22]. Both free drug and lopinavir loaded nanoparticles were studied for *in vitro* release behaviour. For the study, a sealed dialysis bag (MWCO, 12–14 kDa, pore size 2.4 nm), containing free drug or loaded NPs equivalent to 1.5 mg lopinavir was completely submerged in to 50 ml drug release media (PBS containing 0.1% w/v Tween 80, pH 7.4). The temperature of the media was maintained at 37 ± 0.5 ^{o}C and media was stirred at 50 rpm using magnetic bead. The drug release media were completely replaced at pre-determined time intervals to the maintain sink conditions. Cumulative release of lopinavir in sample solution was determined by HPLC.

Obtained data were fitted into zero order, first order, Higuchi and reciprocal-powered time mathematical models for evaluation of release kinetics. Regression coefficient (r^2) and time for 50% dissolution ($t_{50\%}$) were calculated for the best-fit model.

1) Zero order model: $F = k_0 t$,
2) First order model: $\ln(1 - F) = -k_f\, t$,
3) Higuchi model: $F = k_H \sqrt{t}$,
4) Reciprocal powered time model: $(1/F - 1) = m/\, t^b$

Where, F is fraction of drug released up to time t; k_0, k_f, k_H, m and b are model parameters.

f) Stability studies

Stability of prepared formulations was assessed as per International Conference on Harmonization (ICH) Q1A (R2) guidelines (ICH, 2003) [23]. Briefly, lopinavir loaded NP suspensions were stored in sealed glass vials at at 25 ± 2 ^{o}C/60 ± 5% relative humidity in stability chamber (Remi, Mumbai, India). Control samples were stored at 2–8 ^{o}C in a refrigerator. Both of these samples were analyzed at monthly intervals over a period of three months for particle size, zeta potential and EE. Statistical evaluation was done using GraphPad Prism version 5.03 for Windows software (GraphPad Software, San Diego, USA).

4.3.6 *In vitro*/*in vivo* evaluation of optimized SLNs

a) Pharmacokinetic study

i) Selection of animal model

One of the most important facets of biomedical research is selecting the species of laboratory animal best suited for a particular purpose. Use of laboratory animals as model is often based on the premise that animals are more or less similar with respect to many biological characteristics and thus can be compared with humans. More specifically, animal models used during the pre-clinical evaluation are deemed appropriate if metabolites observed in humans (by *in vitro* methods or by clinical studies) are also formed in the animal model [24].

To study the pharmacokinetic behaviour of lopinavir, rat is considered the best animal model due to close similarities in metabolism and disposition characteristics of lopinavir in rats and humans. In a cross species study, Sham et al have demonstrated poor oral bioavailability of lopinavir attributing to extensive first pass metabolism and rapid clearance in both human and rat [25]. Metabolite profiling of lopinavir conducted with human liver microsomes and rat liver microsomes also reveals a close resemblance in metabolic pathways and metabolite formation [26]. Further, researchers have also demonstrated the sensitivity of rat towards the booster effect of ritonavir. Moreover, several researchers have used rat as a model to screen anti-HIV activity and booster effects of ritonavir [27, 28]. Thus, based on available literature, rat was chosen as an animal model to study the drug disposition behavior of various lopinavir formulations.

ii) Validation of animal model

In order to validate rat as an appropriate pharmacokinetic model for human, metabolism studies of lopinavir in rat liver microsomes and human liver microsomes were conducted. From the metabolism data, *in vivo* hepatic clearance of lopinavir (with and without ritonavir) was predicted for both of the species [29].

Hepatic clearance study of lopinavir was performed using established methods adapted from literature [30]. Substrate (lopinavir) and protein (microsomes) concentrations were optimized before the experiment. Results indicate that a maximum of 10 μM substrate and 1 mg /ml protein (of microsomal enzymes) can be used to study linear metabolism of lopinavir. Parent depletion method was used to determine *in vitro* $t_{1/2}$ of drug. The analyte peak areas were respectively converted to percentage drug remaining, using the T= 0 peak area values as 100%. The slope of the linear regression from log-percentage remaining versus incubation time relationships (-k) was used in the conversion to *in vitro* $t_{1/2}$, values by

in vitro $t_{1/2}$ = -0.693/k. Conversion to *in vitro* CL'_{int} (ml/min/kg) was done using the following formula:

$$CL'_{int} = \frac{0.693}{in\ vitro\ t1/2} \text{ x } \frac{\text{ml incubation}}{\text{mg microsomes}} \text{ x } \frac{\text{45 mg microsomes}}{\text{gm liver}} \text{ x } \frac{\text{20 gm liver}}{\text{kg b.w.}}$$

Details of experimental conditions are discussed under microsomal study section (4.3.6 d). Samples were terminated at pre-defined time intervals of 0 min, 5, 10, 15, 30, 45 and 60 min. Results obtained from metabolism studies are presented in Fig. 4.5.

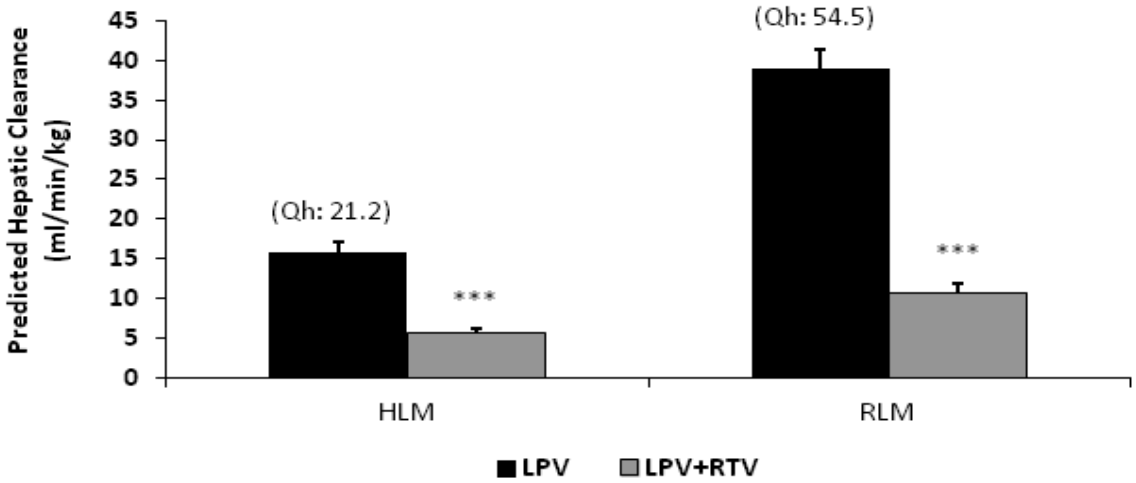

Fig. 4.5: Microsomal clearance study of lopinavir (with and without ritonavir 2.5 µM) in HLM and RLM. Parent depletion method was used to determine hepatic clearance of lopinavir (10 µM).

Result from metabolism study reveals high hepatic clearance of lopinavir in both rat and human. Predicted hepatic clearance of lopinavir for human and rat was 15.8±1.3 ml/min/kg and 38.9±2.5 ml/min/kg respectively. From the data, oral bioavailability of a lopinavir was predicted using following equation [30];

$$F = \left[1 - \left(\frac{Clh}{Qh}\right)\right] x100$$

Where Clh is hepatic clearance and Qh is portal blood flow. Portal blood flow in humans and rats are reported to be 21.2 ml/min/kg and 54.5 ml/min/kg respectively.

The oral bioavailability of lopinavir in rats (~28%) and humans (~25%) were predicted to be poor which agrees well with the reported literatures [31, 32]. Further, from the data, it is also evident that the rat microsomal system responds well towards ritonavir

and nearly similar reduction of hepatic clearance of lopinavir was observed in both of the microsomes.

Hence, from metabolism data, we validated rat as an appropriate model to study pharmacokinetic characteristics of lopinavir, ritonavir and lopinavir/ritonavir co-formulation.

iii) Dose selection and study restrictions

Human equivalent therapeutic dose in rats was calculated using the allometric equation for pharmacokinetic study of lopinavir [33]. As discussed earlier, recommended dose of lopinavir in adult patients for HIV treatment is 400 mg - lopinavir /50 mg - ritonavir. Based on body surface area, scaled down dose of Kaletra® in rat was calculated to be ~ 20 mg/kg lopinavir and 5 mg/kg ritonavir. Therefore, powder equivalent to lopinavir 20 mg/kg (and ritonavir 5 mg/kg) was orally administered to rats assigned for co-formulation group. In all pharmacokinetic studies, lopinavir/ritonavir co-formulation was prepared by crushing Kaletra® equivalent Lopimune® tablets (200 mg/50 mg) and suspending in 0.5% w/v methylcellulose (MC).

The study was restricted to fasted male rats, as a marked sex difference [34] and drug–food interaction [35] effects have been reported on the pharmacokinetic parameters of lopinavir and ritonavir in humans.

Pharmacokinetic studies were performed using male wistar rats, weighing 180–220 g. Animals were fasted overnight (12 h) before dosing and continued on fasting until 4 h post administration of the formulation. Thereafter, rat chow diet was provided *ad libitum*. In all studies, freshly prepared drug formulations were administered.

iv) Pharmacokinetic study design

A) Single dose oral study

For the oral pharmacokinetic study, based on study design, three different treatment groups were taken with five animals in each treatment group. Treatment groups were designated as: Group A (control group) - treated with lopinavir alone (20 mg/kg, lopinavir suspended in 0.5% w/v MC); Group B - treated with lopinavir/ritonavir co-formulation (20/5 mg/kg); Group C- treated with optimized lopinavir SLN formulation (20 mg/kg).

In a separate set of study, effect of lipid on the pharmacokinetics of lopinavir was evaluated by co-administering free lopinavir with blank SLNs (10 ml/kg).

B) Single dose IV bolus study

Intravenous pharmacokinetic studies of lopinavir were conducted following single dose bolus administration (IV, 4 mg/kg, 1 ml/kg) of free lopinavir solution and lopinavir SLNs. For the study, animals were randomly divided into two groups with five animals in each group. Group A (control group) - treated with a free lopinavir solution; Group B - treated with lopinavir loaded SLNs. For intravenous administration, lopinavir was dissolved in PEG:Ethanol:Water pre-mix.

C) Blood collection

Blood samples were collected from the orbital sinus into microfuge tubes containing (10% v/v) anti-coagulant (3.8% w/v sodium citrate) at pre-dose, 0.17, 0.25, 0.5, 1, 2, 3, 4, 6 , 8 and 12 h post dose for oral studies and at pre-dose, 0.08, 0.17, 0.25, 0.5, 1, 2, 4, and 6 h post dose for IV studies. Collected blood samples were kept on ice until further processing. These samples were further harvested for plasma by centrifuging at 4 ^{o}C for 10 min at 650 × g and then stored at –70 ^{o}C until further analysis. The samples were analyzed by a validated HPLC method for estimation of lopinavir in rat plasma matrix.

b) Tissue distribution study

Lopinavir bio-distribution was assessed in male wistar rats (180 ± 20 g; n = 36). The rats were randomly divided into three groups with 12 animals in each group. The groups were designated as: Group A (control group) - treated with lopinavir (20 mg/kg, lopinavir suspended in 0.5% w/v MC) alone; Group B - treated with lopinavir/ritonavir co-formulation (20/5 mg/kg); Group C - treated with the optimized lopinavir SLN formulation.

Three rats from each group were sacrificed at 0.5, 1, 2 and 4 h post-dosing. Individual animals were perfused with heparinized (5 IU) saline (0.9% w/v NaCl) through the portal vein in order to remove circulating blood from body organs before tissue collection. Tissues of interest (liver, spleen and mesenteric lymph nodes) were collected and stored at –70 ^{o}C until further analysis.

As discussed earlier, prior to analysis, tissue samples were thawed to room temperature, minced and homogenized to a fine paste (25% w/v) in a tissue homogenizer (Remi, Mumbai, India) along with methanol:water (1:4) mixture. Lopinavir was extracted from tissue homogenate by adding a protein precipitating agent, acetonitrile in the ratio 1:3 (v/v). Extracted samples were centrifuged (6000 × g for 15 min) and resultant clean supernatant (75 µl) was injected into the HPLC to determine lopinavir concentration in tissue samples.

c) Lymph transport inhibition study

Cycloheximide (CXI) is known to inhibit lymphatic uptake by interfering with secretion process of chylomicrons in enterocytes [36]. To discern the mechanism of SLN uptake, pharmacokinetic studies of free lopinavir and lopinavir SLNs were carried out in presence of CXI.

Based on experimental design, rats were randomly divided into four groups with three rats in each group. Groups were designated as follows: Group A and Group B – rats received (20 mg/kg) either free lopinavir or lopinavir SLNs; Group C and Group D – rats pre-treated with CXI and received either free lopinavir or lopinavir SLNs. Group C and Group D animals were pre-treated with CXI (3 mg/kg) intra-peritoneally (i.p.) 1 h prior to the drug administration. An equal volume of saline (3 mg/kg) was administered (i.p.) to Group A and Group B rats.

d) *In vitro* metabolism stability study

In vitro metabolism stability studies were performed by incubating free lopinavir, lopinavir/ritonavir (ritonavir at an effective concentration of 2.5 µM) co-formulation and lopinavir SLNs with rat intestinal microsomes (RIM) and rat liver microsomes (RLM) (1 mg/ml) at an effective concentration of 10 µM. The metabolism reaction was initiated by addition of NADPH (2 mM) in phosphate buffer (100 mM, pH 7.4). Incubations were performed at 37 ^{o}C in a shaking water bath for 30 min. The reaction was terminated by addition of cold acetonitrile. Samples were vortexed briefly and centrifuged at 6000 × g for 15 min. Resultant clean supernatant (75 µl) was injected into HPLC. Percentage metabolism of lopinavir was determined in all three test conditions.

In a separate set of experiment lopinavir was incubated in enzyme free buffer for 30 min to determine absence of lopinavir degradation in buffer (data not shown).

Effect of excipients present in SLN formulation on metabolic function of the microsomal enzyme system was examined by incubating blank SLNs (SLNs prepared without drug) along with free lopinavir. Any difference in metabolism (compared with free lopinavir alone) was taken as enzyme inhibition.

e) Intestinal uptake study

Everted gut sac studies in rats were performed using established methods adapted from literature [37]. For the study, male wistar rats were fasted overnight for 12 h and sacrificed by cervical dislocation. The rat intestinal segments were identified and separated from the body. A length of 8-10 cm of jejunum was rapidly removed and gently everted over a glass rod. Everted intestine was then slipped off the glass rod and placed in a flat dish

containing Krebs-Henseleit bicarbonate (KHB) buffer oxygenated with O_2/CO_2 (95% / 5%) at 37 ^oC. Further, KHB solution (0.5 ml) was filled into the everted gut sac. The sac was sealed by tying open ends with silk thread. Intestinal sacs were then placed in individual incubation chambers containing free lopinavir (2.5 µg/ml), lopinavir/ritonavir (lopinavir and ritonavir at an effective concentration of 2.5 µg/ml and 0.625 µg/ml, respectively) co-formulation, lopinavir SLNs (2.5 µg/ml), and lucifer yellow (10 µg/ml) prepared in KHB buffer at a maintained temperature of 37 ^oC.

In order to discern the uptake mechanism, permeability studies for lopinavir in free lopinavir, lopinavir/ritonavir co-formulation and lopinavir loaded SLNs were conducted at low temperature or in the presence of specific endocytosis inhibitors; chlorpromazine (CPZ, 10 µg/ml) and nystatin (NYT, 25 µg/ml). After an incubation time of 60 min, intestinal sacs were carefully removed, blotted onto filter paper and contents were collected. Intestinal sacs were rinsed thrice with KHB solution and rinsings were pooled with original content for analysis. Samples were analyzed by a validated HPLC method.

In the present study, lucifer yellow was chosen as a fluorescent hydrophilic paracelluar marker to evaluate epithelial cell tightness over the study period [38]. Lucifer yellow was measured by previously reported spectrofluorimetric method [39] with excitation and emission wavelengths of 418 and 512 nm. Briefly, calibration curve for lucifer yellow was prepared in buffer solution. Mucosal and serosal samples were centrifuged for 10 min at 3000 ×g to precipitate mucus and other solid matter. Samples were appropriately diluted with a blank buffer before analysis.

P_{app} values, expressed in cm/s, were calculated [40] in each experimental condition using the following equation:

$$P_{app} = \left(\frac{dQ}{dt}\right) \text{x} \frac{1}{A \text{ x } C0}$$

Where dQ/dt is the rate of appearance of lopinavir or lucifer yellow in the everted gut sac (receiver compartment), C_o is the initial concentration of lopinavir or lucifer yellow outside everted gut sac (donor compartment) and A is the total cross sectional area of tissue.

4.4 Statistical analysis

All *in vitro* studies were performed in triplicate and data from these experiments are expressed as mean ± SD. Non-compartmental pharmacokinetic analysis was performed using Phoenix® WinNonlin® (Pharsight Inc., Mountain view, CA, USA) to determine various pharmacokinetic parameters. Unpaired *t-test* or Analysis of Variance (ANOVA),

followed by Dunnett's test (Graphpad Prism, version 5.03) was used to assess any significance of difference between means. The significance level was set at 5%.

4.5 Results

4.5.1 Experimental design

a) Preliminary experiments

Critical process variables in preparation of SLN formulations were screened using low resolution Plackett-Burman design (PBD). Particle size and EE of lopinavir loaded SLNs were taken as critical quality attributes. From PBD, amount of lipid, surfactant type, surfactant concentration and ultra-sonication time were found to be most critical variables influencing EE and particle size. For evaluation of the effect of surfactant; type two surfactants, tween 80 and PVA were selected. Formulations prepared with tween 80 (1% w/v) showed low particle size (245.2 ± 2.2 nm) and moderate EE (40.4 ± 3.3%). However, formulations with PVA (1% w/v) showed particle size of 239.5 ± 3.2 nm and EE of 75.6 ± 2.1%. Difference in EE is explained by the difference in saturation solubility of lopinavir in aqueous solution of these surfactants. The saturation solubility of lopinavir in tween 80 and PVA solutions (1% w/v) were 45.8 ± 1.4 µg/ml and 2.5 ± 0.8 µg/ml respectively. Hence, PVA was selected as a surfactant for further trials.

b) Box-Behnken design

Selected critical variables showed statistically significant influence on particle size and EE (Table 4.3). Quadratic equations establishing main effects and interaction effects were determined based on estimation of statistical parameters generated by Design Expert software. Statistical validation of quadratic equations was confirmed by ANOVA. In Fig. 4.6 (a-d), response surface graphs illustrating the effects of critical variables on the particle size and the EE of SLNs are presented.

Effects on particle size (Y_1)

As shown in Table 4.2, particle size of formulations ranged between 218.5 nm (run 1) and 415.0 nm (run 8); this indicated sensitivity of critical variables selected for study. Experiments carried out at the center points (run 1, 6, 13, 16 and 17; n = 5) of the design indicate reproducibility of experiment as coefficient of variation (CV) is less than 2%. Independent factors affecting particle size can be explained by following quadratic equation:

$$Y_1 = 219.7 - 9.76\,(X_1) + 18.3\,(X_2) + 2.19\,(X_3) + 0.75\,(X_1X_2) + 3.53\,(X_1X_3) - 29.90\,(X_2X_3) + 90.34\,(X_1^{\,2}) + 47.96\,(X_2^{\,2}) + 40.49\,(X_3^{\,2})$$

A regression coefficient (r^2) of 0.9432 for the equation indicated a good correlation between observed response and selected critical variables. Residuals were distributed randomly around zero and there was no effect of experimental sequence on the trend of residuals.

Effects on entrapment efficiency (EE, Y_2)

As shown in Table 4.2, EE varied between 45.1% (run 11) to 83.0% (run 1) which indicates that the response was sensitive towards selected factors. Experiments performed at the center points of the design (run 1, 6, 13, 16 and 17; n = 5) confirmed that the experimental method was highly reproducible (CV < 3%). From the data presented in Table 4.3, it is evident that independent factors affecting EE were; concentration of surfactant (X_1), amount of lipid (X_2) and time of ultra-sonication (X_3).

Effect can be explained by following second-order polynomial quadratic equation:

$$Y_2 = 79.80 + 6.70\,(X_1) + 11.61\,(X_2) + 3.99\,(X_3) - 3.55\,(X_1X_2) - 3.40\,(X_1X_3) - 1.27\,(X_2X_3) - 7.44\,(X_1{}^2) - 6.81\,(X_2{}^2) - 8.36\,(X_3{}^2)$$

The regression value of above equation was 0.9866 indicating suitability of the selected design model. Residual analysis showed that residuals were normally distributed around zero and there was no trend of residuals on the outcome.

Table 4.2. Box-Behnken experimental design.

Run	Surfactant concentration (X_1, % w/v)	Lipid amount (X_2, mg)	Ultra-sonication time (X_3, min)	Particle size (Y_1, *nm*)	Entrapment efficiency (Y_2, %)
1	1.0	800	10	218.5	83.0
2	0.5	800	15	367.8	59.8
3	0.5	800	5	372.5	59.2
4	1.5	400	10	299.0	62.0
5	1.0	400	15	366.8	51.8
6	1.0	800	10	220.0	77.0
7	1.5	800	5	327.8	75.8
8	0.5	1200	10	415.0	76.2
9	1.0	1200	5	309.5	80.0
10	1.0	400	5	239.3	55.0
11	0.5	400	10	353.4	45.1
12	1.5	1200	10	364.2	78.9
13	1.0	800	10	222.0	81.0
14	1.5	800	15	335.9	62.2
15	1.0	1200	15	316.2	71.7
16	1.0	800	10	217.0	77.4
17	1.0	800	10	221.0	81.1

a)

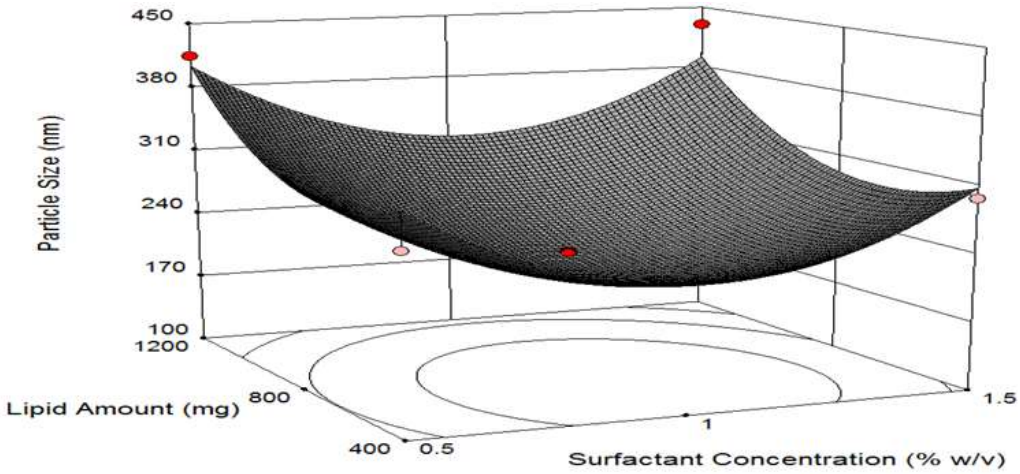
Particle Size (nm)
450
380
310
240
170
100
1200
800
400
Lipid Amount (mg)
0.5
1
1.5
Surfactant Concentration (% w/v)

b)

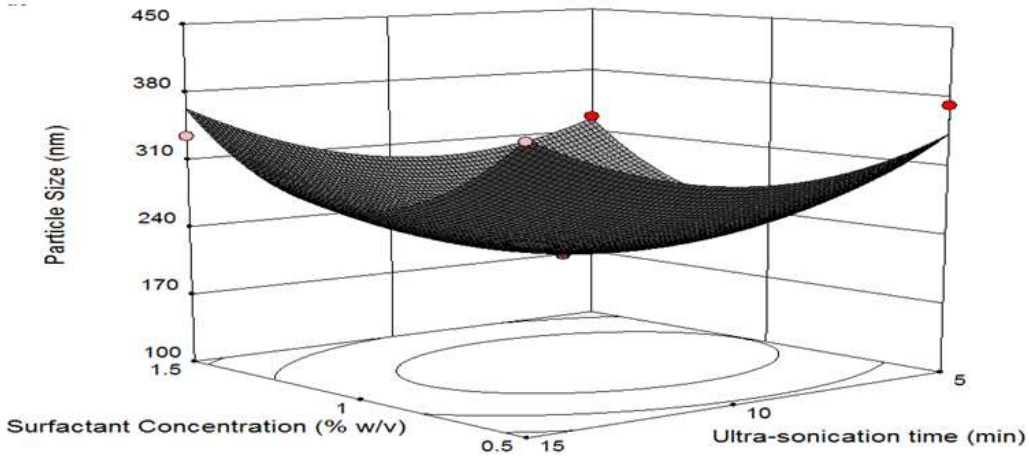
Particle Size (nm)
450
380
310
240
170
100
1.5
1
0.5
Surfactant Concentration (% w/v)
15
10
5
Ultra-sonication time (min)

c)

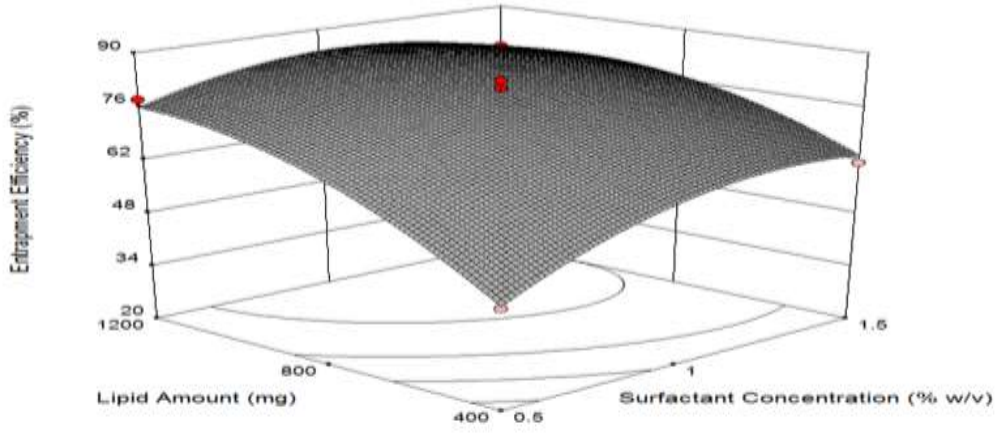
Entrapment Efficiency (%)
90
76
62
48
34
20
1200
800
400
Lipid Amount (mg)
0.5
1
1.5
Surfactant Concentration (% w/v)

d)

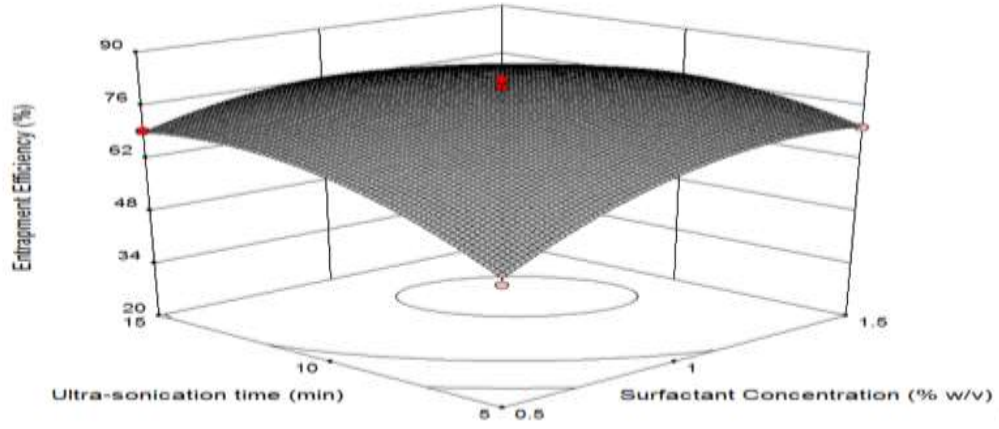
Entrapment Efficiency (%)
90
76
62
48
34
20
15
10
5
Ultra-sonication time (min)
0.5
1
1.5
Surfactant Concentration (% w/v)

Fig. 4.6: **a)** Response surface plot showing effect of surfactant concentration (X_1) and lipid amount (X_2) on particle size; **b)** Response surface plot showing the effect of surfactant concentration (X_1) and ultra-sonication time (X_3) on particle size; **c)** Response surface plot showing the effect of surfactant concentration (X_1) and lipid amount (X_2) on entrapment efficiency; **d)** Response surface plot showing effect of surfactant concentration (X_1) and ultra-sonication time (X_3) on entrapment efficiency.

c) Optimization and validation

To acquire an optimized formulation, desirability function (0.95) was probed using Design Expert software. As shown in Table 4.1, selection of optimum formulation was based on pre-set criteria. Conditions for optimal formulation as predicted by the software were as follows: surfactant concentration = 1.09% (w/v), lipid amount = 880.23 mg and duration of ultra-sonication = 9.05 min. To prove the validity of this statistical model, verification runs (n = 6) with these conditions were carried out; Wilcoxon Sign Rank Test was used to identify statistically significant differences between actual and theoretical values. At $\alpha = 0.05$, there was no statistically significant difference between actual and theoretical values for particle size ($p \geq 0.0867$) and EE ($p \geq 0.875$). This affirms the validity of the proposed model. Optimized formulation exhibited particle size of 223.3 ± 4.3 nm, and EE of 83.1 ± 2.35%.

Table 4.3. Statistical analysis results of particle size and entrapment efficiency (EE).

Source	Particle size (Y_1)				EE (Y_2)			
	Sum of Squares	DF	F-value	P-value	Sum of Squares	DF	F-Value	P-value
Model	68738.63	9	14.54	0.001*	2237.02	9	57.19	0.0001*
X_1	4145.05	1	7.89	0.0262*	176.72	1	40.66	0.0004*
X_2	2679.12	1	5.1	0.049*	1078.8	1	248.22	0.0001*
X_3	2363.28	1	4.5	0.0716#	71.4	1	16.43	0.0049*
X_1X_2	2.25	1	0.0042	0.9497#	50.41	1	11.6	0.0114*
X_1X_3	49.7	1	0.095	0.7674#	46.24	1	10.64	0.0138*
X_2X_3	3576.04	1	6.81	0.035*	6.5	1	1.5	0.2608#
X_1^2	34361.53	1	65.41	0.0001*	232.91	1	53.59	0.0002*
X_2^2	9685.9	1	18.44	0.0036*	195.41	1	44.96	0.0003*
X_3^2	6902.05	1	13.14	0.0085*	294.45	1	67.75	0.0001*
Residual	3677.53	7			30.42	7		
Lack-of -fit	3661.73	3	309.01	0.078#	1.62	3	0.075	0.9702#
Pure error	15.8	4			28.8	4		
Total	72416.16	16			2267.44	16		

*Significant at $p < 0.05$. #Not significant at $p < 0.05$ (non significant lack-of-fit).

4.5.2 Nanoparticles characterization

From SEM photomicrograph, near spherical shape of optimized lopinavir SLNs was evident (Fig. 4.7). Mean particle size, polydispersity index (PDI) (Fig. 4.8) and zeta potential value of optimized lopinavir SLNs (*n* = 6) were 223.3 ± 4.3 nm, 0.21 ± 0.11 and −21.23 ± 2.5 mV respectively. The negative zeta potential was attributed to the presence of free carboxylic acid groups in SA.

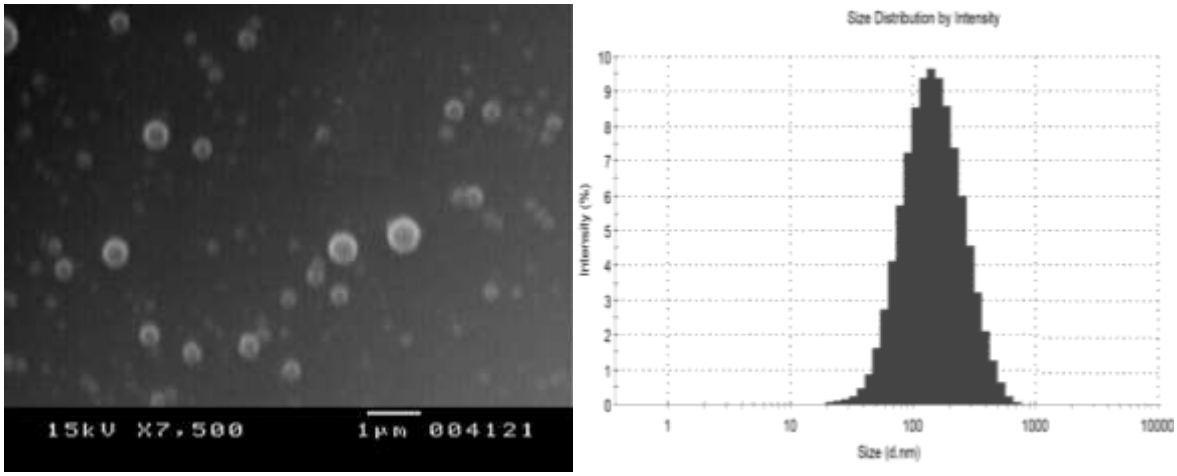

Fig. 4.7 and 4.8: Scanning electron microscopic image (right) and particle size distribution profile (left) of the optimized lopinavir SLNs.

Fig. 4.9 shows DSC thermograms for pure lopinavir, bulk stearic acid (SA, lipid), physical mixture of lopinavir and SA (1:1), blank SLNs and lopinavir SLNs. DSC thermogram for pure lopinavir showed a sharp melting peak at 97.2 ^{o}C while bulk SA showed melting peak at 69.8 ^{o}C. In DSC thermograms of blank and lopinavir SLNs, an additional peak observed at 168.3 ^{o}C was of mannitol (used as cryoprotectant).

Fig. 4.10 represents i*n vitro* drug release profiles of optimized SLNs and free lopinavir. Free lopinavir completely released from dialysis bag within 5 h. Lopinavir SLNs showed a bi-phasic release pattern; this was characterized by an initial rapid release (45%) in first 8 h followed by slow and continuous drug release up to 96 h. Drug release kinetics were studied by fitting data into various mathematical models. From regression analysis, drug release from SLNs was most appropriately described by reciprocal-powered time model (r^2 = 0.9763). In comparison, zero-order kinetics (r^2 = 0.3198), first-order kinetics (r^2 = 0.9437) and Higuchi kinetics (r^2 = 0.8784) showed relatively lower r^2 values. Time taken for 50% drug release ($t_{50\%}$) from SLNs was calculated to be 11.21 h.

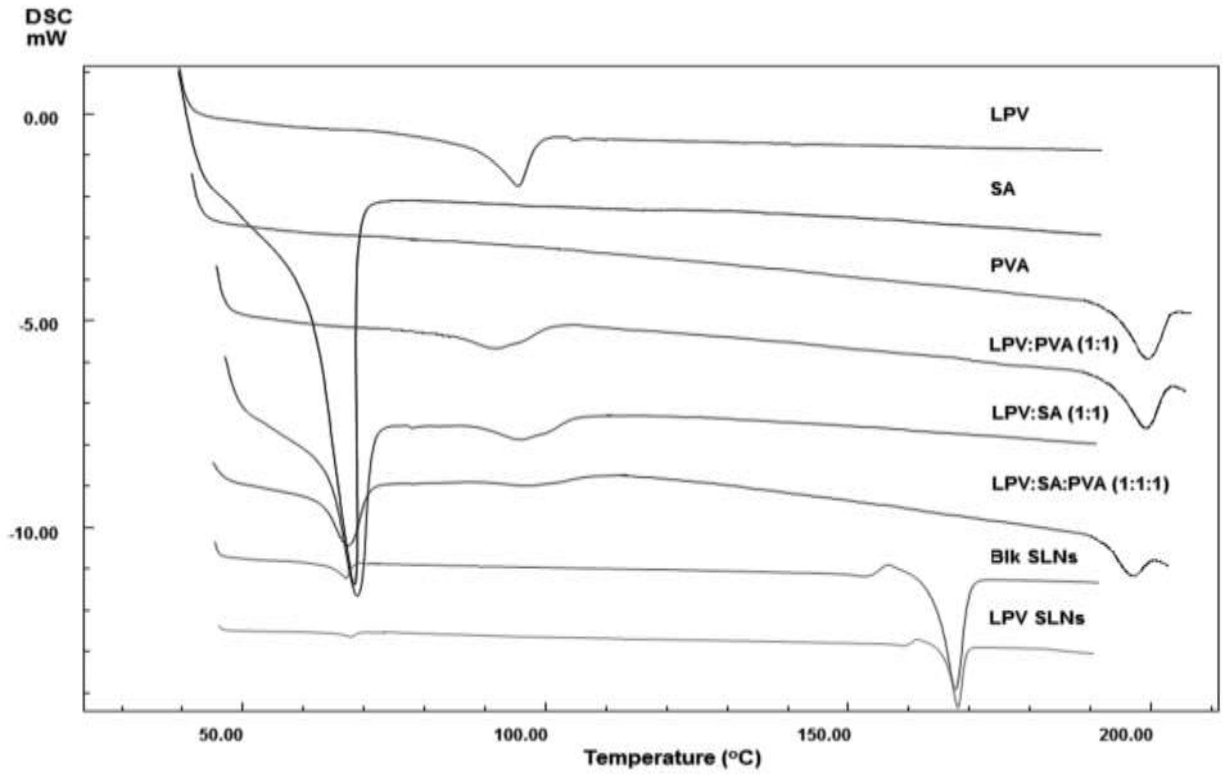

Fig. 4.9: Overlaid DSC thermograms of pure lopinavir, bulk SA (lipid), bulk PVA, physical mixture of lopinavir: SA (1:1), lopinavir: PVA (1:1), lopinavir: SA: PVA (1:1:1), blank SLNs and lopinavir SLNs. LPV, lopinavir; SA, stearic acid; PVA, polyvinyl alcohol; SLNs, solid lipid nanoparticles.

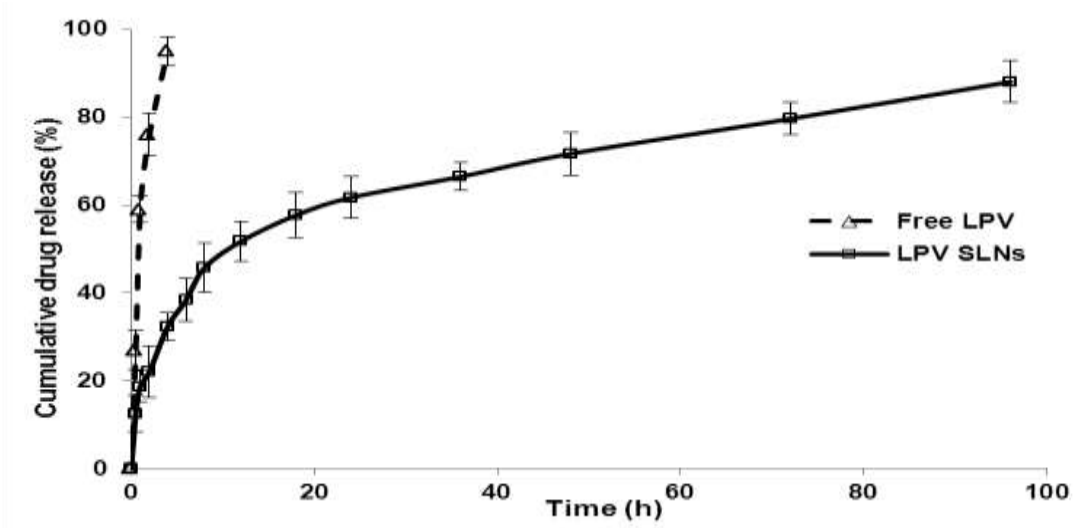

Fig. 4.10: *In vitro* drug release profile of free lopinavir and lopinavir SLNs in PBS pH 7.4. Data are presented as mean ± SD (n = 3).

Stability estimation for optimized lopinavir SLN suspension was done on the basis of particle size, EE, zeta potential and PDI variations during three month study period. Results show (Fig. 4.11) that there was no significant ($p < 0.05$) change in assessed parameters when lopinavir SLNs are stored at 2–8 ^{o}C. Similarly, SLN sample stored at 25 ±

2 ^{o}C/60 ± 5% RH showed no significant change in particle size and zeta potential. However, in these samples, statistically significant ($p < 0.05$) reduction in EE was observed. The EE of SLNs at the end of 3 months was 70% of initial formulation. Hence, storage of SLN under refrigerated condition is recommended.

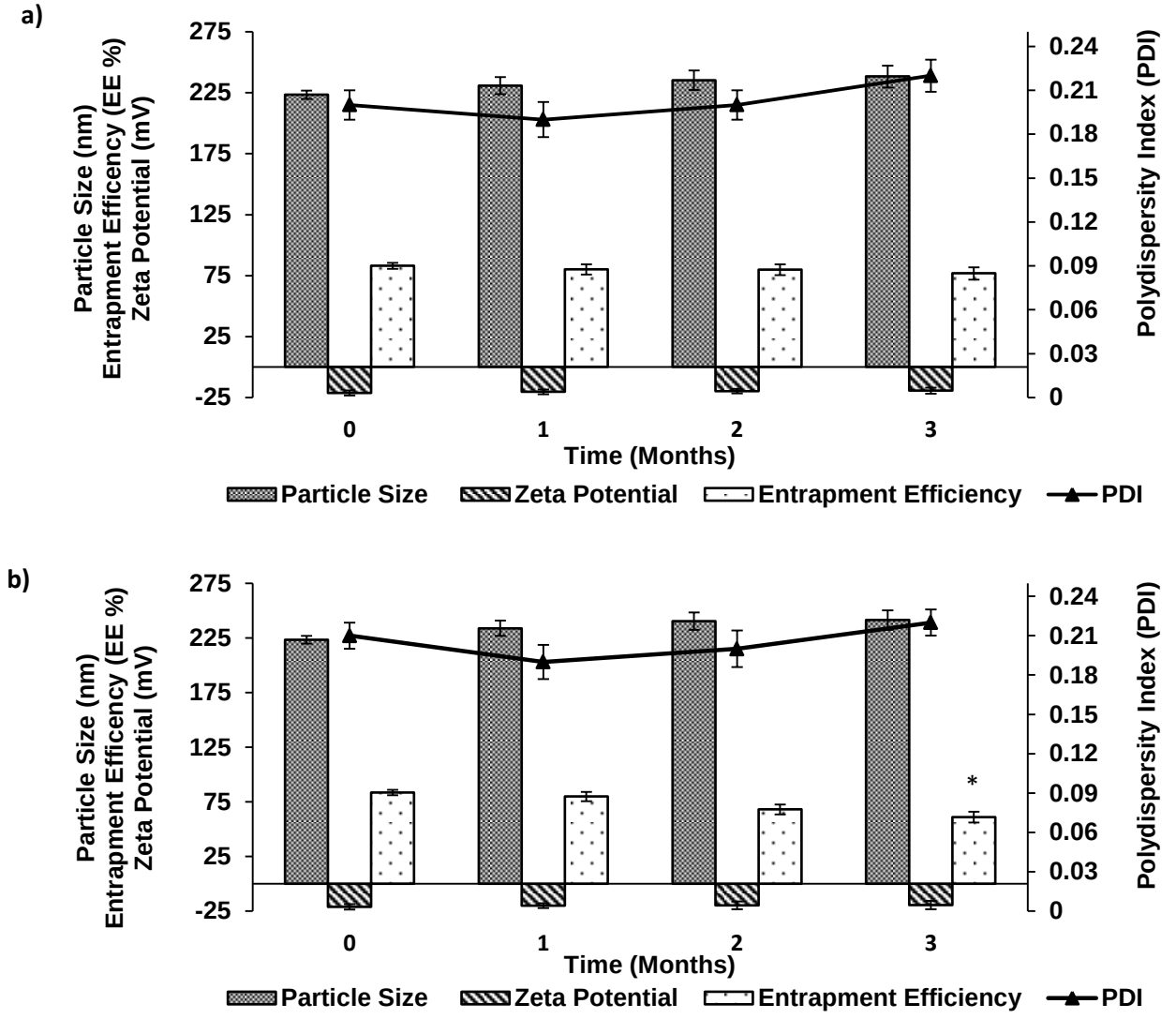

Fig. 4.11: Stability characteristics of lopinavir loaded SLNs in terms of mean particle size, entrapment efficiency (EE), Zeta potential and polydispersity index (PDI) stored at; **a)** 2–8 ^{o}C and **b)** 25 ± 2 ^{o}C and 60% ± 5% RH. The data are expressed as mean ± S.D. of six independent determinations ($n = 6$). *Statistically significance difference ($p < 0.05$) as compared to 0 month EE sample. LPV, lopinavir; SLNs, solid lipid nanoparticles.

4.5.3 *In vitro*/*in vivo* evaluation of optimized nanoparticles

a) Pharmacokinetic studies

Comparative pharmacokinetic performances of free lopinavir, lopinavir/ritonavir co-formulation and optimized lopinavir SLNs following oral administration to male wistar rats are shown in Fig. 4.12 and Table 4.4.

Following oral administration, both lopinavir/ritonavir co-formulation and lopinavir SLNs showed statistically significant improvement in the pharmacokinetics of lopinavir as determined by AUC, C_{max} and mean residence time (MRT).

Co-administration of RTV with lopinavir (Group B) significantly increased lopinavir AUC by 3.7 folds ($p < 0.001$), C_{max} by 2.1 folds ($p < 0.001$) and MRT by 1.5 folds ($p < 0.05$) as compared to free lopinavir (Group A). Whereas, lopinavir SLNs (Group C) increased lopinavir AUC by 5.1 folds ($p < 0.001$), C_{max} by 2.6 folds ($p < 0.001$) and MRT by 1.7 folds ($p < 0.05$). Statistically no significant effect was observed on time to reach maximum plasma concentration (T_{max}) in either of treatment groups as compared to free lopinavir.

Comparative pharmacokinetic parameters of free lopinavir and lopinavir SLNs following IV administration are given in Table 4.4. Statistically significant change in disposition parameters of lopinavir was observed following IV administration of loaded NPs as compared to free lopinavir solution. Total plasma clearance (CL) of lopinavir from SLNs reduced by 36% ($p < 0.01$). On the contrary, a significant increase in $T_{1/2}$ (increased by 2.05 folds, $p < 0.01$), V_d (1.6 folds, $p < 0.05$) and AUC (increased by 2.3 folds, $p < 0.01$) was demonstrated.

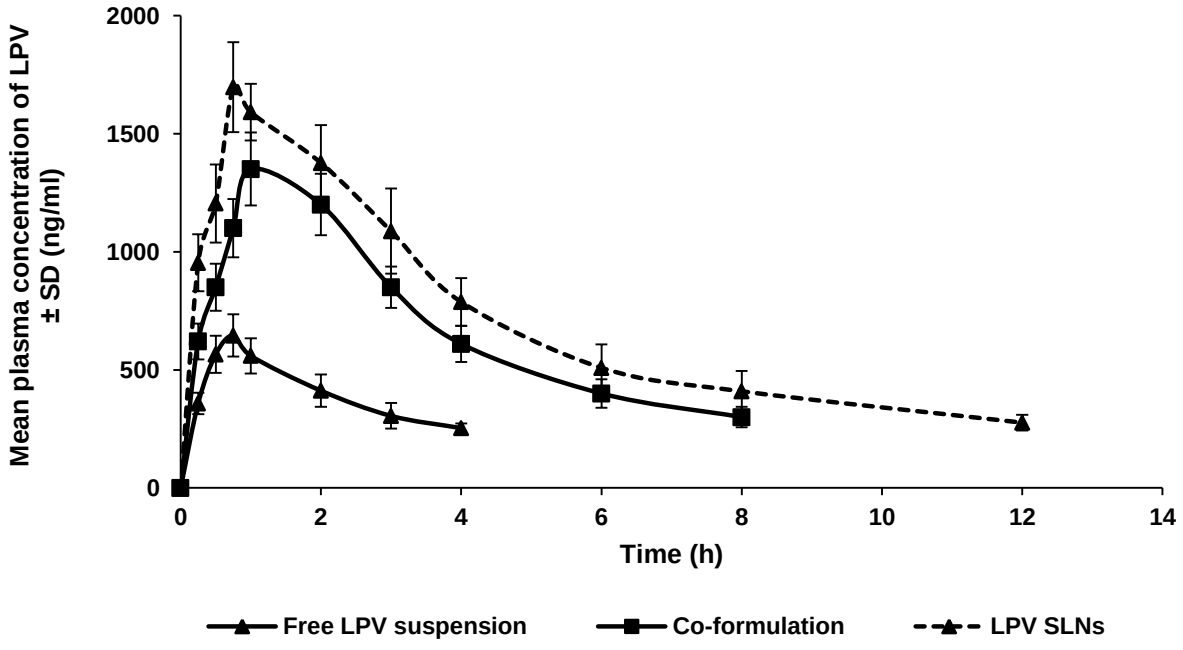

Fig. 4.12: Mean plasma concentration-time profile of lopinavir following oral administration of free lopinavir, lopinavir/ritonavir co-formulation and lopinavir SLNs to wistar rats (n = 5). The data are expressed as mean ± SD. LPV, lopinavir; RTV, ritonavir; SLNs, solid lipid nanoparticles.

To understand the effect of lipid on pharmacokinetics of lopinavir, blank vehicle was co-administered with free lopinavir. Data obtained from study (Fig. 4.13) did not reveal any significant effect of lipid matrix on pharmacokinetic parameters of free lopinavir.

Table 4.4. Pharmacokinetic parameteres of lopinavir post oral and IV administration of free lopinavir, lopinavir/ritonavir co-formulation and lopinavir SLNs to wistar rats.

Oral (20 mg/kg) Parameters	**Free lopinavir (Group A)**	**Lopinavir/RTV (Group B)**	**Lopinavir SLNs (Group C)**
C_{max} (ng/ml)	645.85 ± 89.7	1350.45 ± 113.41***	1694.39 ± 156.59***
T_{max} (h)	0.85(0.75-1.0)	0.89 (0.75-1.0)	1.4 (0.75-2.0)
MRT(h)	5.09 ± 0.25	7.81± 0.47*	8.57 ± 0.52*
AUC (ng/ml*h)	1655.52 ± 53.34	6151.75 ± 112.45***	8402.05 ± 98.59***
F_{rel}		3.72 ± 0.21	5.07 ± 0.35
IV (4 mg/kg) Parameters	**Free lopinavir (Group A)**		**Lopinavir SLNs (Group B)**
C_o (ng/ml)	2342.01 ± 114.17	-	1788.702 ± 170.54
$T_{1/2}$	0.76 ± 0.12	-	1.54± 0.13**
CL (ml/h/kg)	1543.52 ± 129.41	-	985.56 ± 101.23**
V_d (ml/kg)	1658.99 ± 133.09	-	2593.98 ± 298.23*
AUC (ng/ml*h)	2592.10 ± 183.34	-	5879.56 ± 310.25**
F_{el}	-	-	2.3± 0.13

*Statistically no significance difference (p > 0.05) between Group B and C; ***Statistically significance difference (p < 0.001) as compared to Free lopinavir (Group A). The data are expressed as mean ± S.D. LPV, lopinavir; RTV, ritonavir; SLNs, solid lipid nanoparticles.

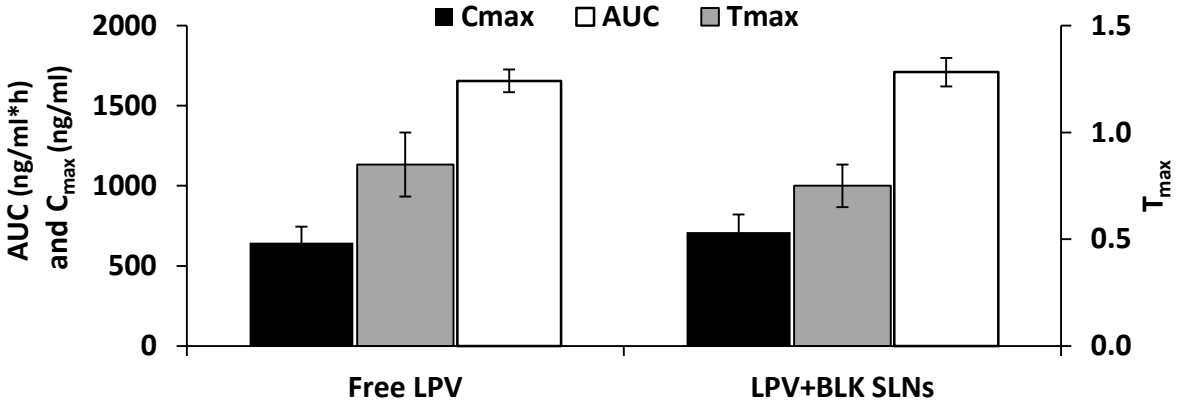

Fig. 4.13: Effect of lipid on pharmacokinetic parameters of free lopinavir following oral administration to wistar rats (n = 5). The data are expressed as mean ± SD. LPV, lopinavir.

b) Tissue-distribution study

The tissue-distribution study was done for free lopinavir, lopinavir/ritonavir co-formulation and lopinavir SLNs to determine the exposure of lopinavir in target organs (liver, spleen and mesenteric lymph nodes).

As shown in Fig. 4.14, statistically significant ($p < 0.01$) accumulation of lopinavir from lopinavir SLNs was observed in all three tissues of interest. In comparison to free drug, in liver tissue, C_{max} of lopinavir from SLN increased by 1.8 folds and AUC increased by 1.9. Similar observation was made in spleen tissue where C_{max} increased by 2.4 folds, AUC increased by 2.3 folds for lopinavir SLNs. In lymph nodes, accumulation of lopinavir from SLN was evident. Here, for lopinavir SLNs, C_{max} increased by 2.5 folds and AUC by 2.6 folds.

Following co-administration of lopinavir with ritonavir, statistically significant ($p < 0.05$) accumulation of lopinavir in liver tissue was observed. In this case, when co-administered with ritonavir, lopinavir's C_{max} increased by 1.3 folds and AUC increased by 1.4 folds. However, for spleen and lymph nodes, no statistically significant change in C_{max} and AUC was observed.

c) Lymphatic transport inhibition study

The data from this experiment (Fig. 4.15) indicated that plasma concentrations of lopinavir from lopinavir SLNs in CXI pre-treated rats (Group D) were significantly lower than saline pre-treated rats (Group B). In CXI pre-treated rats, following oral administration of lopinavir SLNs, C_{max} and $AUC_{0-\infty}$ of lopinavir were significantly reduced ($p < 0.05$) by 31.32 % and 44.44% respectively. However, statistically no significant change in plasma exposure of free lopinavir was observed in CXI pre-treated rats.

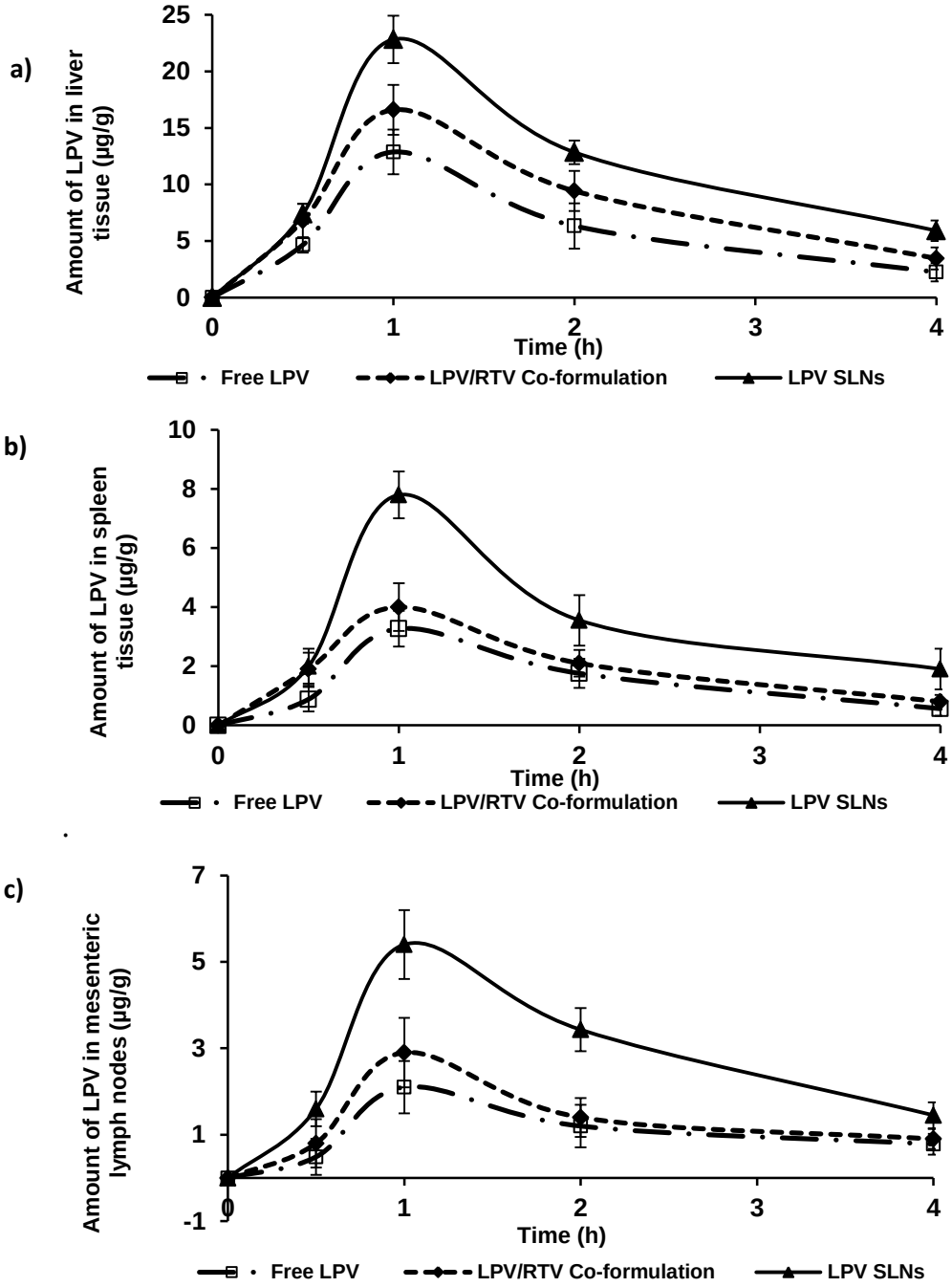

Fig. 4.14: Tissue distribution study of free lopinavir, lopinavir/ritonavir co-formulation and lopinavir loaded SLNs following oral administration to wistar rats. Three animals were sacrificed at each time point to harvest **a)** liver, **b)** spleen and **c)** mesenteric lymph node tissues. The data
are expressed as mean ± SD. LPV, lopinavir; RTV, ritonavir; SLNs, solid lipid nanoparticles.

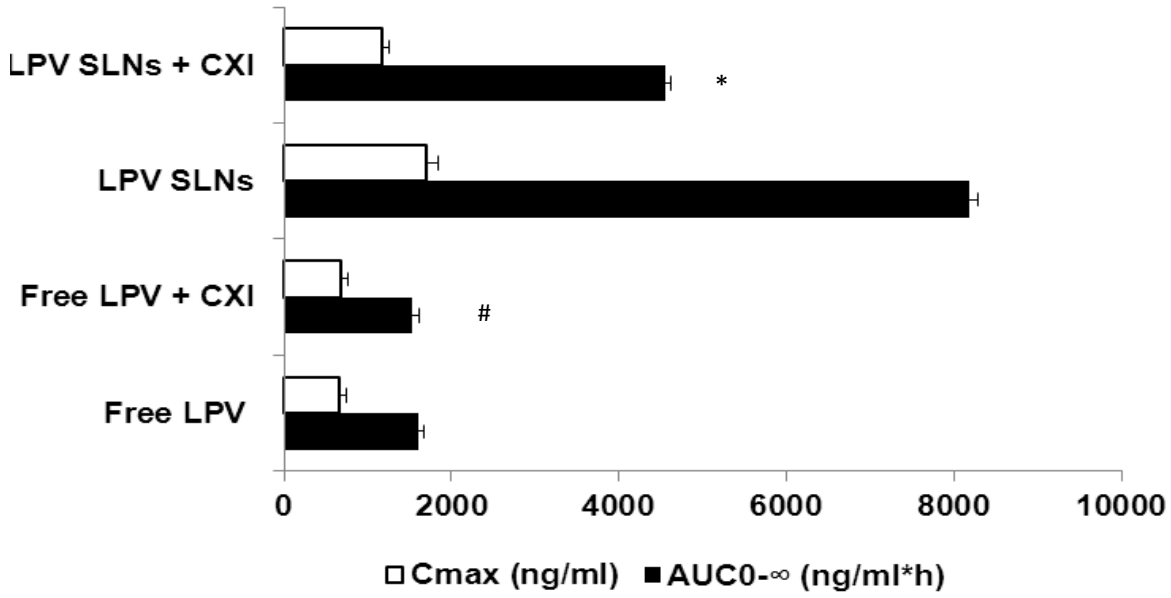

Fig. 4.15: Lymphatic transport inhibition study of lopinavir SLNs in normal rats (n = 3). To block lymph transport, rats were intra-peritoneally pre-treated with CXI (3 mg/kg) 1 h prior to the drug administration. [#]Statistically no significance difference (p> 0.05) as compared to free lopinavir; [*]Statistically significance difference (p< 0.05) as compared to LPV SLNs. The data are expressed as mean ± S.D. CXI, cycloheximide; LPV, lopinavir; SLNs, solid lipid nanoparticles.

d) *In vitro* metabolism stability study

Results obtained from *in vitro* metabolism stability studies are shown in Fig. 4.16. Mean percentage metabolism of lopinavir was reduced significantly (p < 0.001) upon co-incubation with RTV (metabolism of 8.5% in RIMs; 7.8% in RLMs) as compared to free lopinavir (metabolism of 89.2% in RIMs; 81.3% in RLMs) after 30 min of incubation period in both of the microsomes. Similarly, mean percentage metabolism of lopinavir in lopinavir SLNs (metabolism of 14.1% in RIMs; 18.4% in RLMs) was found to significantly (p < 0.001) reduce as compared to free lopinavir. However, statistically no significant change in metabolism of free lopinavir was observed upon co-incubation with blank SLNs.

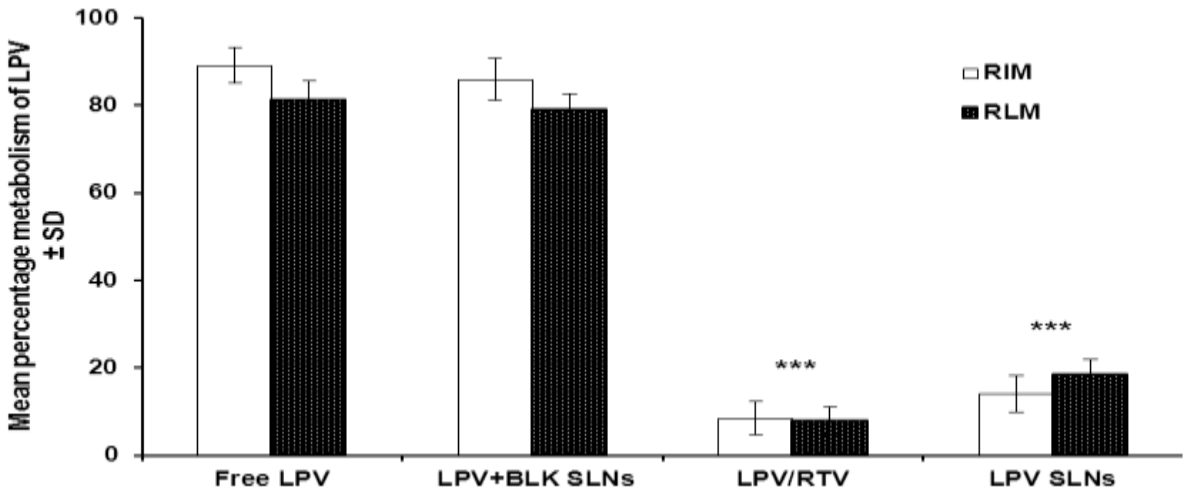

Fig. 4.16: Metabolism stability of free LPV, LPV/RTV co-formulation and LPV SLNs after 30 min incubation with RIM and RLM at1 mg/ml protein concentration. ***Statistically significance difference ($p < 0.001$) as compared to Free LPV. The data are expressed as mean ± S.D. LPV, lopinavir; RTV, ritonavir; SLNs, solid lipid nanoparticles; RIM, rat intestinal microsomes; RLM, rat liver microsomes.

e) Nanoparticles uptake study

Table 4.5 presents a comparison of apparent permeability (P_{app}) values of lopinavir after 60 min incubation through rat everted gut sacs. Experimental results demonstrated a significant increase in P_{app} values of lopinavir in lopinavir/ritonavir co-formulation and lopinavir SLNs as compared to free lopinavir (control group at 37 ^{o}C). Co-administration of ritonavir with lopinavir significantly increased P_{app} of lopinavir by 2.7 folds ($p < 0.01$) as compared to control group. Whereas, the P_{app} of lopinavir SLNs was found to increase by 1.9 folds ($p < 0.01$) as compared to control group.

In order to investigate the mechanism of SLNs uptake into everted gut sac, intestinal uptake study of lopinavir was further performed at 4 ^{o}C and in presence of CPZ and NYT. Results revealed that low incubation temperature (4 ^{o}C) and presence of specific inhibitors significantly ($p < 0.05$) reduced the intestinal uptake of NPs. As shown in Table 4.5, intestinal uptake of SLNs at 4 ^{o}C was reduced by about 25 % than 37 ^{o}C control. The P_{app} of lopinavir SLNs was reduced by 27% and 38% than control after co-incubation with CPZ and NYT respectively.

However, treatment conditions (reduced temperature and presence of endocytic uptake inhibitors) did not bring any significant change in P_{app} values of free lopinavir, lopinavir/ritonavir co-formulation and lucifer yellow.

Table 4.5. Effect of incubation temperature and endocytic uptake inhibitors (chlorpromazine, 10 μg/ml and nystatin, 25 μg/ml) on intestinal permeability of free lopinavir, and lopinavir loaded SLNs.

Groups	P_{app} ($\times 10^{-5}$ cm/s)			
	Control (37 °C)	at 4 °C	(+)CPZ	(+)NYT
Free lopinavir	2.62 ± 0.31	2.71± 0.31	2.85 ± 0.28	2.71 ± 0.29
LPV/RTV Co-formulation	6.98 ± 0.36$^{**,\#}$	7.12± 0.26$^{\#}$	7.21 ± 0.48$^{\#}$	6.88 ± 0.41$^{\#}$
Lopinavir SLNs	5.18 ± 0.36**	3.89± 0.16$^{@}$	3.76 ± 0.21$^{@}$	3.22 ± 0.14$^{@}$
Lucifer Yellow	0.18± 0.03	0.21± 0.02$^{\#}$	0.16± 0.02$^{\#}$	0.19± 0.01$^{\#}$

**Statistically significance difference ($p < 0.01$) as compared with Free lopinavir; $^{\#}$Statistically no significance difference ($p > 0.05$); $^{@}$Statistically significance difference ($p < 0.05$) as compared with lopinavir SLNs without inhibitor. The data are expressed as mean ± S.D. LPV, lopinavir; RTV, ritonavir; SLNs, solid lipid nanoparticles; CPZ, chlorpromazine; NYT, nystatin.

4.6 Discussion

4.6.1 Experimental design

Utility of statistical design in screening of variables and manufacture of SLNs was reaffirmed from the results of experimental design. Fig. 4.6a-b shows the effect of surfactant concentration and lipid amount on particle size at fixed ultra-sonication time. It was observed that an increase in amount of lipid caused a corresponding increase in particle size. With increasing lipid amount in external phase, interfacial tension between lipid and aqueous phase increases, leading to coalesce and increase in particle size [41].

For a fixed amount of lipid, effect of surfactant concentration on particle size was non-linear (Fig. 4.6a). Increase in PVA concentration up to 1% w/v decreased particle size. Beyond this concentration, particle size increased. The initial reduction of particle size by PVA is due to reduction of interfacial tension between lipid and aqueous phase and stabilization of newly formed particles (due to steric stabilizing effect) [42]. However, at higher concentrations, hydrophobic interactions between PVA molecules dominate, leading to aggregation and increase in particle size.

From Fig. 4.6b, it is evident that the curvature of ultra-sonication time is gradual. However, surfactant concentration shows significant curvature in the same figure. Hence, we infer that within selected limits, ultra-sonication time does not influence particle size significantly.

Effect of surfactant concentration and lipid amount on the EE is shown in Table 3 and illustrated in Fig 4.6c. Steep curvature for EE when viewed from lipid axis indicates that with the increasing amount of lipid, EE increases. With increase in lipid amount,

lopinavir's entrapment in lipophilic matrix increases. Higher amount of lipid also provides an additional number of particles into which lopinavir gets entrapped.

From Fig. 4.6c, at fixed ultra-sonication time, EE significantly increases by increasing both amounts of surfactant and lipid. This effect may be explained by increased viscosity of medium which prevents rapid diffusion of lopinavir into the bulk of medium increasing its EE [43]. With increasing surfactant concentration, it is also possible that lopinavir gets entrapped in surfactant layer covering SLN surface leading to higher EE.

From Fig. 4.6d, it is evident that ultra-sonication time has a positive effect on EE. As time of ultra-sonication increases, there are relative, but insignificant ($p < 0.05$) reduction in particle size. This increases the surface area available for drug accommodation. The overall effect is increased in EE with an increase in ultra-sonication time.

4.6.2 Nanoparticles characterization

Optimized formulation exhibited particles in nanometric size with high EE and low PDI value (Fig. 4.8). Low PDI indicates that optimal conditions are suitable for the production of stable lopinavir NPs with narrow size distribution.

In Fig. 4.9, absence of lopinavir peak in thermograms of SLN indicates that lopinavir was present in amorphous form within a lipid matrix. No shift in peak position for lopinavir or SA was observed in physical mixture, indicating absence of incompatibility between SA and lopinavir.

In SLNs manufactured by hot melt emulsion technique, majority of incorporated drug remains at the core of the lipid matrix [42]. However, a portion of the drug remains bound at lipid-surfactant interface. This disparity in drug distribution can result in bi-phasic drug release pattern from SLN. As evident from Fig. 4.10, lopinavir loaded SLN presented similar bi-phasic drug release pattern; initial burst release due to surface presence of lopinavir followed by more sustained release due to drug embedded in core of lipid matrix. Due to hydrophobic nature, stearic acid reduced drug dissolution and drug release when included in the formulation.

The drug release kinetics of encapsulated drugs in nanoparticles is a major determinant for its biological effect. Thus, evaluation of drug release kinetics is of paramount importance in the nanodrug delivery system. Mathematical modeling of drug release kinetics provides a basis for the study of mass transport mechanisms that are involved in the control of drug release.

Reciprocal time release model takes into account both diffusion and dissolution controlled process. This model has been shown to be superior to other mathematical models

for drug release from NPs [44]. Moreover, the reciprocal time release model can also be used to get $t_{50\%}$ value. The bi-phasic drug release pattern from NPs can be useful in giving an initial loading dose (of loosely bound drug); later, drugs inside NPs can provide can provide a controlled release effect. This helps in improving mean retention time of the drug and its plasma exposure. Hence, the bioavailability of the drug improves as a consequence of metabolic protection, lower clearance and increased retention. Increased bioavailability also increases the therapeutic efficacy and reduces the overall dose of the drug [45].

Various methods are available to assess the drug release from nanoparticulate systems. Use of dialysis bag for release studies is widely reported technique and convenient to perform [46]. However, it suffers from certain drawbacks. It has been reported that slow equilibration of drug with outer media limits an accurate analysis of initial drug levels in formulations where the burst release is high. Therefore, in such cases true drug release profile could be underestimated.

4.6.3 *In vitro*/*in vivo* evaluation

A series of comparative pharmacokinetic studies were conducted to assess *in vivo* performance lopinavir SLNs in comparison with marketed formulation. Further, mechanistic studies were performed to discern the mechanism involved in the pharmacokinetic improvement of lopinavir in SLNs.

From oral pharmacokinetic studies and published literature, it is evident that lopinavir exhibits poor bioavailability, due to both high first-pass metabolism and P-gp efflux [47]. Significant improvement in plasma exposure of lopinavir in the presence of ritonavir (co-formulation) could be attributed to reduced first-pass metabolism and/or P-gp efflux. For the same reason, ritonavir is co-formulated with lopinavir as a pharmacokinetic booster in the marketed formulation.

From our study, lopinavir SLNs demonstrated significant ($p < 0.05$) increase in plasma exposure compared to free lopinavir (Fig. 4.12). High lopinavir exposure could be possibly due to reduced first pass metabolism/P-gp efflux and or improved intestinal permeability of encapsulated lopinavir. Additionally, uptake of lopinavir SLNs by the lymphatic route also helps in bypassing first-pass metabolism and P-gp efflux thus increasing bioavailability of lopinavir.

In order to validate the role of metabolic protection in improving the oral bioavailability, single dose IV study of lopinavir SLNs was carried out. From data, a significant reduction in plasma clearance and extended half-life indicates the significant role of metabolic protection (in the liver) in improving the oral bioavailability of encapsulated

lopinavir. Further, from pharmacokinetic data, it is also evident that relative bioavailability obtained from oral study is considerably higher than intravenous study. This suggests the involvement of absorption factors in enhancing plasma exposure of lopinavir such as improved permeability, avoidance of first pass metabolism and lymphatic transport of SLNs.

Further, we performed metabolism studies in tandem with IV studies to verify the fact that nanoparticles offers metabolic protection to encapsulated drug. *In vitro* metabolism stability studies conducted with RIM and RLM illustrate that lopinavir undergoes extensive metabolism; mediated exclusively via Phase-I microsomal enzymes of gut and liver. It was also evident from the result that SLNs could offer metabolic protection to lopinavir which is akin to ritonavir. Further, data evaluate the inhibitory action of ritonavir on CYP activity. No significant change in lopinavir metabolism in presence of blank SLNs suggests the protective nature of SLNs to entrapped drug than the inhibitory action of excipient to enzyme activity.

From the result, it is concluded that drastic increase in plasma levels of lopinavir after co-administration with ritonavir is probably due to inhibition of CYP 3A enzyme system by ritonavir. Similarly, metabolic protection offered by SLNs to lopinavir (gut wall and liver) aids in achieving longer circulation time leading to higher plasma exposure which concurs well with *in vivo* data.

Rat everted gut sac model was used to investigate intestinal permeability and uptake mechanisms of lopinavir presented in co-formulation and SLNs. From the study, significant increase in P_{app} of free lopinavir in the presence of ritonavir reveals considerable role of P-gp in limiting oral absorption of lopinavir. However, in this study, we have not considered the use of control inhibitors for CYP; attributing outcome of study to P-gp modulation alone may not be accurate. In the present model, we could not distinguish the role of transporter from metabolism.

A significant increase in P_{app} of lopinavir SLNs as compared to free drug suggested that SLNs could efficiently cross the intestinal barriers. Improved permeability of drug fabricated into nanoparticles is attributed to its active uptake through endocytosis (phagocytosis/pinocytosis) process, M-cells and extended protection to loaded drug against gut metabolizing enzymes and efflux transporters like P-gp. It is widely reported that low temperature (4 ^{o}C) could arrest the energy dependent processes including endocytosis. Hence, to understand the role of active mechanisms in the uptake process of SLNs, we carried out the everted gut sac study at two different temperatures; 37 ^{o}C (control) and 4 ^{o}C.

The results indicate significant reduction in P_{app} value of lopinavir SLNs at lower temperature as compared to optimal incubation temperature (37 ^{o}C). On the contrary, no significant effect of incubation temperature on intestinal permeability of free lopinavir was observed. This implied that uptake of NPs in everted gut sacs could be possibly a result of an active uptake process.

Further, to establish uptake mechanisms, studies were carried out with specific endocytosis (phagocytosis/pinocytosis) process inhibitors. CPZ and NYT were selected as uptake inhibitors because of their ability to inhibit clathrin coated pit associated receptors and abolishing caveolae function respectively [48]. Results from this study demonstrated a significant reduction in P_{app} of lopinavir SLNs in the presence of specific endocytic uptake inhibitors. This indicates that uptake of lopinavir SLNs occurs by endocytosis process. Further, it could be deduced that both clathrin and caveolae mediated endocytosis mechanisms were involved in the uptake of lopinavir SLNs.

Similar studies were also performed with free lopinavir and lopinavir/ritonavir co-formulation using uptake inhibitors. From P_{app} values presented in Table 4.5, it is evident that uptake of either free lopinavir or lopinavir/ritonavir co-formulation was unaffected by the presence of uptake inhibitors. From this, we concluded that endocytosis plays a trivial role in the uptake of lopinavir. It also signifies a significant role of passive diffusion in absorption of free lopinavir.

In the present study, lucifer yellow was used as a paracellular marker. Low P_{app} values of lucifer yellow across the experimental conditions indicate the integrity of the cell membrane during the experiments.

In order to establish *in vivo* performance of lopinavir SLNs at targeted organs, tissue distribution study was conducted and compared against the distribution pattern of free lopinavir and marketed formulation. Data obtained from tissue distribution studies indicate high localization of lopinavir in liver tissues as compared to spleen and lymph nodes. Superior blood perfusion to liver compared to other organs may result in accumulation of free lopinavir in the liver. In case of loaded SLNs, higher distribution was seen in the spleen and lymph nodes. This indicates lymphatic uptake of SLNs following oral administration. Moreover, it is also reported that nanoparticles, larger than 200 nm after oral administration, are selectively transported to liver and spleen and are eliminated via monocytes and macrophages [49]. Selective distribution of lopinavir SLNs to these organs is thought to enhance lopinavir concentration and drug distribution (V_d) as observed in pharmacokinetic

studies. Such distribution pattern of SLNs following oral administration is in close agreement with the previously reported literature [49].

Similarly, following administration of the co-formulation, higher accumulation of lopinavir in liver tissues is attributed to metabolic protection offered to lopinavir by ritonavir. This augments well with the results from *in vitro* metabolism stability data. However, it is noteworthy that the ritonavir co-administration failed to increase lopinavir concentration in poorly perfused organs like spleen and lymph nodes, while, lopinavir loaded SLNs produced significantly higher levels in these organs.

It has been reported that lipid nanoparticles reach the lymphatic system either by direct endocytosis/transcytosis uptake by membranous epithelial cells (M-cells) covering Payer's patches in intestine or by conversion into triglyceride-rich lipoprotein. Size of chylomicron precludes their absorption into blood capillaries and therefore they are secreted into the lymphatic system [50]. To corroborate this hypothesis, oral pharmacokinetic studies were further carried out in the presence of a lymph transport inhibitor, CXI. The CXI is known to block lymphatic transport pathway by hampering the chylomicron formation without causing damage to other active and passive absorption pathways [36].

In contrast to free lopinavir, presence of CXI significantly reduces plasma exposure of lopinavir SLNs. This affirms lymphatic uptake as a possible mechanism of nanoparticle absorption. From this study, we could demonstrate the significant role of lymphatic transport in absorption of orally administered SLNs. However, we could not deduce the role of other uptake/transport mechanisms. Passive absorption followed by portal transport is the most preferred route of free drug absorption. Therefore, it can be concluded that SLNs show selective preference for lymphatic system over conventional portal transport.

It is reported that viral reservoirs present in lymphoidal organs are poorly accessed by conventional therapy. In conventional therapy, minimum effective concentration of the drug can not be maintained for the necessary time duration at the site of HIV localization. Higher distribution of lopinavir SLNs in such tissues at all-time points assures higher lopinavir availability in these reservoirs. Thus, as compared to conventional lopinavir/ritonvir therapy, better therapeutic outcome of lopinavir from lopinavir SLNs could be expected.

4.7 Conclusions

Lopinavir was successfully fabricated into SLNs with high EE and desirable particle size range. Processing conditions for the manufacture of these lopinavir SLNs were identified and optimized using DoE with good correlation between actual and predicted values. Plasma exposure of lopinavir from lopinavir SLNs was comparable to exposure obtained from lopinavir/ritonavir co-formulation. Metabolic protection and increased intestinal permeability were demonstrated as possible reasons for improving lopinavir oral bioavailability in either of the formulations. Relatively higher distribution of lopinavir SLNs in poorly perfused lymphoidal tissues as compared to lopinavir/ritonavir co-administration suggests that lopinavir loaded SLNs could be safer and more effective alternative to currently marketed co-formulation. In conclusion, formulating SLNs for poorly soluble lopinavir was an effective approach in improving its oral bioavailability and lopinavir exposure to HIV reservoirs which may prove beneficial in the treatment of HIV infected patients. Additionally, this investigation can also form the basis for the use of SLNs in designing lymph-targeted oral delivery system for other HIV-protease inhibitors.

Polymeric nanoparticles

4.8 Introduction

Polymer-based nanoparticles are nano-sized polymeric colloidal particles in which a drug of interest can be conjugated or adsorbed onto the surface or encapsulated inside their polymeric matrix. By virtue of encapsulating labile drugs inside a nanocarrier, the solubility and stability of therapeutic agents can be enhanced, providing a chance to re-evaluate the therapeutic potential of drugs because of poor pharmacokinetics. A variety of natural or synthetic biodegradable polymers as well as non-biodegradable polymers have been employed for the fabrication of polymeric nanoparticles. However, synthetic polymers such as poly-lactic-co-glycolic acid (PLGA), poly-ε-caprolactone (PCL), polyalkylcyanoacrylates, polymethylmethacrylates (Eudragits) and natural polymers like chitosan and pullulan are most widely used for fabrication of polymeric nanoparticles [51, 52].

Polymeric nanoparticles provide an attractive alternative for long-term delivery of therapeutic agents meant for chronic administration. By virtue of controlled release, improved bioavailability and targeted delivery these drug loaded NPs cut overall cost of medicine, reduce risks of toxicity thus, improve patient compliance and are superior to conventional formulation [53]. Among the various NPs, PLGA based polymeric nanoparticles have been widely investigated for delivery of antiretroviral drugs [54].

Poly-ε-caprolactone (PCL) is semi-crystalline biodegradable and biocompatible polyester with low glass transition temperature and melting point. It is non-toxic and non-mutagenic polymer. Post administration, PCL is degraded slowly by hydrolysis of its ester linkages in systemic circulation. Owing to hydrophobic, slow degradation and low melting point, PCL is considered to be most suitable polymer for delivering drugs that require frequent and chronic administration like lopinavir. In comparison with other biodegradable polymers like PLA and PLGA, it demonstrates greater stability in the GI environment and a negligible tendency to generate acidic impurities during degradation. Moreover, it is considerably economical than other polymers such as polyglycolide, polylactide, and their co-polymers [55-57].Therefore, in the present work, we selected PCL as one of the polymeric carriers for oral delivery of lopinavir.

Pullulan is a non-toxic, non-immunogenic, biodegradable and neutral linear polysaccharide consisting of α-1, 6 linked maltotriose residues. This unique linkage pattern is believed to be responsible for the structural flexibility and solubility of pullulan, resulting in distinct film- and fiber-forming characteristics not exhibited by other polysaccharides [58, 59]. In the recent past, pullulan is widely investigated for its biomedical applications in

various aspects such as targeted drug, gene delivery and diagnostic imaging using quantum dots [60].

Pullulan cannot self-associate in aqueous solutions due to its high water solubility. It can be chemically derivatized to alter its water solubility or provide reactive groups. To widen its application, several derivatives of pullulan have been synthesized in recent past [61, 62]. Most pullulan derivatizations are intended to reduce its water solubility or to introduce charged or reactive groups for functionality. In line with this, Zhang et al have explored the potential of hydrophobized pullulan as a drug delivery carrier to encapsulate anticancer drug; epirubicin [63]. Pullulan acetate (PA) is a well explored derivative of pullulan that can form self-aggregating colloidal nanoparticles in aqueous environments with an inner hydrophobic core. Hydrophobic pockets of pullulan acetate nanoparticles make this polymer suitable for delivery of lipophilic drugs like lopinavir [64].

In the present work, different nanoparticulate delivery systems for lopinavir have been proposed using biodegradable and biocompatible polymers such as poly-ε-caprolactone and pullulan acetate. Emulsion-solvent evaporation method was employed for the fabrication of lopinavir nanocarriers. This technique is demonstrated to have some advantages compared with other methods such as rapid and easy preparation process with more critical variables to control particle size and great potentials in promoting large-scale production [65].

Primary objectives of the present work were to i) prepare and characterize lopinavir loaded polymeric nanoparticles and to ii) compare *in vivo* performance of lopinavir loaded nanoparticles with the currently marketed lopinavir/ritonavir co-formulation.

Lopinavir loaded poly- ε-caprolactone nanoparticles (PCL NPs) were rationally designed and optimized using Plackett–Burman Design and Box–Behnken Design (BBD) and data were statistically analyzed using Design Expert software. Prepared nanoparticles were extensively characterized for particle size, surface morphology and charge, drug encapsulation efficiency and *in vitro* drug release. *In vivo* performances of loaded nanocarriers were extensively evaluated in male wistar rats.

4.9 Materials

Lopinavir (purity > 99%) was obtained as a gift sample from Mylan Laboratories, Hyderabad, India. Pullulan (Mw = 200 KDa) was purchased from Hayashibara (Tokyo, Japan). Poly-ε-caprolactone (Molecular weight 65,000 g/mol) was purchased from Polysciences, Inc., Warrington, USA. Rat intestinal microsomes (RIM), rat liver microsomes (RLM) and NADPH were procured from BD Gentest, Woburn, USA. HPLC

grade acetonitrile, ammonium acetate, heparin, methanol, methylene chloride (DCM), potassium dihydrogen phosphate and sodium citrate were purchased from Merck Laboratories, Mumbai, India. Methyl cellulose (molecular weight 14 KDa, viscosity 15 cps) and Tween 80 were purchased from S.D. Fine Chemicals Ltd, Mumbai, India. A Milli-Q water purification system (Millipore, MA, USA) was used for obtaining high quality HPLC grade water.

4.10 Methodology

4.10.1 Experimental Design for PCL NPs

Low resolution PBD, a factorial design matrix, was used to identify critical formulation and manufacturing factors in the preparation of lopinavir loaded NPs. A total of 8 factors were studied at two levels to determine their effect on two responses, viz., entrapment efficiency (EE) and particle size (nm) of loaded NPs. The variables studied were: Amount of polymer, type of surfactant (tween 80 and poloxamer 407), concentration of surfactant, type of an external phase (DCM and chloroform), volume of external phase, speed of homogenization, time of homogenization, rate of external phase addition (rapid and slow).

Based on particle size and EE data obtained from PBD, we selected tween 80 (as surfactant) and DCM (as external phase solvent) for preparation and optimization of lopinavir loaded NPs. Three critical factors including the concentration of surfactant, amount of polymer and time of homogenization were identified in the optimization process. From these initial experiments, limits and range for identified critical factors were set for subsequent optimization studies using BBD.

BBD, a sub-type of response surface methodology (RSM), was employed to develop quadratic models for optimization process and to reduce the number of experimental trials. A 17-run, 3-factor, 3-level BBD was constructed to evaluate main effects, interaction effects and quadratic effects of identified initial factors. Non-linear quadratic model generated by BBD design was in the following form:

$$Y = b_0 + b_1X_1 + b_2X_2 + b_3X_3 + b_{12}X_1X_2 + b_{13}X_1X_3 + b_{23}X_2X_3 + b_{11}X_1^2 + b_{22}X_2^2 + b_{33}X_3^2$$

Where, Y is measured response associated with each factor level combination; b_0- b_{33} are regression coefficients of respective factors and their interaction terms computed from observed experimental values of Y and X_1, X_2, X_3 are the coded levels of independent factors. The terms X_1X_2, X_2X_3, X_3X_1 and X_i^2 (i = 1, 2 or 3) represent the interaction and

quadratic terms respectively. Dependent and independent factors selected are shown in Table 4.6.

Critical factors evaluated in this study were concentration of surfactant (X_1), amount of polymer (X_2) and time of homogenization (X_3). Responses studied were particle size (Y_1) and EE (Y_2). Experiment design matrix generated by the software is shown in Table 4.7.

Table 4.6. Critical factors and their levels in the Box-Behnken Design (BBD).

Critical Factors	Levels used		
	Low (-1)	**Medium (0)**	**High (+1)**
Independent			
X_1 = Surfactant concentration (% w/v)	0.5	1	1.5
X_2 =Polymer amount (mg)	100	200	300
X_3 = Time of homogenization (min)	15	30	45
Dependent		**Constraints**	
Y_1 = Particle size (nm)		Minimum	
Y_2 = Entrapment efficiency (%)		Maximize	

Table 4.7. Box-Behnken experimental design

Run	Critical Factors			Response Variables	
	Surfactant concentration (X_1, % w/v)	**Polymer amount (X_2, mg)**	**Homogenation time (X_3, min)**	**Particle size (Y_1, *nm*)**	**Entrapment efficiency (Y_2, %)**
1	1.0	200	30	170.5	92.3
2	1.0	100	45	138.4	78.5
3	1.0	200	30	174.1	92.8
4	0.5	200	15	215.0	81.1
5	0.5	300	30	204.2	86.6
6	1.5	100	30	188.9	80.3
7	1.0	200	30	178.4	88.8
8	1.0	300	45	176.9	93.4
9	1.5	200	15	232.6	88.7
10	1.0	300	15	212.1	89.0
11	0.5	200	45	174.2	87.8
12	1.5	300	30	230.7	94.4
13	0.5	100	30	165.1	73.5
14	1.0	200	30	171.4	87.5
15	1.0	200	30	172.2	87.2
16	1.5	200	45	208.6	92.3
17	1.0	100	15	163.3	76.8

4.10.2 Preparation of poly-ε-caprolactone nanoparticles (PCL NPs)

Lopinavir loaded PCL NPs were prepared by previously reported oil-in-water emulsion-solvent evaporation technique [66] with minor modifications. This method was adopted for manufacturing formulations listed in Box-Behnken Design (BBD). The manufacturing conditions and component ranges were selected after initial screening using Plackett-Burman Design (PBD). Briefly, lopinavir (10 mg) and specific amount of polymer (100 mg to 300 mg) were dissolved in 5 ml of DCM, which constituted organic phase. This organic phase was slowly added into the 50 ml aqueous phase containing tween 80 (0.5% w/v to 1.5% w/v) under magnetic stirring (800 rpm) to form a primary emulsion. Primary emulsion was further subjected to high speed homogenization (at 5000 rpm, Polytron PT 3100D, Kinematica, Switzerland) for specific time period (15 min to 45 min). Resultant colloidal preparation was centrifuged at 20,000 × g for 45 min to obtain lopinavir loaded NPs. Prepared NPs were washed three times with water to remove adherent free drug from the outer surface of NPs. Washed NPs were re-suspended in water and subjected to pre-freezing at –80 ^{o}C for 6 h. Further, freeze-drying was carried for 12 h at –110 ^{o}C in a lyophilizer (Coolsafe 110-4, Scanvac, Denmark). Five percent mannitol was used as a cryoprotectant. This lyophilized powder was stored in sealed glass containers at room temperature till further use. The scheme of PCL NPs preparation is illustrated in Fig. 4.17.

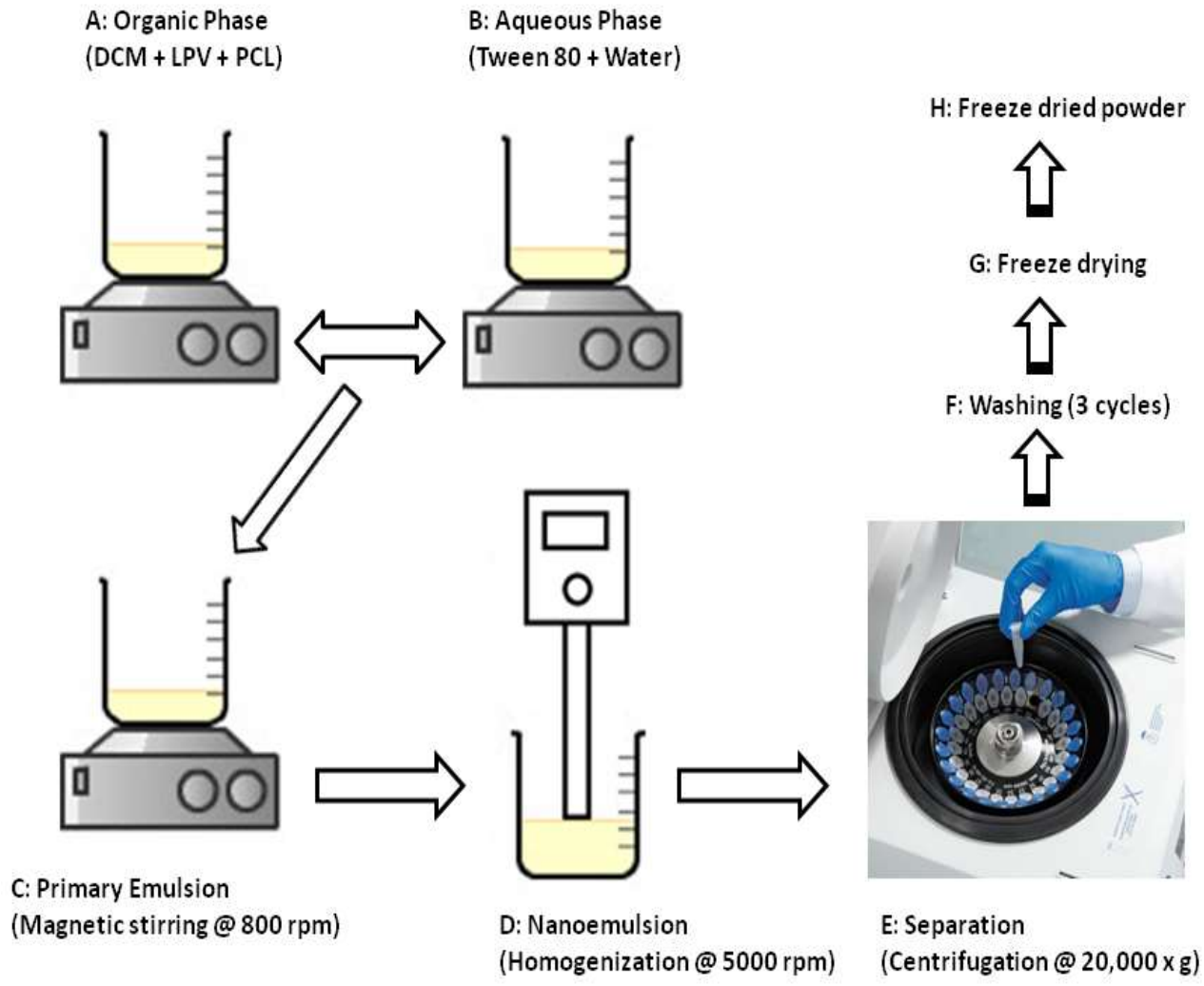

Fig. 4.17: Schematic representation of preparation of PCL NPs by emulsion solvent evaporation method.

4.10.3 Synthesis and preparation of pullulan acetate nanoparticles (PA NPs)

4.10.3.1 Synthesis of pullulan acetate

Pullulan acetate (PA), as hydrophobized pullulan, was synthesized by previously reported Motozato's method [67]. Briefly, 2 g of pullulan was dissolved by vigorous stirring in 20 ml of formamide maintained at 54 ^{o}C. For acetylation of pullulan, 6 ml pyridine and 15 ml of acetic anhydride was added to the above solution while maintaining the temperature at the 54 ^{o}C for 48 h. A dark-brown precipitate was obtained that was further purified by triturating with 1000 ml distilled water and 500 ml methanol. The solid material was vacuum-dried for 24 h, to finally obtain the product.

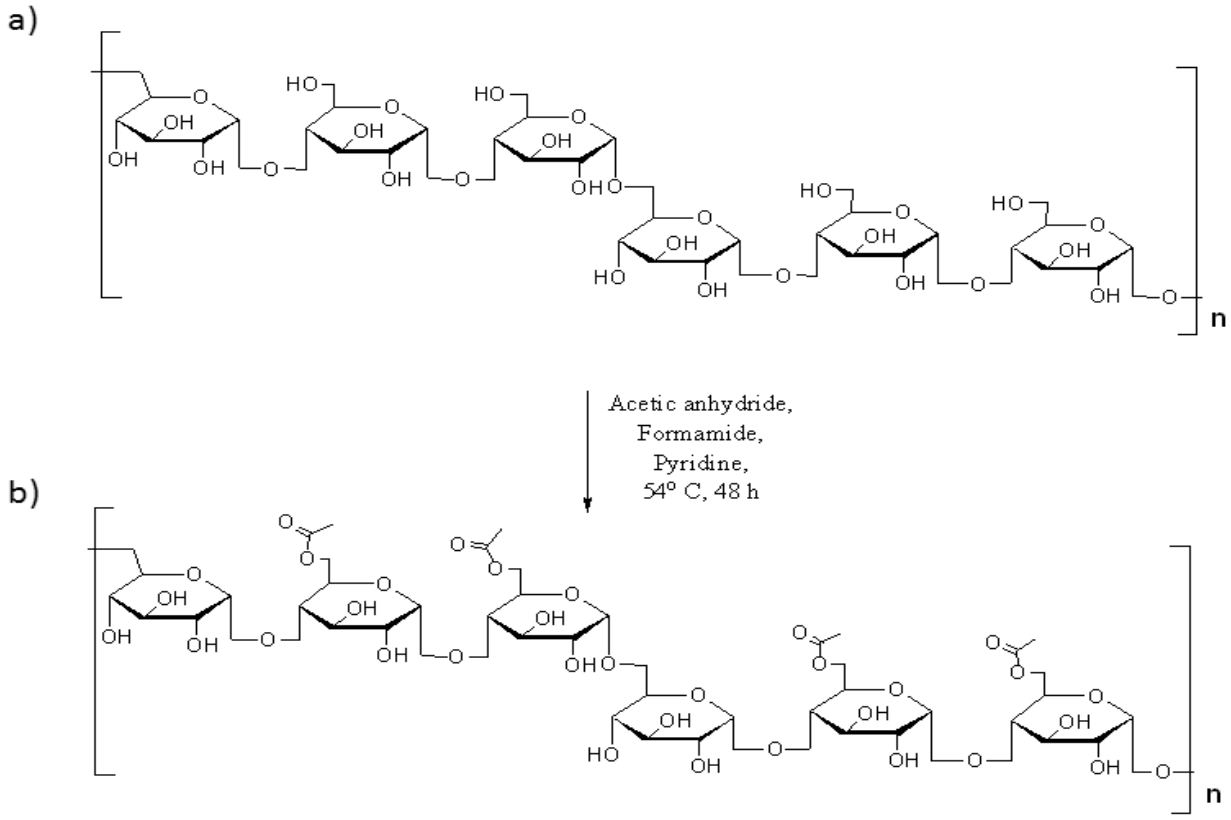

Fig. 4.18: Chemical structures of pullulan and PA.

4.10.3.2Characterization of pullulan acetate

a) FT-IR spectroscopy

Fourier transform infrared (FT-IR) spectra of pullulan and PA were recorded on a FT-IR 4200 (JASCO, USA) spectrometer in the range of 4000–400 cm^{-1} by KBr pellet method (1% sample in KBr). The samples were vacuum dried before FT-IR scan. A total of 40 scans were taken for each sample.

b) ^{1}H NMR spectroscopy

The proton nuclear magnetic resonance (^{1}H NMR) spectra were recorded on a Shielded Varian Inova spectrometer at 500 MHz (International Equipment Trading Ltd., Vernon Hills, USA) using tetramethylsilane (TMS) as an internal standard. Samples were dissolved in deuterated dimethyl sulfoxide (DMSO-d_6) before analysis. All NMR spectra were acquired at ambient temperature.

The degree of substitution (DS) in PA for acetyl groups was calculated from the integration value of acetyl protons (A) observed at 1.8–2.2 ppm and the OH protons and H-1 to H-6 protons (B) of pullulan moiety observed at more than 3.5 ppm. The DS values were calculated by the NMR method using the following equation:

$DS = \frac{10A}{(3B+A)}$, derived from the equation: $\frac{A}{3x} = \frac{B}{\{7+(3-x)\}}$ (corresponding to area for each hydrogen in a glucose unit), where x equals DS [63].

c) Preparation of PA NPs

Lopinavir loaded PA NPs were prepared according to the previously reported oil-in-water emulsion-solvent evaporation technique [66] with minor modifications. Briefly, accurately weighed quantities of lopinavir (10 mg) and PA (100 mg) were dissolved in 5 ml of DCM, this constituted organic phase. To form the primary emulsion, the organic phase was dropped into 50 ml aqueous PVA (0.5%, w/w) solution by means of a syringe fitted with needle (Internal diameter - 0.75 mm), positioned a few centimeters above the surface of the medium under gentle magnetic stirring (800 rpm). The primary emulsion was further subjected to high speed homogenization (at 5000 rpm, Polytron PT 3100D, Kinematica, Switzerland) for 15 min. The resulting colloidal preparation was centrifuged at 20,000 × g for 45 min to obtain lopinavir loaded PA NPs. To remove the adherent free drug and excess PVA, the pellet was re-suspended in deionized water and centrifuged three times at 20,000 × g for 15 min each. Washed NPs were re-suspended in deionized water and subjected to pre-freezing at –80 ^{o}C for 6 h. Further, freeze-drying was carried for 24 h at –110 ^{o}C in a lyophilizer (Coolsafe 110-4, Scanvac, Denmark). Mannitol (5% w/v) was used as a cryoprotectant. This lyophilized powder was stored in sealed glass containers at room temperature till further use. The scheme of PA NPs preparation is illustrated in Fig. 4.19.

4.10.4 Nanoparticles characterization

Prepared nanoparticles were characterized for particle size, size distribution, surface charge, surface morphology, thermal analysis, encapsulation efficiency, release kinetics and storage stability as discussed in earlier sections (4.4.5 a-f). For PA NPs, DSC scans were taken for liquid dispersions without adding mannitol.

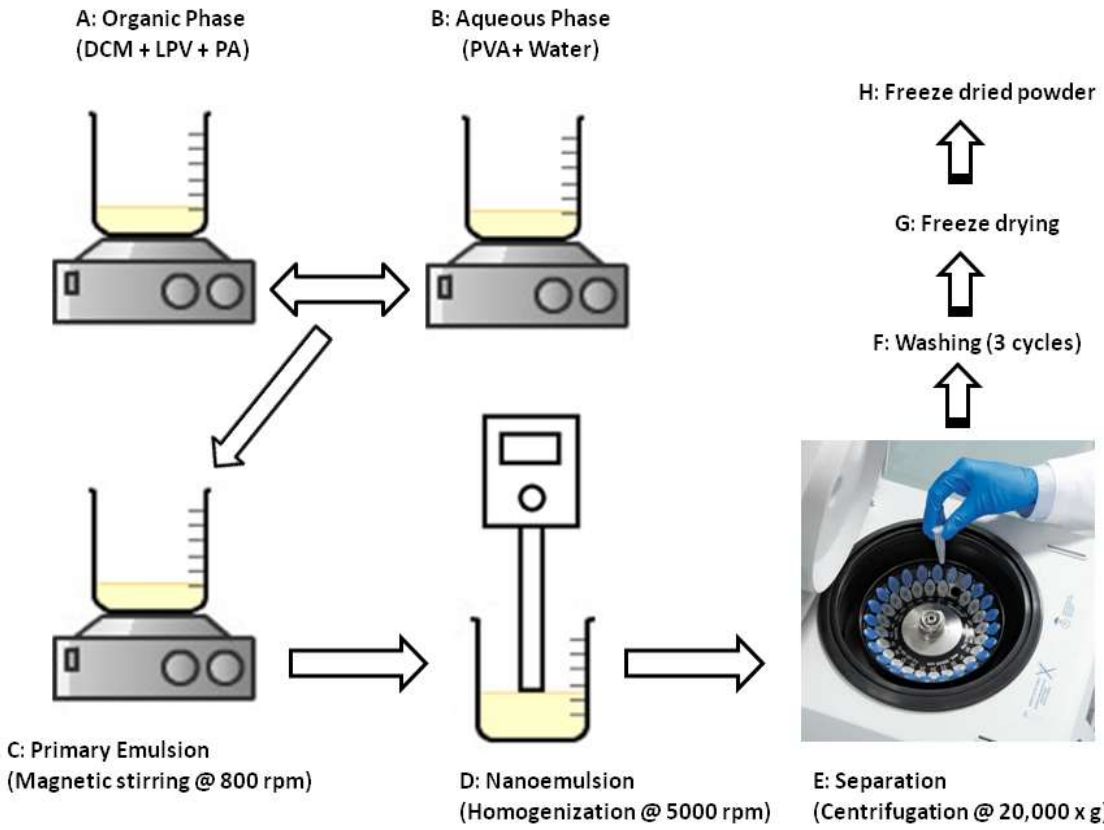

Fig. 4.19: Schematic representation of preparation of PA NPs by emulsion solvent evaporation method.

4.10.5 *In vitro/ in vivo* evaluation

a) Pharmacokinetic study design

i) Single dose oral study

Pharmacokinetic studies were conducted following oral (20 mg/kg, 10 ml/kg) administration of free lopinavir suspension, lopinavir/ritonavir co-formulation and lopinavir loaded PCL NPs/PA NPs. In pharmacokinetic studies, animals were randomly divided into three groups; Group A (control group) - treated with lopinavir alone; Group B - treated with co-formulation; Group C- treated with lopinavir loaded NPs.

ii) Single dose IV bolus study

Intravenous pharmacokinetic studies of lopinavir were conducted following single dose bolus administration (IV, 4 mg/kg, 1 ml/kg) of free lopinavir solution and lopinavir loaded nanoparticles formulations (PCL NPs and PA NPs). For the study, animals were randomly divided into two groups with five animals in each group. Group A (control group) - treated with a free lopinavir solution; Group B - treated with either PCL NPs or PA NPs.

For pharmacokinetic study of each formulation, separate set of animals were used in the control group.

iii) Blood collection

Blood samples were collected from the orbital sinus into microfuge tubes containing anti-coagulant (3.8% w/v sodium citrate) at pre-dose, 0.17, 0.25, 0.5, 1, 2, 3, 4, 6 , 8 and 12 h post dose for oral studies and at pre-dose, 0.08, 0.17, 0.25, 0.5, 1, 2, 4, and 6 h post dose for IV studies. Collected blood samples were kept on ice until further processing. These samples were further harvested for plasma by centrifuging at 4 ^{o}C for 10 min at 650 × g and then stored at –70 ^{o}C until further analysis. The samples were analyzed by a validated HPLC method for estimation of lopinavir in rat plasma matrix.

b) Tissue distribution study

To study the bio-distribution pattern of polymeric NPs, 36 male wistar rats (180 ± 20 g) were randomly divided into three groups with 12 animals in each group. The groups were designated as: Group A (control group) - treated with lopinavir (20 mg/kg, lopinavir suspended in 0.5% w/v MC) alone; Group B - treated with lopinavir/ritonavir co-formulation (20/5 mg/kg); Group C - treated with lopinavir loaded PCL NPs/ PA NPs.

Three rats from each group were sacrificed at 0.5, 1, 2 and 4 h post-dosing. Individual animals were perfused with heparinized (5 IU) saline (0.9% w/v NaCl) through the portal vein in order to remove circulating blood from body organs before tissue collection. Tissues of interest (liver, spleen and mesenteric lymph nodes) were collected and stored at –70 ^{o}C until further analysis.

c) *In vitro* metabolism stability study

In vitro metabolism stability studies were performed by incubating free lopinavir, lopinavir/ritonavir (ritonavir at an effective concentration of 1.25 µM) co-formulation and lopinavir polymeric nanoparticles (PCL NPs & PA NPs) with rat intestinal microsomes (RIM) and rat liver microsomes (RLM) (1 mg/ml) at an effective concentration of 5µM. Reaction was initiated by addition of NADPH (2 mM) in phosphate buffer (100 mM, pH 7.4). Incubations were performed at 37 ^{o}C in a shaking water bath for 30 min. The reaction was terminated by addition of cold acetonitrile. Samples were vortexed briefly and centrifuged at 6000 × g for 15 min. Resultant clean supernatant (75 µl) was injected into the HPLC. Percentage metabolism of lopinavir was determined in all three test conditions. In a separate set of experiment, free lopinavir was incubated with reaction buffer without enzymes for 30 min to ensure stability of free lopinavir in the reaction buffer. No non-enzymatic degradation of lopinavir was observed.

Enzyme inhibition due to formulation excipient present in NPs was investigated by incubating blank NPs (NPs prepared without drug) along with free lopinavir; difference in metabolism (compared with free lopinavir alone) was taken as a sign of enzyme inhibition.

d) Intestinal uptake study

Everted gut sac studies in rats were performed using established methods adapted from literature [37]. As discussed earlier, Intestinal sacs were placed in individual incubation chambers containing free lopinavir (2.5 µg/ml), lopinavir/ritonavir (lopinavir and ritonavir at an effective concentration of 2.5 µg/ml and 0.625 µg/ml, respectively) co-formulation, lopinavir loaded PCL NPs/PA NPs (2.5 µg/ml), and lucifer yellow (10 µg/ml) prepared in KHB buffer at a maintained temperature of 37 ^{o}C.

In order to discern the uptake mechanism, permeability studies for lopinavir in free lopinavir, co-formulation and loaded NPs were conducted at low temperature or in the presence of specific endocytosis inhibitors; chlorpromazine (CPZ, 10 µg/ml) and nystatin (NYT, 25 µg/ml). After an incubation time of 60 min, intestinal sacs were carefully removed, blotted onto filter paper and contents were collected. Intestinal sacs were rinsed thrice with KHB solution and rinsings were pooled with original content for analysis. Samples were analyzed by a validated HPLC method.

P_{app} values, expressed in cm/s, were calculated in each experimental condition using the following equation [40]:

$$P_{app} = \left(\frac{dQ}{dt}\right) x \frac{1}{A \times C0}$$

Where dQ/dt is the rate of appearance of lopinavir in the everted gut sac (receiver compartment), C_o is the initial concentration of lopinavir outside everted gut sac (donor compartment) and A is the total cross sectional area of tissue.

4.10.6 Statistical Analysis

As discussed in section no. 4.4, various statistical tests were employed to assess any significance of difference between means.

4.11 Results

4.11.1 Experimental design for PCL NPs

Selected critical factors showed a statistically significant effect on observed responses for particle size and EE (Table 4.7). Quadratic equations establishing main effects and interaction factors were determined based on estimation of statistical parameters generated by software. Statistical validation of quadratic equations was confirmed by

ANOVA. Three dimensional response surface graphs for illustrating the effects of selected critical factors on selected responses are shown in Fig. 4.20 (a-d).

a) Effects on particle size (Y_1)

As shown in Table 4.7, particle size of formulations ranged between 138.4 nm (run 2) and 232.6 nm (run 9), indicating sensitivity toward critical factors selected for the study. Experiments carried out at the center points (run 1, 3, 7, 14 and 15; n = 5) of the design indicate reproducibility of experiment as coefficient of variation (CV) is less than 2%. Independent factors affecting particle size were concentration of surfactant (X_1), amount of polymer (X_2) and duration of homogenization (X_3) (Table 4.8).

These effects can be explained by following quadratic equation:

$$Y_1 = 176.80 + 12.50\,(X_1) + 21.13\,(X_2) - 15.63\,(X_3) + 0.75\,(X_1X_2) - 4.25\,(X_1X_3) - 2.5\,(X_2X_3) + 27.35\,(X_1^2) - 7.4\,(X_2^2) + 3.1\,(X_3^2)$$

Regression coefficient (r^2) of the above equation was 0.9563, indicating a good correlation between observed response and selected critical factors. The residuals were distributed randomly around zero and there was no effect of experimental sequence on the trend of residuals.

b) Effects on entrapment efficiency (EE, Y_2)

As shown in Table 4.7, EE varied between 73.5% (run 13) to 94.4% (run 12) which indicates that the response was sensitive towards selected factors. Experiments performed at the center points of the design (run 1, 3, 7, 14 and 15; n = 5) confirmed that the experimental method was highly reproducible (CV < 3%). Data presented in Table 4.8 show that independent factors affecting EE were concentration of surfactant (X_1), amount of polymer (X_2) and time of homogenization (X_3).

Effect can be explained by following second-order polynomial quadratic equation:

$$Y_2 = 90.7 + 3.38\,(X_1) + 6.88\,(X_2) + 2.00\,(X_3) + 0.25\,(X_1X_2) - 0.5\,(X_1X_3) + 0.5\,(X_2X_3) - 2.23\,(X_1^2) - 5.23\,(X_2^2) - 1.48\,(X_3^2)$$

The regression value of above equation was found to be 0.922 indicating suitability of selected design model. Analysis of residuals indicated that residuals were normally distributed around zero.

a)

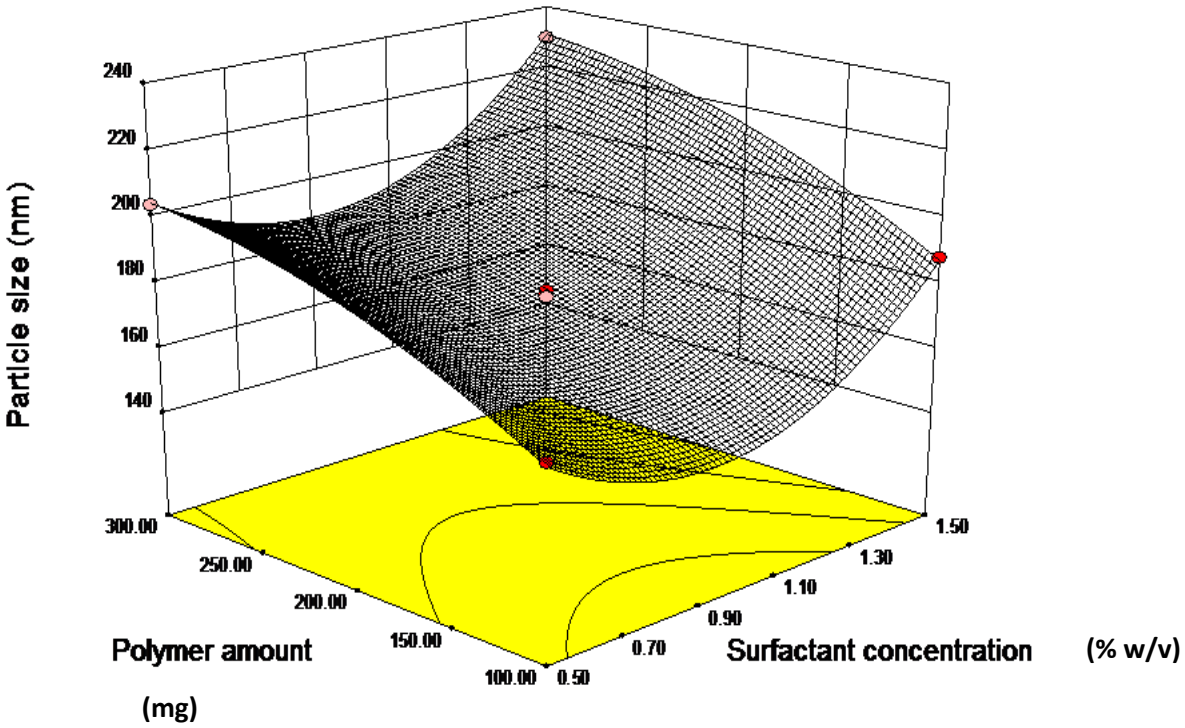
Particle size (nm)
240
220
200
180
160
140
300.00
250.00
200.00
150.00
100.00
Polymer amount
(mg)
0.50
0.70
0.90
1.10
1.30
1.50
Surfactant concentration
(% w/v)

b)

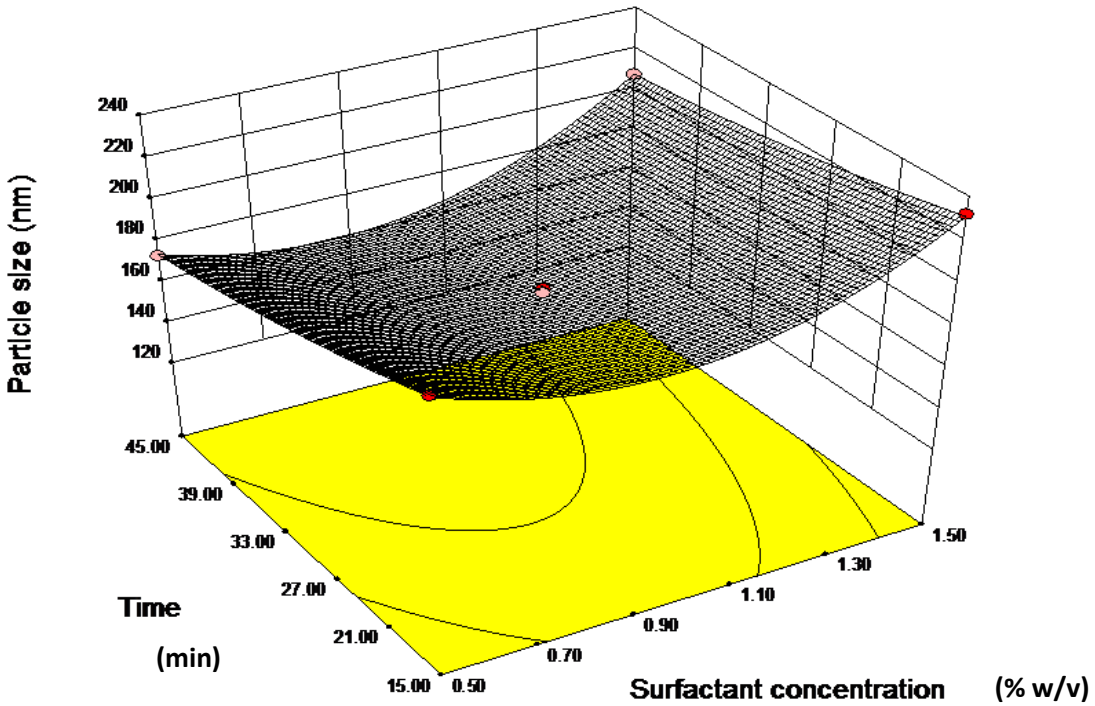
Particle size (nm)
240
220
200
180
160
140
120
45.00
39.00
33.00
27.00
21.00
15.00
Time
(min)
0.50
0.70
0.90
1.10
1.30
1.50
Surfactant concentration
(% w/v)

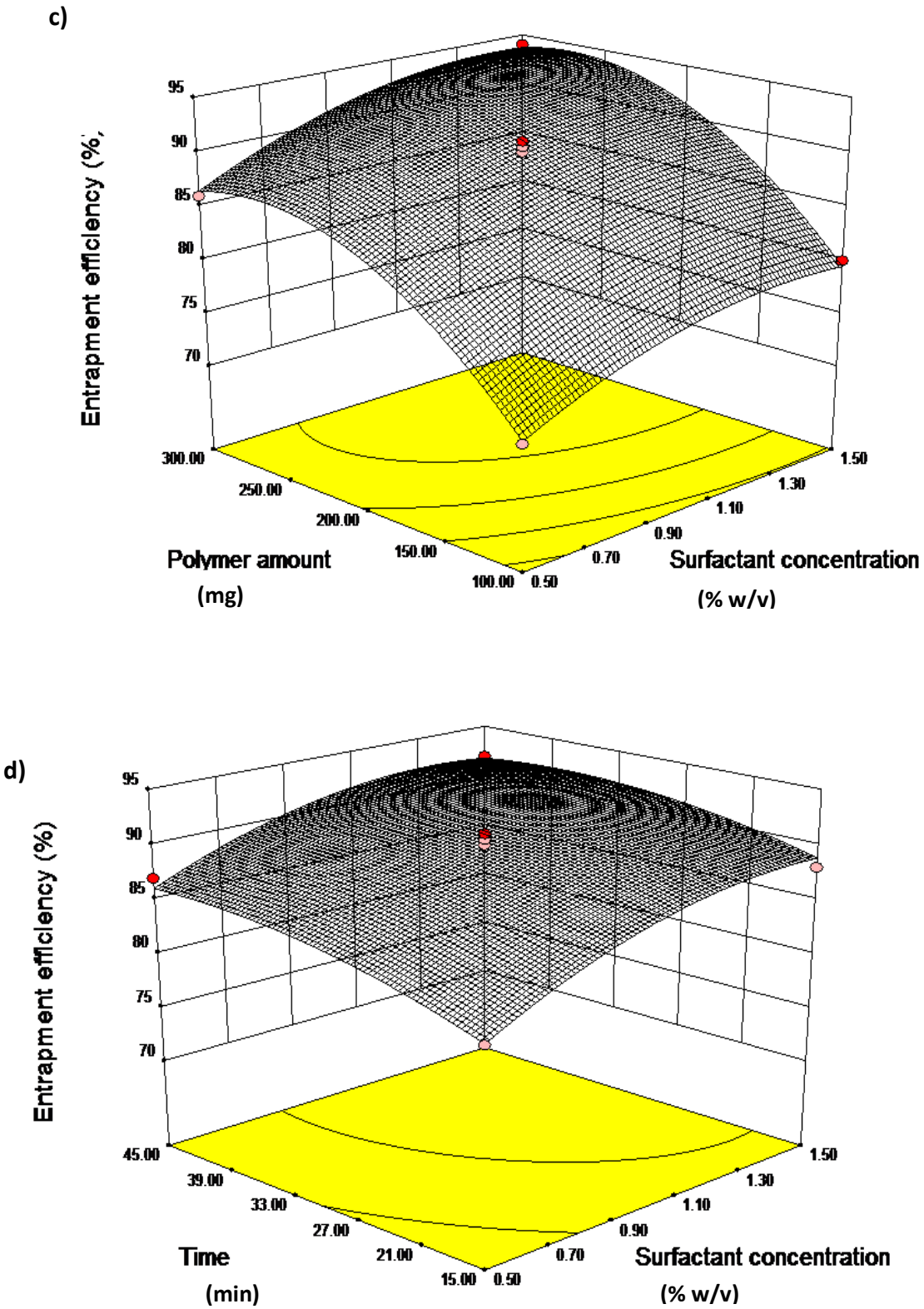

Fig. 4.20: **a)** Response surface plot showing the effect of polymer amount and surfactant concentration on particle size; **b)** Response surface plot showing the effect of time of homogenization and surfactant concentration on particle size; **c)** Response surface plot showing the effect of polymer amount and surfactant concentration on entrapment efficiency; **d)** Response surface plot showing the effect of time of homogenization and surfactant concentration on entrapment efficiency.

Table 4.8. Statistical analysis results of particle size and entrapment efficiency (EE).

Source	Particle size (Y_1)				EE (Y_2)			
	Sum of Squares	DF	F-value	P-value	Sum of Squares	DF	F-value	P-value
Model	10247.33	9	635.07	0.0001*	659.95	9	126.74	0.0001*
X_1	1250.00	1	697.21	0.0001*	91.12	1	157.50	0.0001*
X_2	3570.13	1	1991.30	0.0001*	378.12	1	653.55	0.0001*
X_3	1953.13	1	1089.39	0.0001*	32	1	55.31	0.0001*
X_1X_2	2.25	1	1.25	0.2996#	0.25	1	0.43	0.5320#
X_1X_3	72.25	1	40.30	0.0004*	1	1	1.73	0.2300#
X_2X_3	25.00	1	13.94	0.0073*	1	1	1.73	0.2300#
X_1^2	3149.57	1	1756.73	0.0001*	20.84	1	36.03	0.0005*
X_2^2	230.57	1	128.60	0.0001*	114.95	1	198.67	0.0001*
X_3^2	40.46	1	22.57	0.0021*	9.16	1	15.83	0.0053*
Residual	12.55	7			4.05	7		
Lack-of-fit	9.75	3	4.64	0.0861#	3.25	3	5.42	0.0681#
Pure error	2.80	4			0.8	4		
Total	10259.88	16			664	16		

*Significant at $\alpha < 0.05$, #Not significant at $\alpha < 0.05$.

c) Optimization and validation

Desirability function (0.98) was probed using Design-Expert software to acquire an optimized formulation. Selection of optimum formulation was based on pre-set criteria as shown in Table 4.6. Conditions for optimal formulation as predicted by the software were as follows: surfactant concentration = 1.36 % w/v, polymer amount = 270.74 mg and the duration of homogenization = 40.15 min. To prove the validity of this statistical model, verification runs (n = 6) with these conditions were carried out and Wilcoxon Signed Rank Test was used to identify any statistically significant difference between actual and theoretical values. At α = 0.05, there was no statistically significant difference between actual and theoretical values for particle size (p < 0.0732) and EE (p < 0.8543) thus affirming validity of the proposed model. Optimized formulation exhibited particle size of 195.3 ± 2.3 nm, and EE of 93.95 ± 1.23%.

4.11.2 Synthesis and characterization of PA

PA was synthesized by replacing free hydroxyl groups present in glucose units of pullulan with the acetate groups (Fig. 4.18). Comparison of the FT-IR spectra of pullulan (Fig. 4.21(a)) and PA (Fig. 4.21 (b)) confirms the introduction of acetate groups in PA (Fig. 4.21 (b)), as indicated by the C=O stretching at 1752 cm^{-1}, C-O stretching at 1250 cm^{-1} and 1109 cm^{-1}, CH_3 deformation at 1370 cm^{-1} and presence of O–C=O bend at 603 cm^{-1}. The peak at 3470 cm^{-1} originating from stretching vibration of the hydroxyl (-OH) group became relatively weak following acetylation in PA further indicating the substitution of free -OH groups.

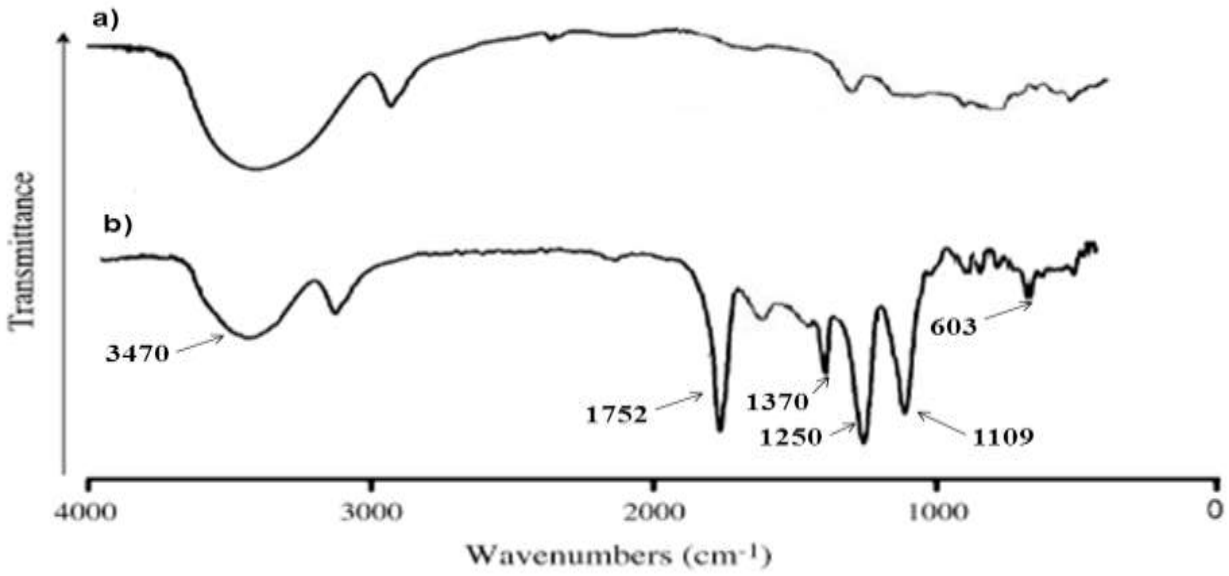

Fig. 4.21: FT-IR spectra of pullulan (a) and pullulan acetate (b).

Comparative ^{1}H NMR spectra of pullulan and PA dissolved in DMSO-d_6 is shown in Fig. 4.22. Intensity of hydroxyl proton signals of PA observed at 4.5–5.6 ppm decreased in comparison with pullulan. The ^{1}H NMR spectra of PA also demonstrated the introduction of additional methyl proton signals at 1.8–2.2 ppm, which can be assigned to the acetyl groups. The acetylation of pullulan was successful with the procedure followed. However, we could not precisely assign few proton signals observed at 3 ppm and above due to the complexity of the signals.

The calculated value of DS, post acetylation, was 2.91. Results indicate that nearly all the hydroxyl (-OH) groups have been substituted by acetyl moiety. Higher DS would render more hydrophobicity to PA [68] that could further accommodate more amount of drug thereby increasing the EE.

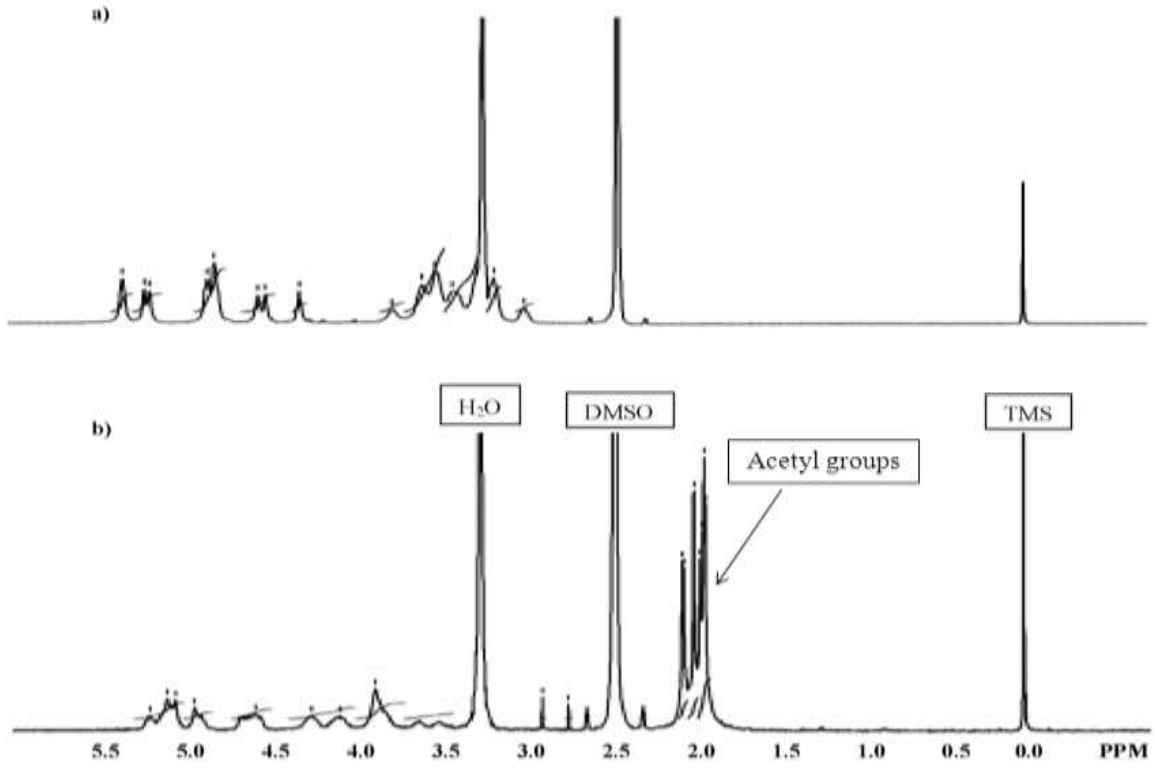

Fig. 4.22: ^{1}H NMR spectra of pullulan (a) and pullulan acetate (b) in DMSO-d_6.

4.11.3 Characterization of PCL NPs and PA NPs

SEM studies revealed that lopinavir loaded PCL NPs and PA NPs were almost spherical in shape (Fig. 4.23). Data from the particle size analysis demonstrated a unimodal size distribution of prepared nanoparticles. Mean particle size, polydispersity index (PDI) and zeta potential value of optimized PCL NPs (n = 6) were 195.3 ± 2.3 nm, 0.10 ± 0.01 and −19.74 ± 2.1 mV respectively. Whereas, mean particle size and the PDI of lopinavir loaded PA NPs (n = 6) were 197 ± 4 nm and 0.11 ± 0.01 respectively. The mean zeta potential value of lopinavir loaded PA NPs was -3 ± 1 mV.

The EE studies demonstrated high efficiency of the polymeric NPs in encapsulating lopinavir. EE of PCL NPs and PA NPs were 93.95 ± 1.23 and 76.5 ± 3.5% respectively. High EE could be possibly due to hydrophobic interactions between lopinavir and polymer molecules.

a)

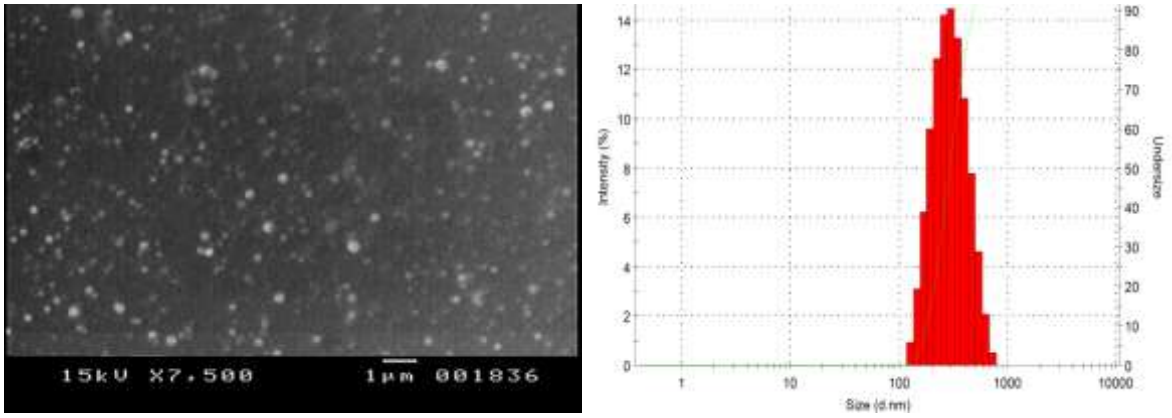

b)

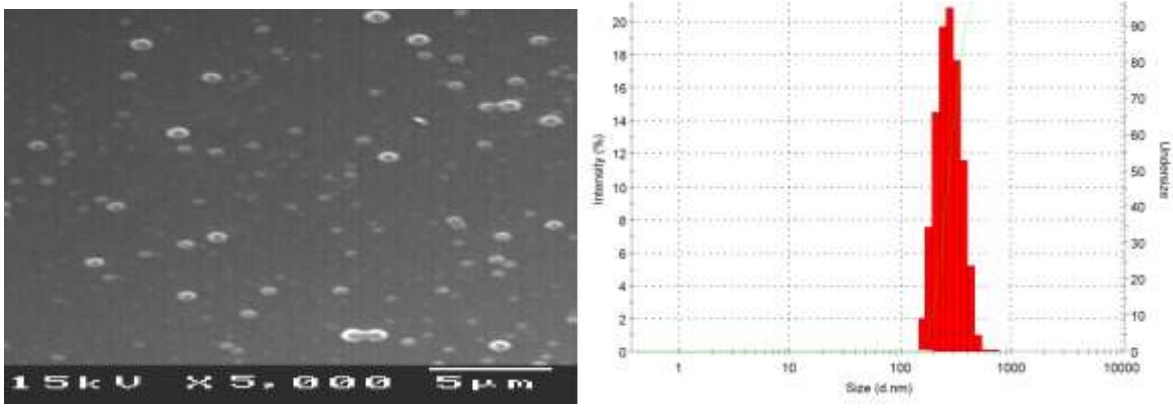

Fig. 4.23: Scanning electron microscopic images (left side) and Particle size distribution profiles (right side) of **a)** PCL NPs and **b)** PA NPs.

Fig. 4.24 (a and b) shows DSC thermograms for pure lopinavir, pure polymers (PCL and PA), physical mixture of lopinavir and polymer (1:1), blank NPs and lopinavir loaded polymeric nanoparticles (PCL NPs and PA NPs). DSC thermogram for pure lopinavir and lopinavir in physical mixture showed a sharp melting peak at 97.2 ^{o}C. PCL showed melting peak at 56.3 ^{o}C whereas, no endothermic peak was observed for pullulan acetate across the scanning range up to 200 ^{o}C. In DSC thermograms of blank and PCL loaded NPs, an additional peak observed at 168.3 ^{o}C was of mannitol (used as cryoprotectant).

In vitro drug release profile of nanoparticles formulations (PCL NPs and PA NPs) and free lopinavir are presented in Fig. 4.25. Free lopinavir showed complete dissolution within 5 h. Unlike free lopinavir, polymeric nanoparticles showed a bi-phasic release pattern, which was characterized by an initial rapid release followed by slow and continuous drug release. In the initial phase, PCL NPs showed 60% drug release in first 10 h followed by a slow and continuous drug release up to 75 h. Whereas, PA NPs exhibited 53% drug release in the first 8 h followed by a slow and continuous drug release.

a)

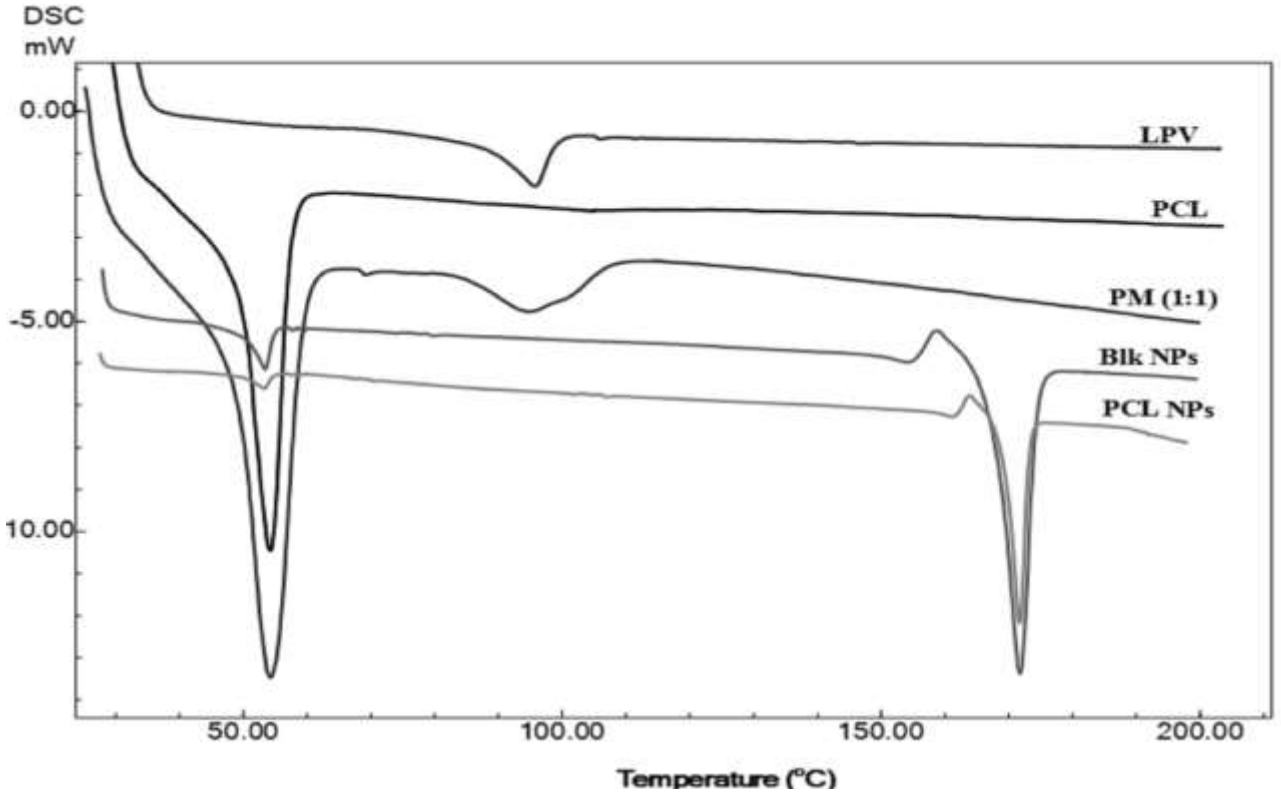

b)

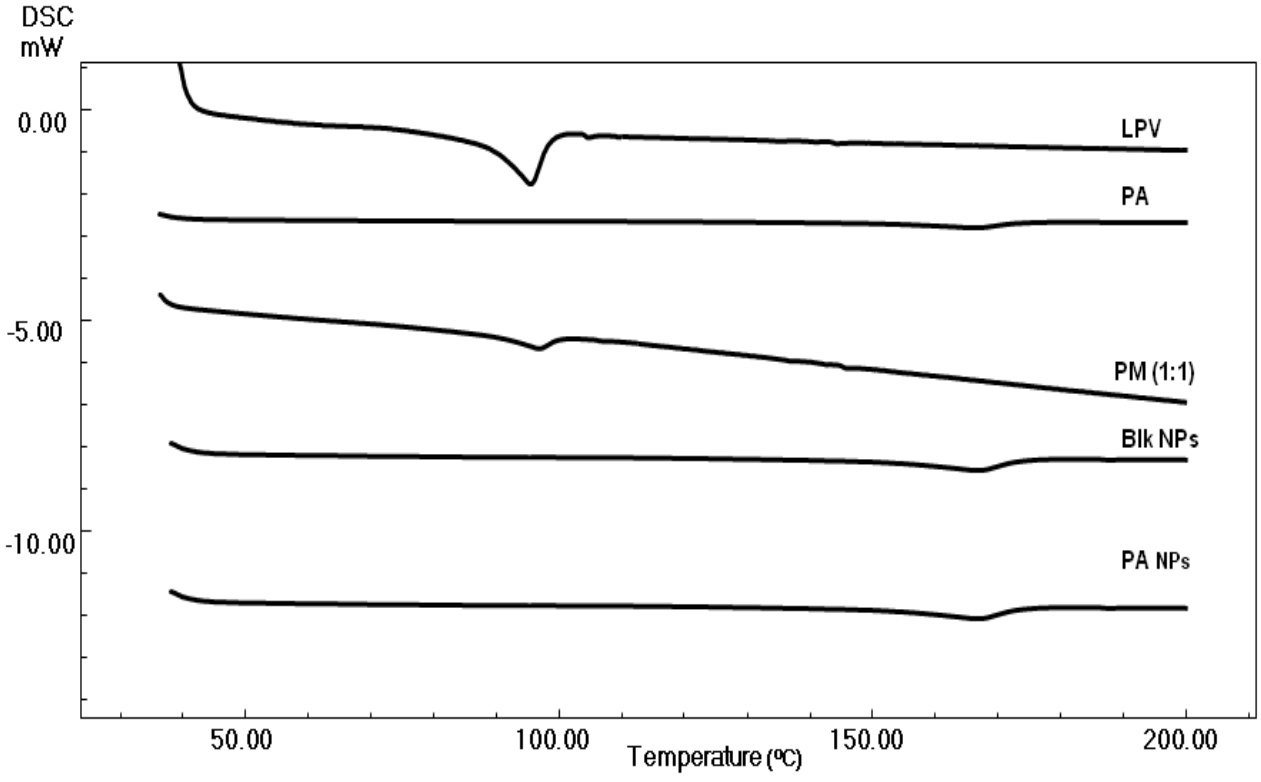

Fig. 4.24: **a)** Overlaid DSC thermograms of LPV, PCL, PM, blank NPs and LPV NPs. LPV, lopinavir; PCL, poly-ε-caprolactone; PM, physical mixture (1:1); NPs, nanoparticles. **b)** Overlaid DSC thermograms of LPV, PA, PM, blank NPs and PA NPs. LPV, lopinavir; PA, pullulan acetate; PM, physical mixture (1:1); NPs, nanoparticles.

Drug release kinetics was studied by fitting data into various mathematical models. From regression analysis, drug release from PCL NPs was most appropriately described by reciprocal-powered time model (r^2 = 0.9877). In comparison, zero-order kinetics (r^2 = 0.2873), first-order kinetics (r^2 = 0.9399) and Higuchi kinetics (r^2 = 0.8987) showed relatively lower r^2 values. Time taken for 50% drug release ($t_{50\%}$) and mean dissolution time (MDT) from NPs was calculated to be 7.34 h and 51.9 h respectively.

A similar observation was made for PA NPs drug release profile. From regression analysis, it is evident that reciprocal-powered time model (r^2 = 0.988) was best suited for PA NPs release profile. In comparison, zero-order kinetics (r^2 = 0.287), first-order kinetics (r^2 = 0.939) and Higuchi kinetics (r^2 = 0.898) showed relatively lower r^2 values. Times taken for 50% drug release ($t_{50\%}$) and mean dissolution time MDT from NPs were calculated to be 6.96 h and 40.71 h respectively.

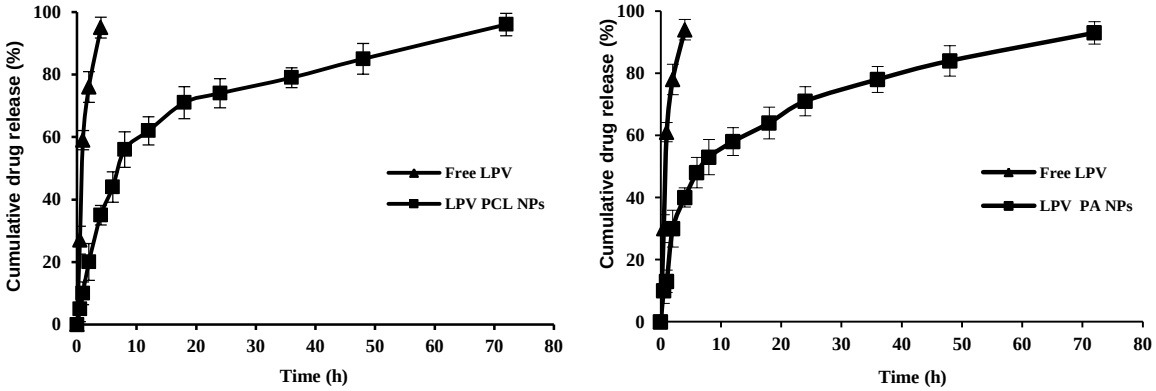

Fig. 4.25: *In vitro* drug release profiles of lopinavir loaded PCL NPs (left side) and PA NPs (right side) in simulated blood pH condition (PBS, pH 7.4). The data are expressed as mean ± SD (*n* = 6). LPV, lopinavir; PCL, poly-ε-caprolactone, PA NPs, pullulan acetate nanoparticles.

Formulation stability of NPs was evaluated by measuring particle size, zeta potential, PDI and EE at 0, 1, 2 and 3 months of storage at ambient temperature. As shown in the Fig. 4.26, mean particle diameter, zeta potential and EE of NPs were not significantly affected by storage at ambient temperature. From the same Fig, small change in PDI values was observed over time. However, for all samples, upon storage, PDI values remained below 0.2 suggesting that the particle population remained fairly homogeneous without any significant aggregation in NP dispersion during storage.

a)

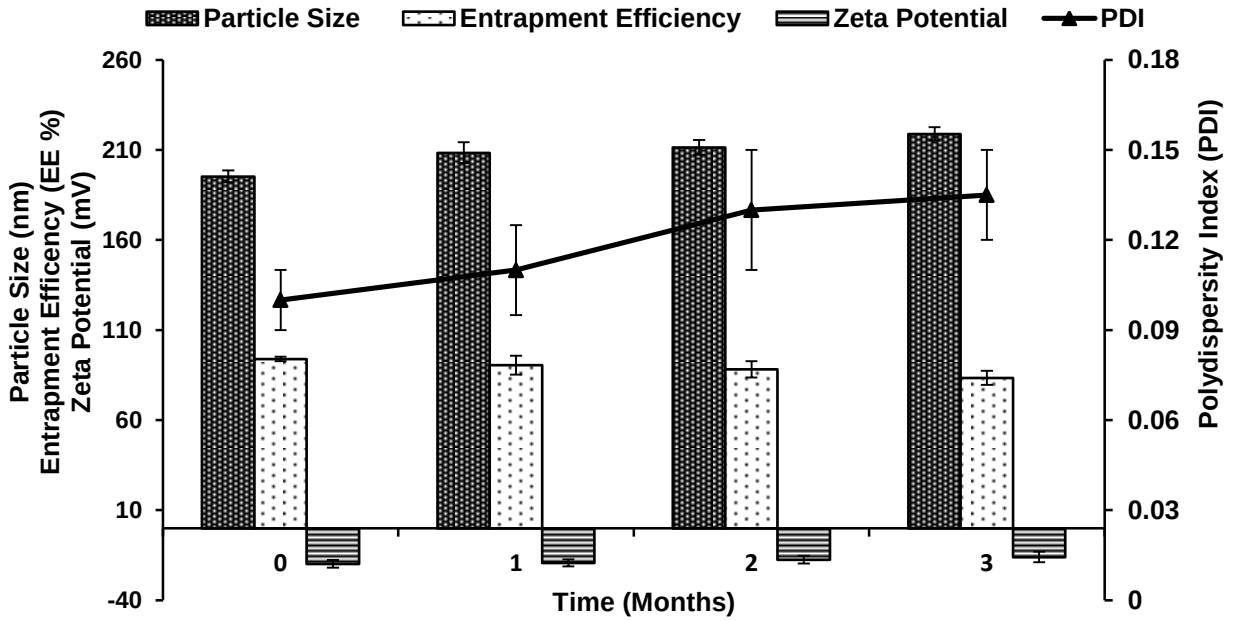

b)

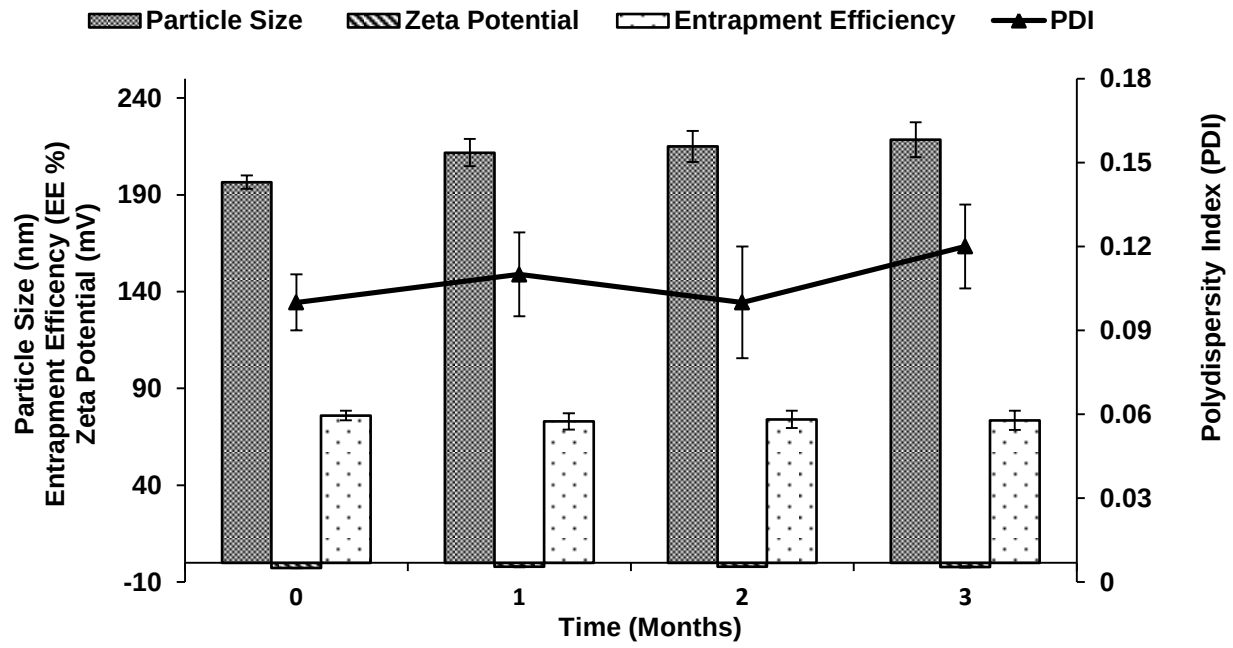

Fig 4.26: Stability characteristics of lopinavir loaded **a)** PCL NPs **b)** PA NPs in terms of mean particle size, entrapment efficiency (EE), Zeta potential and polydispersity index (PDI) stored at 25 ± 2 ^{o}C and 60% ± 5% RH. The data are expressed as mean ± SD of six independent determinations (n = 6). LPV, lopinavir; PCL, poly-ε-caprolactone; PA, pullulan acetate.

4.11.3 *In vitro*/*in vivo* evaluation of nanoparticles

a) Pharmacokinetic studies

The *in vivo* behaviour of lopinavir loaded nanoparticles formulations were assessed by performing pharmacokinetic studies in male wistar rats. Pharmacokinetic behaviour of free lopinavir, lopinavir/ritonavir co-formulation and lopinavir loaded nanoparticles formulations after oral administration is shown in Fig. 4.27 and Fig. 4.28.

Following oral administration, both co-formulation and lopinavir NPs showed statistically significant improvement in pharmacokinetics of lopinavir as determined by area under the curve (AUC), maximum plasma concentration (C_{max}) and mean residence time (MRT) (Table 4.9 and 4.10).

Co-administration of ritonavir with lopinavir (Group B) significantly increased lopinavir AUC by 3.7 folds ($p < 0.001$), C_{max} by 2.0 folds ($p < 0.001$) and MRT by 1.5 folds ($p < 0.05$) as compared to free lopinavir (Group A).

On the other hand, PCL NPs significantly increased AUC by 4.4 folds ($p < 0.001$), C_{max} by 3.0 folds ($p < 0.001$) and MRT by 1.30 folds ($p < 0.05$) as compared to free lopinavir. Similarly, following oral administration of PA NPs, AUC, C_{max} and MRT of loaded lopinavir increased by 2.3 folds ($p < 0.01$), 1.64 folds ($p < 0.05$) and 1.3 folds ($p < 0.05$) respectively. However, statistically no significant difference in T_{max} was observed in either of the formulations as compared to free lopinavir.

Comparative pharmacokinetic parameters of free lopinavir and lopinavir NPs post IV administration are summarized in Table 4.9 and Table 4.10. Statistically significant change in disposition parameters of lopinavir was observed following IV administration of loaded NPs as compared to a free lopinavir solution. Total plasma clearance (CL) of lopinavir from PCL NPs reduced by 27% ($p < 0.05$), whereas, a significant ($p < 0.01$) increase in half-life (increased by 1.82 folds, $p < 0.01$), and AUC (increased by 1.91 folds) was observed.

In case of PA NPs, as compared to free lopinavir solution, total plasma clearance (CL) of lopinavir was reduced by 22% ($p < 0.05$). A significant ($p < 0.01$) increase in half-life (increased by 1.59 folds), and AUC (increased by 1.80 folds) value of lopinavir was observed upon loading in to PA NPs.

Table 4.9 Pharmacokinetic parameters of lopinavir following oral and IV administrations of free lopinavir, lopinavir co-formulation and PCL NPs to rats (20 mg/kg; $n = 5$)

Oral (20 mg/kg) Parameters	**Free lopinavir (Group A)**	**Co-formulation (Group B)**	**PCL NPs (Group C)**
C_{max} (ng/ml)	645.85 ± 67.70	1260.41 ± 113.41***	1893.13 ± 220.16***
T_{max} (h)	0.85(0.75-1.0)	0.85 (0. 5-1.0)	1.1 (0.75-2.0)
MRT(h)	4.99 ± 0.50	7.81± 0.49*	6.51± 0.49*
AUC (ng/ml*h)	1555.52 ± 53.34	6051.75 ± 132.41***	6829.44 ± 98.59***
F_{rel}	-	3.89 ± 0.21	4.39± 0.42
IV (4 mg/kg) Parameters	**Free lopinavir (Group A)**		**PCL NPs (Group B)**
C_o (ng/ml)	2534.01 ± 134.12	-	1874.16 ± 120.14**
$T_{1/2}$	0.72 ± 0.05	-	1.32 ± 0.01**
CL (ml/h/kg)	1543.59 ± 107.34	-	1134.28 ± 95.13*
V_d (ml/kg)	1578.59 ± 116.54	-	1924.20 ± 109.45*
AUC (ng/ml*h)	2592.41 ± 215.23	-	4951.00 ± 321.34**
F_{rel}	-	-	1. 91± 0.12

Statistically significance difference (*$p < 0.05$; **$p < 0.01$;***$p < 0.001$) as compared to Free lopinavir (Group A). The data are expressed as mean ± S.D. T_{max} values in bracket are expressed in range. LPV, lopinavir; PCL, poly-ε-caprolactone; C_{max}, maximum plasma concentration; T_{max}, time to reach maximum plasma concentration; MRT mean residence time; AUC, area under the curve; F_{rel}, relative bioavailability

Table 4.10 Pharmacokinetic parameters of lopinavir following oral and IV administrations of free lopinavir, lopinavir co-formulation and PA NPs to rats (20 mg/kg).

Oral (20 mg/kg) Parameters	**Free Lopinavir (Group A)**	**Co-formulation (Group B)**	**PA NPs (Group C)**
C_{max} (ng/ml)	646.15 ± 67.70	1259.18 ± 123.51***	1060.34 ± 86.51*
T_{max} (h)	0.75 (0.5-1.0)	0.80 (0.5-1.0)	0.75 (0.5-1.0)
MRT(h)	5.19 ± 0.19	7.67± 0.17*	6.75 ± 0.25*
AUC (ng/ml*h)	1620.82 ± 59.32	6192.15 ± 123.15***	3782.50 ± 76.87**
F_{rel}	-	3.82± 0.31	2.32 ± 0.26
IV (4 mg/kg) Parameters	**Free Lopinavir (Group A)**		**PA NPs (Group B)**
C_o (ng/ml)	2423.01 ± 124.18	-	1981.17 ± 111.12*
$T_{1/2}$	0.75 ± 0.11	-	1.19 ± 0.02**
CL (ml/h/kg)	1531.51 ± 121.14	-	1191.23 ± 85.11*
V_d (ml/kg)	1650.59 ± 123.58	-	1884.10 ± 99.15*
AUC (ng/ml*h)	2612.11 ± 195.13	-	4778.02 ± 342.31**
F_{rel}	-	-	1.8± 0.11

Statistically significance difference (*$p < 0.05$; **$p < 0.01$) as compared to Free lopinavir (Group A). The data are expressed as mean ± S.D. T_{max} values in bracket are expressed in range. LPV, lopinavir; PA NPs, pullulan acetate nanoparticles; C_{max}, maximum plasma concentration; T_{max}, time to reach maximum plasma concentration; MRT mean residence time; AUC, area under the curve; F_{rel}, relative bioavailability.

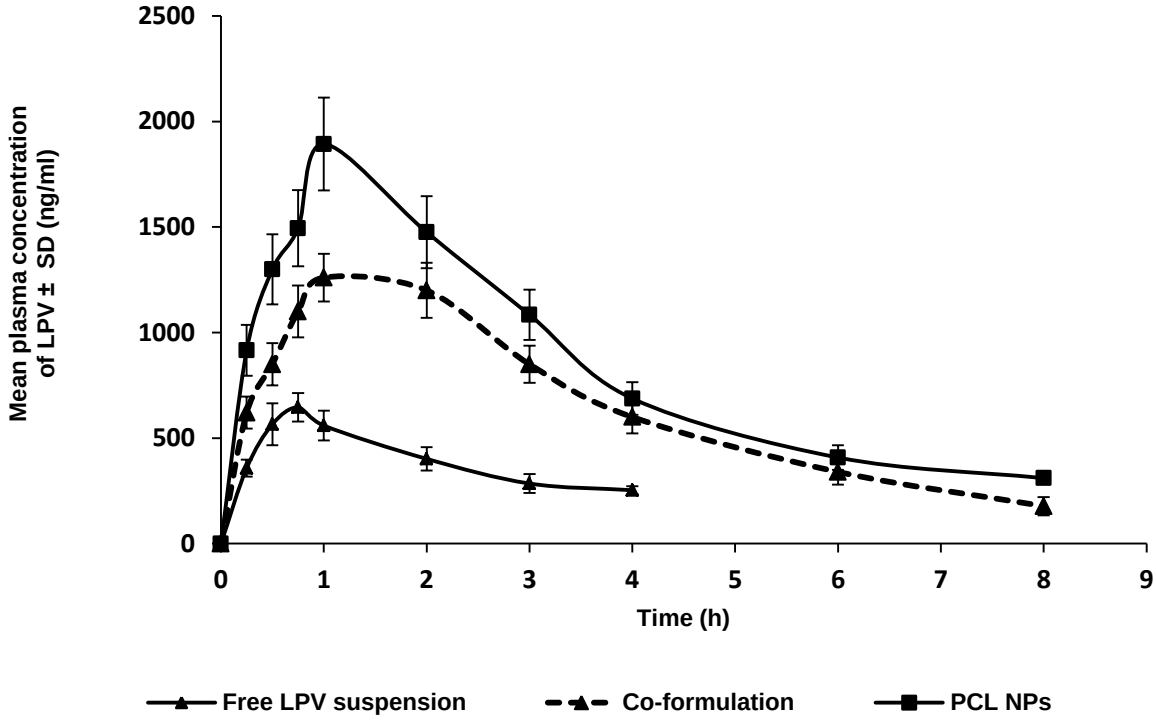

Fig. 4.27: Mean plasma concentration versus time profile of free lopinavir and PCL NPs after oral administration to male wistar rats (n = 5). The data are expressed as mean ± S.D. LPV, lopinavir; NPs, nanoparticles.

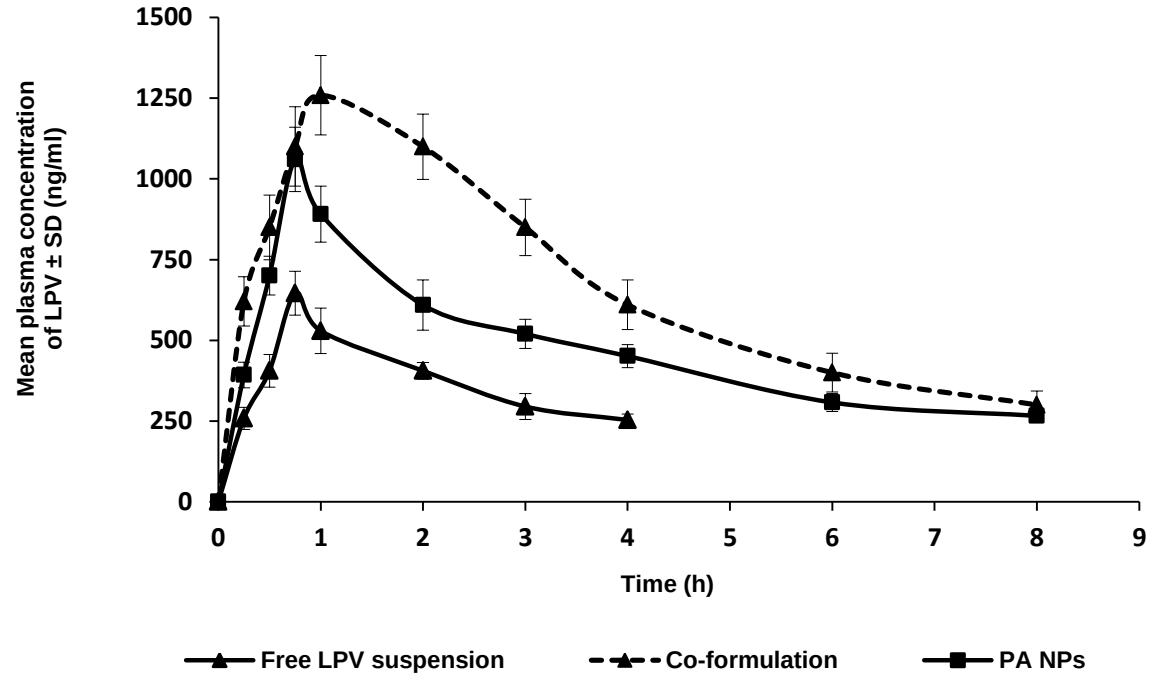

Fig. 4.28: Mean plasma concentration versus time profile of free lopinavir and PA NPs after oral administration to male wistar rats (n = 5). The data are expressed as mean ± S.D. LPV, lopinavir; NPs, nanoparticles.

b) Tissue-distribution study

In order to establish *in vivo* performance of lopinavir loaded PCL NPs and PA NPs at targeted organs, tissue distribution studies were conducted and compared with the distribution pattern of free lopinavir. As shown in Fig. 4.29, it is evident that lopinavir from loaded NPs was significantly ($p < 0.01$) accumulated in the liver (AUC increased by 2.7 folds, C_{max} increased by 3.2 folds), spleen (AUC increased by 2.10 folds; $p < 0.01$, C_{max} increased by 1.6 folds; $p < 0.05$) and lymph node tissues (AUC increased by 1.70 folds; $p < 0.05$, C_{max} increased by 1.9 folds; $p < 0.01$) as compared to free lopinavir post-oral administration.

Correspondingly, lopinavir from PA NPs showed significantly ($p < 0.05$) higher accumulation (Fig. 4.30) in liver (AUC increased by 1.69 folds, C_{max} increased by 1.60 folds) and spleen tissues (AUC increased by 1.53 folds; C_{max} increased by 1.64 folds). Whereas, marginally higher, though the statistically insignificant accumulation of lopinavir from PA NPs in mesenteric lymph node tissues was observed.

Following the co-administration of lopinavir with ritonavir, statistically significant ($p < 0.05$) accumulation of lopinavir in liver tissue was observed. In this case, when co-administered with ritonavir, lopinavir's C_{max} increased by 1.58 folds and AUC increased by 1.4 folds. However, for spleen and lymph nodes, no statistically significant change in C_{max} and AUC was observed.

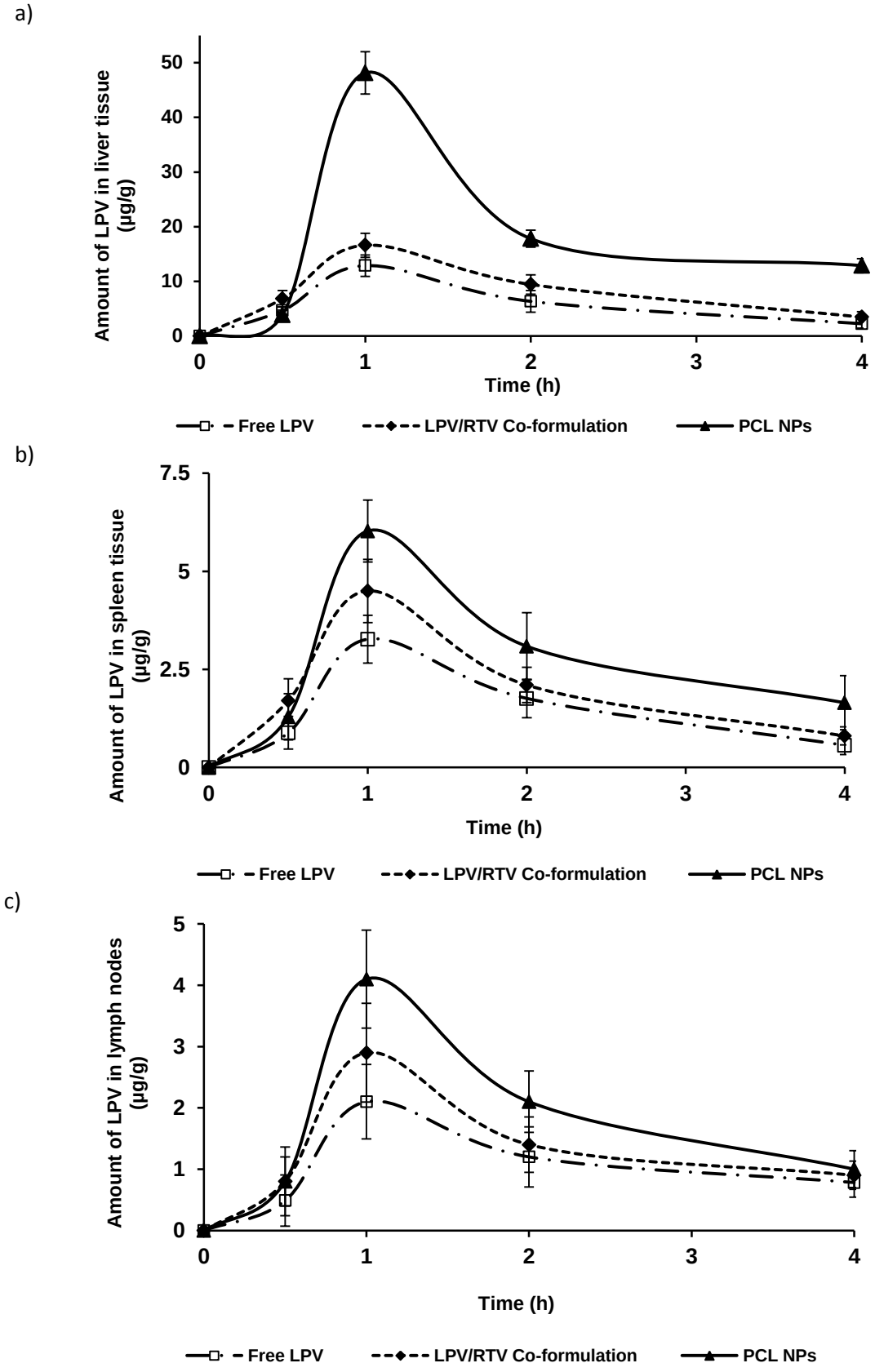

Fig. 4.29: Tissue distribution study of free lopinavir, lopinavir/ritonavir co-formulation and lopinavir loaded PCL NPs following oral administration to wistar rats. Three animals were sacrificed at each time point to harvest **a)** liver, **b)** spleen and **c)** mesenteric lymph node tissues. The data are expressed as mean ± S.D. LPV, lopinavir; RTV, ritonavir; NPs, nanoparticles.

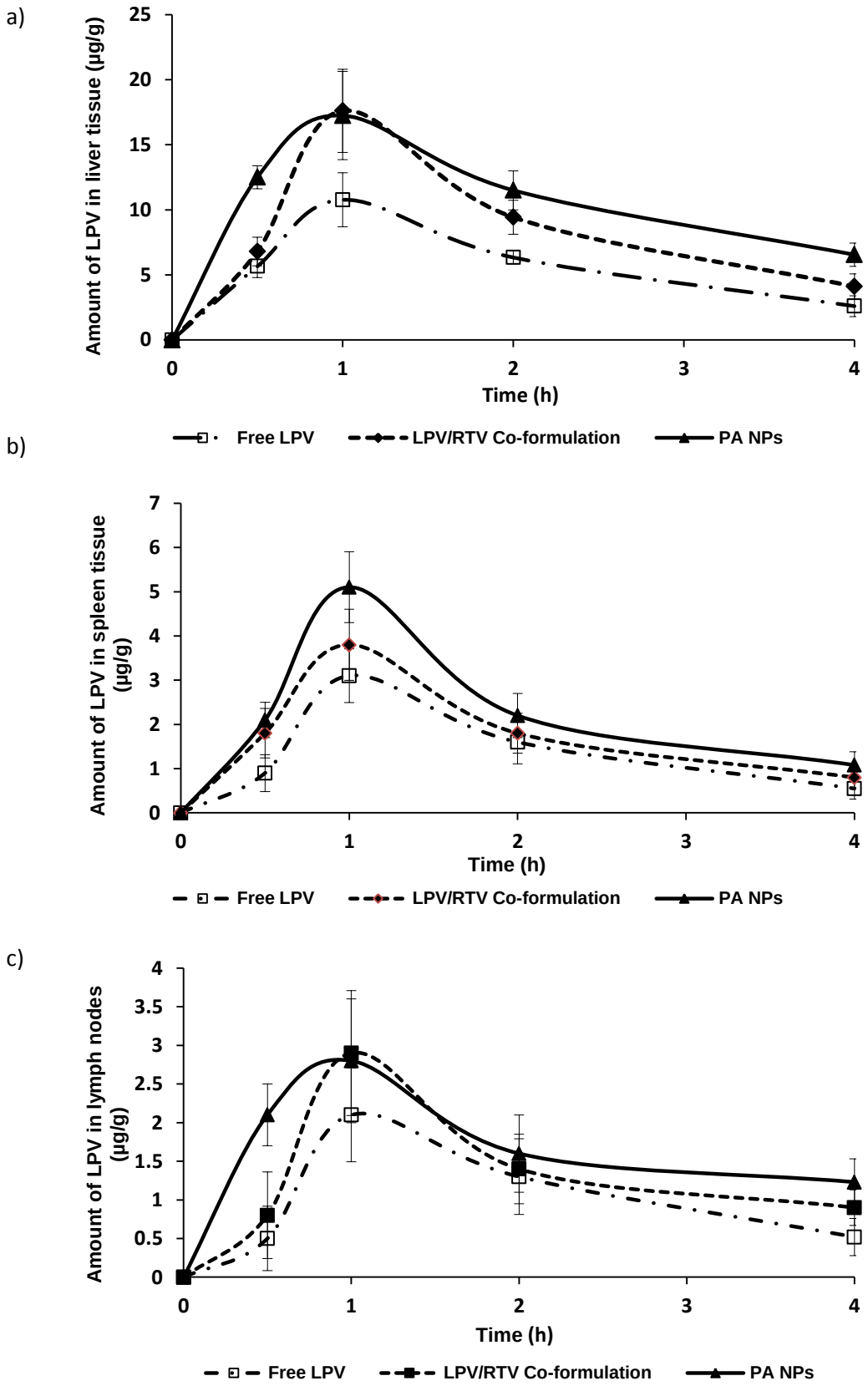

Fig. 4.30: Tissue distribution study of free lopinavir, lopinavir/ritonavir co-formulation and lopinavir loaded PA NPs following oral administration to wistar rats. Three animals were sacrificed at each time point to harvest **a)** liver, **b)** spleen and **c)** mesenteric lymph node tissues. The data are expressed as mean ± S.D. LPV, lopinavir; RTV, ritonavir; PA NPs, pullulan acetate nanoparticles.

c) *In vitro* metabolism stability study

Results obtained from *in vitro* metabolic stability studies using RIMs and RLMs are shown in Fig. 4.31. Mean percentage metabolism of lopinavir was reduced significantly ($p < 0.001$) upon co-incubation with ritonavir (metabolism of 10.1% in RIMs; 9.2% in RLMs) as compared to free lopinavir (metabolism of 89.2% in RIMs; 81.3% in RLMs) after 30 min of incubation period in both of the microsomes.

Similarly, in comparison with the control group, metabolism of lopinavir in loaded PCL NPs (24% in RIMs; 22% in RLMs) and PA NPs (35% in RIMs; 29% in RLMs) decreased significantly ($p < 0.001$). No statistically significant change (< 3%) in metabolism of free lopinavir was observed upon co-incubation with blank NPs.

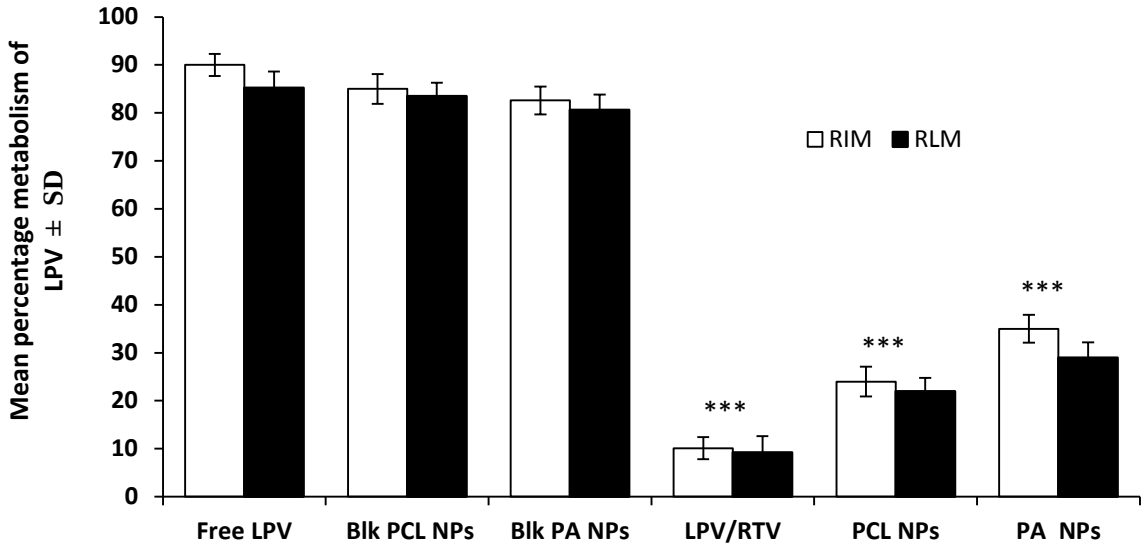

Fig. 4.31: Metabolism stability of free LPV, LPV/RTV co-formulation and LPV NPs after 30 min incubation with RIM and RLM at1 mg/ml protein concentration. ***Statistically significance difference ($p < 0.001$) as compared to Free LPV. The data are expressed as mean ± S.D. LPV, lopinavir; RTV, ritonavir; PCL, poly-ε-caprolactone; PA NPs, pullulan acetate nanoparticles; RIM, rat intestinal microsomes; RLM, rat liver microsomes.

d) Nanoparticles uptake study

Data obtained from permeability studies are shown in Table 4.11. Experimental results indicate a significant increase in apparent permeability (P_{app}) of lopinavir in the presence of ritonavir and upon loading into NPs as compared to free lopinavir. The P_{app} values of PCL NPs and PA NPs were found to increase by 1.88 folds ($p < 0.01$) and 1.61 folds ($p < 0.01$) respectively. Low incubation temperature (4 ^{o}C) and presence of specific inhibitors significantly ($p < 0.05$) reduced the intestinal uptake of NPs. As shown in Table 4.11, intestinal uptake of PCL NPs and PA NPs at 4 ^{o}C was only about 39% ($p < 0.01$) and

44% ($p < 0.01$) of that at the 37 ^{o}C respectively. In co-incubation with CPZ, the P_{app} values of PCL NPs and PA NPs reduced by 37% and 30% respectively. Similarly, in the presence of the NYT, P_{app} of PCL NPs and PA NPs significantly decreased by 34% and 39% respectively.

Table 4.11. Effect of incubation temperature and endocytic uptake inhibitors (chlorpromazine, 10 μg/ml and nystatin, 25 μg/ml) on intestinal permeability of free lopinavir, and lopinavir loaded polymeric nanoparticles.

Groups	P_{app} ($\times 10^{-5}$ cm/s)			
	Control (37 ^{o}C)	at 4 ^{o}C	(+)CPZ	(+)NYT
Free lopinavir	2.58 ± 0.31	2.63 ± 0.29	2.72 ± 0.32	2.44 ± 0.22
LPV/RTV Co-formulation	6.68 ± 0.31$^{**,\#}$	6.92± 0.29$^{\#}$	6.81 ± 0.38$^{\#}$	6.72 ± 0.32$^{\#}$
Lopinavir PCL NPs	4.86 ± 0.35**	1.90 ± 0.24$^{@@}$	3.06 ± 0.21$^{@}$	3.22 ± 0.26$^{@}$
Lopinavir PA NPs	4.16 ± 0.41**	1.85 ± 0.27$^{@@}$	2.91 ± 0.23$^{@}$	2.54 ± 0.24$^{@}$
Lucifer Yellow	0.25± 0.04	0.28± 0.03$^{\#}$	0.22± 0.05$^{\#}$	0.29± 0.03$^{\#}$

**Statistically significance difference ($p < 0.01$) as compared with Free lopinavir; $^{\#}$Statistically no significance difference ($p > 0.05$) as compared with respective control group (37 ^{o}C); $^{@}$Statistically significance difference ($p < 0.05$) as compared with respective control group (37 ^{o}C). The data are expressed as mean ± S.D. LPV, lopinavir; RTV, ritonavir; PCL, poly-ε-caprolactone; PA NPs, pullulan acetate nanoparticles; CPZ, chlorpromazine; NYT, nystatin

4.12 Discussion

4.12.1 Experimental Design for PCL NPs

Results of experimental design provided considerable useful information and reaffirmed utility of statistical design for the conduct of experiments. From Fig 4.20a, for a given concentration of surfactant, an increase in polymer amount leads to significant increase in particle size. This could be due to increase in viscosity of the continuous phase with the increase in the amount of polymer which results in reduction of evaporation rate of organic phase thereby leading to formation of larger particles [69]. It is also evident that at constant polymer amount, with an increase in surfactant concentration up to an optimal level, particle size decreases; beyond this, an increase in particle size is seen. The initial reduction of particle size by surfactant was attributed to reduction of interfacial tension between dispersed organic phase and dispersion media (aqueous phase) [70]. However, at higher surfactant concentrations, hydrophobic interactions between surfactant molecules dominate, leading to aggregation and increase in particle size.

As shown in Fig 4.20 b, increase in length of homogenization time resulted in reduced particle size. Longer duration of homogenization results in increased energy input that prevents agglomeration of NPs.

Effect of surfactant concentration and polymer amount on the EE at a constant homogenization time is shown in Table 4.7and illustrated in Fig 4.20c. A steep curvature for EE when viewed from polymer axis indicates that, with increasing amounts of polymer, EE increases. This is expected because with increasing amount of polymer, the lipophilic drug lopinavir gets better entrapped in the hydrophobic polymeric matrix. Higher amount of polymer also provides an additional number of particles into which lopinavir gets entrapped.

Likewise, from Fig 4.16c at fixed homogenization time, it is evident that with increasing surfactant concentration, EE of lopinavir increases. This is because more lopinavir molecules get entrapped within the surfactant layer present at the surface of NPs, leading to a high EE [71]. Further, with increasing polymer and surfactant concentration, viscosity of the medium increases, preventing rapid diffusion of lopinavir into the bulk of medium leading to higher EE [72].

From the polynomial equation for EE and Fig 4.20 d, it is evident that homogenization time has a positive effect on EE. With increasing homogenization time, energy input increases, leading to reduction of particle size and increase in surface area which increases EE.

4.12.2 Nanoparticles characterization

Fabricated polymeric nanoparticles of lopinavir exhibited particles in the nano size range with high EE and low PDI value. Low value of PDI indicates the usefulness of the proposed method in producing stable polymeric NPs with a relatively narrow size distribution.

The oil-in-water emulsion-solvent evaporation technique is widely used method for preparation of polymeric nanoparticles. Several researchers have validated the application of solvent evaporation in the encapsulation of hydrophobic compounds by producing nanoparticles with high EE [65].

Data from zeta potential studies indicated strong negative surface charge on PCL NPs. Negative zeta potential acquired on the surface was probably due to the presence of lactone residues on the polymeric matrix surface. However, the weak negative zeta potential of PA NPs was attributed to the presence of weakly ionized acetate functional groups on the polymeric surface.

From the stability data, it can be concluded that the polymeric based lopinavir nanoparticles were stable for at least 3 months upon storage at ambient temperature. No significant particle aggregation was seen in any of the formulations. It is assumed that due to high surface charge leading to strong electrostatic repulsion is involved in providing stability to PCL NPs. The particle stability of PA NPs was attributed to steric stabilization effect of PVA. It is reported that PVA adsorbs onto the NP surface and creates a repulsive barrier that prevents particle aggregation during storage [18]. However, extensive stability studies need to be performed to fix the shelf-life of NPs in different storage conditions.

In Fig 4.24 absence of lopinavir peak in thermograms of loaded NP formulations (PCL NPs and PA NPs) indicate that the majority of lopinavir is present in amorphous form within the polymeric matrix. No shift in peak position for lopinavir or PCL was observed in physical mixture, indicating absence of incompatibility between PCL and lopinavir.

The drug release profile indicates bi-phasic release pattern from loaded NPs. Initial rapid release may be due to the presence of lopinavir molecules on the surface of NPs entrapped in surfactant layer. In the second phase, the observed slow release is due to slow diffusion of the entrapped drug from NPs matrix.

4.12.3 *In vitro/in vivo* evaluation

In vivo performances of lopinavir loaded polymeric nanoparticles formulations were evaluated against the marketed formulation of lopinavir in male wistar rats. Series of comparative pharmacokinetic studies were conducted to understand mechanisms involved in the pharmacokinetic improvement of lopinavir NPs.

From oral the pharmacokinetic studies, it is evident that lopinavir has poor bioavailability; presumably due to high first-pass metabolism, rapid clearance and P-gp efflux. Results obtained from co-administration group demonstrated booster effect of ritonavir on pharmacokinetics of lopinavir as indicated by AUC, C_{max} and CL. Significant improvement in plasma exposure of lopinavir could be attributed to reduced first-pass metabolism and/or P-gp efflux.

Similarly, lopinavir loaded polymeric nanoparticles demonstrated significant improvement in the oral pharmacokinetics of lopinavir. High plasma exposure of lopinavir from polymeric nanoparticles could be possibly a result of reduced metabolism/P-gp efflux and/or increased intestinal permeability of lopinavir upon loading.

To understand *in vivo* clearance modulation of lopinavir upon loading, nanoparticles were intravenously injected to rats and apparent rate of elimination was calculated. A significant reduction in plasma clearance and extended half-life following IV administration

indicates metabolic protection (in the liver) offered by polymeric NPs to encapsulated lopinavir. Further, from pharmacokinetic data, it is also evident that the relative bioavailability obtained from oral study is considerably higher than intravenous study. This suggests that apart from diminished clearance, other factors such as improved permeability and avoidance of first-pass metabolism is contributing significant role in enhancing the oral bioavailability of polymeric nanoparticles.

We undertook *in vitro* metabolism stability studies in order to substantiate metabolic protection extended by nanoparticles to encapsulated lopinavir. Metabolism studies conducted with RIM and RLM illustrate extensive metabolism of free lopinavir and also demonstrated that NPs could offer metabolic protection to loaded drug. Metabolic protection offered by NPs to lopinavir (gut wall and hepatic) aids in achieving longer circulation time by bypassing first pass metabolism leading to higher plasma exposure of lopinavir. *In vitro* data agrees well with *in vivo* behaviour of lopinavir.

Intestinal uptake of NPs was investigated in rat everted gut sac model to explore the uptake mechanism and contribution of absorption in improving oral bioavailability of lopinavir NPs. A significant increase in P_{app} of lopinavir NPs as compared to free lopinavir suggested that NPs could efficiently cross intestinal barriers. Improved permeability of drug fabricated into nanoparticles is attributed to its active uptake through endocytosis (phagocytosis/pinocytosis) processes. Further, extended protection to loaded drug against gut metabolizing enzymes and modulation of P-gp function could also improve the intestinal permeability of lopinavir [73]. However, we could not evaluate the possible role of P-gp modulation in permeability of lopinavir NPs.

It is widely reported that at lower temperatures (4 ^{o}C), energy dependent processes like endocytosis could be blocked [74]. Hence, to discern the uptake mechanism, we carried out a permeability study of lopinavir NPs at two different temperatures ie at 37 ^{o}C (control) and 4 ^{o}C. The data from the study indicates significant reduction in P_{app} value of lopinavir NPs. However, no significant effect of incubation temperature on intestinal permeability of free lopinavir was observed. This implied that uptake of NPs in everted gut sacs could be possibly a result of energy dependent active uptake process.

Further, it has been reported that specific endocytic uptake inhibitors like chlorpromazine (CPZ) and nystatin (NYT) could reduce uptake of NPs by either inhibiting clathrin coated pit associated receptors at cell surface or abolishing caveolae function respectively [48]. Hence, to identify the mechanism of nanoparticles uptake, intestinal everted gut sac study was extended and performed in the presence of CPZ and NYT. From

the study results, it could be deduced that both clathrin- and caveolae mediated endocytosis mechanisms were involved in the uptake of lopinavir NPs. From this, we concluded that endocytosis plays a trivial role in the uptake of lopinavir. It also signifies a significant role of passive diffusion in absorption of free lopinavir. Moreover, no significant change in P_{app} value of free lopinavir in the presence of CPZ and NYT also overrules interaction of CPZ and NYT with P-gp and other transporter systems.

In order to establish *in vivo* performance of lopinavir NPs at targeted organs, tissue distribution studies were conducted and compared with the distribution pattern of free lopinavir and marketed co-formulation. As shown in Fig. 4.29 & 4.30, lopinavir in loaded NPs significantly accumulated in the liver, spleen and lymph node tissues in comparison to free lopinavir. Data suggests that following oral administration nanoparticles are taken up into the lymphatic system and transported to lymphoidal organs. Various researchers have reported the similar behaviour of orally administered NPs [75]. It has been reported that the M-cells covering Peyer's patches take up NPs by a combination of endocytosis and/or transcytosis mechanism. The size of these particles takes them to the lymphatic system through relatively larger openings rather than blood capillaries whose pore sizes are tiny. However, we could not observe a significant accumulation of lopinavir following oral administration of PA NPs in lymph node tissue. Higher localization of lopinavir in liver tissue than other tissues could be possibly due to superior blood perfusion to the liver. Moreover, it is reported that kuffer cells present in the liver have remarkable ability to engulf nanoparticles that may further lead to high localization of nanoparticles to liver [76].

From results, it is notable that though ritonavir co-administration (in marketed formulation) was able to improve the plasma exposure of lopinavir significantly, but failed to maintain high concentrations at viral reservoir sites as compared to nanoparticles (with the exception of PA NPs).

In a similar study, Destache et al. have demonstrated significant improvement of lopinavir exposure (over 8 folds) following intra-peritoneal administration of lopinavir loaded PLGA NPs as compared to free lopinavir. Further, higher distribution of NPs to liver, kidney, spleen and brain was also reported [77]. Our data are in reasonable agreement with the previously reported data. However, in our case, nanoparticles formulations were administered by oral route. Apparently, these results should be viewed with sagaciousness as route of administration in both cases are different.

It is reported that the HIV remains viable in the lymphoid organs, the main viral reservoir sites, even when sufficient concentration of the anti-HIV drug is available in the

blood circulation. The majority of the anti-retroviral drugs (including lopinavir co-formulation) are unable to reach these viral reservoir sites. Hence, for better therapeutic efficacy, it is desirable to have higher amounts of lopinavir for longer duration of time in lymphoid organs (liver, spleen and lymph nodes). In the present work, we demonstrated that with the use of lopinavir nanocarriers, better distribution of lopinavir could be achieved at targeted organs in comparison with lopinavir/ritonavir co-formulation. Therefore, in conclusion, lopinavir loaded polymeric nanoparticles could be a better alternative than conventional lopinavir therapy for treatment of HIV infection and prevention of its relapse.

4.13 Conclusions

Lopinavir was successfully fabricated in polymeric nanocarriers; PCL and PA with high EE and desirable particle size range. The method used in the manufacture of NPs was robust and yielded nearly monodisperse particles of nanometric size (~200 nm). Critical factors for manufacturing PCL NPs were identified and optimized using DoE with good correlation between actual and predicted values. Optimized lopinavir PCL NPs showed a significant increase in oral bioavailability as compared to free lopinavir suspension. We have shown that hydrophobically modified pullulan nanoparticles are promising carriers to improve oral bioavailability of lopinavir. Compared to the free drug, we also demonstrated that lopinavir in polymeric nanoparticles was metabolized to a lesser extent in the liver and gut. Moreover, metabolic protection and lymphatic uptake of NPs helped in achieving a significantly higher bioavailability of lopinavir than free drug. In summary, lopinavir loaded NPs could prove effective in addressing a major delivery challenge for anti-HIV drugs in reaching the viral reservoir sites that are normally inaccessible by conventional therapy. In conclusion, formulating PCL and PA NPs for poorly soluble lopinavir was an effective approach in improving its exposure to HIV reservoirs and reducing dose which may prove beneficial in the treatment of HIV infected patients.

References

1. Gastaldi L, Battaglia L, Peira E, Chirio D, Muntoni E, Solazzi I, et al. Solid lipid nanoparticles as vehicles of drugs to the brain: Current state of the art. Eur J Pharm Biopharm. 2014; 87: 433-444
2. Onoue S, Yamada S, Chan HK. Nanodrugs: pharmacokinetics and safety. Int J Nanomedicine. 2014; 9: 1025-37.
3. Kalepu S, Manthina M, Padavala V. Oral lipid-based drug delivery systems–an overview. Acta Pharm Sin B. 2013; **3**: 361-372.

4. Iqbal MA, Md S, Sahni JK, Baboota S, Dang S, Ali J. Nanostructured lipid carriers system: recent advances in drug delivery. J Drug Target. 2012; 20: 813-30.
5. Das S, Ng WK, Tan RB. Are nanostructured lipid carriers (NLCs) better than solid lipid nanoparticles (SLNs): development, characterizations and comparative evaluations of clotrimazole-loaded SLNs and NLCs? Eur J Pharm Sci. 2012 30; 47:139-51.
6. Radomska-Soukharev A. Stability of lipid excipients in solid lipid nanoparticles. Adv Drug Deliv Rev. 2007; 59: 411-8.
7. Mehnert W, Mäder K. Solid lipid nanoparticles: Production, characterization and applications. Adv Drug Deliver Rev. 2001; 47: 165-196.
8. Pardeshi C, Rajput P, Belgamwar V, Tekade A, Patil G, Chaudhary K, Sonje A. Solid lipid based nanocarriers: an overview. Acta Pharm. 2012; 62: 433-72.
9. Manjunath K, Venkateswarlu V.Pharmacokinetics, tissue distribution and bioavailability of clozapine solid lipid nanoparticles after intravenous and intraduodenal administration. J Control Release. 2005; 107: 215-28.
10. Manjunath K, Venkateswarlu V. Pharmacokinetics, tissue distribution and bioavailability of nitrendipine solid lipid nanoparticles after intravenous and intraduodenal administration. J Drug Target. 2006; 14: 632-45.
11. Ning Y, Zhang H, Dong F, Liu X, Wu J, Yang B. Direct synthesis of polymerizable surfactant-stabilized nanoparticles: the macromolecular monomers for fabricating nanoparticle-polymer composites. Nanotechnology. 2010; 21: 285604.
12. Awad TS, Helgason T, Kristbergsson K, Weiss J, Decker EA, McClements DJ. Temperature scanning ultrasonic velocity study of complex thermal transformations in solid lipid nanoparticles. Langmuir. 2008; 24: 12779-84.
13. zur Mühlen A, Schwarz C, Mehnert W. Solid lipid nanoparticles (SLN) for controlled drug delivery – Drug release and release mechanism. Eur J Pharm Biopharm. 1998; 45: 149-55.
14. Ojewole E, Mackraj I, Naidoo P, Govender T. Exploring the use of novel drug delivery systems for antiretroviral drugs. Eur J Pharm Biopharm. 2008; 70: 697-710.
15. Wong HL, Chattopadhyay N, Wu XY, Bendayan R. Nanotechnology applications for improved delivery of antiretroviral drugs to the brain. Adv Drug Del Rev. 2010; 62: 503-515.
16. Wavikar P, Vavia P. Nanolipidgel for enhanced skin deposition and improved antifungal activity. AAPS PharmSciTech. 2013; 14: 222-33.

17. Jiao J, Burgess DJ. Rheology and stability of water-in-oil-in-water multiple emulsions containing Span 83 and Tween 80.AAPS PharmSci. 2003; 5: E7.
18. Lee A, Tsai HY, Yates MZ. Steric stabilization of thermally responsive N-isopropylacryl -amide particles by poly (vinyl alcohol). Langmuir. 2010; 26:18055-60.
19. Severino P, Pinho SC, Souto EB, Santana MH. Polymorphism, crystallinity and hydrophilic-lipophilic balance of stearic acid and stearic acid-capric/caprylic triglyceride matrices for production of stable nanoparticles. Colloids Surf B Biointerfaces. 2011; 86: 125-30.
20. Castelli F, Puglia C, Sarpietro MG, Rizza L, Bonina F. Characterization of indomethacin-loaded lipid nanoparticles by differential scanning calorimetry. Int J Pharm 2005; 304: 231-238.
21. Yue PF, Lu XY, Zhang ZZ, Yuan HL, Zhu WF, Zheng Q, et al. The study on the entrapment efficiency and in *vitro* release of puerarin submicron emulsion. AAPS PharmSciTech. 2009; 10: 376-83.
22. Shah M, Pathak K. Development and statistical optimization of solid lipid nanoparticles of simvastatin by using 2^3 Full-Factorial Design. AAPS PharmSciTech. 2010; 11: 489-496.
23. ICH Q 1 A (R2). Stability testing of new drug substances and products. (CPMP/ICH/2736/99). Available from: URL: http://www.emea.eu.int/pdfs/human/ich/273699en.pdf
24. McGonigle P, Ruggeri B. Animal models of human disease: challenges in enabling translation. Biochem Pharmacol. 2014; 87: 162-71.
25. Sham HL, Kempf DJ, Molla A, Marsh KC, Kumar GN, Chen CM, et al. ABT-378, a highly potent inhibitor of the human immunodeficiency virus protease. Antimicrob Agents Chemother. 1998; 42: 3218-24.
26. MolKumar GN, Jayanti V, Lee RD, Whittern DN, Uchic J, Thomas S, et al. In vitro metabolism of the HIV-1 protease inhibitor ABT-378: species comparison and metabolite identification. Drug Metab and Dispos. 1999; 27: 86-91.
27. Goffinet C, Allespach I, Keppler OT. HIV-susceptible transgenic rats allow rapid preclinical testing of antiviral compounds targeting virus entry or reverse transcription. Proc Natl Acad Sci U S A. 2007; 104: 1015-20.
28. Huang W, Calvo M, Karu K, Olausen HR, Bathgate G, Okuse K, et al. A clinically relevant rodent model of the HIV antiretroviral drug stavudine induced painful peripheral neuropathy. Pain. 2013; 154: 560-75.

29. Kumar GN, Jayanti VK, Johnson MK, Uchic J, Thomas S, Lee RD, et al. Metabolism and disposition of the HIV-1 protease inhibitor lopinavir (ABT 378) given in combination with ritonavir in rats, dogs, and humans. Pharm Res. 2004; 21: 1622-30.
30. Obach RS. Prediction of human clearance of twenty-nine drugs from hepatic microsomal intrinsic clearance data: An examination of in vitro half-life approach and nonspecific binding to microsomes. Drug Metab Dispos. 1999; 27: 1350-9.
31. Zha W, Zha BS, Zhou F, Zhou H, Wang G. The cellular pharmacokinetics of HIV protease inhibitors: current knowledge and future perspectives. Curr Drug Metab. 2012 ; 13: 1174-83.
32. Wong HL, Chattopadhyay N, Wu XY, Bendayan R. Nanotechnology applications for improved delivery of antiretroviral drugs to the brain. Adv Drug Del Rev. 2010; 62: 503-515.
33. Sahneh FD, Scoglio CM, Monteiro-Riviere NA, Riviere JE.Predicting the impact of biocorona formation kinetics on interspecies extrapolations of nanoparticle biodistribution modeling. Nanomedicine (Lond). 2014; 17: 1-9.
34. Umeh OC, Currier JS, Park JG, Cramer Y, Hermes AE, Fletcher CV. Sex differences in lopinavir and ritonavir pharmacokinetics among HIV-infected women and men. J Clin Pharmacol. 2011; 51: 1665-73.
35. Klein CE, Chiu YL, Awni W, Zhu T, Heuser RS, Doan T,The tablet formulation of lopinavir/ritonavir provides similar bioavailability to the soft-gelatin capsule formulation with less pharmacokinetic variability and diminished food effect. J Acquir Immune Defic Syndr. 2007; 44: 401-10.
36. Dahan A, Hoffman A. Evaluation of a chylomicron flow blocking approach to investigate the intestinal lymphatic transport of lipophilic drugs. Eur J Pharm Sci. 2005; 24: 381-8.
37. Barthe L1, Woodley J, Houin G.The improved everted gut sac: a simple method to study intestinal P-glycoprotein. Fundam Clin Pharmacol. 1999;13: 154-68.
38. Lacombe O, Woodley J, Solleux C, Delbos J-M, Boursier-Neyret C, Houin G. Localisation of drug permeability along the rat small intestine, using markers of the paracelluar, transcellular and some transporter routes. Eur J Pharm Sci. 2004; 23: 385-91.
39. Parsa A, Saadati R, Abbasian Z, Azad Aramaki S, Dadashzadeh S. Enhanced permeability

of etoposide across everted sacs of rat small intestine by vitamin E-TPGS. Iran J Pharm Res. 2013 Winter; 12: 37-46.

40. Barthe L, Woodley J, Houin G. Gastrointestinal absorption of drugs: methods and studies. Fundam Clin Pharmacol. 1999; 13: 154-68.
41. Quintanar-Guerrero D, Tamayo-Esquivel D, Ganem-Quintanar A, Allémann E, Doelker E. Adaptation and optimization of the emulsification-diffusion technique to prepare lipidic nanospheres. Eur J Pharm Sci. 2005; 26: 211-8.
42. Hao J, Fang X, Zhou Y, Wang J, Guo F, Li F, Peng X. Development and optimization of solid lipid nanoparticle formulation for ophthalmic delivery of chloramphenicol using a Box-Behnken design. Int J Nanomedicine. 2011; 6: 683-692.
43. Yang YY, Chung TS, Bai XL, Chan WK. Effect of preparation conditions on morphology and release profiles of biodegradable polymeric microspheres containing protein fabricated by double-emulsion method. Chem Eng Sci. 2000; 55: 2223-2236.
44. Barzegar-Jalali M, Adibkia K, Valizadeh H, Shadbad MR, Nokhodchi A, Omidi Y, et al. Kinetic analysis of drug release from nanoparticles. J Pharm Pharm Sci. 2008; 11: 167-77.
45. Gajendiran M, Gopi V, Elangovan V, Murali RV, Balasubramanian S. Isoniazid loaded core shell nanoparticles derived from PLGA-PEG-PLGA tri-block copolymers: *in vitro* and in vivo drug release. Colloids Surf B Biointerfaces. 2013; 104: 107-15.
46. Hua S. Comparison of in vitro dialysis release methods of loperamide-encapsulated liposomal gel for topical drug delivery. Int J Nanomedicine. 2014; 9: 735-44.
47. Chandwani1 A, Shuter J. Lopinavir/ritonavir in the treatment of HIV-1 infection: a review. Ther Clin Risk Manag. 2008; 4; 1023-1033.
48. Roger E, Lagarce F, Garcion E, Benoit JP. Lipid nanocarriers improve paclitaxel transport throughout human intestinal epithelial cells by using vesicle-mediated transcytosis. J Cont Rel. 2009; 140: 174-181.
49. Qi J, Lu Y, Wu W. Absorption, disposition and pharmacokinetics of solid lipid nanoparticles. Curr Drug Metab. 2012; 13: 418-28.
50. Porter CJ, Trevaskis NL, Charman WN. Lipids and lipid based formulations: optimizing the oral delivery of lipophilic drugs. Nat Rev Drug Discov. 2007;6 : 231-48.
51. Wurm FR, Weiss CK. Nanoparticles from renewable polymers.Front Chem. 2014; 2: 49.
52. Chan JM, Valencia PM, Zhang L, Langer R, Farokhzad OC. Polymeric nanoparticles for drug delivery. Methods Mol Biol. 2010; 624:163-75.

53. Matsumura Y. The drug discovery by nanomedicine and its clinical experience. Jpn J Clin Oncol. 2014; 44: 515-25.
54. Shibata A, McMullen E, Pham A, Belshan M, Sanford B, Zhou Y, et al. Polymeric nanoparticles containing combination antiretroviral drugs for HIV type 1 treatment. AIDS Res Hum Retroviruses. 2013; 29: 746-54.
55. Woodruff MA, Hutmacher DW. The return of a forgotten polymer-polycaprolactone in the 21st century. Prog Polym Sci. 2010; 35: 1217-1256.
56. Ulery BD, Nair LS, Laurencin CT. Biomedical applications of biodegradable polymers. J Polym Sci B Polym Phys. 2011; 49: 832-864.
57. Shah LK, Amiji MM. Intracellular delivery of saquinavir in biodegradable polymeric nanoparticles for HIV/AIDS. Pharm Res. 2006; 23: 2638-2645.
58. Leathers TD. Biotechnological production and applications of pullulan. Appl Microbiol Biotechnol. 2003; 62: 468-73.
59. Akiyoshi K, Deguchi S, Moriguchi N, Yamaguchi S, Sunamoto J. Self-aggregates of hydrophobized polysaccharides in water. Formation and characteristics of nanoparticles. Macromolecules. 1993; 26: 3062-3068.
60. Lee SJ, Hong GY, Jeong YI, Kang MS, Oh JS, Song CE, et al. Paclitaxel incorporated nanoparticles of hydrophobized polysaccharide and their antitumor activity. Int J Pharm. 2012; 433: 121-8.
61. Hong GY, Jeong YI, Lee SJ, Lee E, Oh JS, Lee HC. Combination of paclitaxel- and retinoic acid-incorporated nanoparticles for the treatment of CT-26 colon carcinoma. Arch Pharm Res. 2011; 34: 407-17.
62. Tang HB, Li L, Chen H, Zhou ZM, Chen HL, Li XM, et al. Stability and *in vivo* evaluation of pullulan acetate as a drug nanocarrier. Drug Deliv. 2010; 17: 552-8.
63. Zhang HZ, Gao FP, Liu LR, Li XM, Zhou ZM, Yang XD, Zhang QQ. Pullulan acetate nanoparticles prepared by solvent diffusion method for epirubicin chemotherapy. Colloids Surf B Biointerfaces. 2009; 71: 19-26.
64. Jung SW, Jeong YI, Kim SH. Characterization of hydrophobized pullulan with various hydrophobicities. Int J Pharm. 2003; 254: 109-21.
65. Reis CP, Neufeld R J, Ribeiro AJ, Veiga F. Nanoencapsulation I. Methods for preparation of drug-loaded polymeric nanoparticles. Nanomedicine: Nanotechnology, Biology and Medicine.2006; 2: 8-21.

66. Byun Y, Hwang JB, Bang SH, Darby D, Cooksey K, Dawson PL, et al. Formulation and characterization of α-tocopherol loaded poly-ε-caprolactone (PCL) nanoparticles. LWT-Food Sci Technol. 2011; 44: 24-28.
67. Motozato Y, Ihara H, Tomoda T, Hirayama C. Preparation of gel permeation chromatographic properties of pullulan spheres. J Chromatogr Sci. 1986; 355: 434.
68. Teramoto N, Shibata M. Synthesis and properties of pullulan acetate. Thermal properties, biodegradability, and a semi-clear gel formation in organic solvents. Carbohydr Polym. 2006; 6: 476-481.
69. Lamprecht A, Ubrich N, Hombreiro PM, Lehr C, Hoffman M, Maincent P. Influences of process parameters on nanoparticle preparation performed by a double emulsion pressure homogenization technique. Int J Pharm. 2000; 196: 177-182.
70. Ma Y, Zheng Y, Zeng X, Jiang L, Chen H, Liu R, et al. Novel docetaxel-loaded nanoparticles based on PCL-Tween 80 copolymer for cancer treatment. Int J Nanomedicine. 2011; 6: 267-2688.
71. Mayank S, Krishna C, Mishra A, Pathak K. Oral solid compritol 888 ATO nanosuspension of simvastatin: optimization and biodistribution studies. Drug Dev Ind Pharm. 2011; 37: 526-537.
72. Yang Y, Chung T, Bai X, Chan, W. Effect of preparation conditions on morphology and release profiles of biodegradable polymeric microspheres containing protein fabricated by double-emulsion method. Chem Eng Sci. 2000; 55: 2223-2236.
73. Sharma P, Garg S. Pure drug and polymer based nanotechnologies for the improved solubility, stability, bioavailability and targeting of anti-HIV drugs. Adv Drug Deliv Rev. 2010; 62: 491–502.
74. Zhang Z, Gao F, Bu H, Xiao J, Li Y. Solid lipid nanoparticles loading candesartan cilexetil enhance oral bioavailability: in vitro characteristics and absorption mechanism in rats. Nanomedicine 2012; 8: 740–747.
75. Owens DE 3rd, Peppas NA. Opsonization, biodistribution, and pharmacokinetics of polymeric nanoparticles. Int J Pharm. 2006; 307: 93-102.
76. Almeida JP, Chen AL, Foster A, Drezek R. In vivo biodistribution of nanoparticles. Nanomedicine (Lond). 2011; 6: 815-35.
77. Destache CJ, Belgum T, Goede M, Shibata A, Belshan MA. Antiretroviral release from poly(DL-lactide-co-glycolide) nanoparticles in mice. J Antimicrob Chemother. 2010; 65: 2183-7.

Chapter 5

In vitro Cytotoxicity Assessment

5.1 Introduction

The primary goal for nanoparticle entrapment of drugs are either enhanced delivery to, or uptake by, target cells and or a reduction in the toxicity of free drug to off-target sites. Although nanoparticles have tremendous potential for a host of applications, their adverse effects on living cells have raised serious concerns recently for their use in the healthcare and consumer sectors. Entrapment of nanoparticles in the mononuclear phagocytic system of liver and spleen that leads to organ toxicity is one of the major concerns in nanoparticulate drug delivery systems [1]. It is reported that nanoparticles are taken up into the reticulo-endothelial cells through various energy dependent endocytosis process. Inside the cell, nanoparticles interact with various organelles and are digested by lysosomal enzymes and drug will be released [2].

De Jong et al. have reported that cynoacrylate and polystyrene nanoparticles could cause transient alterations in liver function and acute inflammation attributed to their active accumulation into macrophage cells of liver. In addition, these nanoparticles significantly reduced antioxidant defences of hepatocytes probably as a result of local release of oxidative species. Observed toxicities of ingested nanoparticles were attributed to the size and bio incompatible nature of polymers [3]. Moreover, various researchers have also reported the significant impact of surface charge of nanoparticles on normal physiology of systemic circulation like cellular integrity of erythrocytes, platelets aggregation and blood coagulation [4].

Several *in vitro* nanotoxicity assays examine nanoparticles influence on a single, homogeneous, immortal cell type. The cell types chosen for toxicological study should be a true representative of cellular components that are deemed to be exposed to nanoparticles following administration [5]. Therefore, in the present work, cell toxicity studies (MTT assay and hemolysis tests) were conducted to assess biocompatibility of developed nanoparticles (SLNs, PCL NPs and PA NPs) with macrophages; an integral part of reticulo-endothelial system.

5.2 Materials

The RAW 264.7 mouse macrophage cell line was obtained from American Type Culture Collection (ATCC) USA. 3-(4,5-dimethylthiazol-2-y1)-2,5-diphenyltetrazolium bromide (MTT), cyanmethemoglobin reagent (CMH) and hemoglobin standards were purchased from Sigma Chemical Co. (St. Louis, MO, USA). Dulbecco's modified Eagle's

medium (DMEM), Ca^{++}/Mg^{++}-free Dulbecco's phosphate-buffered saline (DPBS), Triton X-100, fetal bovine serum (FBS), penicillin and streptomycin for cell culture were obtained from Invitrogen-Gibco (Grand Island, NY, USA). Different concentrations of blank nanoparticles (0.5 mg/ml and 2 mg/ml) were prepared by appropriate dilutions of nanoparticles pellet, obtained after centrifugation (20,000 x g for 15 min), in deionized sterile water.

5.3 Methodology

5.3.1 MTT assay

In order to determine the cell toxicity, previously reported MTT (3-(4,5-Dimethylthiazol-2-yl)-2,5-diphenyltetrazolium bromide) assay was performed using RAW 264.7 mouse macrophage cell lines [6]. In brief, RAW 264.7 cells (mouse monocyte macrophages) harvested from growing cells as a monolayer were seeded onto 96-well plates (5,000 cells/well), and incubated for 24 h. The prepared blank nanoparticles were appropriately diluted with media buffer to get final concentrations of 0.5 mg/ml and 2 mg/ml. The media in the wells were replaced with 100 µl of diluted nanoparticles dispersions and incubated for 4h. Later, to remove nanoparticles, cells were washed with 100 µl of PBS solution, and incubated with fresh media and cultured in 5% CO_2, at 37 ^oC for 48 h. At the end of the incubation period, 10 µl of 10 mg/ml concentration of MTT was added to each well and incubated further for 3 h at 37 ^oC. DMSO (200 µl) was then added to each well to dissolve the internalized purple formazan crystals. Each sample was tested in triplicates. The UV absorbance at 570 nm was measured using a Microplate Reader (spectramax plus384, Micromolecular, USA). The results were expressed as a percentage of the absorbance of the non-treated cells. In the present experiment, Triton X-100 (0.5 % and 2%) was used as a positive control.

5.3.2 Hemolysis test

Hemolysis test in rat blood was performed using established methods adapted from literature [7]. Briefly, the total hemoglobin concentration of heparinized whole blood was measured using the cyanmethemoglobin (CMH) method against a hemoglobin concentration standard curve at an absorbance wavelength of 540 nm. The blood was then diluted to a hemoglobin concentration of 10 mg/ml with Ca^{++}/Mg^{++}-free DPBS. Blank nanoparticles samples (SLNs, PCL NPs and PA NPs) at two different mass concentrations (0.5 mg/ml and 2 mg/ml) and positive and negative controls were analyzed in triplicate.

To determine extent of hemolysis, an aliquot (100 µl) of nanoparticle suspension in water was added to microcentrifuge tubes, followed by the addition of 700 µl of Ca^{++}/Mg^{++}-free

DPBS. Within 3 min, equal amount of diluted blood was added to each of the tubes. The tubes were incubated in a 37 ^{o}C water bath for 4 h with gentle inversion of the sample tubes every 30 min. Following the incubation, the tubes were centrifuged at 800 x g for 15 min at room temperature. The supernatants were mixed in a 1:1 ratio with CMH reagent and analyzed at 540 nm. Sample absorbance was corrected for background interference (i.e., nanoparticles in DPBS without blood). The concentration of cell-free hemoglobin in each sample was assessed from the hemoglobin standard curve and by accounting for the 16-fold dilution factor for the samples and controls. Water was used as a negative control and Triton X-100 (0.5% and 2% v/v) was used as a positive control. Following equation was used to determine the extent of hemolysis:

$$\text{Hemolysis (\%)} = \frac{\text{Cell-free hemoglobin concentration}}{\text{Total hemoglobin concentration}} \text{ x } 100$$

5.4 Results and discussion

Assays of metabolic activity are the most common methods used to determine cell viability following nanoparticle exposure. Of these assays, the MTT assay in live cells is considered to be most reliable and sensitive method to measure cytostatic activity (shift from proliferation to quiescence) of potential medicinal agents and toxic materials [7]. In this, MTT [3-(4,5-dimethylthiazol-2-yl)-2,5-diphenyltetrazolium bromide] is reduced to purple formazan, which can be detected spectrophotometrically.

Hemolysis of erythrocytes in response to nanoparticles can be a measure of both membrane disruption and extreme cellular toxicity. This test is especially important for nanoparticles that are intended to be directly introduced into the bloodstream. The spectrophotometric detection of hemoglobin is an extremely sensitive technique to measure extent of hemolysis [7]. It has been widely employed by various researchers to predict the impact of size, surface charge and constituents of nanoparticles on cellular integrity of blood [7, 5].

From MTT assay (Fig. 5.1), it is evident that even after prolonged contact with the cells (4 h), developed nanoparticles exhibited low cytotoxicity (< 10%) up to 2 mg/ml. Similar results were observed in hemolysis study (Fig. 5.2). Co-incubation of nanoparticles with blood did not reveal any significant hemolysis. From *in vitro* data, it is evident which the polymers used in preparation of nanoparticles are biocompatible.

Polymers like stearic acid, PCL and pullulan acetate are reported to be biocompatible and biodegradable [7-9]. Moreover, it is also reported that anionic nanoparticles (all the three nanoparticles carry anionic surface charge) are generally nontoxic than cationically charged nanoparticles [3, 4]. Data obtained from cytotoxicity studies are in close agreement with previous reports.

In conclusion, from study, it is evident that developed nanoparticles are safe and biocompatible. However, thorough pre-clinical investigation needs to be conducted before extrapolating the obtained results to humans.

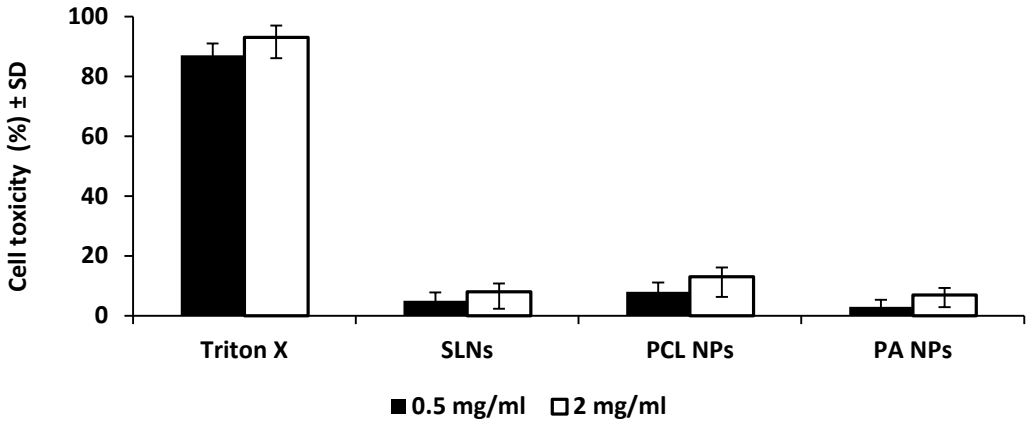

Fig. 5.1: Cytotoxicity study of blank nanoparticles in mouse macrophage cells. Triton X was used as positive control at two concentration levels; 0.5 % (v/v) and 2% (v/v). Cells were incubated with blank NPs for 4h. Cell toxicity was measured by the MTT cell proliferation method.

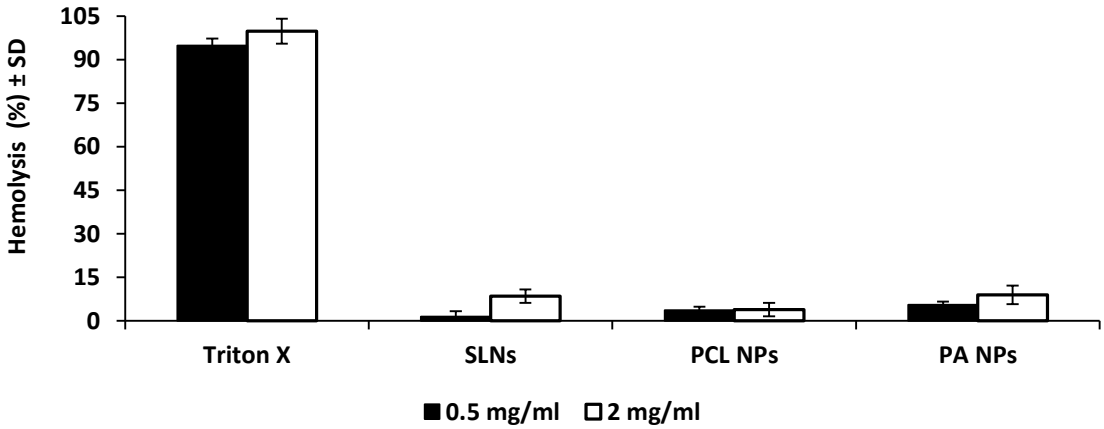

Fig. 5.2: *In vitro* hemolysis test results for diluted rat blood exposed to various particles. Triton X was used as positive control at two concentration levels; 0.5 % (v/v) and 2% (v/v). Blood was incubated with blank nanoparticles for 4h. Extent of hemolysis (hemoglobin) was measured by cyanmethemoglobin (CMH) method.

References

1. Yah CS, Simate GS, Iyuke SE Nanoparticles toxicity and their routes of exposures. Pak J Pharm Sci. 2012; 25: 477-91.
2. Adjei IM, Sharma B, Labhasetwar V. Nanoparticles: cellular uptake and cytotoxicity. Adv Exp Med Biol. 2014; 811: 73-91.
3. De Jong WH, Borm PJ. Drug delivery and nanoparticles: applications and hazards. Int J Nanomedicine. 2008; 3: 133-49.
4. Gupta AK, Gupta M. Synthesis and surface engineering of iron oxide nanoparticles for biomedical applications. Biomaterials. 2005; 26: 3995-4021.
5. Love SA, Maurer-Jones MA, Thompson JW, Lin YS, Haynes CL. Assessing nanoparticle toxicity. Annu Rev Anal Chem (Palo Alto Calif). 2012; 5: 181-205.
6. Sargent JM. The use of the MTT assay to study drug resistance in fresh tumor samples. Recent Results Cancer Res. 2003; 161:13-25.
7. Choi J, Reipa V, Hitchins VM, Goering PL, Malinauskas RA. Physicochemical characterization and *in vitro* hemolysis evaluation of silver nanoparticles. Toxicol Sci. 2011; 123: 133-43.
8. Severino P, Pinho SC, Souto EB, Santana MH. Polymorphism, crystallinity and hydrophilic-lipophilic balance of stearic acid and stearic acid-capric/caprylic triglyceride matrices for production of stable nanoparticles. Colloids Surf B Biointerfaces. 2011; 86: 125-30.
9. Woodruff MA, Hutmacher DW. The return of a forgotten polymer-polycaprolactone in the 21st century. Prog Polym Sci. 2010; 35: 1217-1256.
10. Zhang HZ, Gao FP, Liu LR, Li XM, Zhou ZM, Yang XD, Zhang QQ. Pullulan acetate nanoparticles prepared by solvent diffusion method for epirubicin chemotherapy. Colloids Surf B Biointerfaces. 2009; 71: 19-26.

Chapter 6

Conclusions

6.1 Conclusions

Nanotechnology-based platforms for systemic delivery of antiretroviral drugs have attracted several researchers worldwide in the recent past. The advent of nanotechnology has brought new dimensions to the current strategies for effective treatment of HIV/AIDS. There are emerging novel approaches in which nanotechnology can enhance patient compliance and therapeutic outcome of the present therapy. In the present work, studies were aimed to design and characterize nanoparticulate delivery systems to improve therapeutic efficacy of lopinavir by selective distribution of drug to reasonably inaccessible viral reservoir sites.

An accurate, precise and robust analytical method is an integral part of formulation development and pharmacokinetic evaluation of dosage forms. Therefore, analytical and bioanalytical methods were developed and critically validated for analysis of lopinavir in aqueous and biological samples using high-performance liquid chromatography (HPLC). Both the analytical and bioanalytical methods were found to be sensitive and selective towards lopinavir. The validated bioanalytical method was successfully employed for pharmacokinetic evaluation of various formulations of lopinavir. Developed bioanalytical method was found superior to other reported methods for determination of lopinavir in rat plasma samples.

Pre-formulation studies are important to establish physicochemical properties of a drug prior to formulation development. Data from pre-formulation studies demonstrated pH independent ionization pattern of lopinavir with a maximum aqueous solubility of ~2.5 µg/ml. Thermal analysis indicated lopinavir as a crystalline material with a sharp melting point at ~97 ºC. The partition co-efficient of lopinavir was found to be 4.2 indicating the lipophilic nature of the drug. The results of the drug-excipient studies indicated no significant interaction with most of the excipients used in the preparation of nanoparticles formulations.

For preparation of lipid based (SA) and polymeric nanocarriesrs (PCL and PA) of lopinavir, hot homogenization and solvent-evaporation techniques were found suitable respectively. Nanoparticles characteristics such as particle size and size distribution, surface charge and encapsulation efficiency were found to be dependent on various formulation and process parameters. Manufacturing parameters such as amount of polymer, concentration of emulsifier and process parameter such as time of homogenization/sonication were identified as critical variables, in preparation of lopinavir nanoparticles (SLNs, PCL NPs and PA

NPs). Lopinavir loaded SLNs and PCL NPs were rationally optimized using a low resolution Plackett–Burman design followed by Box-Behnken design. The optimized experimental conditions provided good quality nanoparticles with reproducible characteristics. The particle size analysis and microscopic imaging revealed that prepared nanoparticles (both lipid based and polymeric) were near spherical in shape with particle size ~200 nm. Optimized nanoparticles showed high encapsulation efficiency (>90%) for lopinavir. Pullulan acetate was explored as a potential carrier system for oral delivery of lopinavir. Pullulan acetate was successfully synthesized from pullulan and extensively characterized by IR and NMR techniques. PA NPs exhibited moderate EE (>70%) and unimodal size distribution.

Lopinavir loaded nanoparticles showed bi-phasic drug release pattern with the initial bust release followed by slow and continuous release up to 75 h. Drug release from all of the three formulations followed reciprocal-powered time model. Drug release from SLNs ($t_{50\%}$ 11.21 h) was relatively slower than other two polymeric nanoparticles; PCL (7.34 h) and PA NPs (6.96 h). Polymeric nanoparticles showed good stability in dispersed state when stored at room temperature (25 ± 2 ^{o}C/60 ± 5% RH) for 3 months. On the contrary, SLNs were stable only at refrigerated condition. SLNs showed significant loss in EE over 3 months of storage at room temperature. Stability assessment of formulation was based on particle size, PDI, surface charge and entrapment efficiency.

Oral pharmacokinetic studies in rat confirmed the poor bioavailability of free lopinavir attributed to first pass metabolism, P-gp efflux and poor solubility. Intravenous studies revealed rapid clearance of lopinavir leading to poor plasma exposure and short half-life (~0.7 h). *In vitro* metabolism studies indicated CYP dependent extensive metabolism of lopinavir in gut and liver, contributing to pre-systemic metabolism of drug. Everted gut sac studies illustrate poor permeability of free lopinavir probably due to P-gp efflux.

A series of studies (both *in vitro* and *in vivo*) were conducted to understand booster effects of ritonavir on pharmacokinetic of lopinavir. Co-administration of ritonavir showed high plasma exposure of lopinavir following oral administration. *In vitro* metabolism and permeability studies revealed that improvement in oral bioavailability of lopinavir could be probably due to the inhibitory action of ritonavir on CYP mediated metabolism and P-gp medicated efflux of lopinavir.

Comparative pharmacokinetic evaluations of developed nanoparticles were conducted and compared against marketed formulation (Kaletra; a co-formulation of

lopinavir and ritonavir). Studies demonstrated that co-administration of ritonavir though significantly improves plasma exposure of lopinavir, but not sufficient enough to maintain high concentration in lymphoidal organs.

On the contrary, *in vivo* pharmacokinetic and bio-distribution studies in rat indicated that SLNs and PCL NPs are potential carriers for effective delivery of lopinavir with promising enhanced plasma exposure and drug distribution to viral reservoir sites.

PA NPs though found effective in improving oral bioavailability (against free lopinavir) but failed to produce high concentrations of lopinavir both in plasma and lymphoidal tissues in comparison with currently marketed formulation.

Several mechanistic studies were conducted to explain the *in vivo* performances of delivered nanoparticles. Intestinal permeability studies conducted with endocytic uptake inhibitors suggest the significant role of clathrin and caveolae in nanoparticles uptake. It also indicates that nanoparticles are efficient in crossing intestinal barriers by surpassing P-gp efflux leading to improvement in oral bioavailability.

Further, pharmacokinetic studies conducted in CXI pre-treated rat following oral administration of SLNs exhibited significant drop in plasma exposure of lopinavir. Study suggests the possible involvement of lymphatic uptake and selective transport of nanoparticles to lymphoidal organs. Nanoparticles uptake data are in close agreement of tissue distribution studies. *In vitro* metabolism studies conducted with intestine and liver microsomes affirms the role of metabolic protection offered by nanoparticles to loaded drug during systemic circulation.

The pharmacokinetic profile of lopinavir was found to be altered when delivered in nanoparticles. A multi fold increase in plasma exposure of lopinavir, as characterized by AUC and C_{max}, was observed with loaded nanoparticles. Similarly, an increase in half life and volume of distribution following nanoparticles administration indicates increase in drug residence time in the systemic circulation and addition distribution of drug to poorly perfused organs (spleen and lymph nodes) and cells (macrophages and monocytes). Tissue distribution studies of nanoparticles reveal improved availability of drug for longer duration in these viral reservoir sites. The selective and enhanced distribution of drug to lymphoidal organs may provide sufficient concentration of lopinavir leading to the reduced possibility of viral resistance and relapse of infection. Studies also indicated good compatibility of developed formulations following oral administration to male wistar rats without any acute side effects. *In vitro* cytotoxicity studies further support the safety of developed formulation.

Thus, delivery of lopinavir using nanoparticles would be advantageous over available conventional formulation with selective distribution to the site of action over an extended duration. In HIV/AIDS patients, orally delivered nanoparticles would be preferentially localized to GALT and other lymphoidal organs that are widely considered as 'Trojan horse' for HIV infection. Moreover, it may also offer the benefit of ritonavir free therapy along with reduced dose and dosing frequency, leading to decreased untoward effects, improved patient compliance and clinical management of infection.

6.2 Future scope and directions

In order to establish the benefit risk ratio, further studies are needed to be conducted for the developed formulations in real clinical patients. Current therapy demands chronic administration of the drug which could cause drug accumulation and non linearity in pharmacokinetics due to modulation of certain transporters/enzyme proteins. Multiple and chronic dosing pharmacokinetic studies would address the effectiveness of the nanoparticulate drug delivery systems in such cases. Additionally, *in vitro* cell uptake studies in different immune cells may be carried out to investigate the intracellular concentration of the drug at viral replication sites. In the present work, pullulan acetate a novel polymer was explored as a potential carrier for oral delivery of lopinavir. Further studies are needed to be conducted to optimize PA NPs. Furthermore, safety aspects of PA should be evaluated before extrapolation of data to humans.

Appendix

LIST OF PUBLICATIONS (From Thesis Work)

1. Vats R, Aditya N and Ravi PR. Simple, rapid and validated LC determination of lopinavir in rat plasma and its application in pharmacokinetic studies. **Sci. Pharm.** 2011; 79: 849–863. (IF 0.9).

2. Ravi PR, Vats R, Thakur R, Srivani S and Aditya N. Effect of grapefruit juice and ritonavir on pharmacokinetics of lopinavir in wistar rats. **Phytother. Res.** 2012; 26:1490–5. (IF 2.1).

3. Ravi PR, Vats R, Dalal V, Gadekar N and Aditya N. Design, optimization and evaluation of Poly-ε-Caprolactone (PCL) based polymeric nanoparticles for oral delivery of lopinavir. **Drug Dev. Ind. Pharm.** 2013 [Epub ahead of print]. http://dx.doi.org/10.3109/03639045.2013.850710.

4. Ravi PR, Vats R, Gadekar N and Aditya N. A hybrid design to optimize preparation of lopinavir loaded solid lipid nanoparticles and comparative pharmacokinetic evaluation with marketed lopinavir/ritonavir co-formulation. **J. Pharm. Pharmacol.** 2014; 66: 912–26. (IF 2.1). http://dx.doi.org/10.1111/jphp.12217.

5. Ravi PR, Vats R, Balija J and Aditya N. Modified pullulan nanoparticles for oral delivery of anti-HIV drug lopinavir: formulation and pharmacokinetic evaluation. **Carbohydr. Polym.** 2014; 110: 320–8 (IF 3.8). http://dx.doi.org/10.1016/j.carbpol.2014.03.099.

LIST OF PUBLICATIONS (Outside Thesis Work)

1. Vats R, Kanthikiran VSV, Arla R, Veeraraghavan S and Rajak S. Drug-drug interaction study to assess the effects of atorvastatin co-administration on pharmacokinetics and anti-thrombotic properties of cilostazol in male Wistar rats. **Biopharm. Drug Dispos.** 2012; 33: 455–65. (IF 2.1).

2. Vats R, Kanthikiran VSV, Arla R, Veeraraghavan S, Rajak S and Aditya N. Effect of multidosecilostazol on pharmacokinetic and lipid Profile of atorvastatin in male wistar rats. **J. Pharm. Pharmacol.** 2012; 64: 1638–45. (IF 2.1).

3. Aditya N, Vats R and Ravi PR. Development, validation and pharmacokinetic application of liquid chromatographic method for estimation of raloxifene hydrochloride in rabbit plasma. **Acta. Chromatogr.** 2012; 24:559–573. (IF 1.1).

4. Ravi PR, Vats R and Reddy KU. Validation of a simple, rapid and sensitive LC method for quantification of riluzole in rat plasma and its pharmacokinetic application. **J. Bioanal. Biomed.** 2012. http://dx.doi.org/10.4172/1948-593X.S6-007

5. Ravi PR, Vats R and Reddy KU. Effect of ciprofloxacin and grapefruit juice on oral pharmacokinetics of riluzole in wistar rats. **J. Pharm. Pharmacol.** 2013; 65: 337–44. (IF 2.1).

6. Aditya N, Ravi PR, Kathuria H, and Vats R. Lipid nanoparticles for oral delivery of raloxifene: optimization, stability, in vivo evaluation and uptake mechanism. **Eur. J Pharm. Biopharm.** 2013. http://dx.doi.org/10.1016/j.ejpb.2013.12.015 (IF 4.8).

7. Aditya N, Ravi PR, Ranjan AS and Vats R. Poly (ε-caprolactone) nanocapsules for oral delivery of raloxifene: process optimization by hybrid design approach, in vitro and in vivo evaluation. **J. Microencapsul.** 2014; 31: 508–18 (IF 1.8). http://dx.doi.org/10.3109/02652048.2014.885603.

8. Ravi PR, Vats R and Gadekar N. Development and validation of simple, rapid and sensitive LC-PDA ultra violet method for quantification of nebivolol in rat plasma and its pharmacokinetic application. (Accepted for publication in **Acta Chromatogr.** and scheduled for issue no 2, 2015). (IF 1.1).

LIST OF CONFERENCE PRESENTATIONS (From Thesis Work)

1. Vats R, Aditya N and Ravi PR. Conference Proceeding: Polymeric nanoparticles of lopinavir to improve its oral bioavailability. **39th Annual Meeting and Exposition of the Controlled Release Society, Quebec City, Canada**; 15/07/2012.

2. Vats R, Aditya N and PR Ravi. Enhanced oral bioavailability of lopinavir from pullulan acetate nanoparticles: in vitro and in vivo evaluation. **3rd Nano Today Conference, Biopolis, Singapore**; 12/2013.

3. Vats R, Aditya N and Ravi PR. Conference Proceeding: Development and optimization of PCl nanoparticles for oral delivery of lopinavir using Box-Behnken statistical design. **13th International Symposium of CRS-Indian Chapter, Mumbai, India**; 01/2013.

4. Vats R, Aditya N and PR Ravi. ADME of lopinavir loaded solid lipid nanoparticles in normal and hepatic impaired Wistar rats. **6th International Symposium on DMPK, NIPER, Mohali, India**; 2/2014.

LIST OF CONFERENCE PRESENTATIONS (Outside Thesis Work)

1. Vats R, Kanthikiran VSV and Arla R. Conference Proceeding: Pharmacokinetic and pharmacodynamics drug interaction between cilostazol and atorvastatin" in male SD rats, **40th Annual Conference of Indian Pharmacological Society, NIPER, Mohali**; 18/07/2010.

2. Aditya N, Vats R, U Avula and PR Ravi. Design of polymeric nanocapsules for raloxifene hydrochloride by multiple emulsion method (w/o/w) using rotatable central composite design model, **10th International Nano Medicine and Drug Delivery (NanoDDS'12) Symposium, Atlantic City, NJ,** USA; 10/2012.

3. Aditya N, Vats R and PR Ravi. Self-organizing soyalecithin-chitosan nanoparticles for oral delivery of raloxifene. **3rd Nano Today Conference, Biopolis, Singapore**; 12/2013.

4. Aditya N, Vats R, H Kathuria and PR Ravi. Solid lipid nanoparticles for oral delivery of raloxifene: optimization, pharmacokinetic evaluation, bio-distribution and uptake studies. **13th International Symposium of Controlled Release Society, Indian Chapter, Mumbai, India**; 01/2013.

Biography of Dr Punna Rao Ravi

Dr Punna Rao Ravi is working as Assistant Professor in Department of Pharmacy, BITS-Pilani, Hyderabad Campus. He obtained his B.Pharm, M.Pharm and PhD degrees in Pharmaceutical Sciences from BITS-Pilani University, Rajasthan. He has been working as a faculty member in BITS-Pilani since year 2000. He has many publications in reputed international and national peer-reviewed journals and has presented papers in scientific conference both in India and abroad. He has successfully completed government sponsored research projects and is expecting more grants from scientific funding agencies.

Biography of Rahul Vats

Mr Rahul Vats has completed his B.Pharm from Northern India Engineering College, Lucknow and M. Pharm from Manipal University, Manipal, Karnataka. Post M.Pharm, he has worked in Pharmacokinetics and Drug Metabolism departments of Torrent Research Centre, Gandhinagar and Lupin Research Park, Pune where he was exposed to nuances of bioanalysis and pharmacokinetic tools and techniques. He joined BITS-Pilani, Hyderabad campus as a PhD scholar-cum-lecturer in July 2010. He has authored/co-authored research papers in renowned international peer-reviewed journals. He has also presented scientific posters/papers in reputed international and national conferences.